EXPERIMENTAL STUDY OF PIANO KEY WEIR

A THESIS

Submitted in partial fulfilment of the requirements for the award of the degree of

DOCTOR OF PHILOSOPHY

in

WATER RESOURCES DEVELOPMENT & MANAGEMENT

by

GOPAL DAS SINGHAL

M.C. CENTRAL LIBRARY
ACC No. G20549
Date 23/2/11
I.I.T. ROORKEE

DEPARTMENT OF WATER RESOURCES DEVELOPMENT & MANAGEMENT
INDIAN INSTITUTE OF TECHNOLOGY ROORKEE
ROORKEE - 247 667 (INDIA)

JULY, 2009

6.7.2 Variation of Discharge Coefficient with H_T/p for L/W as 4.84 136

6.7.3 Variation of Discharge Coefficient with H_T/p for L/W as 7.4 137

6.7.4 Variation of Discharge Coefficient with Froude No. and H_T/p 138

6.7.4.1 Variation of discharge coefficient with Froude No. and H_T/p for L/W as 3.56 138

6.7.4.2 Variation of discharge coefficient with Froude No. and H_T/p for L/W as 4.84 139

6.7.4.3 Variation of discharge coefficient with Froude No. and H_T/p for L/W as 7.4 140

6.7.5 Variation of Discharge Coefficient with Froude No. and H_T/p in Two Distinct Segments 141

6.7.5.1 Variation of discharge coefficient with Froude No. and H_T/p upto 0.4for L/W as 3.56 141

6.7.5.2 Variation of discharge coefficient with Froude No. and H_T/p greater than 0.4 for L/W as 3.56 142

6.7.5.3 Variation of discharge coefficient with Froude No. and H_T/p upto 0.4 for L/W as 4.84 143

6.7.5.4 Variation of discharge coefficient with Froude No. and H_T/p greater than 0.4 for L/W as 4.84 144

6.7.5.5 Variation of discharge coefficient with Froude No. and H_T/p upto 0.4 for L/W as 7.4 145

6.7.5.6 Variation of Discharge Coefficient with Froude No. and H_T/p greater than 0.4 for L/W as 7.4 146

6.7.6 Variation of Discharge Coefficient with Froude No., H_T/p and L/W 147

6.8 RESULT AND DISCUSSION 148

6.9 SUMMARY 152

CHAPTER 7 CONCLUSIONS AND FUTURE SCOPE OF WORK 153

7.1 CONCLUSIONS 153

7.2 FUTURE SCOPE OF WORK 154

REFERENCES 155

APPENDIX-A DATA RELATED TO FIVE PHASE EXPERIEMNTS 158

APPENDIX-B DATA RELATED TO CASE STUDY 168

APPENDIX-C DATA RELATED TO STUDY OF Cd VARATION 170

Froude No. and h/p for L/W as 3.56
6.5.7.2 Variation of discharge coefficient with Froude No. and h/p for L/W as 4.84 114
6.5.7.3 Variation of discharge coefficient with Froude No. and h/p for L/W as 7.4 116
6.5.8 Variation of Discharge Coefficient with Froude No. and h/p in Two Distinct Segments 118
6.5.8.1 Variation of discharge coefficient with Froude No. and h/p upto 0.4 for L/W as 3.56 118
6.5.8.2 Variation of discharge coefficient with Froude No. and h/p greater than 0.4 for L/W as 3.56 120
6.5.8.3 Variation of discharge coefficient with Froude No. and h/p upto 0.4 for L/W as 4.84 122
6.5.8.4 Variation of discharge coefficient with Froude No. and h/p greater than 0.4 for L/W as 4.84 124
6.5.8.5 Variation of discharge coefficient with Froude No. and h/p upto 0.4 for L/W as 7.4 126
6.5.8.6 Variation of discharge coefficient with Froude No. and h/p greater than 0.4 For L/W as 7.4 128
6.5.9 Variation of Discharge Coefficient with Froude No., h/p and L/W 130
6.6 VARIATION OF DISCHARGE COEFFICIENT FOR DOWNSTREAM SIDES OVER-HANGING TYPE OF PIANO KEY WEIR WITH CONSIDERING VELOCITY HEAD OF APPROACH FLOW 131
6.6.1 Variation of Discharge Coefficient with H_T/p for L/W as 4.84 131
6.6.2 Variation of Discharge Coefficient with Froude No. and H_T/p for L/W as 4.84 132
6.6.3 Variation of Discharge Coefficient with Froude No. and H_T/p in Two Distinct Segments 133
6.6.3.1 Variation of discharge coefficient with Froude No. and H_T/p upto 0.4 for L/W as 4.84 133
6.6.3.2 Variation of discharge coefficient with Froude No. and H_T/p greater than 0.4 for L/W as 4.84 134
6.7 VARIATION OF DISCHARGE COEFFICIENT FOR BOTH SIDES OVER-HANGING TYPE OF PIANO KEY WEIR WITH CONSIDERING VELOCITY HEAD OF APPROACH FLOW 135
6.7.1 Variation of Discharge Coefficient with H_T/p for L/W as 3.56 135

CHAPTER 6 ANALYSIS OF DISCHARGE COEFFICIENT 92

6.1 GENERAL 92

6.2 DATA CONSIDERATION 92

6.3 VARIATION OF DISCHARGE COEFFICIENT 93

6.3.1 Basics 93

6.3.2 Cases Considered 94

6.4 VARIATION OF DISCHARGE COEFFICIENT FOR DOWNSTREAM SIDES OVER-HANGING TYPE OF PIANO KEY WEIR 94

6.4.1 Variation of Discharge Coefficient with Froude No. for *L/W* as 4.84 94

6.4.2 Variation of Discharge Coefficient with *h/p* for *L/W* as 4.84 96

6.4.3 Variation of Discharge Coefficient with Froude No. and *h/p* for *L/W* as 4.84 97

6.4.4 Variation of Discharge Coefficient with Froude No. and *h/p* in Two Distinct Segments 99

6.4.4.1 Variation of discharge coefficient with Froude no. and *h/p* upto 0.4 for *L/W* as 4.84 99

6.4.4.2 Variation of discharge coefficient with Froude no. and *h/p* greater than 0.4 for *L/W* as 4.84 101

6.5 VARIATION OF DISCHARGE COEFFICIENT FOR BOTH SIDES OVER-HANGING TYPE OF PIANO KEY WEIR 103

6.5.1 Variation of Discharge Coefficient with Froude No. for *L/W* as 3.56 103

6.5.2 Variation of Discharge Coefficient with Froude No. for *L/W* as 4.84 105

6.5.3 Variation of Discharge Coefficient with Froude No. for *L/W* as 7.4 106

6.5.4 Variation of Discharge Coefficient with h/p for *L/W* as 3.56 108

6.5.5 Variation of Discharge Coefficient with *h/p* for *L/W* as 4.84 109

6.5.6 Variation of Discharge Coefficient with h/p for *L/W* as 7.4 111

6.5.7 Variation of Discharge Coefficient with Froude No. and *h/p* 112

6.5.7.1 Variation of discharge coefficient with 112

©INDIAN INSTITUTE OF TECHNOLOGY ROORKEE, ROORKEE, 2009
ALL RIGHTS RESERVED

INDIAN INSTITUTE OF TECHNOLOGY ROORKEE
ROORKEE

CANDIDATE'S DECLARATION

I hereby certify that the work which is being presented in the thesis entitled **EXPERIMENTAL STUDY OF PIANO KEY WEIR** in partial fulfilment of the requirements for the award of the degree of Doctor of Philosophy and submitted in the Department of Water Resources Development & Management of the Indian Institute of Technology Roorkee, Roorkee, is an authentic record of my own work carried out during the period from January 2005 to July 2009 under the supervision of Dr. Nayan Sharma, Professor, Department of Water Resources Development & Management and Dr. C.S.P. Ojha, Professor, Department of Civil Engineering, Indian Institute of Technology Roorkee, Roorkee.

The matter presented in this thesis has not been submitted by me for the award of any other degree of this or any other Institute.

Gopal

(GOPAL DAS SINGHAL)

This is to certify that the above statement made by the candidate is correct to the best of our knowledge.

(C.S.P.OJHA)
Supervisor
Date: July 20th 2009

(NAYAN SHARMA)
Supervisor

The Ph.D. Viva-Voce Examination of **Mr. Gopal Das Singhal**, Research Scholar, has been held on _____

Signature of Supervisors

Signature of External Examiner

Dedicated
To
My Beloved Wife
'Sonal'

ABSTRACT

As projects are reassessed for safety, provision for an increased estimate of the probable maximum flood (PMF) has to be made in many cases. It is therefore necessary to provide more flood storage and/or larger capacity for spillways to pass the PMF safely. An innovative and effective way of increasing the spillway capacity is to use a Labyrinth weir. The concept of the Labyrinth weir is to vary the plan shape of the crest to increase the effective crest length. This increases the discharge per unit width of the spillway for a given operating head. A Labyrinth weir has advantages compared to the straight over flow weir and the standard ogee crest. Labyrinth weirs can be used to increase outlet capacity for a given spillway crest elevation and length or to increase storage by raising the crest while maintaining spillway capacity.

A new concept of a Labyrinth weir has been proposed with a new shape like black and white Piano keys when viewed in plan. Keeping in view the relatively reported better performance of Piano Key Weirs in comparison to linear and Labyrinth weirs, following objectives are considered for the present study: (i) to perform experiments on different configurations of Piano Key Weir, varying in term of presence/absence of ramp in upstream and downstream for one side and both side overhanging and varying ratio of any two consecutive limbs, (ii) to identify the situations which lead to increase in the magnification ratio of discharge passing through the Piano Key Weir, (iii) to quantify the maximum achievable magnification ratio and associated hydraulic conditions, (iv) to identify the parameters influencing the variation of discharge coefficient and study the role of considering the total head versus the head over the crest and (v) to develop a set of relationships for the variation of discharge coefficient and to identify the most suitable relationship

The work includes details of five phases of experiments. Initial phase of experiments (phase -I to IV) which were planned with different configurations of Piano Key Weir, i.e. with or without ramp and one or two side overhanging (u/s & d/s) indicate that Piano Key Weir with presence of ramp and two sides overhanging (u/s & d/s) provides a higher discharge under same head when compared with other Piano Key Weir configurations with lesser number of ramps and/or over-hangings. In phase-V experiments, filling were introduced in the ramps but these were not found to increase the discharge. Thus, ramps with no planar discontinuity were found to be best performing. In phase-V experiments, also modification were introduced into inlet limb of Piano Key

Weir but it was again observed that such an inlet modification was of no practical significance as it did not lead to any increase in the discharge.

The ratio (r) of Piano Key Weir to linear weir discharge for a given head was always more than one and when compared with Labyrinth weir (based on computational only) was always higher than the Labyrinth weir. This finding is in conformity with the literature. The ratio (r) was found to increase with magnification ratio L/W. However, at larger value of L/W, the ratio (r) was observed to tend to approach a limiting value in the proximity of four.

For a very large value of L/W, where L is the perimeter of the Piano-Key Weir crest and W is the width of the channel, it was observed that variation of ratio of inlet and outlet cell width did influence the ratio r and the performance was best when two cells were of same width. Any deviation from this ratio was found to have a negative effect on ratio r at larger L/W ratios.

Among the several options attempted to develop relationship for C_d variations for two different configurations of Piano Key Weir, i.e. one side and both side overhanging, it was found that for one side overhanging Piano Key Weir, C_d variations as a function of (i) Froude number, Fr (ii) h/p (head over the weir, h and weir height as p) and (iii) Fr and h/p leads to development of several relationships with a relatively higher values of statistical fits, i.e. Coefficient of Determination (R^2) indicating the appropriateness of different functional relationships. However, the perusal of function relationships for both side overhanging indicates relatively poor performance of C_d variation only as function of Fr. Also, the C_d variation with h/p as only variational parameter doesn't appear to work so well ($R^2 = 0.80$) when compared with counterpart for one side overhanging ($R^2 = 0.96$).

The use of total head is also explored in the analysis of C_d variations. However, no significant improvements are observed into development of C_d relationships. This may be because of the reason that velocity heads are very small in the experiments performed. Study also indicates that for lower value of L/W, say as 3.56 and 4.84, the functional relationship of C_d variation in term of Fr and h/p appears to be most suitable choice. However, for larger value of L/W as 7.4, relationship is strongly dominated by h/p. Evaluation of the data collected at field scale model using (i) $C_d = f(Fr)$, (ii) $C_d = f(h/p)$ & (iii) $C_d = f(h/p, Fr)$ indicates that the use of $C_d = f(h/p, Fr)$ very well works with the field scale model results.

ACKNOWLEDGEMENTS

I am immensely grateful to my supervisors Dr. Nayan Shama, Professor, Dept. of WRD&M, and Dr. C.S.P. Ojha, Professor, Deptt. of Civil Engineering, IIT Roorkee for their stipulated guidance, unwavering support and encouragement. This thesis could not have attained its present form, both in content and presentation, without their active interest, direction and guidance.

I express my heartfelt thanks and gratitude to Prof. Ram Pal Singh, Professor and Head, Department of WRD&M, IIT Roorkee for his utmost co-operation, help and support through out the course of my research work.

I express my sincere thanks to Prof. Devadutta Das, Prof. Gopal Chauhan, Prof. M.L. Kansal, Prof Deepak Khare, Prof Raj pal Singh, Dr. S. K. Mishra, Department of WRD&M, IIT Roorkee for their valuable suggestions and words of encouragement. I also express my sincere thanks to all distinguished faculty and staff members, for their suggestions and timely help.

I wish to thank Dr. Ajay Gairola, Associate Professor Department of Civil Engineering, member Student Research Committee, for giving their valuable suggestions and words of encouragement.

I am thankful to Prof. H. O. Gupta, Professor Electric Engineering Department for giving his moral support and advice in various ways. I am highly obliged and express sincere thanks to Mrs. Kusam Gupta.

I express my sincere thank to official and technical staff of Deptt. Of Water Resources Development and Management, IIT Roorkee. Also, special thanks go to Mr. Beer Singh Chauhan for their help in experimental study of my research work. I warmly thank Mr. Kedar Singh for giving me valuable suggestion during my experimental work for my research work. I am also thankful to Mr. Neeraj Kumar and Mr. Pradeep Kumar for their help in my thesis preparation. I am also thankful to all the lab members for the help they rendered in giving this thesis a final shape.

I thank my collaborators for the kind support they have provided during the course of this research work. I express my thanks to Mrs. Archana Sarkar, Scientist, NIH, Roorkee. I wish to express my thanks to Mr. Parwez Akhatar, Mrs. Anupama Nayak, Mr. Romji Singh, Mr. Bidhan Chandra Das and Ms. Shailza Verma for their timely help.

I wish to thank my friend Dr. Amit Kumar Chawla, for his kind gestures/help he provided. I also wish to thank Mr. Narendra Singh Beniwal and Ms. Ruby Beniwal for their constant encouragement and love.

The words prove to be insufficient to express my deep feelings and heartfelt thanks to Dr. Nayan Sharma for his high benevolence and un-hesitated guidance throughout the study period.

I express my deep gratitude to my father, Mr. Kishan Lal Singhal, father in-law, Mr. Anil Singhal, mother, Mrs. Pushpa Singhal and mother in-law, Mrs. Usha Singhal, for their blessings, whole hearted support and co-operation.

I extend my humble thanks to my wife, Ms. Sonal Singhal for their forbearance, understanding and patience throughout the research work.

I would like to thank everybody who was important to the successful realization of thesis, as well as expressing my apology that I could not mentioned personally one by one.

Above all, I express my gratitude from the core of my heart to Lord 'SHIVA' for giving courage, strength and patience to carryout my research work.

(Gopal Das Singhal)

CONTENTS

DESCRIPTION			PAGE NO.
CANDIDATE'S DECLARATION			i
ABSTRACT			ii
ACKNOWLEDGEMENT			iv
CONTENTS			vi
LIST OF FIGURES			xi
LIST OF PLATES			xviii
LIST OF TABLES			xix
LIST OF NOTATIONS			xxii
CHAPTER 1 INTRODUCTION			1
1.1	GENERAL		1
1.2	LABYRINTH WEIR		2
1.3	PIANO KEY WEIR		2
1.4	OBJECTIVES OF THE STUDY		4
1.5	ORGANISATION OF THE THESIS		4
CHAPTER 2 LITERATURE REVIEW			6
2.1	GENERAL		6
2.2	DEVELOPMENT AND FIELD APPLICATIONS OF LABYRINTH WEIR		6
2.3	THEORETICAL CONCEPT OF LABYRINTH WEIR		10
	2.3.1	General	10
	2.3.2	Characteristics of Flows Over Labyrinth Weir	11
	2.3.3	Basics Parameters of Labyrinth Weir	12
	2.3.4	Different Theories of Labyrinth Weir Discharge Coefficient	12
2.4	PIANO KEY WEIR		18
	2.4.1	Flow Characteristics over Piano Key Weir	18
	2.4.2	Review of the Existing Model Study of Piano Key Weir	19
2.5	SUMMARY		20

CHAPTER 3 EXPERIMENTAL PROGRAMME 21

3.1 INTRODUCTION 21

3.2 LABORATORY FLUME AND OTHER EXPERIMENTAL ACCESSORIES 21

3.2.1 Laboratory Flume Used 21

3.2.2 Other Accessories 22

3.3 EXPERIMENTAL PROCEDURE 22

3.4 FIRST PHASE MODEL EXPERIMENTS 23

3.5 PHASE TWO MODEL EXPERIMENTS 31

3.6 PHASE THREE MODEL EXPERIMENTS 37

3.7 PHASE FOUR MODEL EXPERIMENTS 44

3.8 PHASE FIVE MODEL EXPERIMENTS 50

3.9 SUMMARY 53

CHAPTER 4 PERFORMANCE EVALUATION OF PIANO KEY WEIR 54

4.1 GENERAL 54

4.2 DATA ANALYSIS 54

4.3 VALIDITY OF DISCHARGE MEASURING THROUGH V-NOTCH AND SHARP CRESTED WEIR 55

4.4 EVALUATION OF FIRST PHASE EXPERIMENTS 56

4.5 EVALUATION OF SECOND PHASE EXPERIMENTS 63

4.6 EVALUATION OF THIRD PHASE EXPERIMENTS 67

4.7 EVALUATION OF FOURTH PHASE EXPERIMENTS 68

4.8 UATION OF FIFTH PHASE EXPERIMENTS 72

4.9 SUMMARY 75

CHAPTER 5 PIANO KEY WEIR –A CASE STUDY 76

5.1 GENERAL 76

5.2 EXPERIMENTAL STUDIES 76

5.3 ANALYSIS OF LAB-BASED MODEL EXPERIMENTS 86

5.4 ANALYSIS OF COMPREHENSIVE MODEL EXPERIMENTS RESULTS 88

5.5 SUMMARY 91

LIST OF FIGURES

Fig. No.	Description	Page No.
2.1	Side channel spillway – Arizona spillway at Hoover dam, USA	7
2.2	Duckbill spillway – Apartadura spillway, Portugal	7
2.3	Bathtub spillway – Fontenelle dam, USA	8
2.4	Labyrinth weir- Tongue River dam, USA	8
2.5	Design curve - triangular -sharp crested weir	13
2.6	Design curve - trapezoidal - sharp crested weir	14
2.7	Design curves between C_W Vs L/W	15
2.8	Design curves between C_p Vs L/W	16
2.9	Design curve - triangular weir	16
2.10	Design curve - trapezoidal weir	17
2.11	Design curves with quarter-round crest and a triangular weir	18
3.1	Plan of tilting flume and its components used in experiments	22
3.2	Three dimensional view to generalize Piano Key Weir shape	24
3.3	Plan and section of model P_1M_1 (dimensions in mm)	25
3.4	Plan and section of model P_1M_2 (dimensions in mm)	26
3.5	Plan and section of model P_1M_3 (dimensions in mm)	27
3.6	Plan and section of model P_1M_4 (dimensions in mm)	28
3.7	Plan and section of model P_1M_5 (dimensions in mm)	29
3.8	Plan and section of model P_1M_6 (dimensions in mm)	30
3.9	Plan and section of model P_2M_1 (both sides ramping), (dimensions in mm)	31
3.10	Plan and section of model P_2M_2 (both sides ramping), (dimensions in mm)	32
3.11	Plan and section of model P_2M_3 (both sides ramping), (dimensions in mm)	33
3.12	Plan and section of model P_2M_4 (both sides ramping), (dimensions in mm)	34
3.13	Plan and section of model P_2M_5 (both sides ramping), (dimensions in mm)	35
3.14	Plan and section of model P_2M_6 (both sides ramping), (dimensions in mm)	36

3.15	Plan and section of model P_3M_1 (both sides ramping), (dimensions in mm)	38
3.16	Plan and section of model P_3M_2 (both sides ramping), (dimensions in mm)	39
3.17	Plan and section of model P_3M_3 (both sides ramping), (dimensions in mm)	40
3.18	Plan and section of model P_3M_4 (both sides ramping), (dimensions in mm)	41
3.19	Plan and section of model P_3M_5 (both sides ramping), (dimensions in mm)	42
3.20	Plan and section of model P_3M_6 (both sides ramping), (dimensions in mm)	43
3.21	Plan and section of model P_4M_1 (both sides ramping), (dimensions in mm)	45
3.22	Plan and section of model P_4M_2 (both sides ramping), (dimensions in mm)	46
3.23	Plan and section of model P_4M_3 (both sides ramping), (dimensions in mm)	47
3.24	Plan and section of model P_4M_4 (both sides ramping), (dimensions in mm)	48
3.25	Plan and section of model P_4M_5 (both sides ramping), (dimensions in mm)	49
3.26	Plan and section of model P_2M_4 with inlet modification (dimensions in mm)	50
3.27	Plan and section of model P_4M_3 with inlet modification (dimensions in mm)	51
3.28	Plan and section of model P_2M_6 with filling inlet cell modification (dimensions in mm)	51
3.29	Plan and section of model P_2M_2 with filling outlet cell modification (dimensions in mm)	52
3.30	Plan and section of model P_2M_5 with filling outlet cell modification (dimensions in mm)	52
4.1	Plot between Q_{PK}, Q_L and h/p for model P_1M_1	57
4.2	Plot between Q_{PK}, Q_L and h/p for model P_1M_2	57
4.3	Plot between Q_{PK}, Q_L and h/p for model P_1M_3	58
4.4	Plot between Q_{PK}, Q_L and h/p for model P_1M_4	58
4.5	Plot between Q_{PK}, Q_L and h/p for model P_1M_5	59
4.6	Plot between Q_{PK}, Q_L and h/p for model P_1M_6	59
4.7	Plot between r and h/p for model P_1M_1 & P_1M_4	60

	with same p = 12 cm	
4.8	Plot between r and h/p for model P_1M_2 & P_1M_5 with same p = 16 cm	60
4.9	Plot between r and h/p for model P_1M_3 & P_1M_6 with same p = 20 cm	61
4.10	Plot between r and h/p for same L/W = 7.4	61
4.11	Plot between r and h/p for same L/W = 3.56	62
4.12	Plot between r and h/p for all six models	62
4.13	Plot between ΔQ and h/p for model P_2M_1 with both side ramps and without ramps	63
4.14	Plot between ΔQ and h/p for model P_2M_2 with both side ramps and without ramps	64
4.15	Plot between ΔQ and h/p for model P_2M_3 with both side ramps and without ramps	64
4.16	Plot between ΔQ and h/p for model $P_2M_4$with both side ramps and without ramps	65
4.17	Plot between ΔQ and h/p for model P_2M_5 with both side ramps and without ramps	65
4.18	Plot between ΔQ and h/p for model P_2M_6 with both side ramps and without ramps	66
4.19	Plot between r and h/p for all six models with both side ramps	66
4.20	Plot between r and h/p for all six Models of phase three	67
4.21	Plot between r and $h/(a+b)$	68
4.22	Plot between Q_{PK}, Q_L and h/p for model P_4M_1 with both side ramps	69
4.23	Plot between Q_{PK}, Q_L and h/p for model P_4M_2 with both side ramps	69
4.24	Plot between Q_{PK}, Q_L and h/p for model P_4M_3 with both side ramps	70
4.25	Plot between Q_{PK}, Q_L and h/p for model P_4M_4 with both side ramps	70
4.26	Plot between Q_{PK}, Q_L and h/p for model P_4M_5 with both side ramps	71
4.27	Plot between r and h/p for all five models of phase four	71
4.28	Plot between ΔQ and h/p for model P_2M_4 & model P_2M_4 (with improving the hydraulic shape of inlet)	72
4.29	Plot between ΔQ and h/p for model P_4M_3 & model P_4M_3 (with improving the hydraulic shape of inlet)	73

4.30	Plot between ΔQ and h/p for model P_2M_6 (filling inlet cell)	73
4.31	Plot between ΔQ and h/p for model P_2M_2 (filling outlet cell)	74
4.32	Plot between ΔQ and h/p for model P_2M_5 (filling outlet cell)	74
5.1	Plan and section of model C_1M_1 for physical model study (dimensions in mm)	78
5.2	Plan and section of model C_1M_2 for physical model study (dimensions in mm)	79
5.3	Plan and section of model C_1M_3 for physical model study (dimensions in mm)	80
5.4	Plan and section of model C_1M_4 for physical model study (dimensions in mm)	81
5.5	Plan and section of model C_1M_5 for physical model study (dimensions in mm)	82
5.6	Plan and section of model C_1M_6 for physical model study (dimensions in mm)	83
5.7	Plan and section of model C_1M_6 for comprehensive model study (dimensions in mm)	84
5.8	Plan and section of model C_1M_6 for prototype (dimensions in mm)	85
5.9	Plot between ΔQ and h/p for all six models	87
5.10	Plot between r and h/p for all six models	87
5.11	Plot between r and h/p for model C_1M_6	88
5.12	Plot between ΔQ and h/p for model C_1M_6	89
5.13	Comparison of Piano Key Weir by to sharp crested weir with head over the crest for model C_1M_6	89
5.14	Discharge passing over Piano Key Weir and corresponding reservoir level	91
6.1	Plot between Fr and C_d for $L/W = 4.84$	95
6.2	Error analysis between observed and computed C_d for $L/W = 4.84$ using Eq. (6.8)	95
6.3	Plot between h/p and C_d for $L/W = 4.84$	96
6.4	Error analysis between observed and computed C_d for $L/W = 4.84$ using Eq. (6.9)	97
6.5	Graphical plot between Fr and C_d for $L/W = 4.84$	98
6.6	Graphical plot between h/p and C_d for $L/W = 4.84$	98
6.7	Error analysis between observed and computed C_d for $L/W = 4.84$ using Eq. (6.10)	99
6.8	Graphical plot between Fr and C_d for $L/W = 4.84$ and	100

	h/p upto 0.4	
6.9	Graphical plot between h/p and C_d for L/W = 4.84 and h/p upto 0.4	100
6.10	Error analysis between observed and computed C_d for L/W = 4.84 and h/p upto 0.4 using Eq. (6.11)	101
6.11	Graphical plot between Fr and C_d for L/W = 4.84 and h/p greater than 0.4	102
6.12	Graphical plot between h/p and C_d for L/W = 4.84 and h/p greater than 0.4	102
6.13	Error analysis between observed and computed C_d for L/W = 4.84 and h/p greater than 0.4 using Eq. (6.12)	103
6.14	Plot between Fr and C_d for L/W = 3.56	104
6.15	Error analysis between observed and computed C_d for L/W = 3.56 using Eq. (6.13)	104
6.16	Plot between Fr and C_d for L/W = 4.84	105
6.17	Error analysis between observed and computed C_d for L/W = 4.84 using Eq. (6.14)	106
6.18	Plot between Fr and C_d for L/W = 7.4	107
6.19	Error analysis between observed and computed C_d for L/W = 7.4 using Eq. (6.15)	107
6.20	Plot between h/p and C_d for L/W = 3.56	108
6.21	Error analysis between observed and computed C_d for L/W = 3.56 using Eq. (6.16)	109
6.22	Plot between h/p and C_d for L/W = 4.84	110
6.23	Error analysis between observed and computed C_d for L/W = 4.84 using Eq. (6.17)	110
6.24	Plot between h/p and C_d for L/W = 7.4	111
6.25	Error analysis between observed and computed C_d for L/W = 7.4 using Eq. (6.18)	112
6.26	Graphical plot between Fr and C_d for L/W = 3.56	113
6.27	Graphical plot between h/p and C_d for L/W = 3.56	113
6.28	Error analysis between observed and computed C_d for L/W = 3.56 using Eq. (6.19)	114
6.29	Graphical plot between Fr and C_d for L/W = 4.84	115
6.30	Graphical plot between h/p and C_d for L/W = 4.84	115
6.31	Error analysis between observed and computed C_d for L/W = 4.84 using Eq. (6.20)	116
6.32	Graphical plot between Fr and C_d for L/W = 7.4	117

6.33	Graphical Plot between h/p and C_d for L/W = 7.4	117
6.34	Error analysis between observed and computed C_d for L/W = 7.4 using Eq. (6.21)	118
6.35	Graphical plot between Fr and C_d for L/W = 3.56 and h/p upto 0.4	119
6.36	Graphical plot between h/p and C_d for L/W = 3.56 and h/p upto 0.4	119
6.37	Error analysis between observed and computed C_d for L/W = 3.56 and h/p upto 0.4 using Eq. (6.22)	120
6.38	Graphical plot between Fr and C_d for L/W = 3.56 and h/p greater than 0.4	121
6.39	Graphical plot between h/p and C_d for L/W = 3.56 and h/p greater than 0.4	121
6.40	Error analysis between observed and computed C_d for L/W = 3.56 and h/p greater than 0.4 using Eq. (6.23)	122
6.41	Graphical plot between Fr and C_d for L/W = 4.84 and h/p upto 0.4	123
6.42	Graphical plot between h/p and C_d for L/W = 4.84 and h/p upto 0.4	123
6.43	Error analysis between observed and computed C_d for L/W = 4.84 and h/p upto 0.4 using Eq. (6.24)	124
6.44	Graphical plot between Fr and C_d for L/W = 4.84 and h/p greater than 0.4	125
6.45	Graphical plot between h/p and C_d for L/W = 4.84 and h/p greater than 0.4	125
6.46	Error analysis between observed and computed C_d for L/W = 4.84 and h/p greater than 0.4 using Eq. (6.25)	126
6.47	Graphical plot between Fr and C_d for L/W = 7.4 and h/p upto 0.4	127
6.48	Graphical plot between h/p and C_d for L/W = 7.4 and h/p upto 0.4	127
6.49	Error analysis between observed and computed C_d for L/W = 7.4 and h/p upto 0.4 using Eq. (6.26)	128
6.50	Graphical plot between Fr and C_d for L/W = 7.4 and h/p greater than 0.4	129
6.51	Graphical plot between h/p and C_d for L/W = 7.4 and h/p greater than 0.4	129
6.52	Error analysis between observed and computed C_d for L/W = 7.4 and h/p greater than 0.4 using Eq. (6.27)	130
6.53	Error analysis between observed and computed C_d for all value of L/W using Eq. (6.29)	131

6.54	Error analysis between observed and computed C_d for L/W = 4.84 using Eq. (6.30)	132
6.55	Error analysis between observed and computed C_d for L/W = 4.84 using Eq. (6.31)	133
6.56	Error analysis between observed and computed C_d for L/W = 4.84 and H_T/p upto 0.4 using Eq. (6.32)	134
6.57	Error analysis between observed and computed C_d for L/W = 4.84 and H_T/p greater than 0.4 using Eq. (6.33)	135
6.58	Error analysis between observed and computed C_d for L/W = 3.56 using Eq. (6.34)	136
6.59	Error analysis between observed and computed C_d for L/W = 4.84 using Eq. (6.35)	137
6.60	Error analysis between observed and computed C_d for L/W = 7.4 using Eq. (6.36)	138
6.61	Error analysis between observed and computed C_d for L/W = 3.56 using Eq. (6.37)	139
6.62	Error analysis between observed and computed C_d for L/W = 4.84 using Eq. (6.38)	140
6.63	Error analysis between observed and computed C_d for L/W = 7.4 using Eq. (6.39)	141
6.64	Error analysis between observed and computed C_d for L/W = 3.56 and H_T/p upto 0.4 using Eq. (6.40)	142
6.65	Error analysis between observed and computed C_d for L/W = 3.56 and H_T/p greater than 0.4 using Eq. (6.41)	143
6.66	Error analysis between observed and computed C_d for L/W = 4.84 and H_T/p upto 0.4 using Eq. (6.42)	144
6.67	Error analysis between observed and computed C_d for L/W = 4.84 and H_T/p greater than 0.4 using Eq. (6.43)	145
6.68	Error analysis between observed and computed C_d for L/W = 7.4 and H_T/p upto 0.4 using Eq. (6.44)	146
6.69	Error analysis between observed and computed C_d for L/W = 7.4 and H_T/p greater than 0.4 using Eq. (6.45)	147
6.70	Error analysis between observed and computed C_d for all value of L/W using Eq. (6.46)	148
6.71	Performance of C_d relationships using field scale data of Piano Key Weir	149

LIST OF PLATES

Plate No.	Description	Page No.
3.1	Model P_1M_1	25
3.2	Model P_1M_2	26
3.3	Model P_1M_3	27
3.4	Model P_1M_4	28
3.5	Model P_1M_5	29
3.6	Model P_1M_6	30
3.7	Model P_2M_1 (both sides ramping)	31
3.8	Model P_2M_2 (both sides ramping)	32
3.9	Model P_2M_3 (both sides ramping)	33
3.10	Model P_2M_4 (both sides ramping)	34
3.11	Model P_2M_5 (both sides ramping)	35
3.12	Model P_2M_6 (both sides ramping)	36
3.13	Model P_3M_1 (both sides ramping)	38
3.14	Model P_3M_2 (both sides ramping)	39
3.15	Model P_3M_3 (both sides ramping)	40
3.16	Model P_3M_4 (both sides ramping)	41
3.17	Model P_3M_5 (both sides ramping)	42
3.18	Model P_3M_6 (both sides ramping)	43
3.19	Model P_4M_1 (both sides ramping)	45
3.20	Model P_4M_2 (both sides ramping)	46
3.21	Model P_4M_3 (both sides ramping)	47
3.22	Model P_4M_4 (both sides ramping)	48
3.23	Model P_4M_5 (both sides ramping)	49
5.1	Model C_1M_1	78
5.2	Model C_1M_2	79
5.3	Model C_1M_3	80
5.4	Model C_1M_4	81
5.5	Model C_1M_5	82
5.6	Model C_1M_6	83
5.7	Pictorial view of Piano Key Weir model C_1M_6 for comprehensive model study	86
5.8	Running view of Piano Key Weir from d/s with under sluice gate	90
5.9	Running view of Piano Key Weir from u/s with under sluice gate	90

Table No.	Description	Page No.
3.1	Phase one model dimensions	24
3.2	Phase Three Model dimensions	37
3.3	Phase four model dimensions	44
4.1	Results on comparative study between V-notch and sharp crested weir	56
5.1	Piano Key Weir dimensions for model study	77
5.2	Piano Key Weir dimensions for prototype	77
6.1	Average absolute percentage error between observed and computed C_d for one side and both sides overhanging type of Piano Key Weir for L/W as 4.84	150
6.2	Comparison of average absolute percentage error between observed and computed C_d for L/W as 4.84 with h/p and H_T/p for single side overhanging	150
6.3	Comparison of Average absolute percentage difference between observed and computed C_d for L/W as 3.56 with h/p and H_T/p for both side overhanging	151
6.4	Comparison of Average absolute percentage error between observed and computed C_d for L/W as 4.84 with h/p and H_T/p for both side overhanging	151
6.5	Comparison of Average absolute percentage error between observed and computed C_d for L/W as 7.4 with h/p and H_T/p for both side overhanging	152
A.1	Data for discharge coefficient variation analysis for Model P_1M_1	158
A.2	Data for discharge coefficient variation analysis for Model P_1M_2	158
A.3	Data for discharge coefficient variation analysis for Model P_1M_3	159
A.4	Data for discharge coefficient variation analysis for Model P_1M_4	159
A.5	Data for discharge coefficient variation analysis for Model P_1M_5	159
A.6	Data for discharge coefficient variation analysis for Model P_1M_6	160
A.7	Data for discharge coefficient variation analysis for Model P_2M_1	160
A.8	Data for discharge coefficient variation analysis for Model P_2M_2	160
A.9	Data for discharge coefficient variation analysis for Model P_2M_3	161
A.10	Data for discharge coefficient variation analysis for Model P_2M_4	161
A.11	Data for discharge coefficient variation analysis for Model P_2M_5	161
A.12	Data for discharge coefficient variation analysis for Model P_2M_6	162

A.13	Data for discharge coefficient variation analysis for Model P_3M_1	162
A.14	Data for discharge coefficient variation analysis for Model P_3M_2	162
A.15	Data for discharge coefficient variation analysis for Model P_3M_3	163
A.16	Data for discharge coefficient variation analysis for Model P_3M_4	163
A.17	Data for discharge coefficient variation analysis for Model P_3M_5	163
A.18	Data for discharge coefficient variation analysis for Model P_3M_6	164
A.19	Data for discharge coefficient variation analysis for Model P_4M_1	164
A.20	Data for discharge coefficient variation analysis for Model P_4M_2	164
A.21	Data for discharge coefficient variation analysis for Model P_4M_3	165
A.22	Data for discharge coefficient variation analysis for Model P_4M_4	165
A.23	Data for discharge coefficient variation analysis for Model P_4M_5	165
A.24	Data for discharge coefficient variation analysis for Model P_5M_1	166
A.25	Data for discharge coefficient variation analysis for Model P_5M_2	166
A.26	Data for discharge coefficient variation analysis for Model P_5M_3	166
A.27	Data for discharge coefficient variation analysis for Model P_5M_4	167
A.28	Data for discharge coefficient variation analysis for Model P_5M_5	167
B.1	Data for discharge coefficient variation analysis for Model C_1M_1	168
B.2	Data for discharge coefficient variation analysis for Model C_1M_2	168
B.3	Data for discharge coefficient variation analysis for Model C_1M_3	169
B.4	Data for discharge coefficient variation analysis for Model C_1M_4	169
B.5	Data for discharge coefficient variation analysis for Model C_1M_5	169
B.6	Data for discharge coefficient variation analysis for Model C_1M_6	169
C.1	Data for discharge coefficient variation analysis for Model P_2M_1	170
C.2	Data for discharge coefficient variation analysis for Model P_2M_2	170
C.3	Data for discharge coefficient variation analysis for Model P_2M_3	171
C.4	Data for discharge coefficient variation analysis for Model P_2M_4	171
C.5	Data for discharge coefficient variation analysis for Model P_2M_5	171
C.6	Data for discharge coefficient variation analysis for Model P_2M_6	172
C.7	Data for discharge coefficient variation analysis for Model P_3M_1	172
C.8	Data for discharge coefficient variation analysis for Model P_3M_2	172
C.9	Data for discharge coefficient variation analysis for Model P_3M_3	173
C.10	Data for discharge coefficient variation analysis for Model P_3M_4	173
C.11	Data for discharge coefficient variation analysis for Model P_3M_5	173
C.12	Data for discharge coefficient variation analysis for Model P_3M_6	174

C.13 Data for discharge coefficient variation analysis for Model P_4M_3 174
C.14 Data for discharge coefficient variation analysis for Model P_4M_4 174
C.15 Data for discharge coefficient variation analysis for Model P_4M_5 175

The following symbols are used in this thesis

Symbol		Description	Units
a	=	Width of inlet cell	cm
A	=	Flow area upstream of weir	m^2
b	=	Width of outlet cell	cm
B	=	Length of elements	cm
C_d	=	Discharge coefficient of rectangular sharp crested weir; and discharge coefficient of V-notch	---
C_{dm}	=	Discharge magnification coefficient	---
Fr	=	Froude number	---
g	=	Gravitational acceleration	cm/sec^2
H	=	Total depth of water in channel	cm
h	=	Head over the crest (at one meter u/s of the P. K. Weir)	cm
H_e	=	Effective depth of water above vertex at the upstream of V-notch;	cm
K_h	=	Combined effects of fluid properties	----
L	=	Perimeter of Piano Key weir	cm
L/W	=	Length magnification ratio	---
p	=	Crest Height of Piano Key weir	cm
Q	=	Discharge over a rectangular notch	cm^3/sec
Q_L	=	Discharge through sharp crested weir	cm^3/sec
Q_{PK}	=	Discharge through Piano Key weir	cm^3/sec
r	=	ratio of Piano Key Weir discharge to linear weir discharge	---
R^2	=	Squared correlation coefficient	---
W	=	Width of channel	cm
Z	=	Height of crest	cm
ΔQ	=	Difference of Piano Key weir discharge and Rectangular sharp crested weir discharge	cm^3/sec
θ	=	Angle of the V-notch	degree

CHAPTER-1
INTRODUCTION

1.1 GENERAL

A weir is built across a river (or stream) in order to raise level of water on the upstream side and to allow the excess water to flow over its entire length to the downstream side. Thus a weir is similar to a small dam constructed across river, with the difference that whereas in the case of a dam excess water flows to the downstream side, only through a small portion called spillway, the same in the case of a weir flow over its entire length. Spillways represent a substantial portion of total project costs and they play a major role in ensuring safety (Modi and Seth, 1991). Weirs may be classified according to the shape of opening, the shape of crest, the effect of sides on the issuing the nappe and the discharge condition. According to the shape of opening, the weirs may be classified as rectangular, triangular and trapezoidal weirs. According to the shape of the crest, the weirs may be classified as sharp crested weir, narrow crested weir, broad crested weir and ogee shaped weir.

As projects are reassessed for safety, provision for an increased estimate of the probable maximum flood (PMF) has to be made in many cases. It is therefore necessary to provide more flood storage and/or larger capacity for spillways to pass the PMF safely. If the dam can not adequately pass the updated flood, the structure requires modification by increasing the flood storage space, increasing the spillway capacity or using combinations of these two solutions. An innovative and effective way of increasing the spillway capacity is to use a Labyrinth weir. The concept of the Labyrinth weir is to vary the plan shape of the crest to increase the effective crest length (Lempérière and Jun, 2005; and Baud et al. 2002). This increases the discharge per unit width of the spillway for a given operating head.

The ability of the Labyrinth to pass large flows at comparatively low heads has led to many applications. The primary use of Labyrinth weir has been as a spillway for dams. It is particularly suited for use where the spillway width is restricted, or where the flood surcharge space is limited. The Labyrinth is relatively low cost when compared with gated spillways and this has led to its use in conjunction with the raising of dams for increased storage space. Labyrinth weirs can be highly effective in many circumstances (Blanc and Lempérière, 2001).

A Labyrinth weir has advantages compared to the straight over flow weir and the standard ogee crest. The total length of Labyrinth weir is typically three to four times the spillway width. Its capacity varies with head and is typically about twice that of a standard weir or over flow crest of the same width. Labyrinth weirs can be used to increase outlet capacity for a given spillway crest elevation and length or to increase storage by raising the crest while maintaining spillway capacity.

1.2 LABYRINTH WEIR

Labyrinth weirs are polygonal walls, designed to provide a much longer overtopped crest than the length of the spillway. The Labyrinth weir is particularly well-suited for cases where the length of the structure has to be restricted or for rehabilitation of existing spillways (Emiroglu and Baylar, 2005; and Hay and Taylor, 1970). The concept involves a structure where the crest length is developed by triangular or trapezoidal elements which are much longer than the spillway chute width.

This type of spillway is characterized by a broken-axis weir in plan, generally with the same polygonal pattern repeated periodically. Hence, for the same total width, the Labyrinth weir spillway will present larger crest lengths than the same solution.

A Labyrinth weir can pass large discharge at a relatively low head. Its advantage includes relatively low construction and maintenance costs, and more reliable operation, compared with gated spillways. As their application is sometimes difficult in rehabilitation projects due to inappropriate supporting conditions, a new concept of Labyrinth weirs has been proposed with a new shape, called Piano Key Weir (Chi et al., 2006; and Lempérière and Ouamane, 2003). This innovative alternative of Labyrinth weir provides an increase in the stability of the structure which can be placed on the top of most existing or new gravity dams.

1.3 PIANO KEY WEIR

A new concept of a Labyrinth weir has been proposed with a new shape like black and white Piano keys when viewed in plan, this new concept was called the Piano Key Weir (Lempérière and Ouamane, 2003). This innovative design solves most of the problem presented by the original Labyrinth weir, and is also more efficient. Compared with the traditional Labyrinth weir:

- Plan view of the Piano Key Weir is not trapezoidal, but rectangular
- Vertical walls founded on a flat area are replaced by lateral vertical walls and sloping slabs upstream and downstream of the crest. These slabs are partially a cantilever structure, upstream and downstream. Therefore the overall structure is self balanced
- The Piano Key Weir can be positioned on the top of the crest of new or existing gravity dams.
- Application can cover a wide range of specific flows, from 3 to 1000 $m^3/s/ml$.
- Piano Key Weir can increase by a factor about 1.50 to 4.00 times than the specific discharge capacity of straight sharp crested weir.
- From a structural point of view, Piano Key Weir is extremely hyper-static structures, which are solid and simple.

This innovative alternative of Labyrinth weir has a considerably higher specific flow. The Piano Key Weir can increase safety and the storage and/or the flood control efficiency of existing/new dams. For increasing the storage capacity of reservoir, sediment passage from reservoir area through Piano Key Weir ramp is an additional benefit. The outcome of this study is very much relevant to address the dam safety concerns in developing and developed nation in the current context of adverse hydrological consequences due to ongoing global warming phenomenon, intense rainfall like cloud burst and erratic hydrologic condition.

A Piano Key Weir has advantages compared with the straight overflow weir and the standard ogee crest. The total length of the Piano Key Weir is typically three to seven times the spillway width. Its discharging capacity varies with head and is typically about twice that of a straight sharp crested weir or overflow crest of the same width. Piano Key Weir can be used to increase outlet capacity for a given spillway crest elevation and length or to increase storage by raising the crest while maintaining spillway capacity.

The flow downstream of a Piano Key Weir is considerably aerated as per a system of air injection. Consequently the risks of erosion or cavitation are considerably reduced and the cost of new downstream structures or the maintenance of existing ones is reduced. To avoid vibrations in Piano Key Weir, it is advisable to aerate the nappe.

The Piano Key Weir is particularly well suited for cases where the length of the structure has to be restricted or for the rehabilitation of existing spillways. A Piano Key Weir can pass large discharge at a relatively low head. Its advantages include relatively

low construction and maintenance costs and more reliable operation, compared with gated spillways. In addition for a given maximum operation head, a Piano Key Weir can be an economical alternative in terms of dam crest elevation and reservoir storage volume. The ability of the Piano Key Weir to pass large flows at comparatively low heads has led to many applications. The primary use of Piano Key Weir has been as a spillway for dams. It is particularly suited for use where the spillway width is restricted or where the flood surcharge space is limited.

1.4 OBJECTIVES OF THE STUDY

Keeping in view the relatively reported better performance of Piano Key Weirs in comparison to linear and Labyrinth weirs, following objectives are considered for the present study.

1. To perform experiments on different configurations of Piano Key Weir, varying in term of presence/absence of ramp in upstream and downstream for one side and both side overhanging and varying ratio of any two consecutive limbs.
2. To identify the situations which lead to increase in the magnification ratio of discharge passing through the Piano Key Weir.
3. To quantify the maximum achievable magnification ratio and associated hydraulic conditions.
4. To identify the parameters influencing the variation of discharge coefficient and study the role of considering the total head versus the head over the crest
5. To develop a set of relationships for the variation of discharge coefficient and to identify the most suitable relationship

1.5 ORGANISATION OF THE THESIS

To meet the above objectives, the present study is organised as follows:

Chapter 1: It introduces the topic of investigation, underlying objectives and the layout of the thesis.

Chapter 2: The literature reviews relevant to Labyrinth weir, Piano Key Weir and variation of discharge coefficient are included here.

Chapter 3: It provides details of the experimental program.

Chapter 4: It presents the performance evaluation of Piano Key Weir of different shapes and sizes. It also deals with the development of appropriate *L/W* and height of wall of the Piano Key Weir.

Chapter 5: It includes the investigation the case study for a potential application of Piano Key Weir used for Sawara Kuddu Hydro Electric project.

Chapter 6: It includes analysis of collected data and develops a design curve and relationship between *h/p*, Froude No. and discharge coefficient (C_d).

Chapter 7: It summaries the main findings of the present work and provides framework for future investigations.

CHAPTER – 2

LITERATURE REVIEW

2.1 GENERAL

Considering the importance of Piano Key Weir in comparison to other type of weirs, present chapter looks into available practices with particular reference to labyrinth weir/spillway. It also deals with review related to variation of Labyrinth weir discharge coefficient. Finally, it deals with very limited research work on Piano Key Weir to emphasize the need for the present study.

2.2 DEVELOPMENT AND FIELD APPLICATIONS OF LABYRINTH WEIR

Most spillways consist of some form of a weir. The weirs are normally placed perpendicular to the flow direction. The most significant parameters in determining the capacity of a weir are its height relative to the upstream depth, the crest shape and the crest length (Afshar, 1988; and Falvey, 2003). Here, capacity refers to the flow rate or discharge for a given depth of flow over the crest of the weir. Of these parameters, the crest length has the greatest influence on the spillway capacity. In this section, certain examples of existing dams are provided where attempt has been made to increase the crest length.

As the emphasis on dam safety has increased, many spillways must be rehabilitated to increase their capacity without changing the reservoir storage. However, for many spillways, the width of the approach channel or the downstream chute cannot be widened. To increase the crest length but keep the spillway width constant, the crest is often placed at an angle to the centerline of the chute. If the crest is placed parallel with the chute centerline, it is called a side channel spillway (Pinheiro and Silva, 1999), as shown in Fig. 2.1

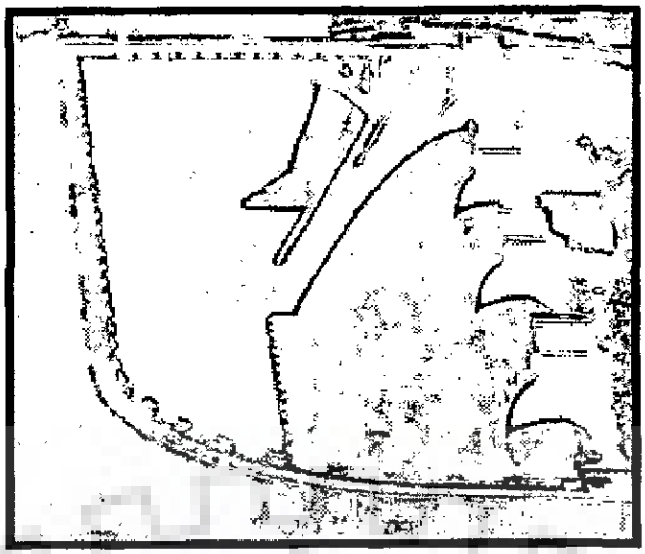

Fig. 2.1 Side channel spillway – Arizona spillway at Hoover dam, USA (Pinheiro and Silva, 1999)

The length can be increased further and can still keep the downstream dimension small by folding the weir into several sections. One implementation of this idea is the duckbill spillway, as shown in Fig. 2.2.

Fig. 2.2 Duckbill spillway – Apartadura spillway, Portugal (Pinheiro and Silva, 1999)

Several cycles of this type of spillway can be placed together to further increase the spillway length. A variation of the duckbill spillway is tile bathtub spillway, as shown in Fig. 2.3. This shape is rectangular instead of the approximately triangular shape of the duckbill.

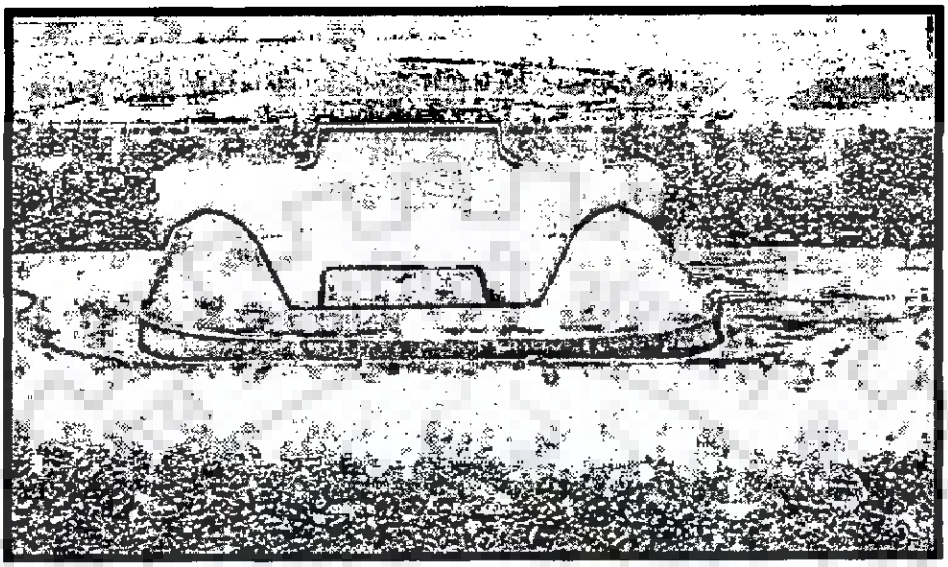

Fig. 2.3 Bathtub spillway – Fontenelle dam, USA (Falvey, 2003)

Several cycles of the bathtub shape can be placed side by side. These weirs are called corrugated, accordion, or folded weirs. If several cycles of the duckbill spillway are placed side by side, the weir is called a Labyrinth weir, as shown in Fig. 2.4.

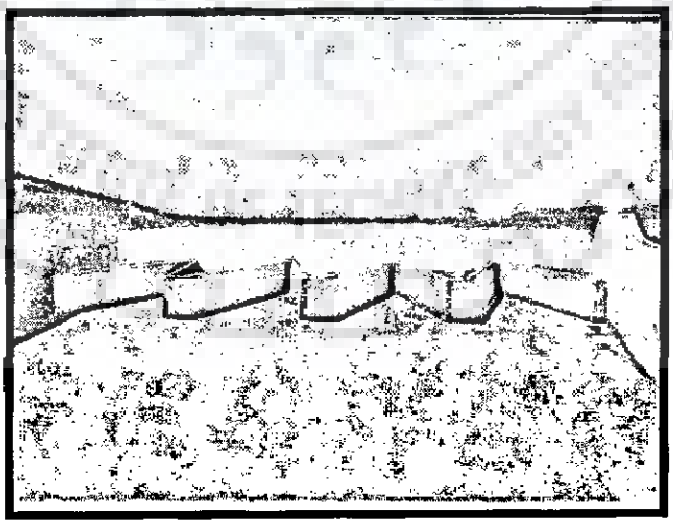

Fig. 2.4 Labyrinth weir- Tongue River dam, USA (Falvey, 2003)

Hydraulic model studies have been conducted at the Portuguese National Laboratory for Harrezza dam (Algeria) in 1980, Dungo dam (Angola) in 1981 and Keddara dam (Algeria) in 1984, and the details are narrated below.

Harrezza Dam

Harrezza dam is a 41 m high earthfill dam. Initial design included an ogee spillway of straight crest, without gates, with three bridge piers and its was located next to the left abutment. At the foot of the spillway there was stilling basin, connected downstream to a 700 m long excavated, rather steep transition channel to the natural river. The weir width was 64.50 m (Four 15.00 m wide spans and three 1.50 m thick piers)

The model tests indicated an upstream head over crest of 2.08 m for a design discharge of 350 m^3/sec. The downstream transition channel to the natural river was to be built in a very soft clay soil. In consequence, the hydraulic model tests led the way to include in the design an armored blanket to protect the transition channel. The existence of this apron made the initially designed spillway non economic solution.

Therefore, a new spillway was designed, next to the right abutment. The downstream transition of the river becoming significantly shorter, but the available width for the entrance zone and spillway weir becoming rather smaller, due to topographical constraints.

The new spillway presents a Labyrinth weir followed by a 230 m long steep channel with variable width (30, 40 to 20 m), a 35 m long stilling basin and finally a transition channel which become almost horizontal.

The Labyrinth weir has three cycles with a total length of 90 m and width 30 and 40 m, includes on the upstream side, three piers, which serve as splitters also.

Model test indicated, for this new solution a quite good behaviour, with an upstream head over crest of 1.90 m for a design discharge of 350 m^3/sec.

Dungo Dam

Dungo dam is a 19 m high earth fill dam. The initial design included a straight ogee crest spillway to be built next to the dam right abutment, without gates, with four bridge piers, and followed downstream by a canal and a stilling basin. The weir total width was approximately 72.50 m. The design discharge of 576 m^3/sec would correspond to an upstream head over crest of 2.50 m.

A large flood occurred during the spillway construction, destroyed the spillway crest and the canal. To rebuild the same spillway was too expensive, so a new spillway was designed located now at the dam left abutment.

The new spillway, much narrower than the initial one, has a Labyrinth weir, followed, similarly, by a canal and a stilling basin. The Labyrinth weir has a total length of 115.50 m and total width of 40.10 m, it has four cycles, and includes splitter piers at both sides upstream and downstream.

The model test confirmed the excellence of this solution, which was finally adopted for construction. The design discharge of 576 m^3/sec was set to an upstream head over crest of 2.40 m.

Keddara Dam

Keddara dam is a 108 m high rockfill dam. The spillway was designed for a 250 m^3/sec discharge and it includes, essentially a Labyrinth weir, a canal and a stilling basin. In this case the Labyrinth weir was adopted since the beginning as the most economical solution. It consists of two cycles and has a total length of 53.77 and a total width of 19.00 m and it includes two bridge splitter piers at the upstream end. The model tests confirmed a well behaved solution with an upstream head over crest of 2.46 m for a design discharge of 250 m^3/sec.

Thus, for dams in operation it is sometimes required to increase the spillway discharge capacity, which may be done either by proposing another spillway or by changing the spillway in weir form.

2.3 LABYRINTH WEIR

2.3.1 General

Labyrinth weirs are polygonal walls, designed to provide a much longer overtopped crest than the length of the spillway. The Labyrinth weir is particularly well-suited for cases where the length of the structure has to be restricted or for rehabilitation of existing spillways. The concept involves a structure where the crest length is developed by triangular or trapezoidal elements which are much longer than the spillway chute width.

This type of weir is characterized by a broken-axis weir in plan, generally with the *same polygonal pattern repeated periodically. Hence, for the same total width, the* Labyrinth weir will present larger crest lengths than the same total width.

A Labyrinth weir has advantages compared to the straight over flow weir and the standard ogee crest. The total length of Labyrinth weir is typically three to four times the spillway width. Its capacity varies with head and is typically about twice that of a standard weir or over flow crest of the same width. Labyrinth weirs can be used to

increase outlet capacity for a given spillway crest elevation and length or to increase storage by raising the crest while maintaining the spillway capacity.

A Labyrinth weir can pass large discharge at a relatively low head. Its advantage includes relatively low construction and maintenance costs, and more reliable operation, compared with gated spillways.

In addition, for a given maximum operation head, a Labyrinth weir can be an economical alternative in terms of dam crest elevation and reservoir storage volume. Although it has a broad range of applications, its complex flow conditions and design have been considered a drawback by designers.

2.3.2 Characteristics of Flows Over Labyrinth Weir

The distinguishing characteristic of this spillway is that the plan shape is not linear but varies using a repeating plan-form. The repeating plan-forms that have been used are U, V and trapezoidal shapes. Using these plan-form shapes for spillways result in a complex flow pattern. Ideally the discharge passing over the Labyrinth should increase in direct proportion of an increase in crest length. However, this is only the case for Labyrinth weirs with low design heads. Qualitatively, as the upstream head increases, the flow pattern using a Labyrinth weir sequentially passes through four basic phases. These phases are fully aerated, partially aerated, transitional and suppressed (Wormleaton and Tsang, 2000).

The fully aerated condition occurs at low upstream heads when the flow falls freely over the entire length of the Labyrinth crest. In this flow condition, the thickness of the nappe and depth of fall of water do not affect the discharge capability of the spillway. As a result, the Labyrinth behaves almost ideally when compared to a linear weir with the same vertical cross section.

In partially aerated phase when head increases, the tail water depth increases particularly between the nappe and the Labyrinth wall, due to convergence of opposing nappes. The higher tail water depths and restricted area at the upstream apexes aeration under the nappe is maintained. A stable air pocket is formed along each side wall and downstream apex of the Labyrinths.

In the transitional phase, the nappe is alternating between intermittent air entrainment and solid water flows. It is difficult at times to distinguish between the partially aerated and transitional phases but transitional region can be easily identified as a discontinuity in the discharge co-efficient curve.

On the suppressed phase, the flow over the Labyrinth crest forms a solid non aerated nappe. The thickness of the nappe and the depth of tail water do not allow air to be drawn under the nappe. As the upstream head increases, this last flow condition eventually leads to full submergence of the Labyrinth weir. Complete submergence of the Labyrinth usually occurs when the flow depth over the crest is greater than the height of the Labyrinth.

2.3.3 Basics Parameters of Labyrinth Weir

The discharge characteristics of Labyrinth weirs are primarily a function of the weir height, p, the depth of flow over the weir, h, the width of the weir, W, the developed length of the Labyrinth, L, and its shape. Thus, the discharge can be expressed as

$$Q = f(h/p, L/W, Shape) \tag{2.1}$$

The shape of a Labyrinth can be rectangular, trapezoidal, or triangular. Analytic development showed that the flow over a skew weir is strongly influenced by the angle the weir forms with the upstream flow direction. For a triangular weir, the angle is related to the L/W ratio by

$$\alpha_{max} = \arcsin(W/L) \tag{2.2}$$

The angle given by this relationship is the maximum value that can be achieved for a Labyrinth weir. For a trapezoidal plan form, the angle is given by

$$\alpha = \arcsin\left(\frac{W-4a}{L-4a}\right) \tag{2.3}$$

where α is side wall angle and a is half apex width.

2.3.4 Different Theories of Labyrinth Weir Discharge Coefficient

Taylor (1968)

In the experiments conducted by Taylor, (1968), the discharge was made dimensionless by dividing the Labyrinth weir flow by the discharge of a linear weir that has the same channel width. This is a clever method of removing the effects of surface tension in the model tests. In this manner, a family of curves that represent the characteristics is given by

$$\frac{Q_{Lab.}}{Q_L} = f(h/p, Shape) \tag{2.4}$$

in which p is weir height; Q_{Lab} is the total discharge of the Labyrinth weir; Q_L is the

discharge of a linear weir having the same width of the Labyrinth weir; and h is head over the weir.

Design charts prepared by Hay and Taylor (1970) are shown in Figs. 2.5 and 2.6. These curves are for a Labyrinth located in a channel.

The discharge for a linear weir in these studies was determined from the weir equation of Kindsvater and Carter (1959):

$$Q_k = C_s L_e h_e^{3/2} \tag{2.5}$$

where L_e is equvlent crest length; h_e is equivalent head on the crest.
in which the discharge coefficient C_s is given by

$$C_k = -3.22 + 0.40\frac{h}{p} \tag{2.6}$$

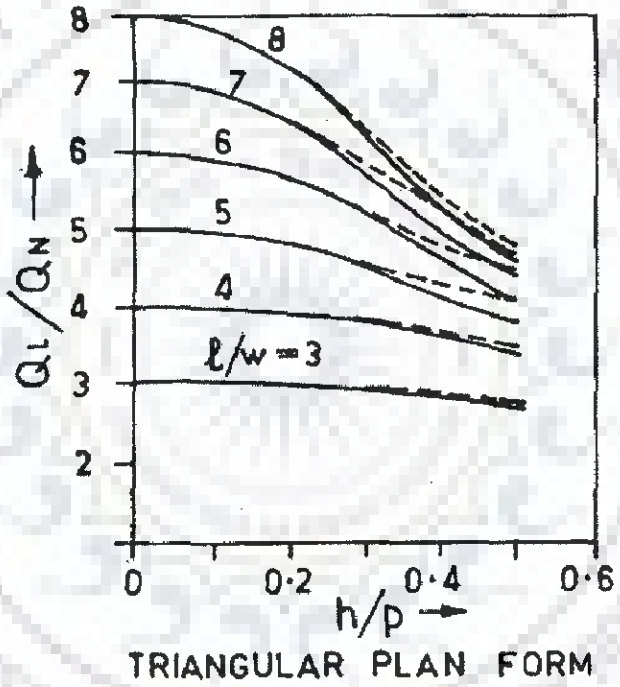

Fig. 2.5 Design curve - triangular -sharp crested weir (Hay and Taylor, 1970)

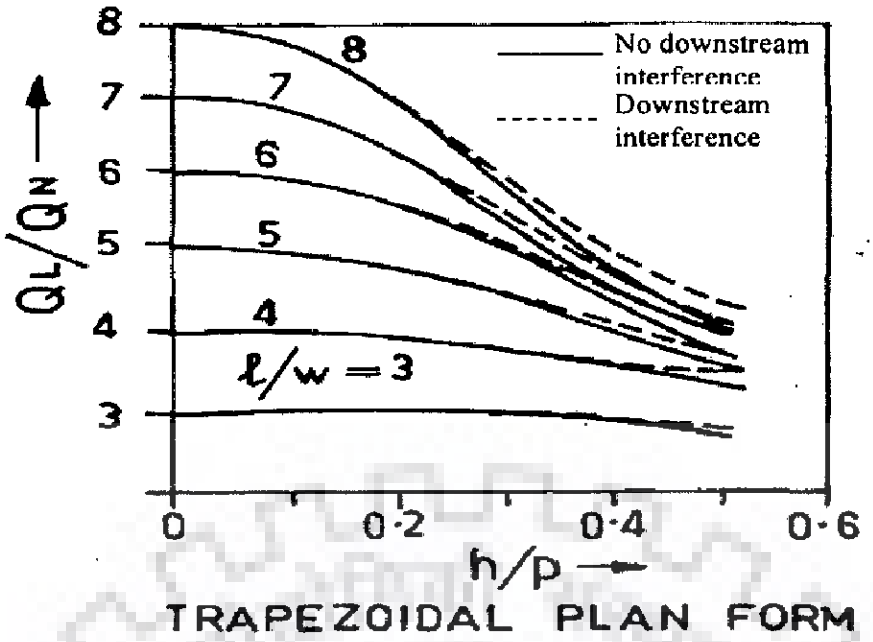

Fig. 2.6 Design curve - trapezoidal - sharp crested weir (Hay and Taylor, 1970)

Darvas (1971)

Darvas (1971) introduced the concept of a discharge coefficient defined as

$$C_w = \frac{Q_{Lab}}{WH_o^{3/2}} \tag{2.7}$$

in which $Q_{Lab.}$ = the total discharge; W = the total width of the Labyrinth weir; C_w is Darvas discharge coefficient; and H_o = the total head on the weir. This coefficient has the units of $ft^{0.5}$/sec. The plots of Darvas are given as a family of curves in which

$$C_w = f(H_o / p, L/W) \tag{2.8}$$

in which L is the development length of the Labyrinth weir and p is weir height. These curves shown in Fig. 2.7

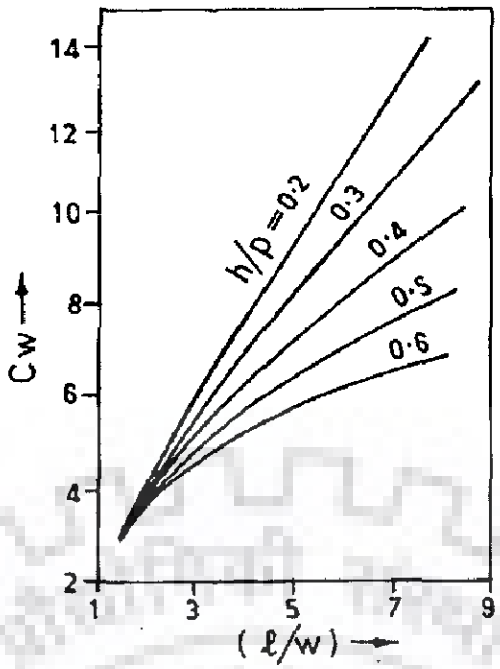

Fig. 2.7 Design curves between C_W Vs L/W (Darvas, 1971)

Mcgalhaes and Lorena (1989)

Megalhaes and Lorena (1989) and Megalhaes (1985) developed curves similar to that of Darvas (1971), except their curves are for a nappe or ogee crest, and the discharge coefficient is given in dimensionless terms by

$$C_p = \frac{Q_{Lab}}{W\sqrt{2g}H_o^{3/2}} \tag{2.9}$$

where H_o is total upstream head; Q_{Lab} is total discharge; C_p is Megalhaes discharge coefficient; W is width of channel; and g is the acceleration of gravity. Design curves are shown in Fig. 2.8.

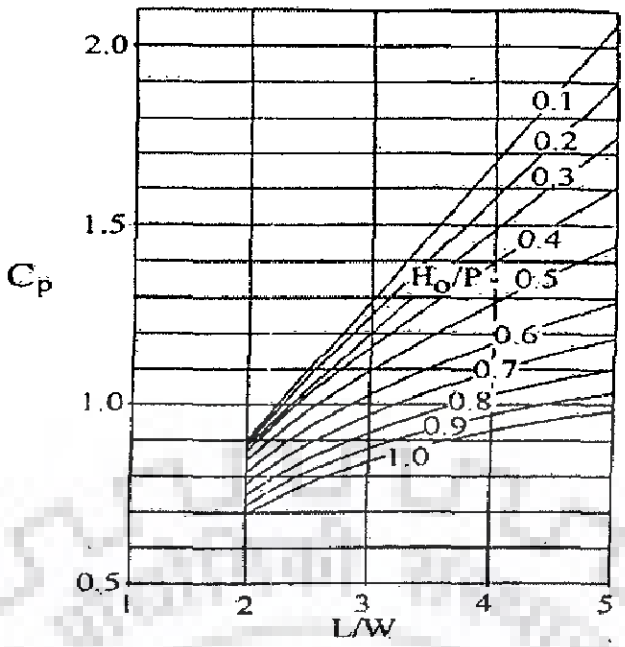

Fig. 2.8 Design curves between C_p Vs L/W (Magalhaes and Lorena, 1989)

Lux (1989)

Lux (1989) introduced another discharge coefficient based on the total upstream head. His relationship for the discharge of one cycle is given by

$$Q_k = C_W \left(\frac{W_c / p}{W_c / (p+k)} \right) W_c H_o \sqrt{g H_o} \qquad (2.10)$$

in which k is a shape constant; H_o is the total upstream head; p is height of weir; W_c is width of channel; C_W is Darvas discharge coefficient and g is the acceleration of gravity. These curves are shown in Figs. 2.9 & 2.10.

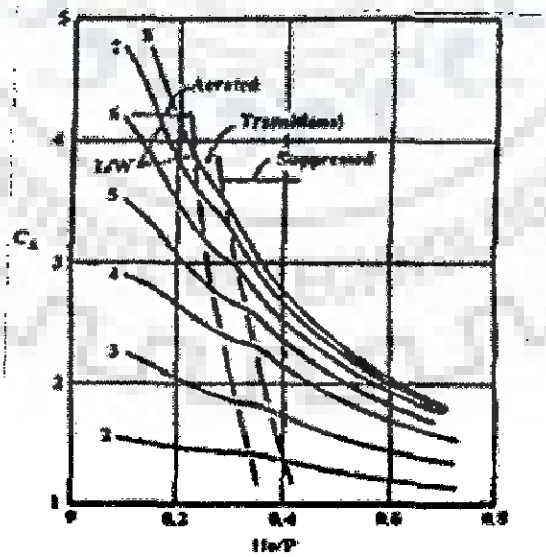

Fig. 2.9 Design curve - triangular weir (Lux, 1985)

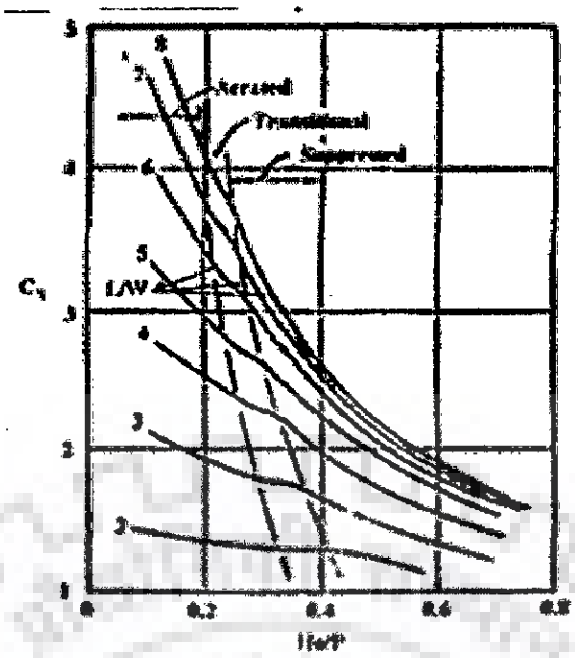

Fig. 2.10 Design curve - trapezoidal weir (Lux, 1985)

Tullis et al. (1995)

Tullis et al. (1995) defined a coefficient that used the total upstream head on the weir. Their equation is

$$Q_{Lab.} = C_T L \frac{2}{3}\sqrt{2g}H^{1.5} \tag{2.11}$$

where C_T is crest coefficients for a weir, H is head over the crest of weir and L is length of weir crest.

This is similar to the conventional weir discharge equation, except that the head is the total upstream head and not the head or, the weir crest. All of the tests were performed in a channel similar to the investigations of Taylor (1968).

The crest coefficients for a triangular weir with a quarter-round crest are shown in Fig. 2.11 as a function of the angle that the weir makes with the flow.

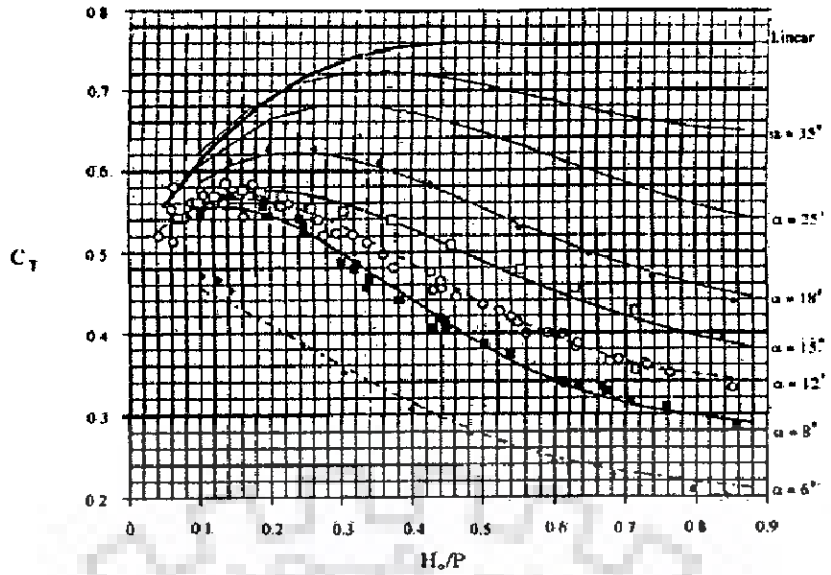

Fig. 2.11 Design curves with quarter-round crest and a triangular weir (Tullis et al., 1995)

2.4 PIANO KEY WEIR

As for Labyrinth weirs, the advantage of Piano Key Weir is to increase the total effective crest length for a given width (Ouamane and Lempérière, 2006). Consequently, it can be used to increase the discharge capacity for a given head or decrease the head for a given discharge. Therefore, the implementation of such a spillway allows a high crest level which can also increase the storage capacity in the reservoir. In addition, beyond economical considerations, Piano Key Weir is a free flow spillway and has a high level of safety and reliability. Moreover floating debris will easily pass over as the water level increases. A key advantage of Piano Key Weir structures is that they can be placed on the crest of most existing or new gravity dams, unlike traditional Labyrinth weirs.

The flow behaviour compared to the conventional Labyrinth structures is quite different. The flow is divided into two parts, one from the inlet of the Piano Key Weir that overflows as a thin screen and another from the outlet, which flows as a jet at the bottom (Leite et al., 2009).

2.4.1 Flow Characteristics over Piano Key Weir

The flow over Piano Key Weir is complicated further by the interference of the jets at the upstream apex of the Piano Key Weir. That is, at high flows, the jets from adjacent crests strike each other. This creates a nappe that is not aerated and can decrease the discharge coefficient of the weir. The degree of impact increases as the angle between the crests decreases and as the flow depth over the crest increases. As a result, for most Piano Key Weirs, the underside of the nappe gets aerated only for low flow depths.

The interference of the jets from adjacent crests means that Piano Key Weirs become less and less effective as the reservoir level rises. At some depth, the flow over a Piano Key Weir is almost the same as the flow over a straight weir.

The nappes from two weirs placed at an angle with each other will have an impact over a limited length of the weir crest.

This impact is called nappe interference. The effect of the nappe interference is to decrease the discharge. Interference occurs when the jets from the two sidewalls and the sidewall intersect.

2.4.2 Review of the Existing Model Study of Piano Key Weir

An initial model investigations and behavior of Piano Key Weir was studied by Lempérière and Ouamane (2003) in terms of a magnification ratio of the Piano Key Weir against sharp-crested linear weir having the same channel width. The results of the test showed that the Piano Key Weirs are simple solutions as safe and easy to operate as traditional free flow spillways and much more efficient. They may improve the flood control by many existing dams.

Behavior of Piano Key Weir was studied by Barcouda et al. (2006) in terms of a magnification ratio of the Piano Key Weir flow for a sharp-crested linear weir having the same channel width. The results of the test show that the Piano Key Weirs are more efficient than the traditional Labyrinth weir and Piano Key Weirs can be an interesting solution for increasing the active storage of reservoir or for improving the safety of dam during extreme flood.

Some models studies were done by Leite et al. (2007) for rehabilation of St-Marc dam at Laboratory of Hydraulic Constructions (LCH) at the Ecole Polytechnique Federal de Lausanne (EPFL), Switzerland. Experimental tests also demonstrated the efficiency of the Piano Key Weir under low heads also.

In Electricite de France (EDF), Laugier (2007) tested the Piano Key Weir to increase the discharge capacity at Golours Dam, in Southwestern France. The preliminary design was based on Lempérière and Ouamane (2003). Some additional tests were carried out on a hydraulic model constructed at the EDF hydraulic Laboratory (EDF-LNHE), and some configurations were studied. This study represents an innovative solution to increase spillway discharge capacity for flood mitigation.

Thus, a very limited research has been conducted on Piano Key Weir. There are no design criteria, design curve developed from the model studies, as well as shape optimization for generalized Piano Key Weir reported in literature.

2.5 SUMMARY

In this chapter various studies related to Labyrinth weir and Piano Key Weir mechanisms and their applications has been reviewed. It is obvious that Piano Key Weir performance depends on a number of factors including shape geometry, flow pattern and related variables. The opinion defers regarding the relative importance of these factors on performance of Labyrinth weir.

The Piano Key Weir uses simple shapes linked in a repetitive manner to form the structure. These two concepts, simplicity and repetition, makes design and construction of Piano Key Weir easy. Having the Piano Key should be considered as a viable alternative.

However, there is no theoretical or empirical design procedure available on Piano Key Weir in the literature. This emphasizes the importance of the present study. The Piano Key Weirs can be used world-wide with various shapes and most often the flow can be considerably increased.

CHAPTER 3
EXPERIMENTAL PROGRAMME

3.1 GENERAL

It is obvious that certain preliminary studies on the performance of Piano Key Weir are necessary in order to identify the discharge passing capacity and depth saving. The effect of different shapes and dimensions of Piano Key Weir with different length magnification ratio is also important and needs detailed investigations. With this in view, the experimental programme was organized in five phases. The Piano Key Weir models were made of perspex sheet and all the experiments were performed in a 50 cm wide flume. In this chapter, five phases of experimental campaign on twenty eight Piano Key Weir models are reported. Details of Piano Key Weir shapes are also provided.

3.2 LABORATORY FLUME AND OTHER EXPERIMENTAL ACCESSORIES

3.2.1 Laboratory Flume Used

An overflowing tank was installed at the upstream head-end to ensure the supply of steady discharge into the experimental flume. The flume used was made of mild steel with side walls made of transparent perspex sheet. Flume has an in-built upstream tank of 40 cm x 90 cm x 115 cm dimensions. Diagrammatic scheme is given in Fig. 3.1. The bed of flume is supported on angle iron sections, the lower ends of which are connected to a shaft, placed length-wise parallel to the central portion of flume below it. Shaft is movable horizontally backwards and forwards with the help of a gearbox and electric motor such that if the shaft moves towards the direction of flow, the front portion of flume moves upwards and lower portion moves downward and vice-versa. This is the mechanism of adjusting the flume to the required slope. The water flowing in the flume falls into a down stream tank installed with V-notch discharge measuring devices, which is connected to down stream of V-notch storage tank. From the down stream of V-notch storage tank, tank water is lifted with the help of a two 10 HP pumps. 10 cm diameter pipes carry water from the storage tank to the upstream constant head tank. The discharge is regulated with the help of a gate valve placed after the constant head tank.

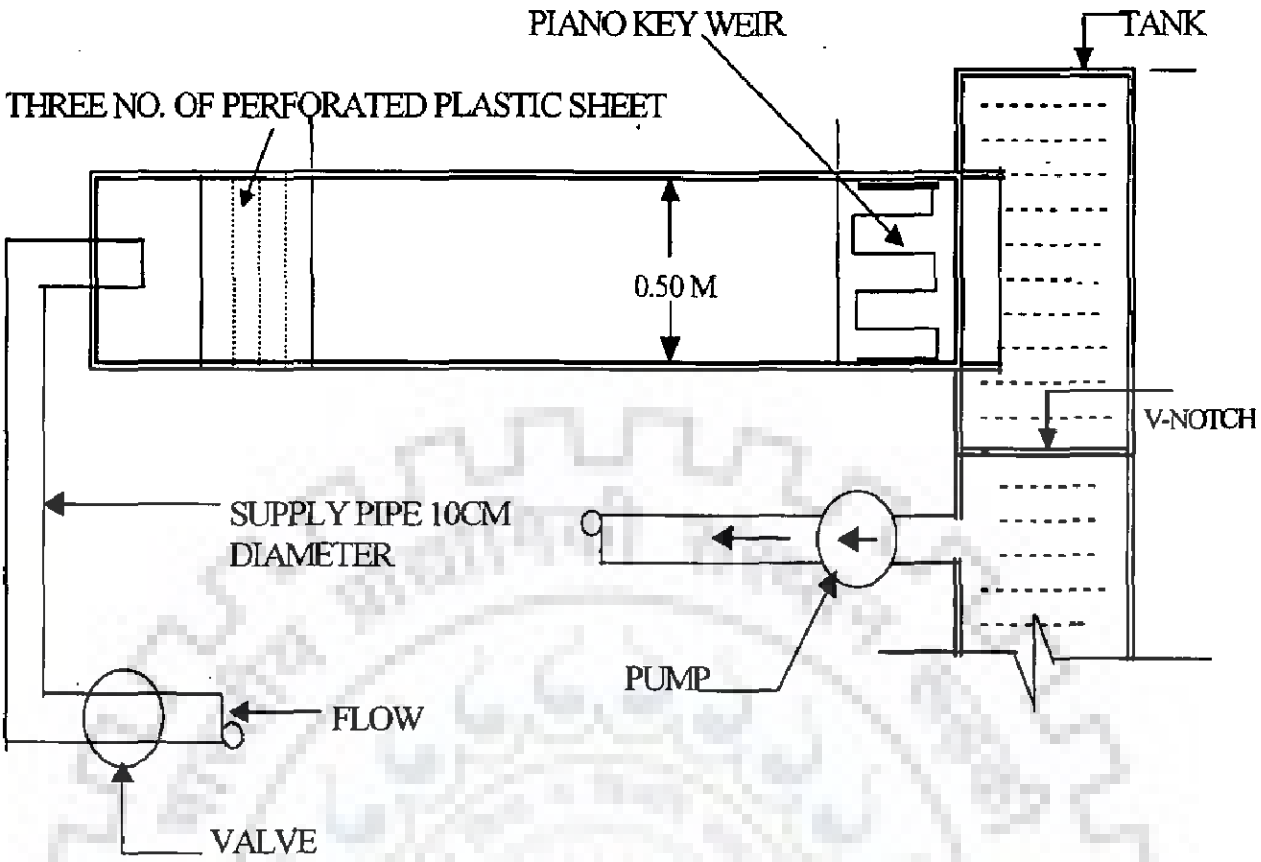

Fig. 3.1 Plan of tilting flume and its components used in experiments

3.2.2 Other Accessories

The depth of flow along the length of flume was measured with the help of a pointer gauge, which could be moved along the hand rails fitted at the top of flume. It was used to measure the head over crest at the upstream of Piano Key Weir.

Head over the V-notch was also measured with the help of pointer gauge. It was used for the measurement of discharge through the Piano Key Weir. 90^0 V-notch was used for the discharge measurement.

3.3 EXPERIMENTAL PROCEDURE

Experiments were conducted in the following steps:

- Before starting the experiment the side rails of the flume were adjusted and were kept parallel to each other and parallel to the bottom of channel.
- The water was supplied to the flume from constant head tank to upstream tank and upstream tank to flume. Supply pipe connected to the pump and the discharge was controlled by a regulating valve.

- Two rows of perforated plastic sheet walls were provided to dampen the surface disturbances/destroy the excess energy of inflow and distribute the flow uniformly in the entire width of the flume.
- A plastic perspex sheet Piano Key Weir was placed at the down stream end of the flume at 8 cm base platform was made. The models were placed at the platform (pre determined location).
- The water which discharges into the tail box was allowed to flow over 90 degree V-notch. After flowing over the notch, the water was discharged into the sump from where it was re-circulated by pump.
- For the measurement of initial and different nappe depth the pointer gauge fixed to a vertical graduated rod was used. The difference of initial reading and different nappe depth readings gave the nappe depth of different discharges.
- After the Piano Key Weir was placed on the plat-form, discharge was slowly allowed into the flume and covered upto maximum discharge. The experiments were run for 10 to 12 different nappe heights.
- The experiments were repeated for all the models with different shapes of Piano Key Weir.

3.4 FIRST PHASE MODEL EXPERIMENTS

The three dimensional view of generalized Piano Key Weir shape is shown in Fig. 3.2. In the first phase of the experiment programme, six selected models of Piano Key Weir have been used. The dimensions of Piano Key Weir models are as indicated below in Table 3.1. In first three models P_1M_1, P_1M_2, and P_1M_3, element configuration is same but slope is different and same with other three models P_1M_4, P_1M_5, and P_1M_6. Plan and sectional view of Piano Key Weir models are as indicated below in Figs. 3.3-3.8. Length of all elements has been kept as 32 cm.

All the models were run for 10 to 12 different nappe heights, discharges. It was endeavored to run all the models for the value of h/p upto unity. All the models have been studied for the value of Piano Key Weir discharge upto 80 l/s. Running view of all the models is shown in plate no. 3.1 to 3.6. These photos depict the behavior of Piano Key Weir.

Table 3.1: Phase one model dimensions

Model No.	Height of Model (p) (cm)	a (cm)	b (cm)	$a + b$ (cm)	L/W	No. of Element
P_1M_1	12	5.00	5.00	10	7.40	5
P_1M_2	16	5.00	5.00	10	7.40	5
P_1M_3	20	5.00	5.00	10	7.40	5
P_1M_4	12	12.50	12.50	25	3.56	2
P_1M_5	16	12.50	12.50	25	3.56	2
P_1M_6	20	12.50	12.50	25	3.56	2

For last elements on the side of the flume, the width of a or b will be divided by 2. The relevant notations used are:

a = Width of inlet cell

B = Length of elements

b = Width of outlet cell

L = Perimeter of Piano Key Weir crest

p = Crest height of Piano Key Weir

Q_L = Discharge through rectangular sharp crested weir

Q_{PK} = discharge through Piano Key Weir

W = Width of channel

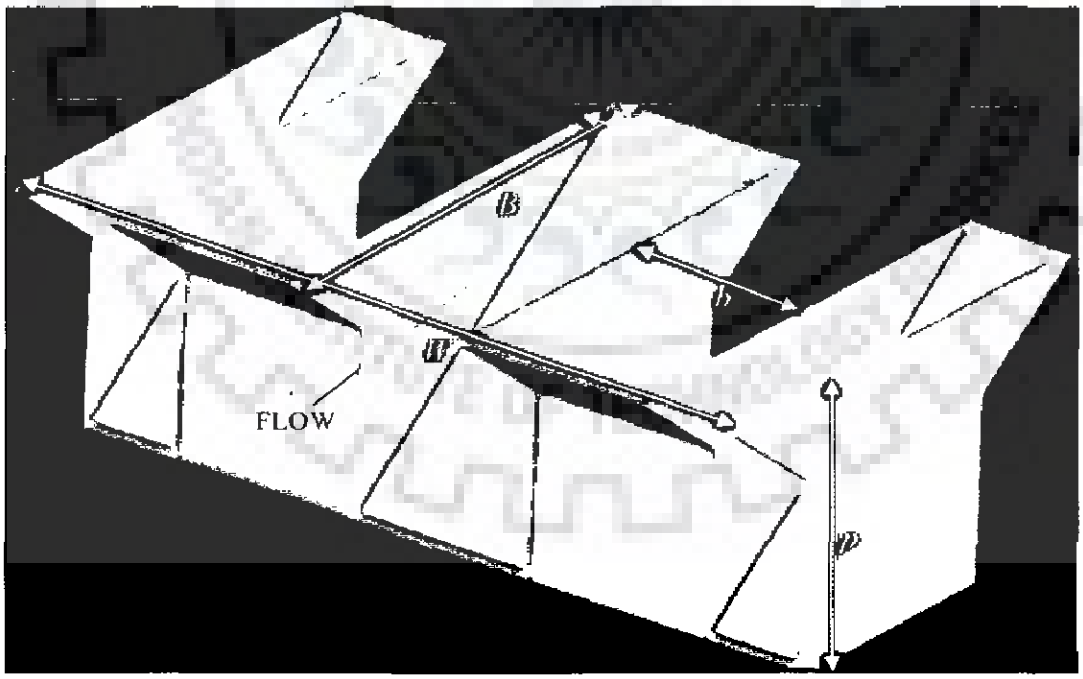

Fig. 3.2 Three dimensional view to generalize Piano Key Weir shape

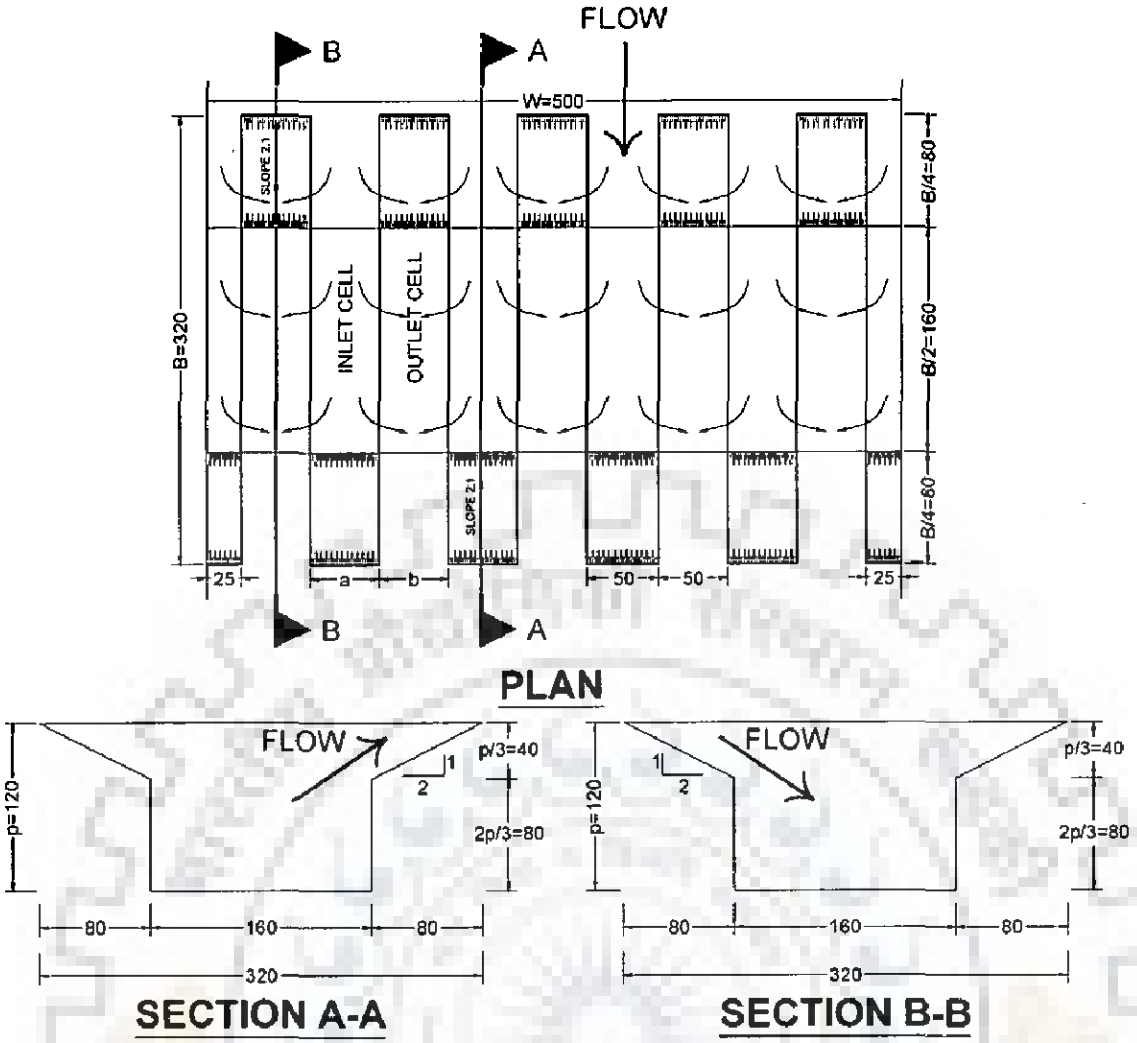

Fig. 3.3 Plan and section of model P_1M_1 (dimensions in mm)

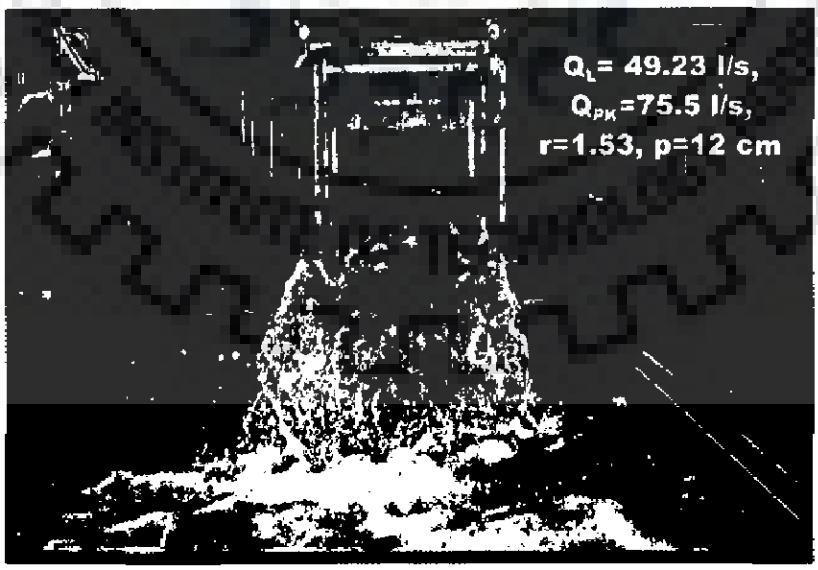

Plate No. 3.1 Model P_1M_1

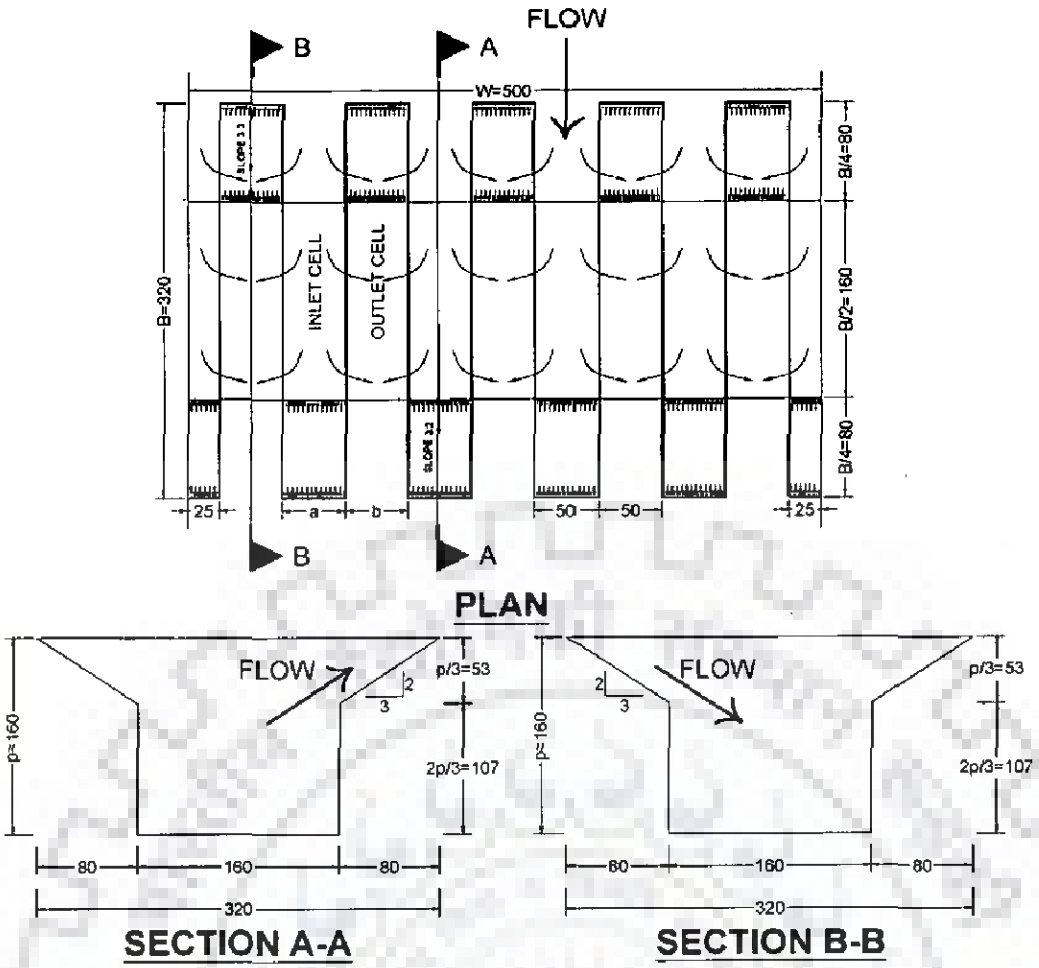

Fig. 3.4 Plan and section of model P_1M_2 (dimensions in mm)

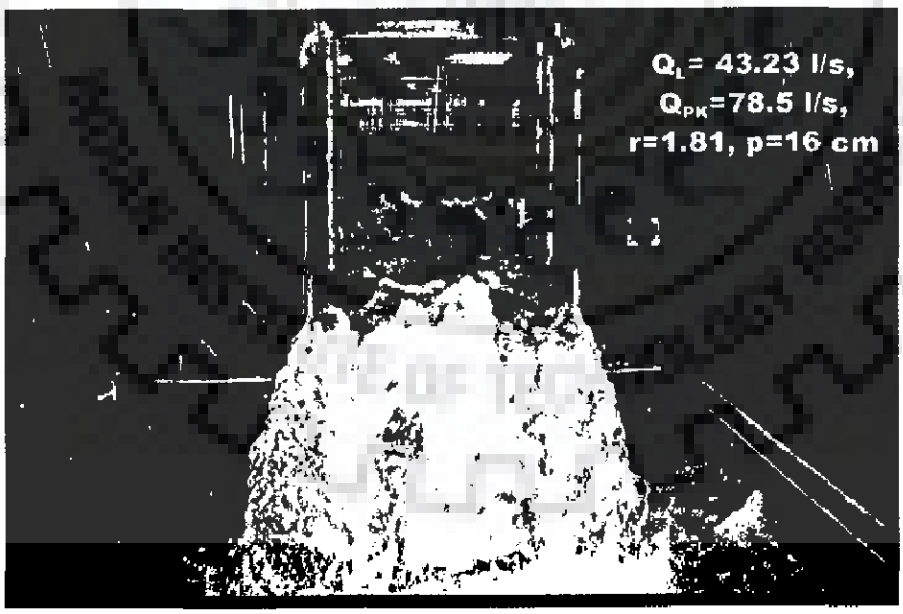

Plate No. 3.2 Model P_1M_2

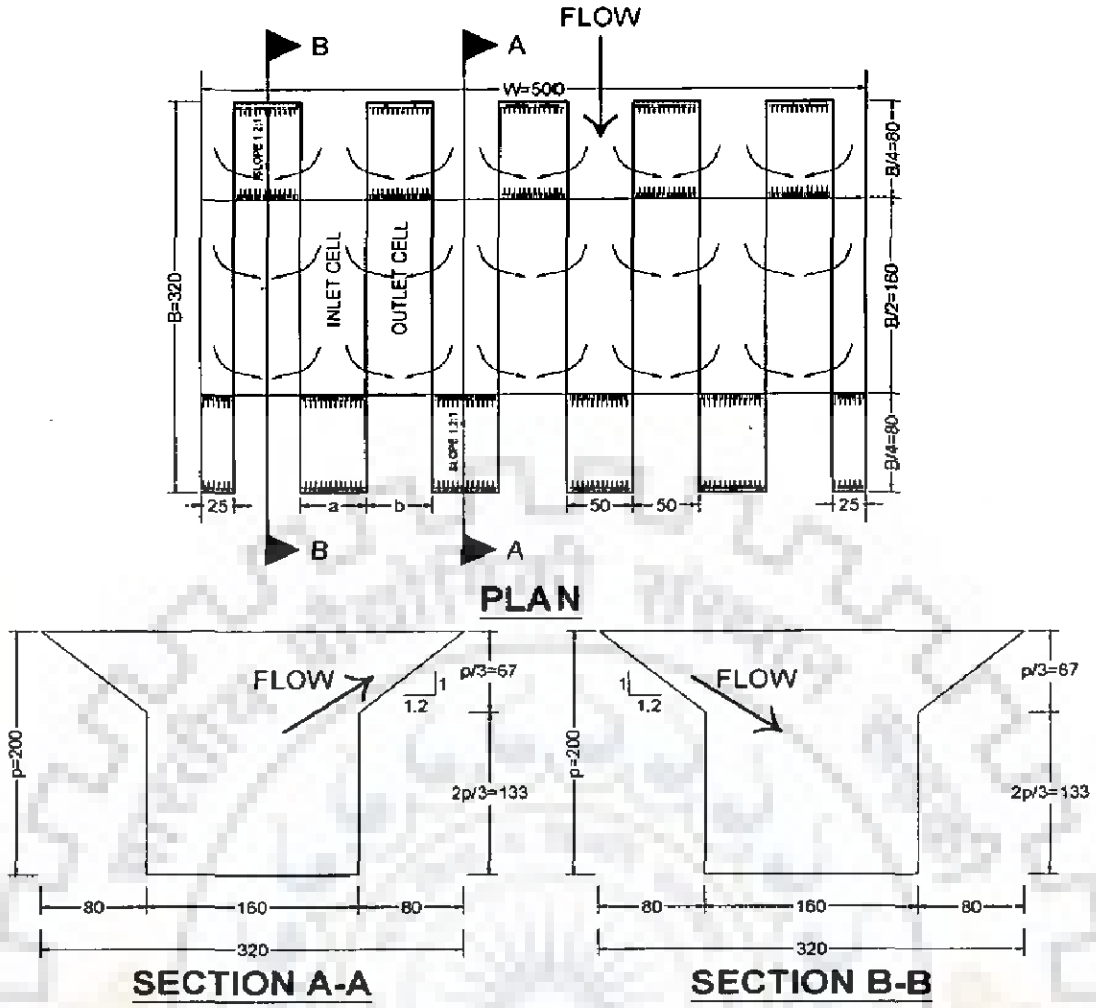

Fig. 3.5 Plan and section of model P_1M_3 (dimensions in mm)

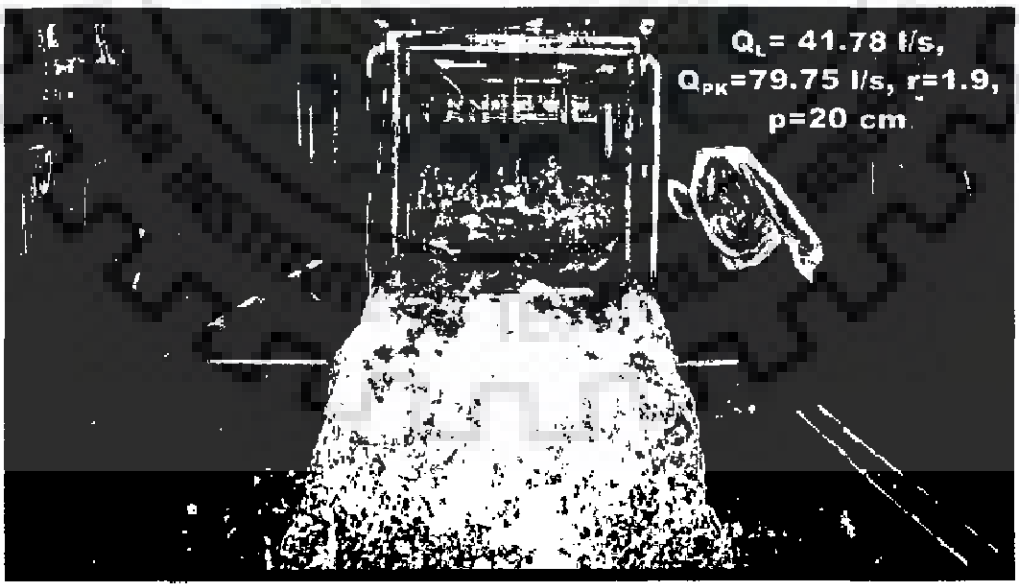

Plate No. 3.3 Model P_1M_3

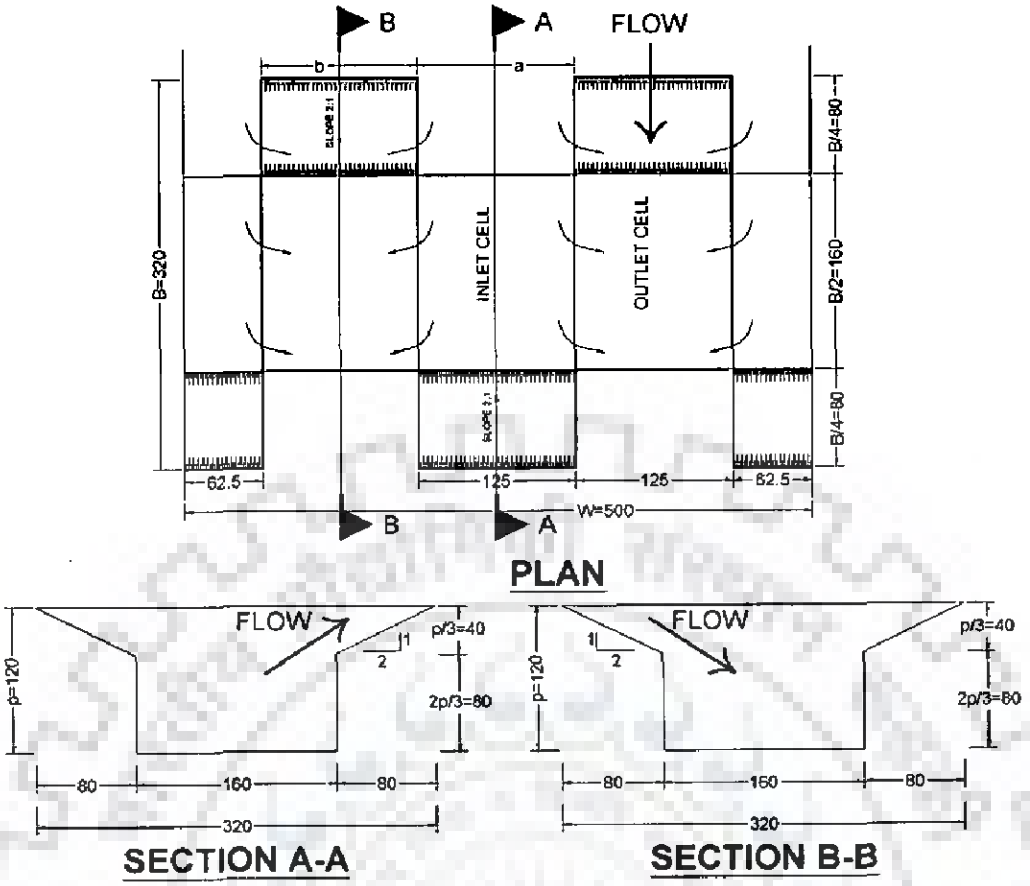

Fig. 3.6 Plan and section of model P_1M_4 (dimensions in mm)

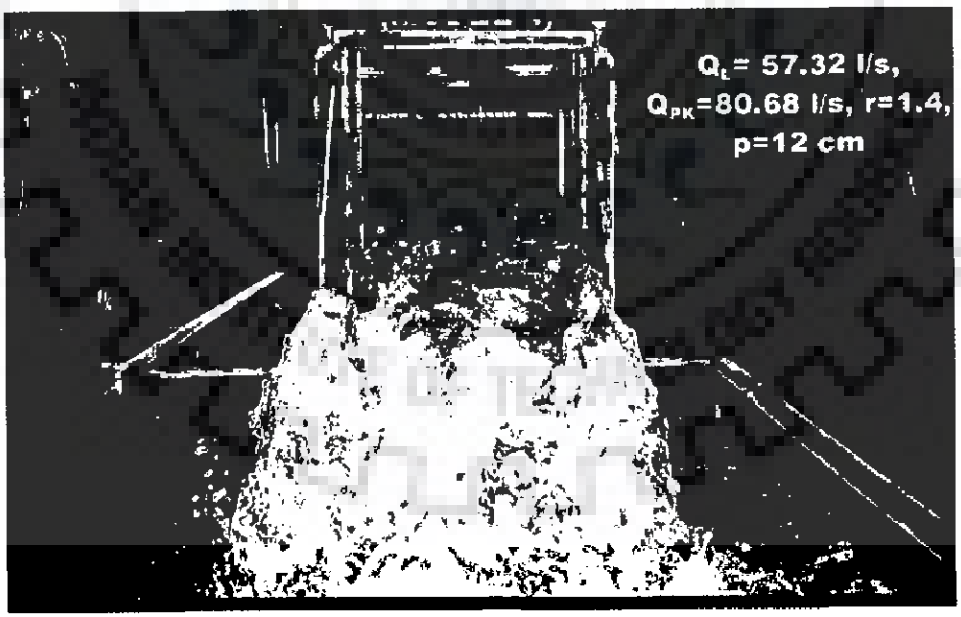

Plate No. 3.4 Model P_1M_4

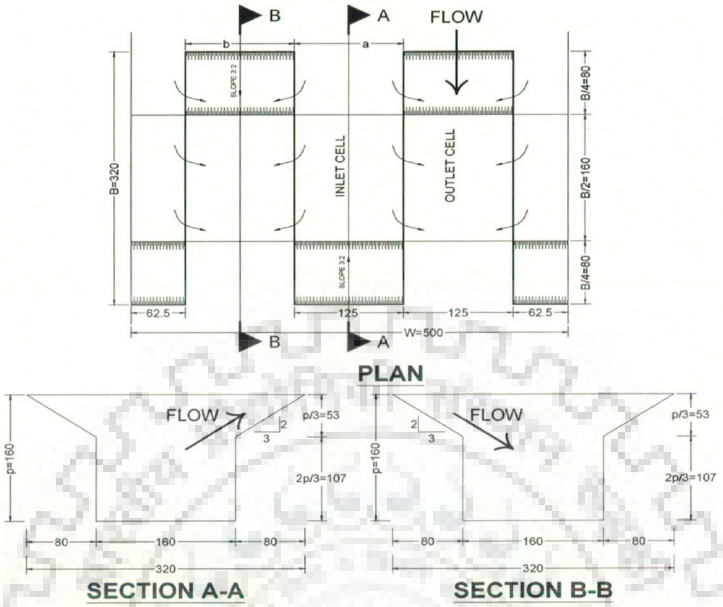

Fig. 3.7 Plan and section of model P_1M_5 (dimensions in mm)

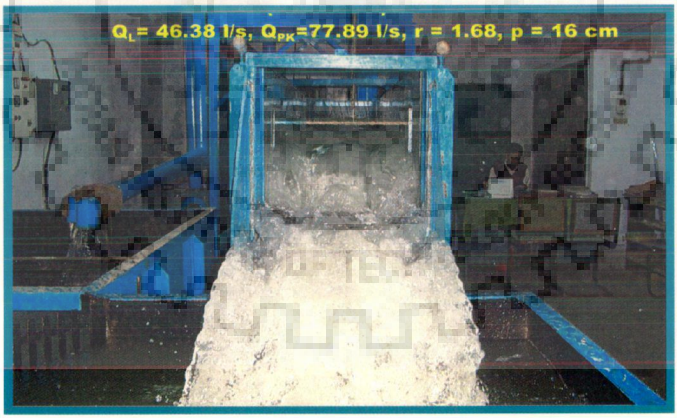

Plate No. 3.5 Model P_1M_5

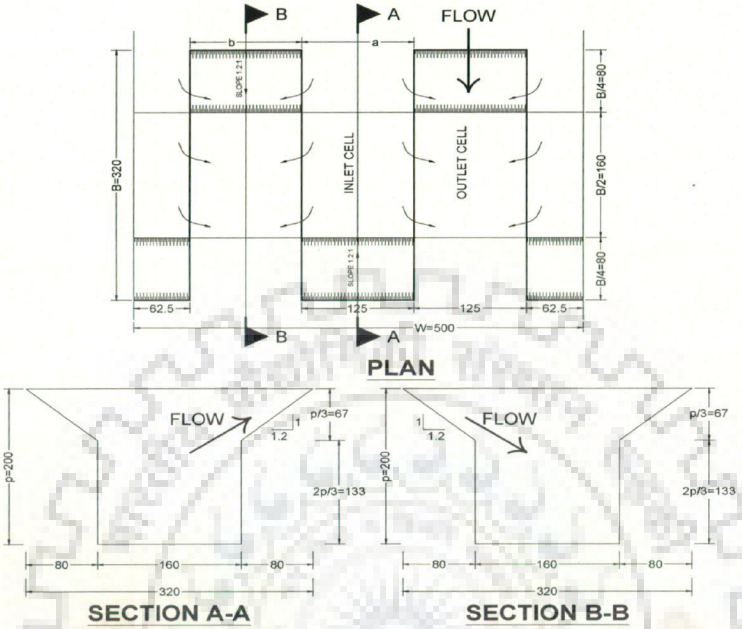

Fig. 3.8 Plan and section of model P_1M_6 (dimensions in mm)

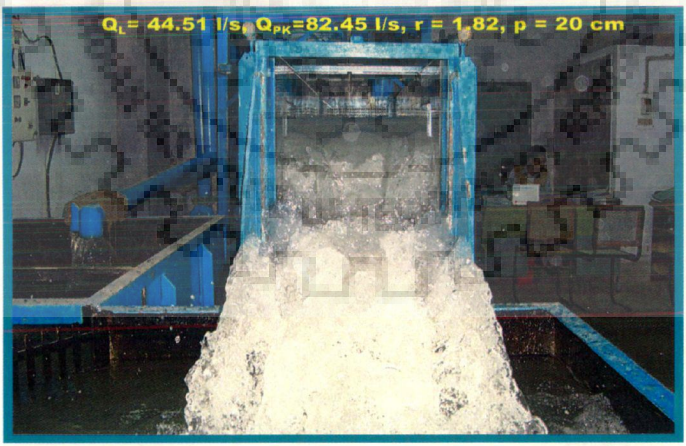

Plate No. 3.6 Model P_1M_6

3.5 PHASE TWO MODEL EXPERIMENTS

From first phase experiment, some modifications have been introduced in the first phase models. In the second phase of the experiment programme, six selected modified models of first phase Piano Key Weir have been used. In the second phase experiment programme, we are providing both sides ramping in the first phase models. The modifications of first phase Piano Key Weir models are shown in Figs. 3.9-3.14. The dimensions of Piano Key Weir models are same as in first phase models.

All the models were run for 10 to 12 different nappe heights and discharges. All the models were tried to run for the value of h/p upto unity. All the models were studied for the value of Piano Key Weir discharge upto 80 l/s. Running view of all the models is shown in plate no. 3.7 to 3.12. These photos show the behavior of Piano Key Weir.

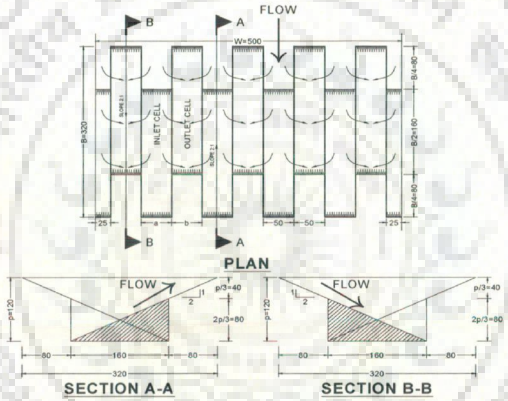

Fig. 3.9 Plan and section of model P_2M_1 (both sides ramping), (dimensions in mm)

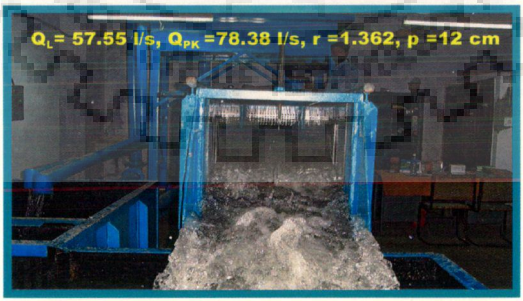

Plate No. 3.7 Model P_2M_1 (both sides ramping)

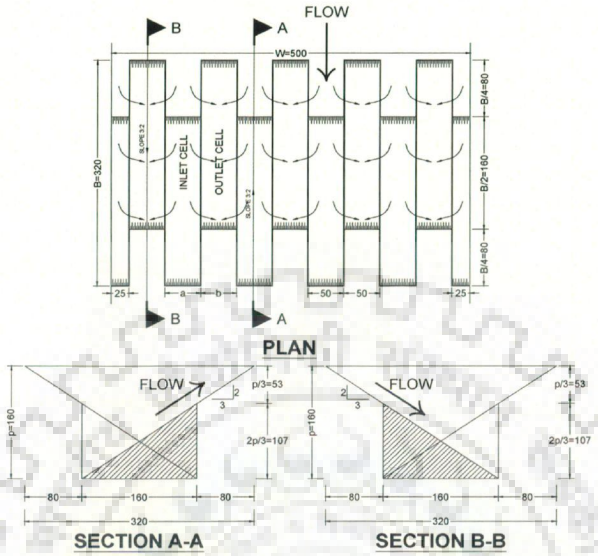

Fig. 3.10 Plan and section of model P_2M_2 (both sides ramping), (dimensions in mm)

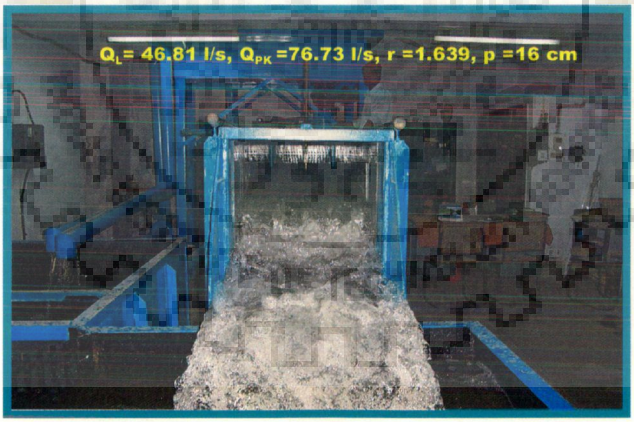

Plate No. 3.8 Model P_2M_2 (both sides ramping)

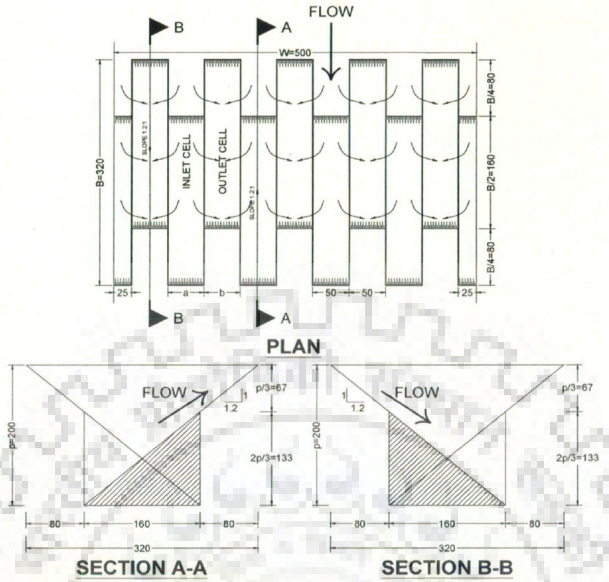

Fig. 3.11 Plan and section of model P_2M_3 (both sides ramping), (dimensions in mm)

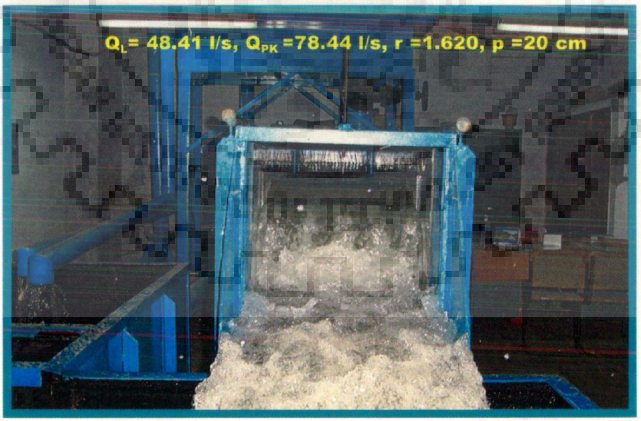

Plate No. 3.9 Model P_2M_3 (both sides ramping)

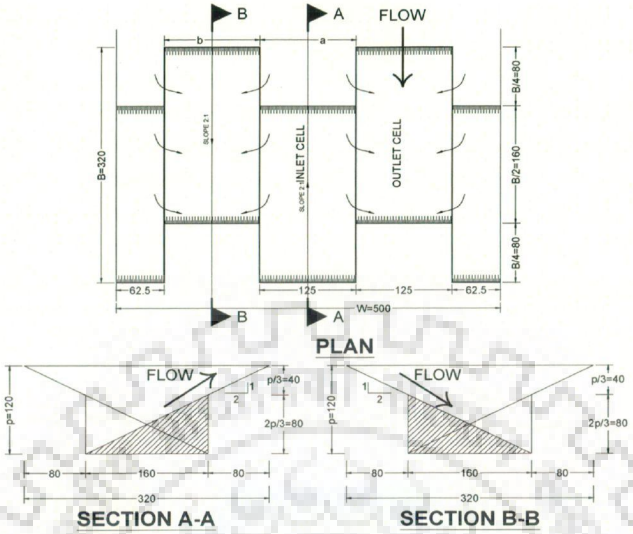

Fig. 3.12 Plan and section of model P_2M_4 (both sides ramping), (dimensions in mm)

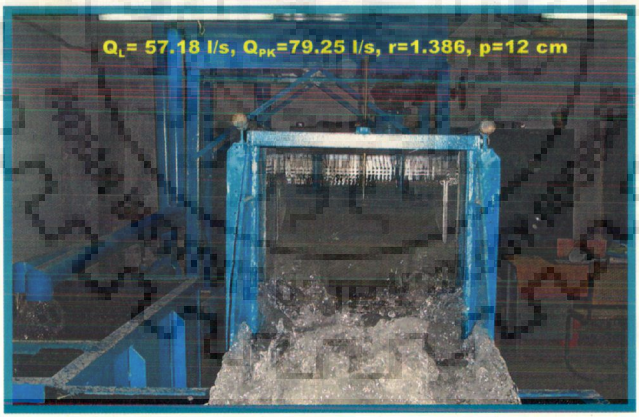

Plate No. 3.10 Model P_2M_4 (both sides ramping)

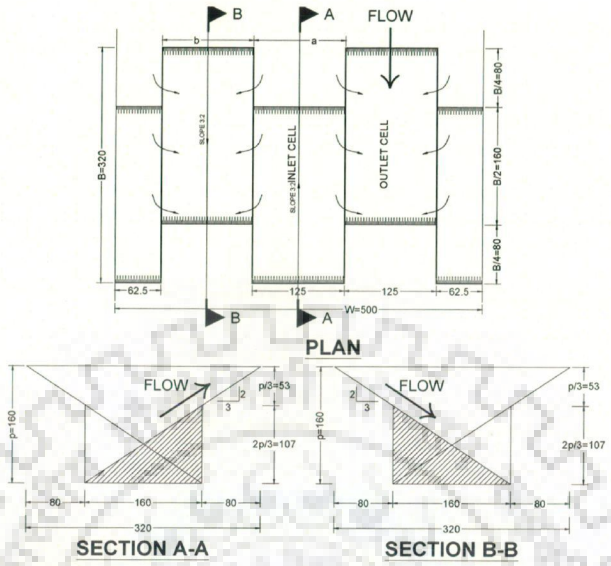

Fig. 3.13 Plan and section of model P_2M_5 (both sides ramping), (dimensions in mm)

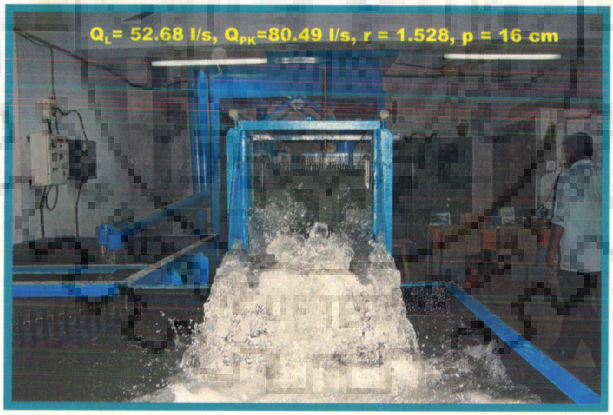

Plate No. 3.11 Model P_2M_5 (both sides ramping)

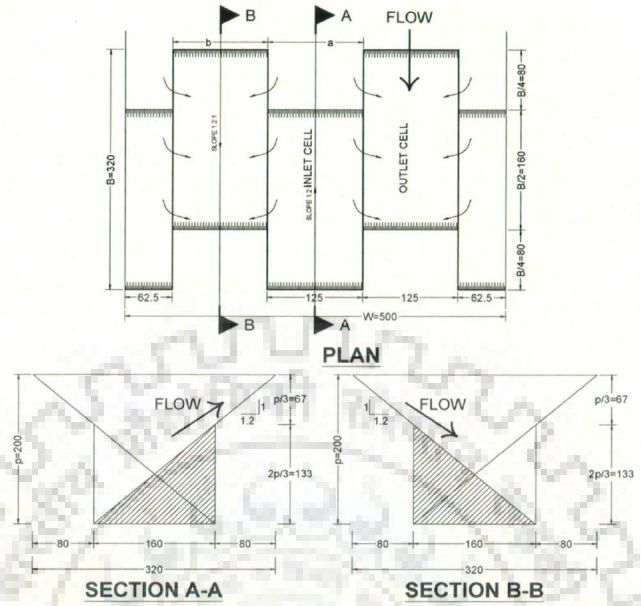

Fig. 3.14 Plan and section of model P_2M_6 (both sides ramping), (dimensions in mm)

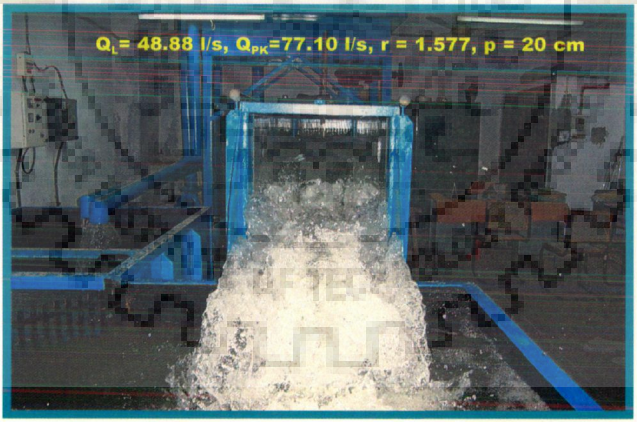

Plate No. 3.12 Model P_2M_6 (both sides ramping)

3.6 PHASE THREE MODEL EXPERIMENTS

In the third phase of the experiment programme, six selected models of Piano Key Weir have been used. The dimensions of Piano Key Weir models are as indicated below in Table 3.2. In third phase experimental models, all six models P_3M_1, P_3M_2, P_3M_3, P_3M_4, P_3M_5, and P_3M_6 have same slope but element configuration is different. Plan and sectional view of Piano Key Weir models P_3M_1, P_3M_2, P_3M_3, P_3M_4, P_3M_5, and P_3M_6 are as shown in Figs. 3.15-3.20. Running view of all the models is shown in plate no. 3.13 to 3.18.

All the models were run for 10 to 12 different nappe heights and discharges. All the models were run for the value of h/p upto unity. All the models have been experimented for the value of Piano Key Weir discharge upto 80 l/s.

Table 3.2: Phase Three Model dimensions

Model No.	Height of Model (p) (cm)	a (cm)	b (cm)	$a+b$ (cm)	L/W	No. of Element
P_3M_1	16	6.00	4.00	10.00	7.40	5
P_3M_2	16	4.00	6.00	10.00	7.40	5
P_3M_3	16	10.00	6.67	16.67	4.84	3
P_3M_4	16	6.67	10.00	16.67	4.84	3
P_3M_5	16	8.33	8.33	16.67	4.84	3
P_3M_6	16	10.00	15.00	25.00	3.56	2

For last elements on the side of the flume, the width of a or b will be divided by 2.

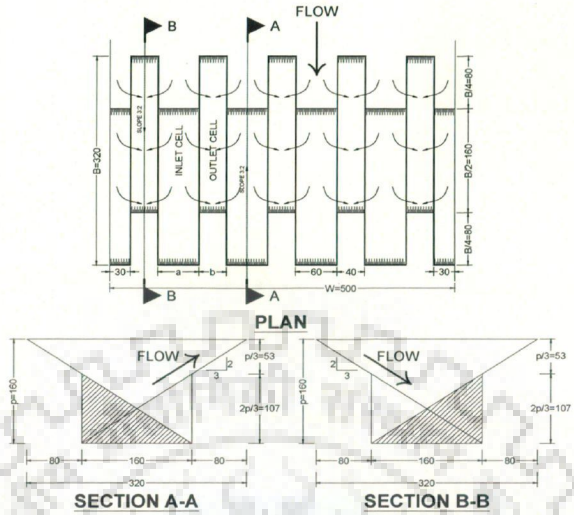

Fig. 3.15 Plan and section of model P_3M_1 (both sides ramping), (dimensions in mm)

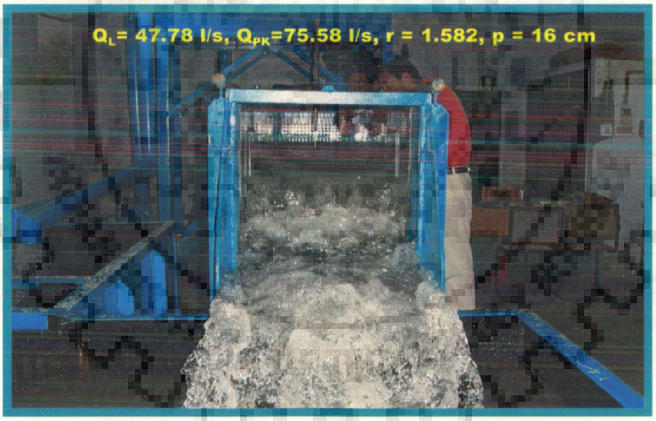

Plate No. 3.13 Model P_3M_1 (both sides ramping)

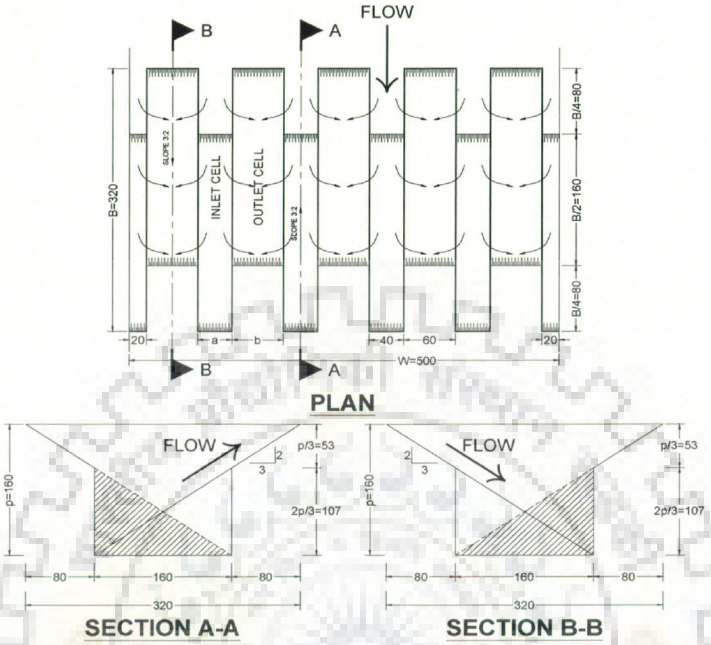

Fig. 3.16 Plan and section of model P_3M_2 (both sides ramping), (dimensions in mm)

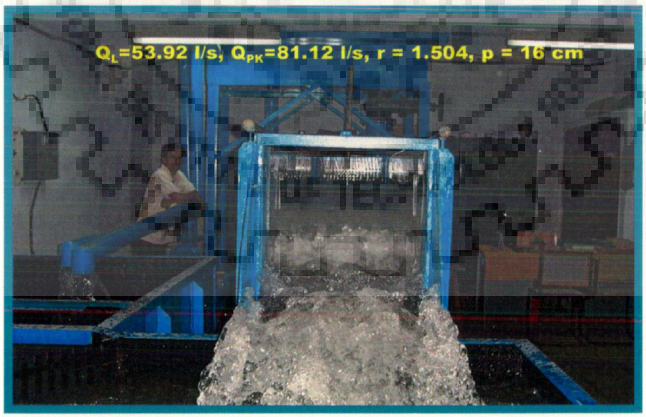

Plate No. 3.14 Model P_3M_2 (both sides ramping)

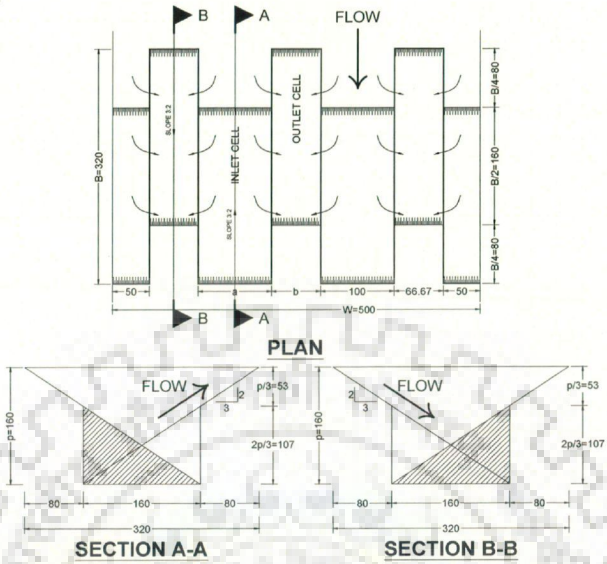

Fig. 3.17 Plan and section of model P_3M_3 (both sides ramping), (dimensions in mm)

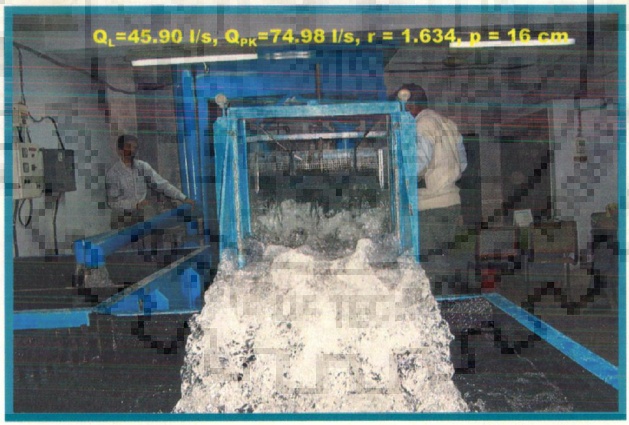

Plate No. 3.15 Model P_3M_3 (both sides ramping)

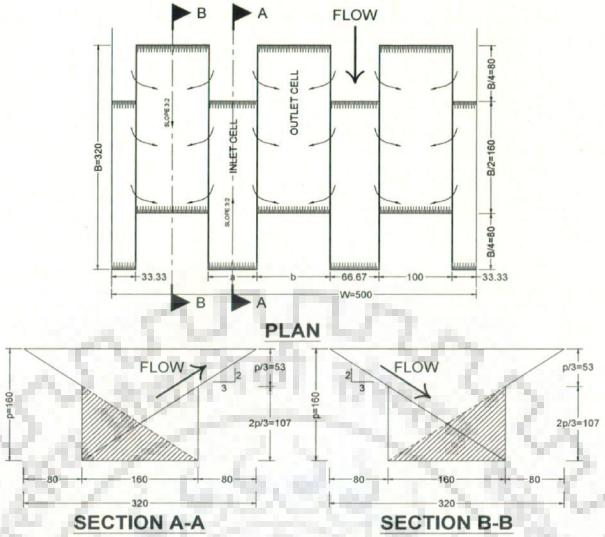

Fig. 3.18 Plan and section of model P_3M_4 (both sides ramping), (dimensions in mm)

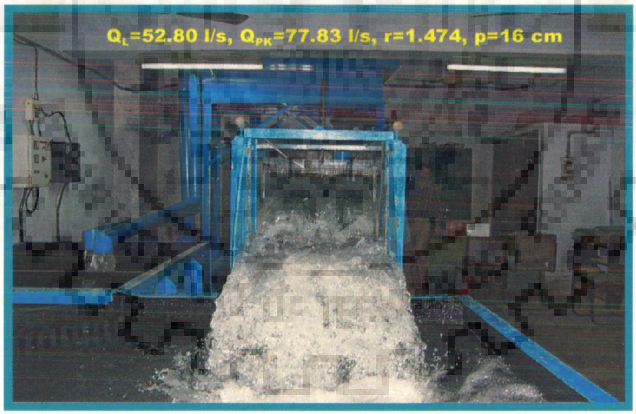

Plate No. 3.16 Model P_3M_4 (both sides ramping)

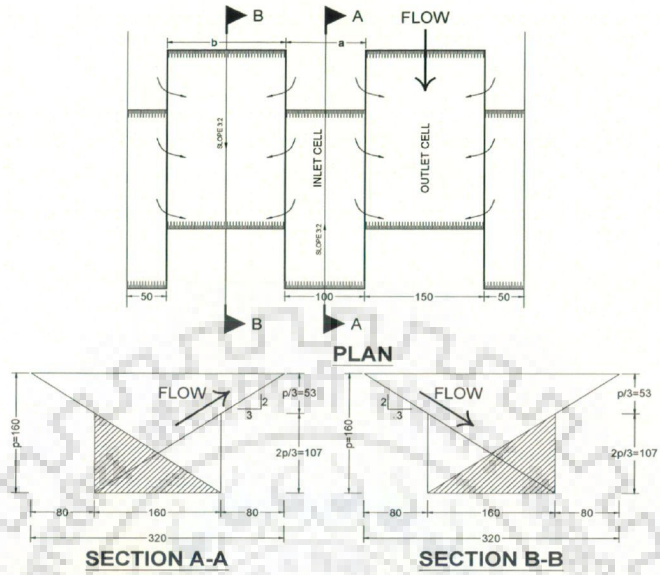

Fig. 3.19 Plan and section of model P_3M_5 (both sides ramping), (dimensions in mm)

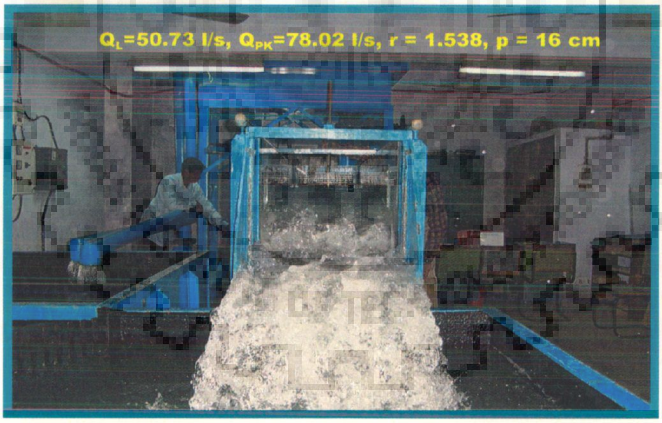

Plate No. 3.17 Model P_3M_5 (both sides ramping)

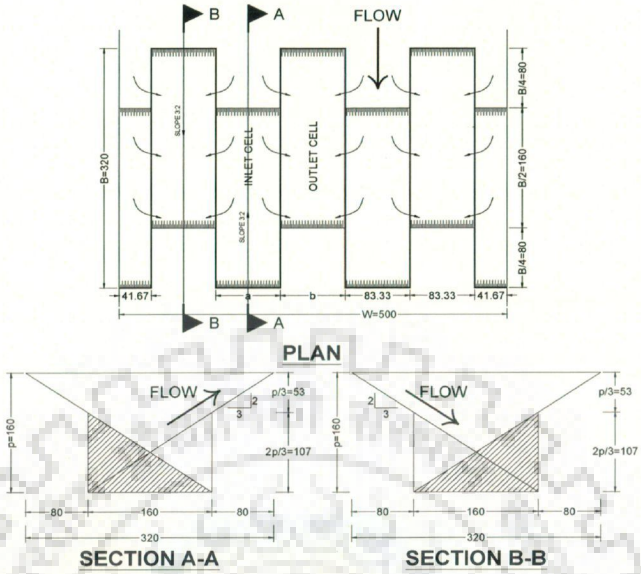

Fig. 3.20 Plan and section of model P_3M_6 (both sides ramping), (dimensions in mm)

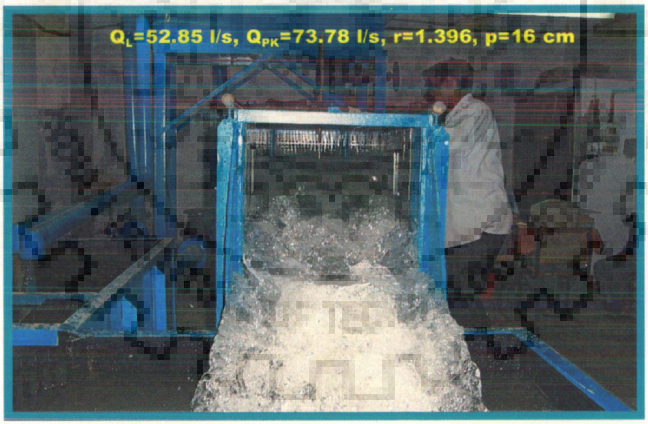

Plate No. 3.18 Model P_3M_6 (both sides ramping)

3.7 PHASE FOUR MODEL EXPERIMENTS

In the fourth phase of the experiment programme, five selected models of Piano Key Weir have been used. The dimensions of Piano Key Weir models are as indicated below in Table 3.3. In fourth phase experimental models, P_4M_1, P_4M_2, and P_4M_3, models have same slope but element configuration is different. P_4M_4, and P_4M_5 models have also same slope but different from P_4M_1, P_4M_2, and P_4M_3, and element configuration is different. Here downstream side over hanging only was considered, not upstream side. Plan and sectional view of Piano Key Weir models P_4M_1, P_4M_2, P_4M_3, P_4M_4, and P_4M_5 are shown in Figs. 3.21-3.25. Running view of all the models is shown in plate no. 3.19 to 3.23.

All the models were run for 10 to 12 different nappe heights and discharges. All the models were endeavored to run for the value of h/p upto unity. All the models have been studied for the value of Piano Key Weir discharge upto 80 l/s.

Table 3.3: Phase four model dimensions

Model No.	Height of Model (p) (cm)	a (cm)	b (cm)	$a+b$ (cm)	L/W	No. of Element
P_4M_1	16	5.00	5.00	10.00	7.40	5
P_4M_2	16	12.50	12.5	25.00	3.56	2
P_4M_3	16	8.33	8.33	16.67	4.84	3
P_4M_4	12	8.33	8.33	16.67	4.84	3
P_4M_5	12	10.00	6.67	16.67	4.84	3

For last elements on the side of the flume, the width of a or b will be divided by 2.

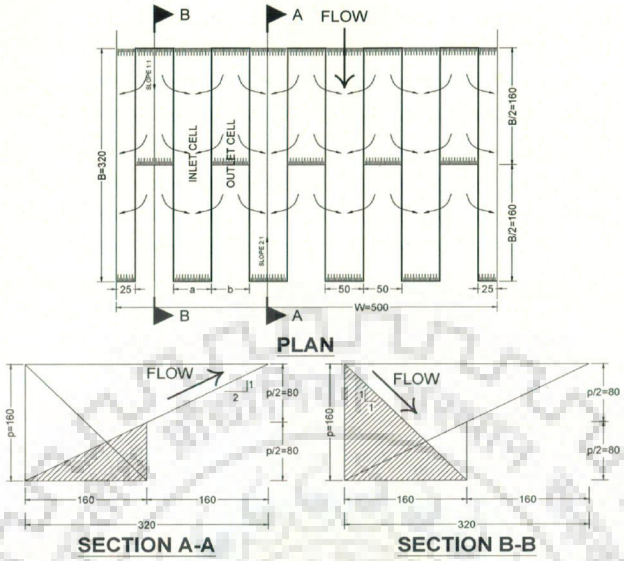

Fig. 3.21 Plan and section of model P_4M_1 (both sides ramping), (dimensions in mm)

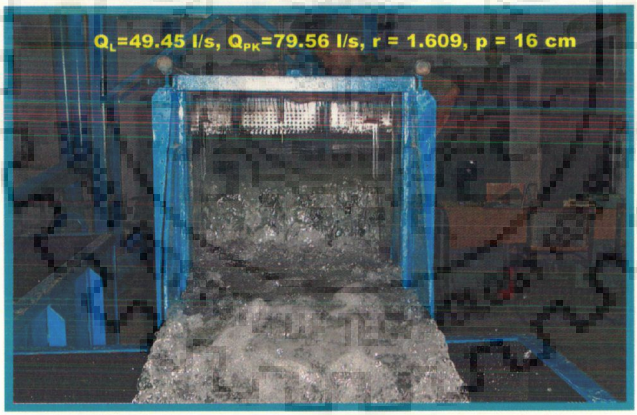

Plate No. 3.19 Model P_4M_1 (both sides ramping)

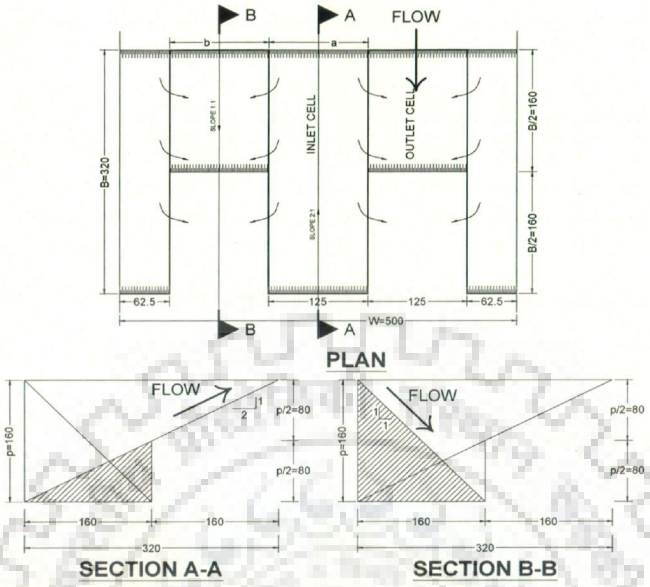

Fig. 3.22 Plan and section of model P_4M_2 (both sides ramping), (dimensions in mm)

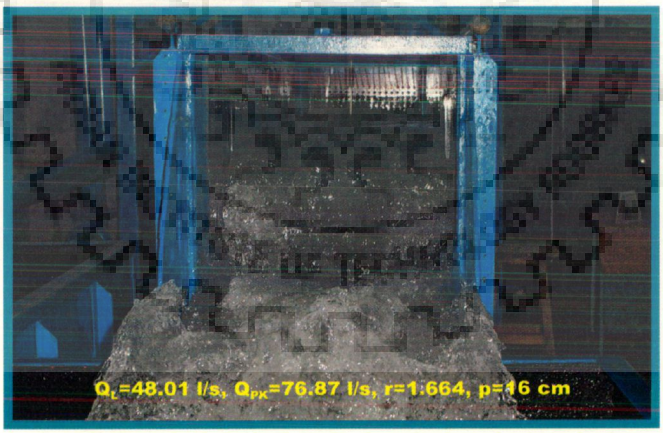

Plate No. 3.20 Model P_4M_2 (both sides ramping)

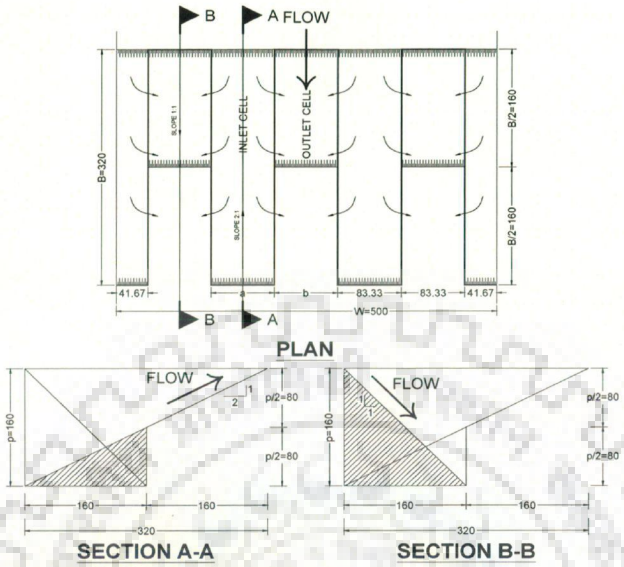

Fig. 3.23 Plan and section of model P_4M_3 (both sides ramping), (dimensions in mm)

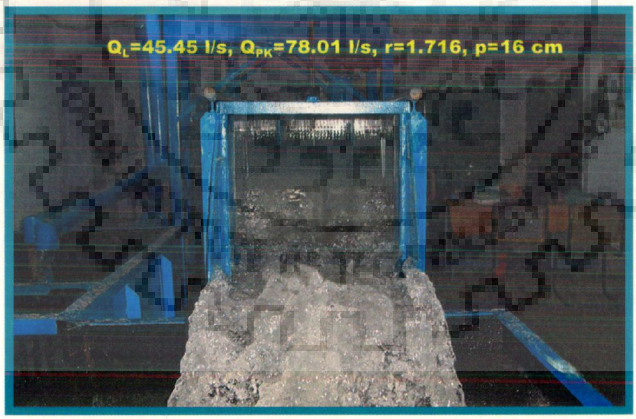

Plate No. 3.21 Model P_4M_3 (both sides ramping)

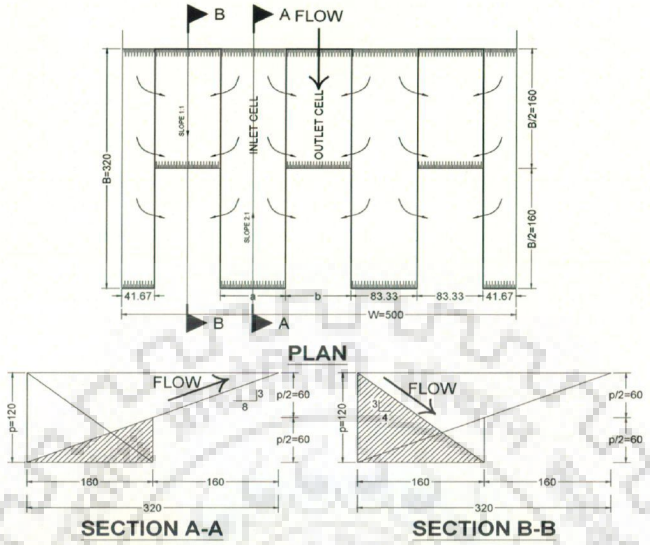

Fig. 3.24 Plan and section of model P_4M_4 (both sides ramping), (dimensions in mm)

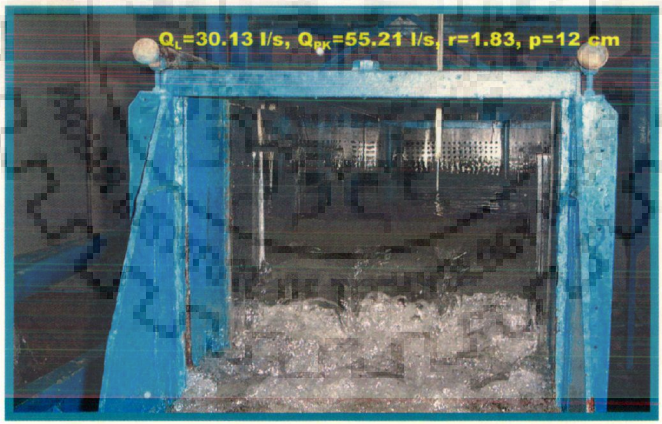

Plate No. 3.22 Model P_4M_4 (both sides ramping)

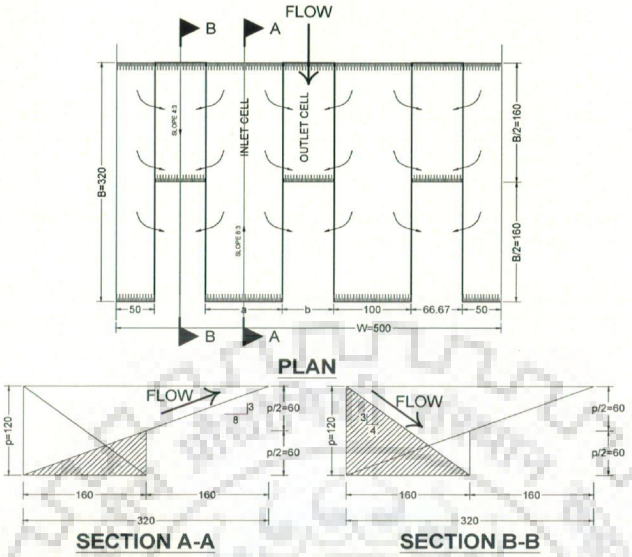

Fig. 3.25 Plan and section of model P_4M_5 (both sides ramping), (dimensions in mm)

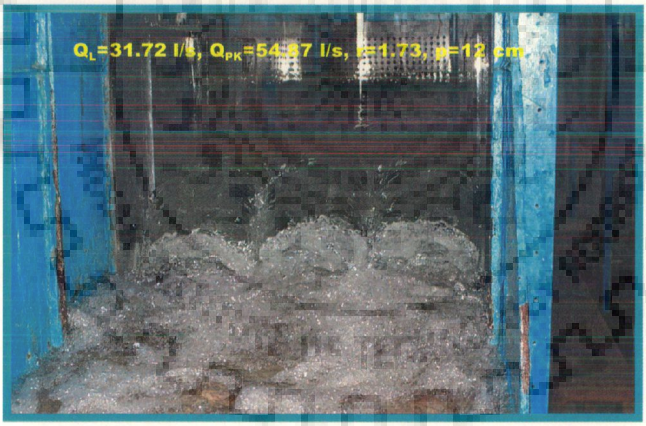

Plate No. 3.23 Model P_4M_5 (both sides ramping)

3.8 PHASE FIVE MODEL EXPERIMENTS

In the fifth phase of the experiment programme, five selected models of Piano Key Weir have been used with some modification in previous models. Inlet modification has been done in the model P_2M_4, and P_4M_3. Filling inlet cell modification has been done in the model P_2M_6 and filling outlet cell modification has been done in the model P_2M_2 and P_2M_5. Modification in the selected models of Piano Key Weir is shown in Figs 3.26-3.30 with plan and sectional view. These modifications were incorporated to see the improvement in the performance of Piano Key Weir.

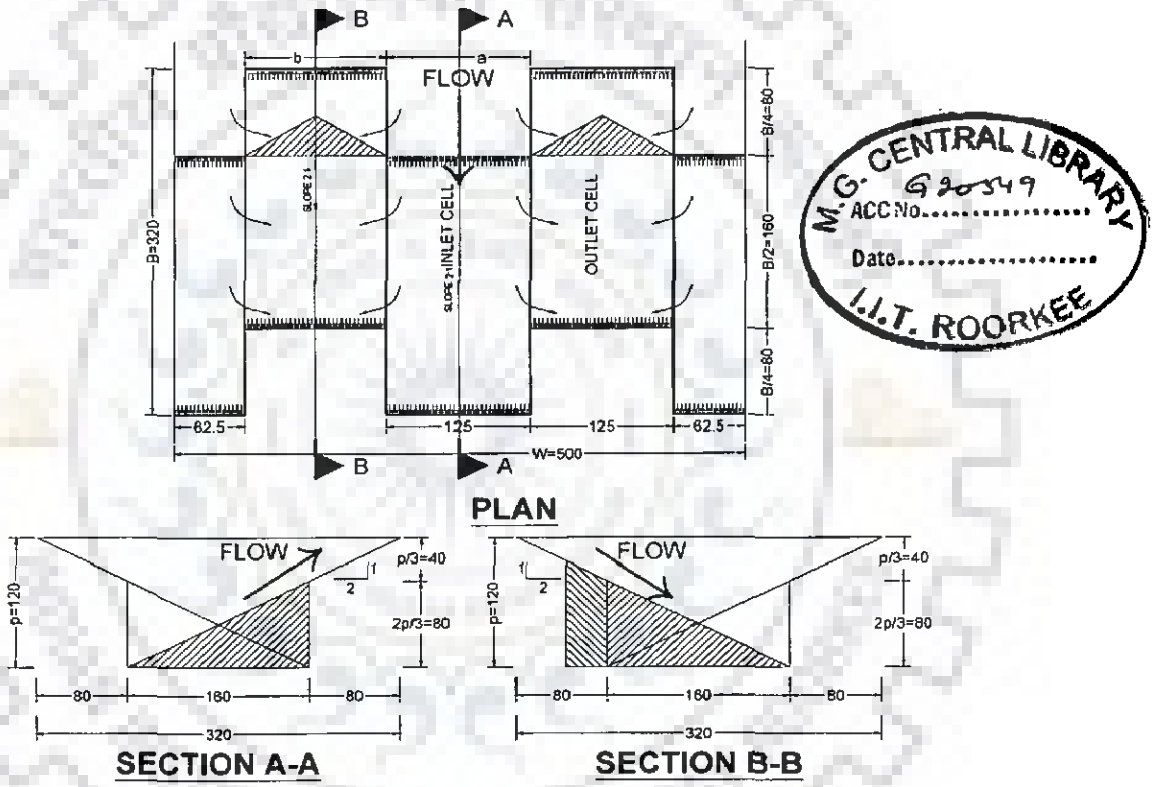

M.G. CENTRAL LIBRARY
G20549
ACC No.....
Date.....
I.I.T. ROORKEE

Fig. 3.26 Plan and section of model P_2M_4 with inlet modification (dimensions in mm)

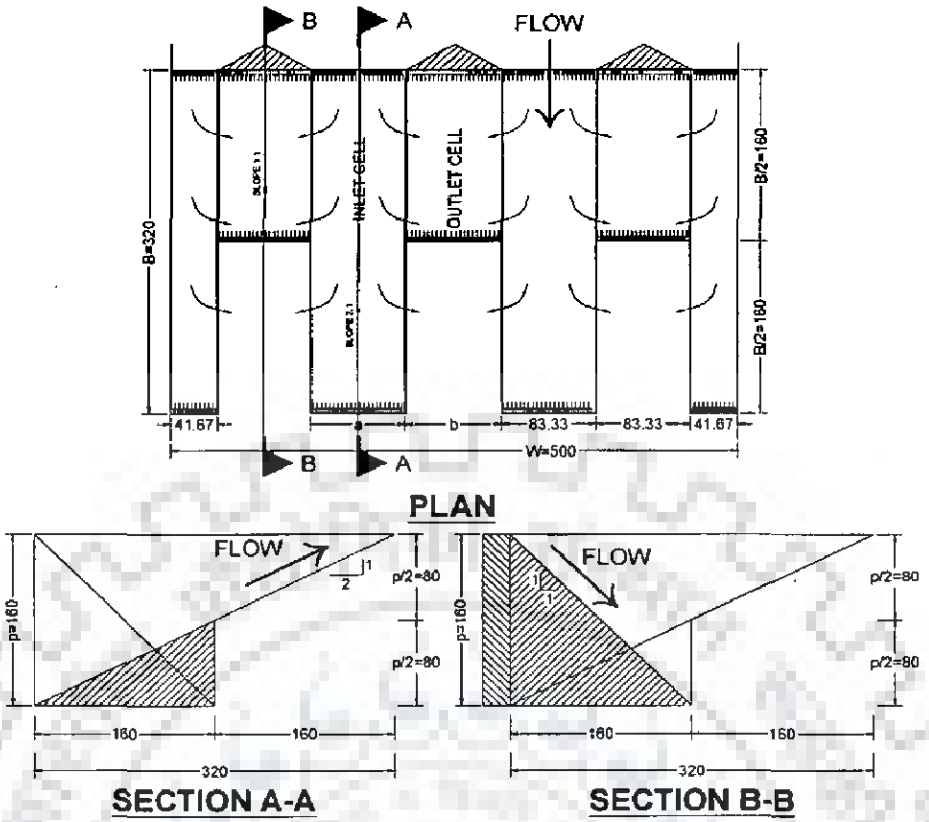

Fig. 3.27 Plan and section of model P_4M_3 with inlet modification (dimensions in mm)

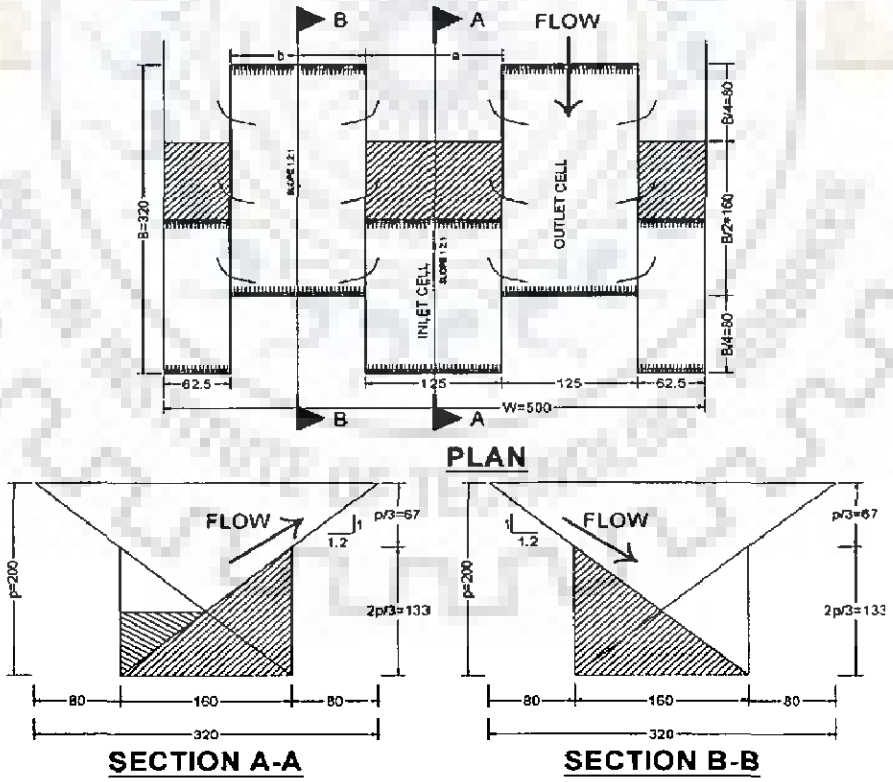

Fig. 3.28 Plan and section of model P_2M_6 with filling inlet cell modification (dimensions in mm)

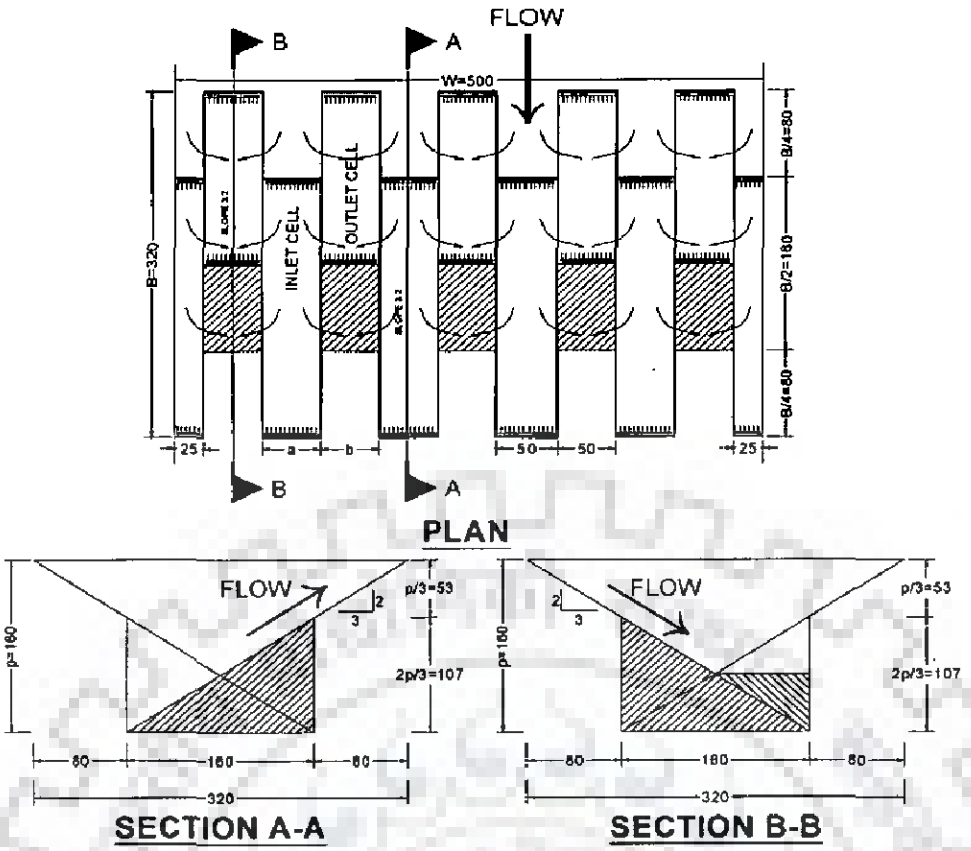

Fig. 3.29 Plan and section of model P_2M_2 with filling outlet cell modification (dimensions in mm)

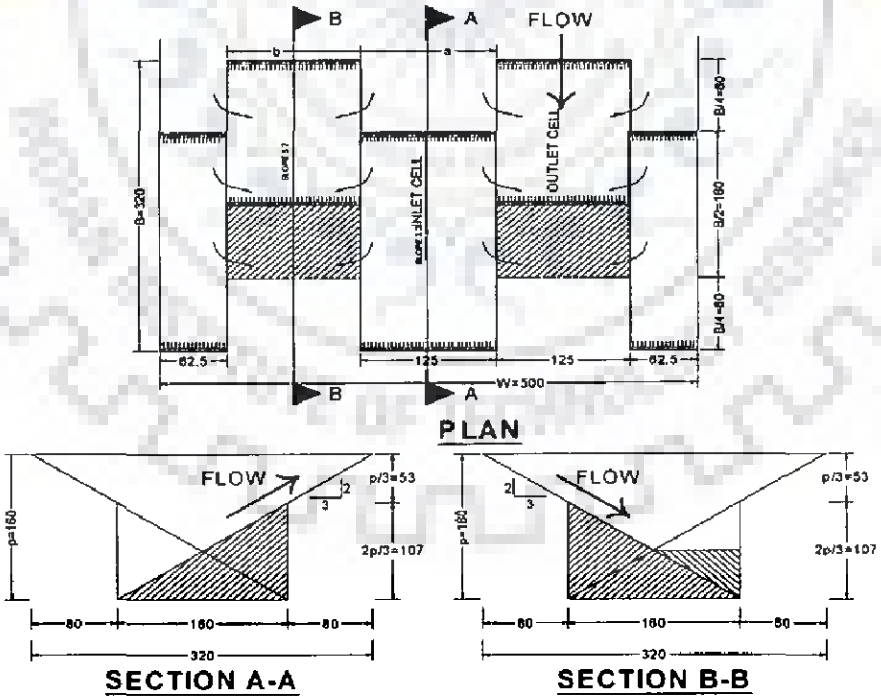

Fig. 3.30 Plan and section of model P_2M_5 with filling outlet cell modification (dimensions in mm)

3.9 SUMMARY

The experimental studies of Piano Key Weir model were performed in five different phases. A simple design of Piano Key Weir was investigated in the first phase experiments and modifications in the preliminary design of first phase model were added in subsequent phases. In order to increase the performance of Piano Key Weir, a ramp is provided in the preliminary designed model in first phase and thus sets the basis for the second phase experiments. Increase in discharge passing capacity was obtained in particular model of second phase experiments. Thereafter, it became obvious to select this particular model from second phase experiment and to carry out rigorous experimental analysis on this selected model. All these investigation were placed in the third phase experiments. Next, the fourth phase experiments were designed with downstream side over-hanging only. Finally model investigation with some modifications in few previous models were carried out and placed in the fifth phase experiments.

CHAPTER 4

PERFORMANCE EVALUATION OF PIANO KEY WEIR

4.1 GENERAL

Considering the fact that Piano Key Weir of different shapes are to be used in field conditions, the objective of these experiments was to identify the Piano Key Weir in which the maximum discharge capacity at different L/W with p (height of weir) could be achieved. To achieve this for different flow conditions, length magnification ratio (L/W) is taken from 3.56 to 7.40. Also, other parameters are taken in different combinations for getting optimum configuration of Piano Key Weir for better performance. Few selected models of Piano Key Weir have been also used with certain modifications in the inlet and outlet cell for improving the performance. This chapter presents the experimental data processing of all these model results.

4.2 DATA ANALYSIS

Some of the steps of the data analysis consist of the following:

- Calculation of discharge through rectangular sharp crested weir is made by the formula,

$$Q_L = \frac{2}{3} C_d \sqrt{2g}.Wh^{3/2} \tag{4.1}$$

where Q_L is the discharge through rectangular sharp crested weir, h is the head over the crest and C_d is coefficient of discharge, W is the width of channel. In Eq. (4.1)

$$C_d = \left[0.605 + \frac{0.08h}{p} + \frac{0.001}{h} \right] \tag{4.2}$$

and p is height of crest

- V-notch is used to measure the discharge through Piano Key Weir (Chow, 1959). The formula used for discharge of V-notch is

$$Q_{PK} = \frac{8}{15} C_d \sqrt{2g} \tan(\theta/2) H_e^{5/2} \tag{4.3}$$

where, $H_e = H + K_h$ (4.4)

Here, H_e is the effective depth of water above vertex at the upstream of V-notch, the quantity K_h represents the combined effects of fluid properties, taken as 0.0008m for 90^0 V-notch, C_d is coefficient of discharge, taken as 0.58 for a 90-degree V-notch only and θ is the angle of the V-notch.

- Difference of Piano Key Weir discharge and rectangular sharp crested weir discharge (ΔQ) is obtained as

$$\Delta Q = Q_{PK} - Q_L \tag{4.5}$$

where, Q_{PK} is the discharge through Piano Key Weir and Q_L is the discharge through rectangular sharp crested weir

- Ratio (r) of Piano Key Weir discharge and linear Weir discharge is

$$r = \left(\frac{Q_{PK}}{Q_L}\right) \tag{4.6}$$

- Calculation of h/p

h is the head over the crest (at one and half meter u/s of the Piano Key Weir) and p is height of Piano Key Weir.

- Calculation of length magnification ratio (L/W)

L is the length of Piano Key Weir crest and W is the effective linear width of element of Piano Key Weir.

Data processing and analysis have been done for each model.

4.3 VALIDITY OF DISCHARGE MEASURING THROUGH V-NOTCH AND SHARP CRESTED WEIR

Sharp crested weir discharge is calculated by Eq. (4.1) and coefficient of discharge for sharp crested weir is taken as 0.72. Discharge through the V-notch is calculated by Eq. (4.3) and coefficient of discharge for 90^o V-notch is taken as 0.58 (Weber et al., 2001). Comparative results of V-notch and sharp crested weir are shown in table 1. From table 4.1, percentage of discharge variation between V-notch and Sharp Crested Weir is -1.0 to 5.5.

Table 4.1: Results on comparative study between V-notch and sharp crested weir

Head over V-Notch (m)	V-Notch Discharge (l/s)	Head over Sharp Crested Weir (m)	Sharp Crested Weir Discharge (l/s)	% of discharge variation
0.31	72.12	0.18	71.37	-1.05
0.29	64.53	0.17	65.06	0.80
0.28	57.09	0.16	57.51	0.72
0.27	50.56	0.15	51.85	2.48
0.25	41.88	0.13	43.37	3.43
0.23	33.57	0.11	35.09	4.33
0.20	25.82	0.10	27.36	5.63
0.19	20.45	0.08	21.60	5.33

4.4 EVALUATION OF FIRST PHASE EXPERIMENTS

The collected data from all six models have been analysed to find best geometric shape. Collected data have been analysed using Eq. 4.1 to 4.6. The graphical representation between discharge and (h/p) for all the six models is shown in Figs. (4.1-4.6). In Figs. 4.1 to 4.6, the discharge passing through Piano Key Weir (Q_{PK}) is observed to be more than the discharge passing through rectangular sharp crested weir because available water way length in Piano Key Weir is more than rectangular sharp crested weir. In Figs. 4.7 to 4.9, r vs h/p for same height of Piano Key Weir has been analysed. It can be seen from Figs. 4.7 to 4.9 that value of r increases with increasing L/W because water-way length increases with increasing L/W. In Figs. 4.10 to 4.11, for same length magnification ratio (L/W), the variation of r is shown with respect to h/p and indicates that r is high when h/p is low. Graphical plots between 'r' and h/p for all six models is shown in Fig. 4.12. From Fig. 4.12, model P_1M_2 is found to perform better.

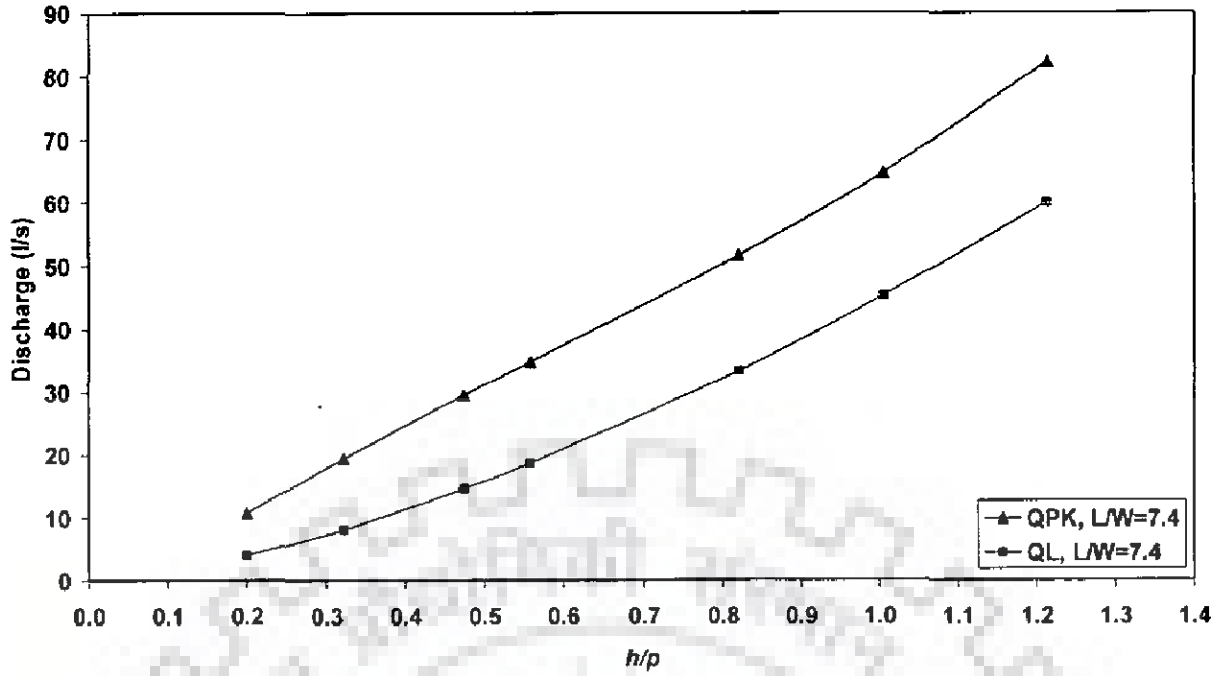

Fig. 4.1 Plot between Q_{PK}, Q_L and h/p for model P_1M_1

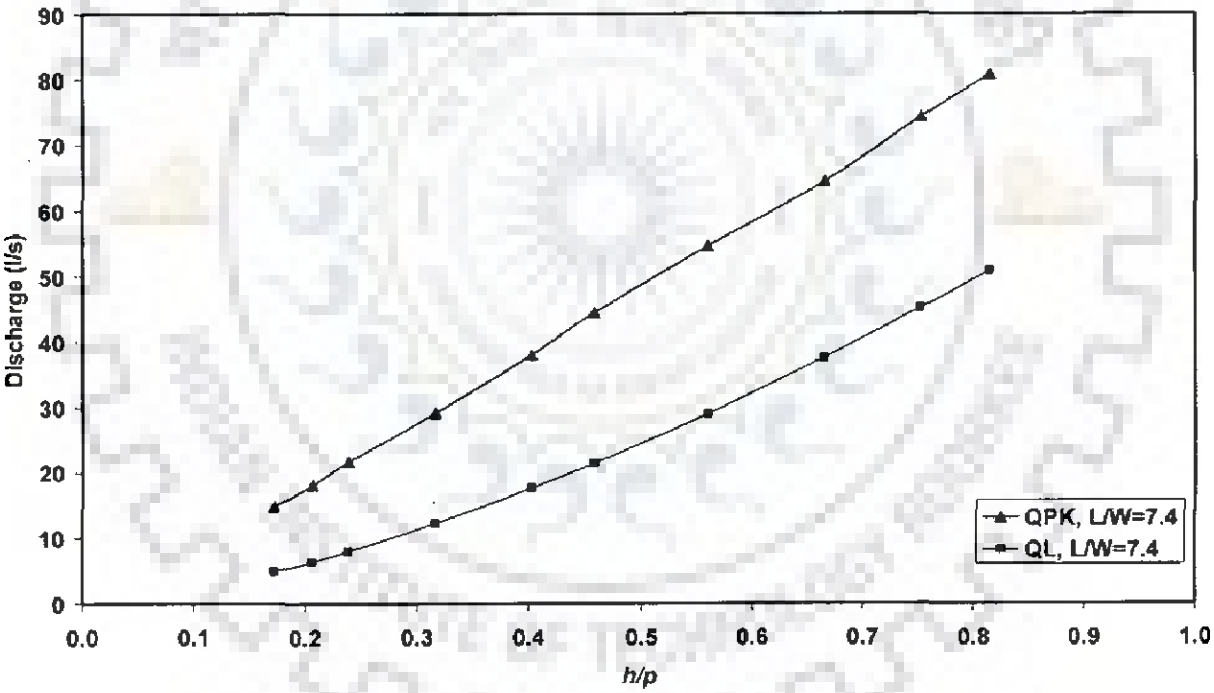

Fig. 4.2 Plot between Q_{PK}, Q_L and h/p for model P_1M_2

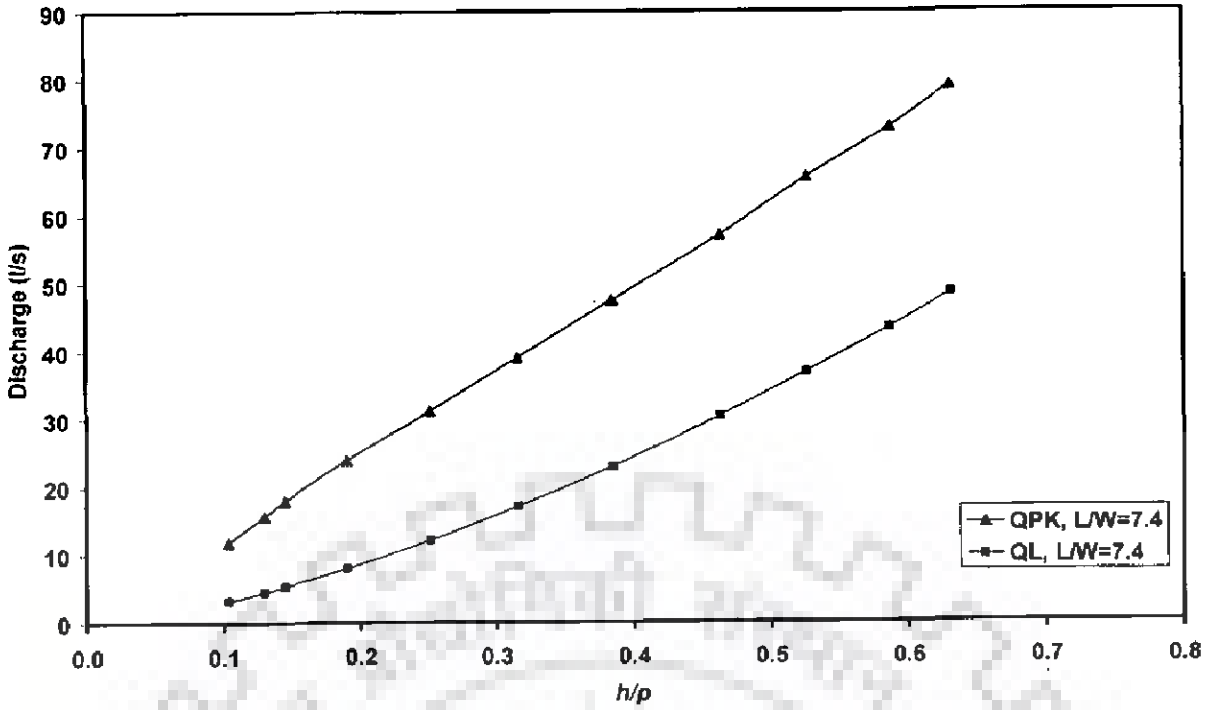

Fig. 4.3 Plot between Q_{PK}, Q_L and h/p for model P_1M_3

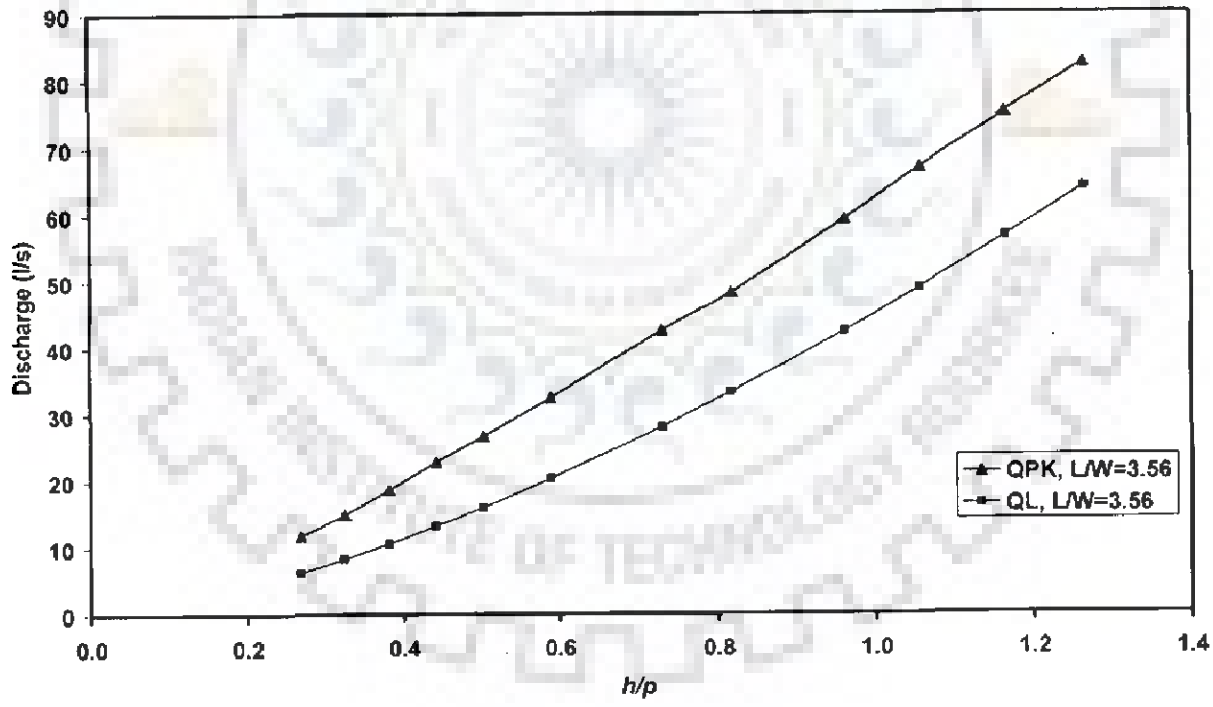

Fig. 4.4 Plot between Q_{PK}, Q_L and h/p for model P_1M_4

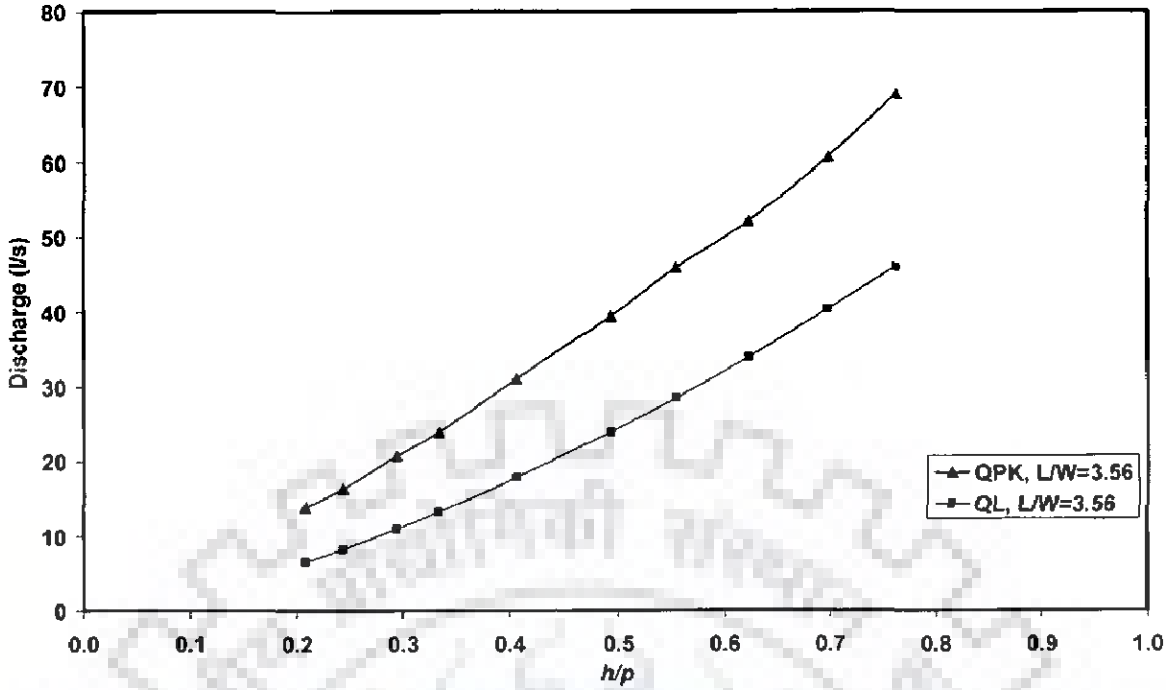

Fig. 4.5 Plot between Q_{PK}, Q_L and h/p for model P_1M_5

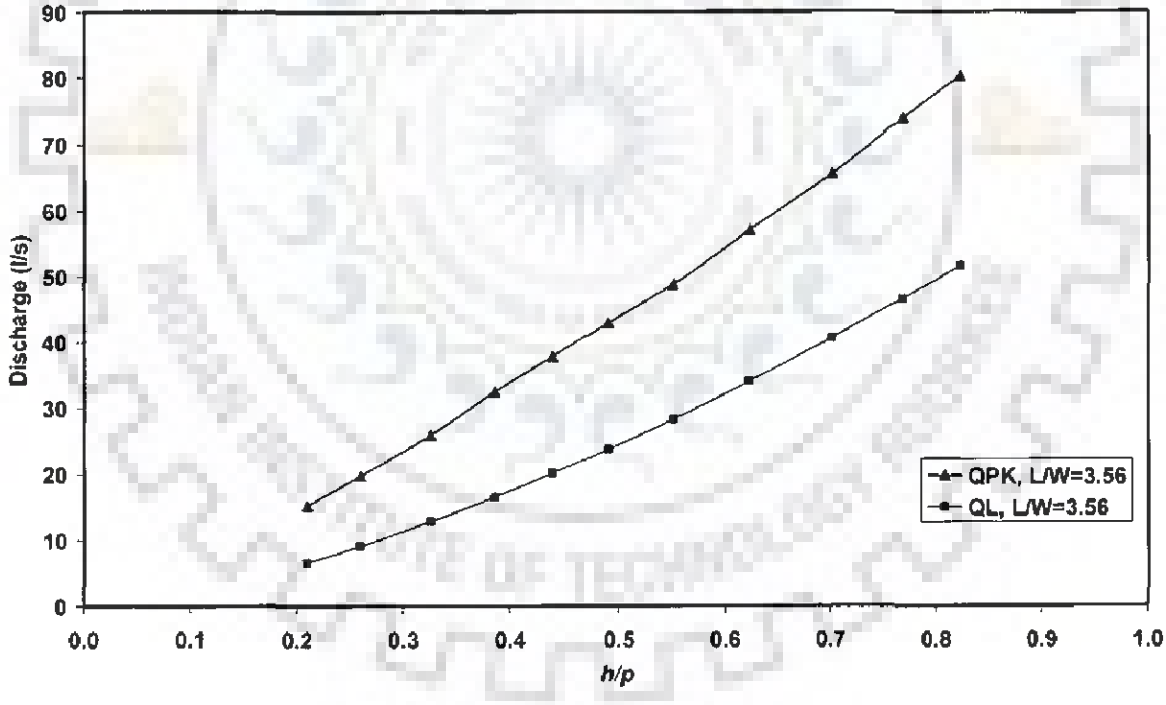

Fig. 4.6 Plot between Q_{PK}, Q_L and h/p for model P_1M_6

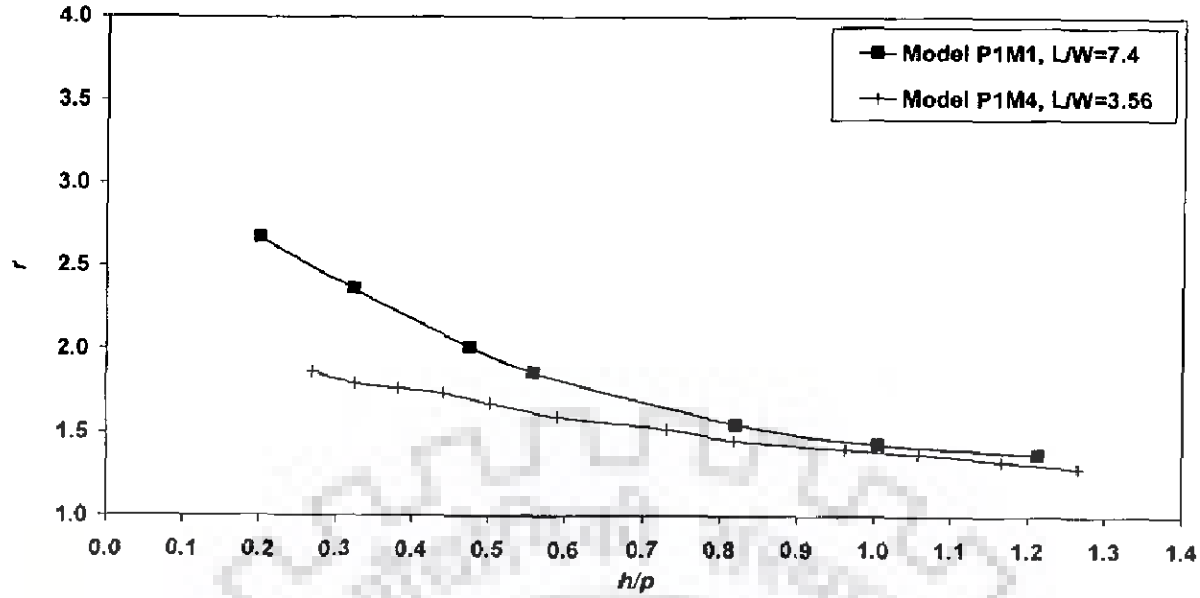

Fig. 4.7 Plot between r and h/p for model P_1M_1 & P_1M_4 with same p = 12 cm

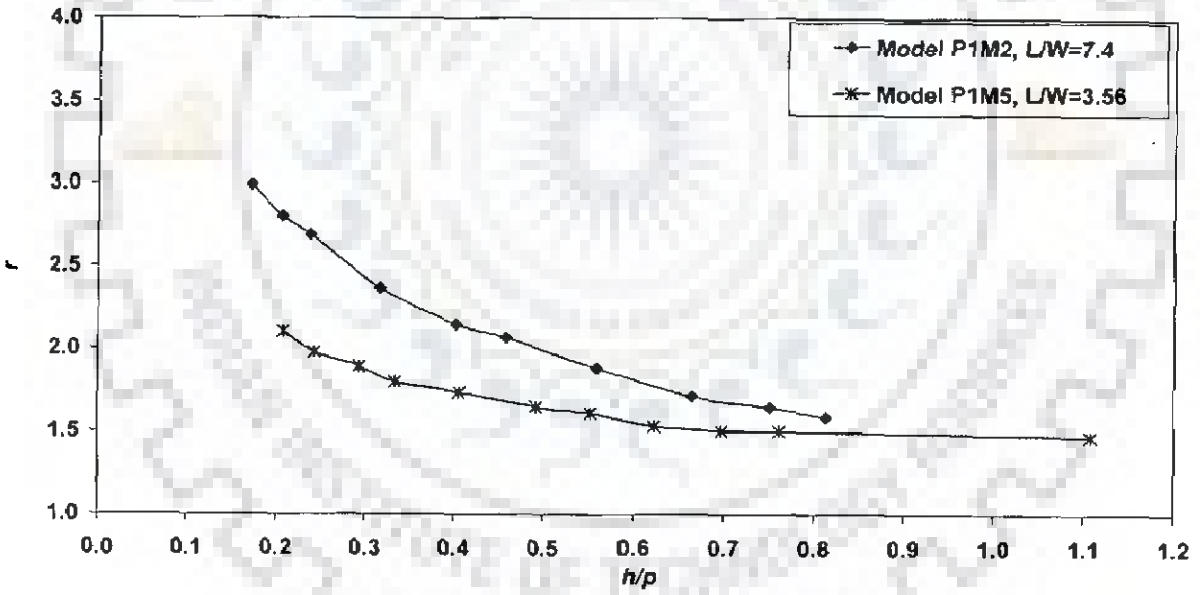

Fig. 4.8 Plot between r and h/p for model P_1M_2 & P_1M_5 with same p = 16 cm

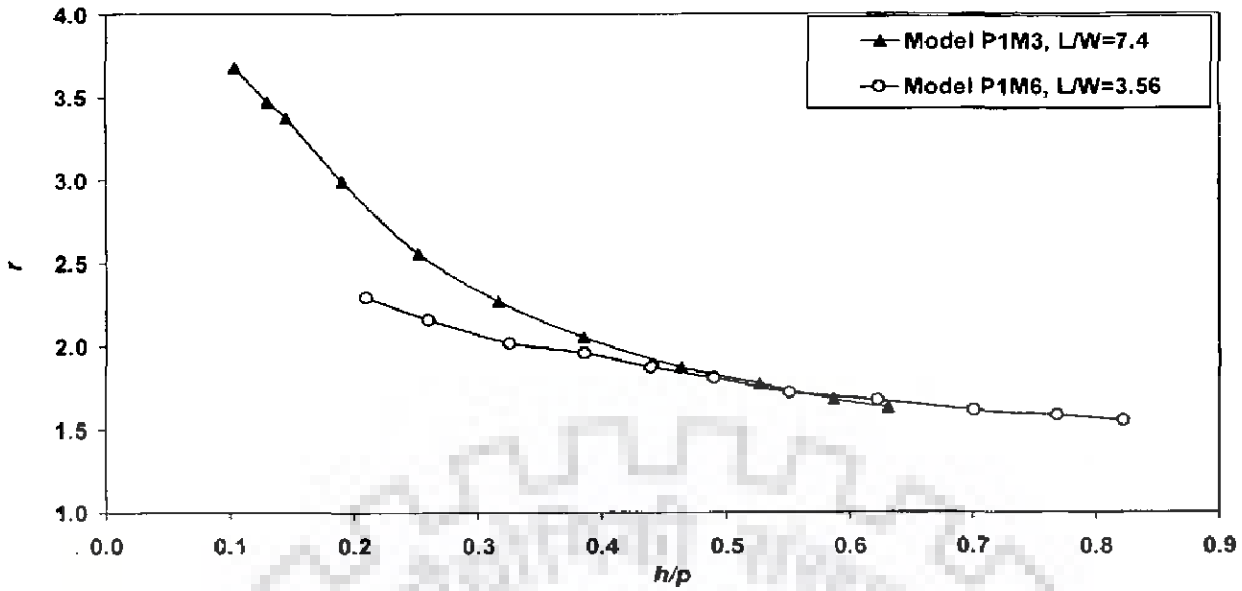

Fig. 4.9 Plot between *r* and *h/p* for model P_1M_3 & P_1M_6 with same *p* = 20 cm

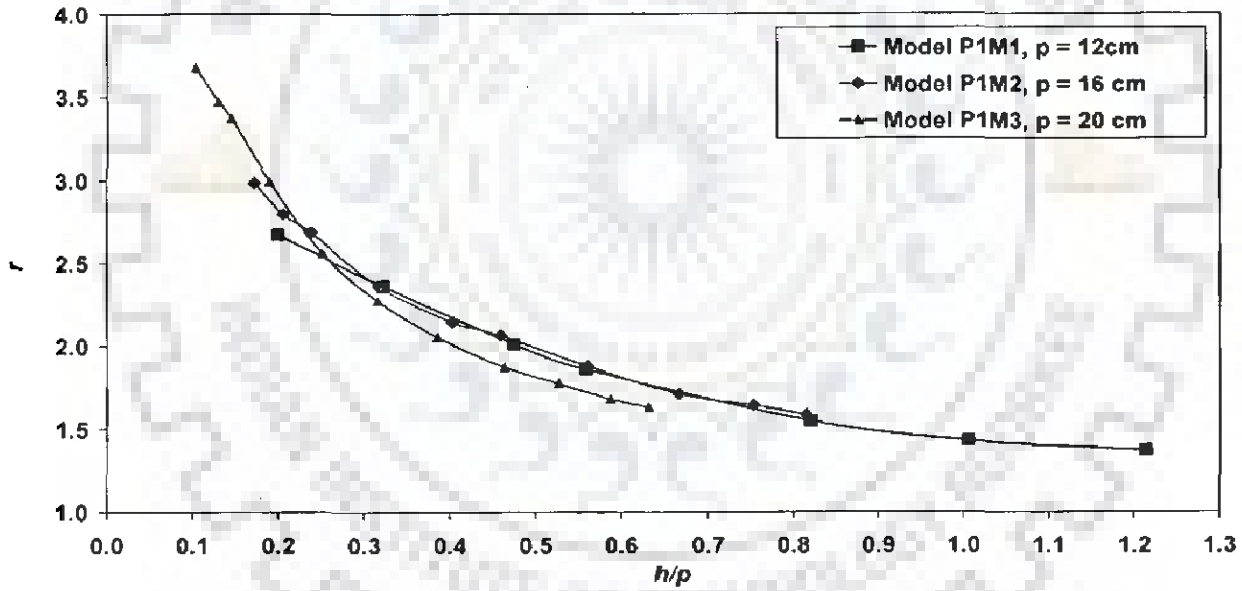

Fig. 4.10 Plot between *r* and *h/p* for same *L/W* = 7.4

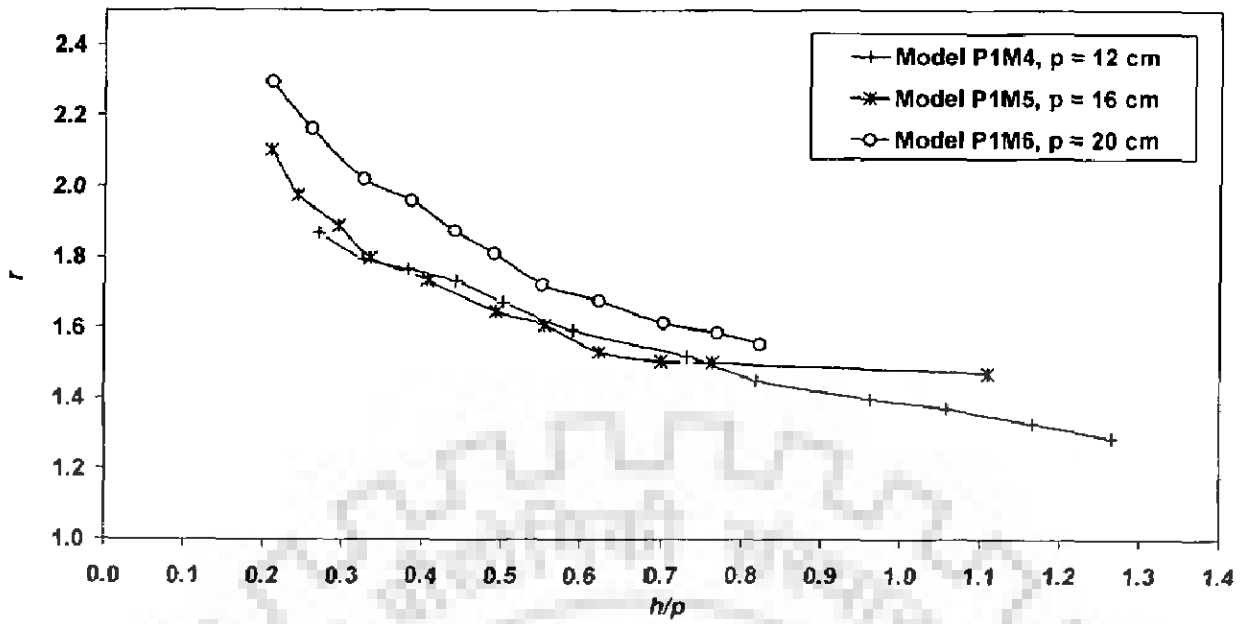

Fig. 4.11 Plot between *r* and *h/p* for same *L/W* = 3.56

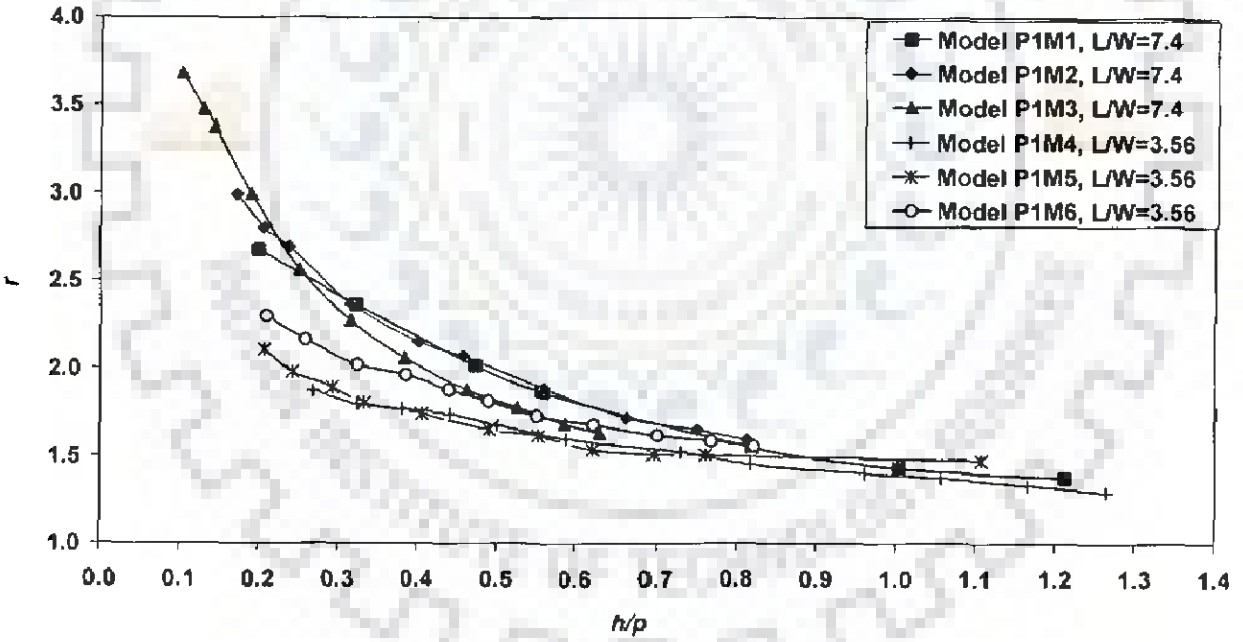

Fig. 4.12 Plot between *r* and *h/p* for all six models

4.5 EVALUATION OF SECOND PHASE EXPERIMENTS

In this phase of experiment, some modifications have been done in the first phase models for increased hydraulic efficiency. In this phase of the experiment, both sides ramps are provided in the first phase models.

The graphical representation between net absolute value of discharge increment (difference between ordinates of Q_L and Q_{PK}) for both side ramps and without ramps against (h/p) for all the six models is shown in Figs. 4.13-4.18. In Figs.4.13 to 4.18, one can see that net absolute value of discharge increment ΔQ is more for both side ramps than without ramps. It can be seen that the discharge increment increases in the presence of ramps. Graphical plots between 'r' and h/p for all six models are shown in Fig. 4.19. From Fig. 4.19, model P_2M_2 is found to perform better.

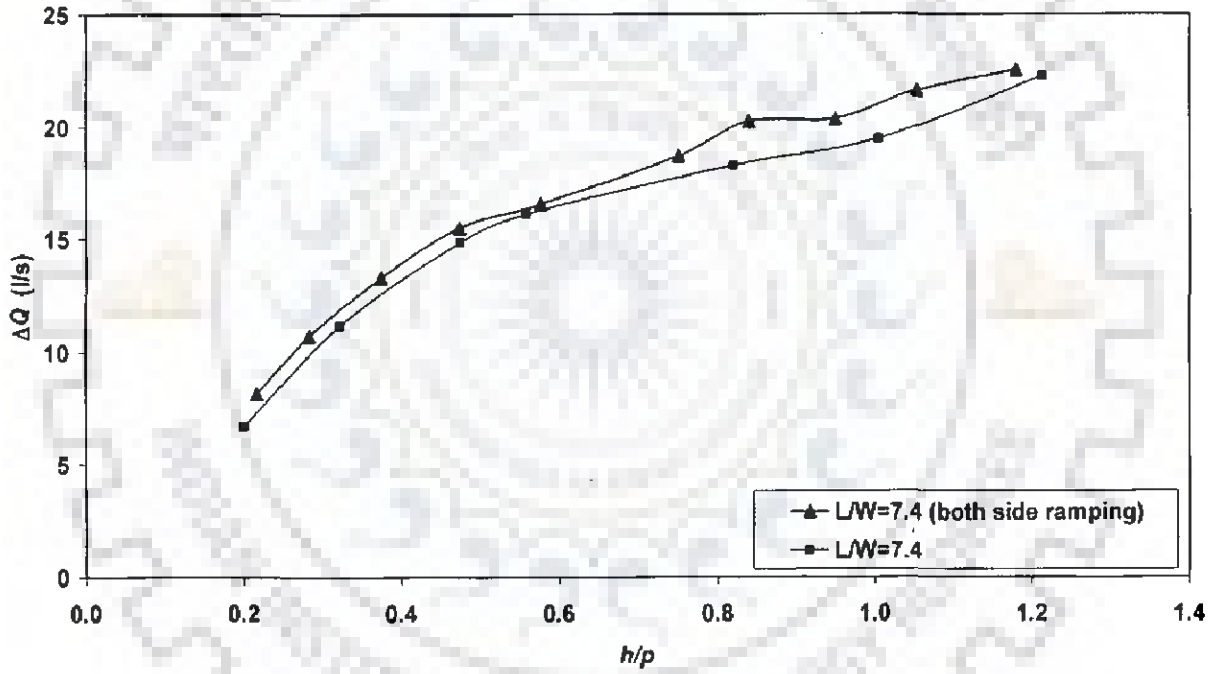

Fig. 4.13 Plot between ΔQ and h/p for model P_2M_1 with both side ramps and without ramps.

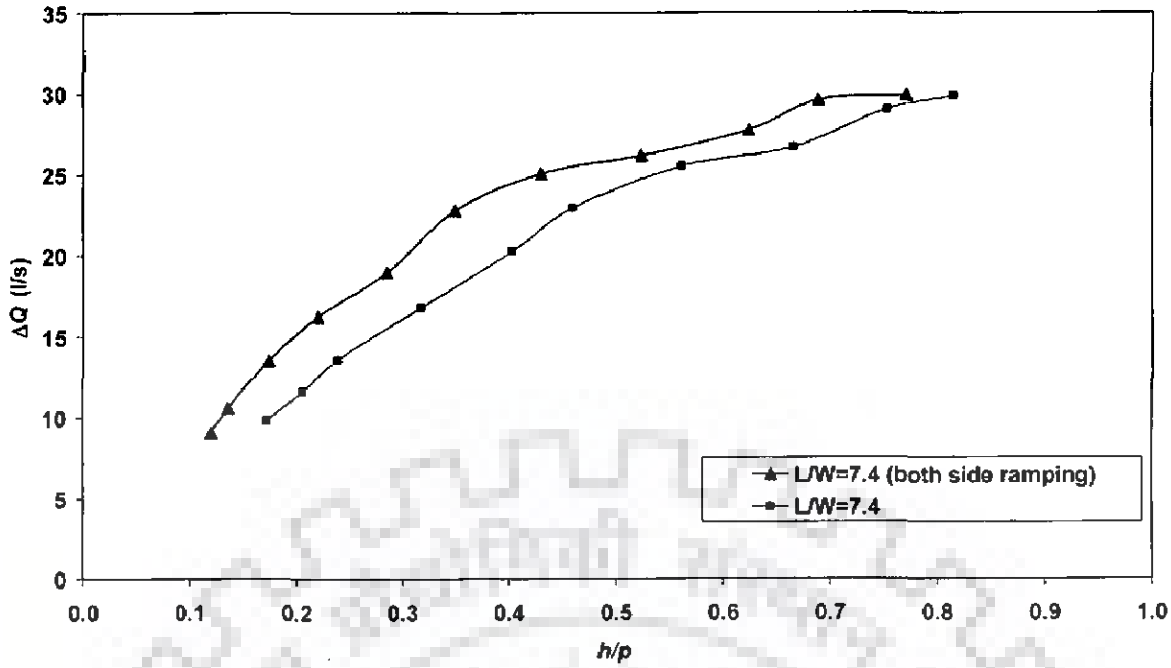

Fig. 4.14 Plot between ΔQ and h/p for model P_2M_2 with both side ramps and without ramps

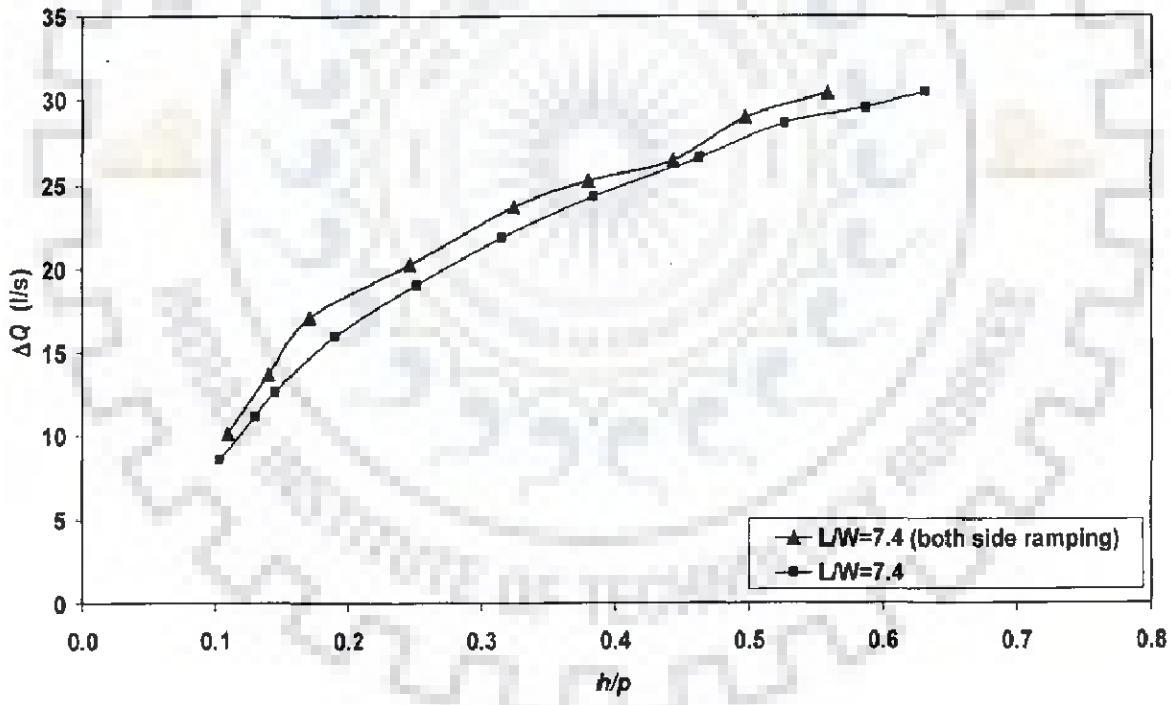

Fig. 4.15 Plot between ΔQ and h/p for model P_2M_3 with both side ramps and without ramps

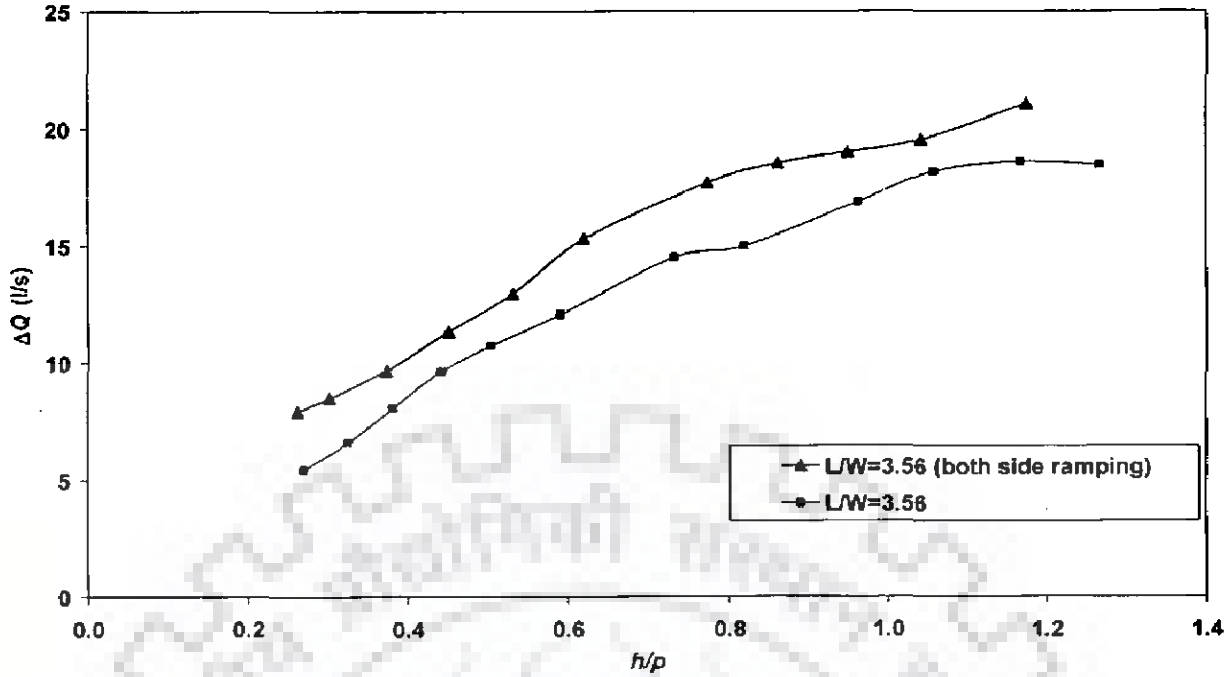

Fig. 4.16 Plot between ΔQ and h/p for model $P_2M_4$with both side ramps and without ramps

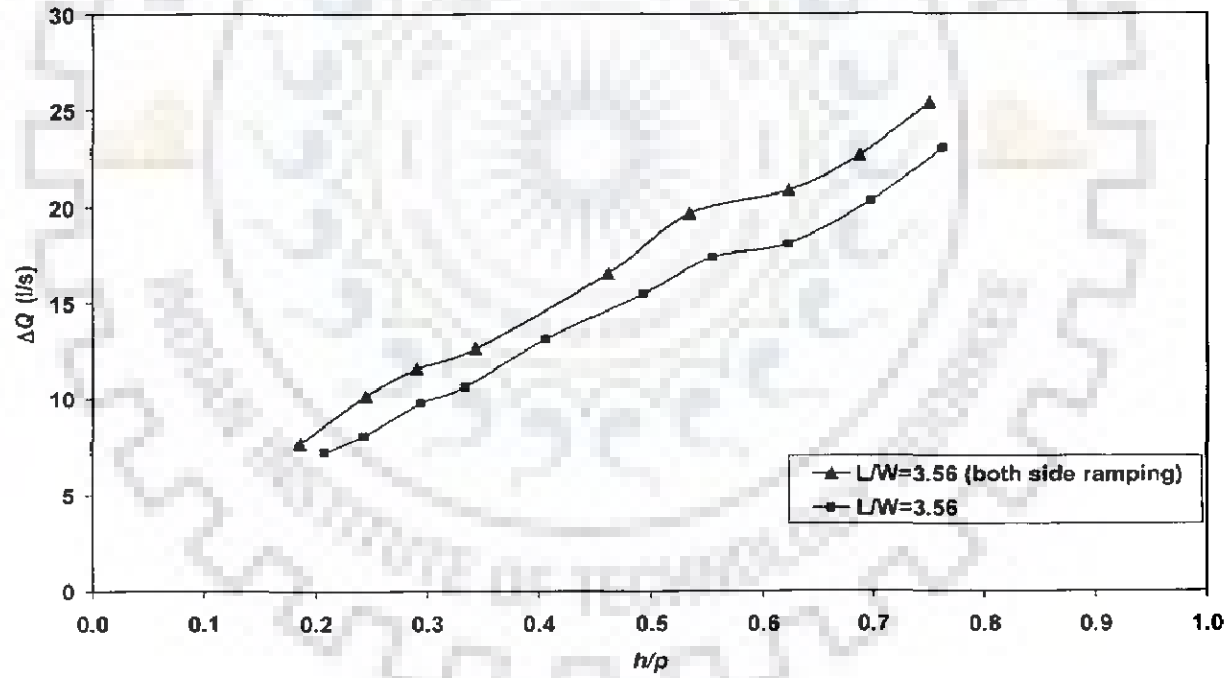

Fig. 4.17 Plot between ΔQ and h/p for model P_2M_5 with both side ramps and without ramps

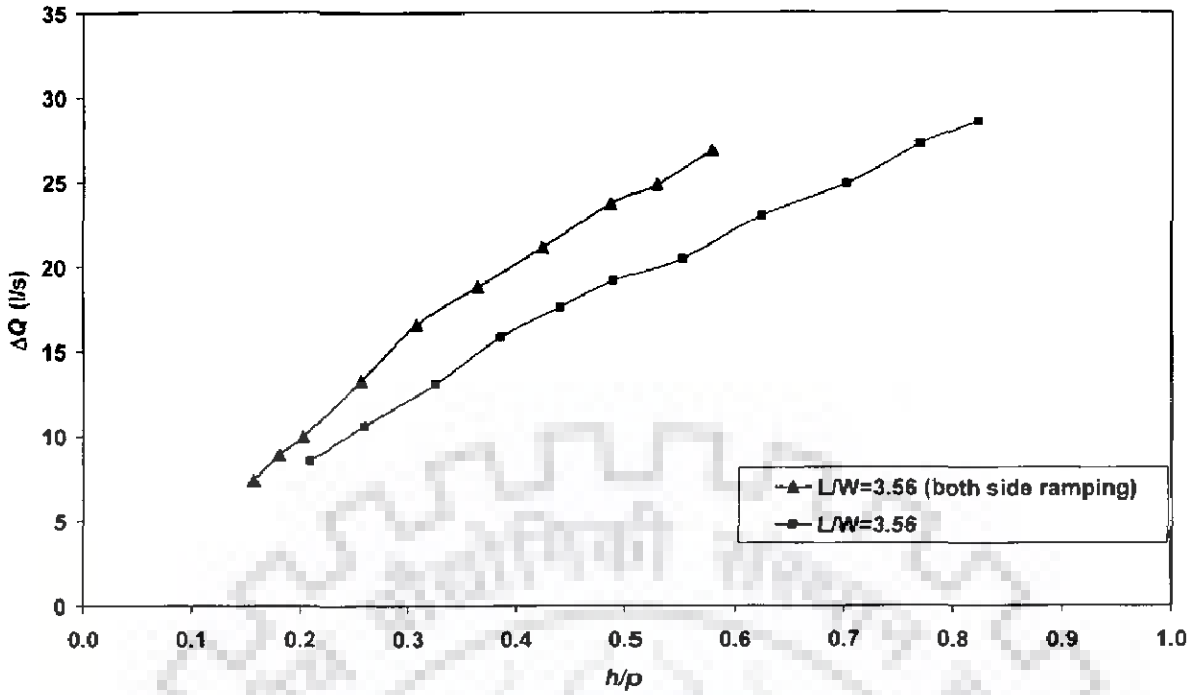

Fig. 4.18 Plot between ΔQ and h/p for model P_2M_6 with both side ramps and without ramps

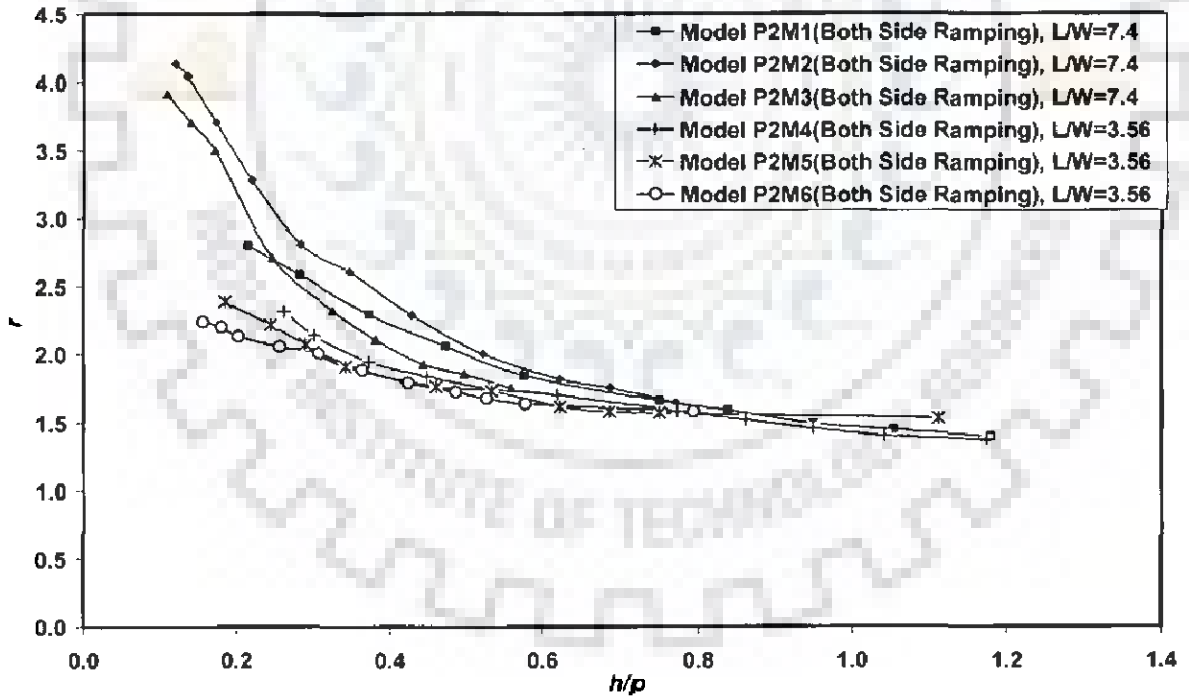

Fig. 4.19 Plot between r and h/p for all six models with both side ramps

4.6 EVALUATION OF THIRD PHASE EXPERIMENTS

The effect of changing widths of inlet and outlet cells has been studied in this phase of experiments. Here, the ratio of inlet to outlet cell is varied from 0.667 to 1.33. The model height is kept as 16 cm and in total six models having ramps and both side overhanging are fabricated and used.

Graphical plots between '*r*' and *h/p* for all six models in this phase are shown in Fig. 4.20. From Fig. 4.20, model P_3M_1 is found to perform better. It is also observed that effect of length magnification ratio *L/W* does not appear significant at *h/p* higher than 0.6.

Graphical plots between '*r*' and *h/(a+b)* for all six models is shown in Fig. 4.21 and this graph highlights the effect of inlet cell width (*a*) and outlet cell width (*b*). In Fig. 4.21, all 16 cm height of Piano Key Weir models have been considered including two second phase models P_2M_2 & P_2M_5 also. It can be seen from Fig. 4.21 that the value of '*r*' increases with increasing *a/b*. But for *L/W* 7.4, it is found that value of '*r*' increases with increasing *a/b* value upto 1, and after that there is no increment in value of *r*. Thus, *a/b* as unity appears to be a reasonable choice for larger *L/W* ratio.

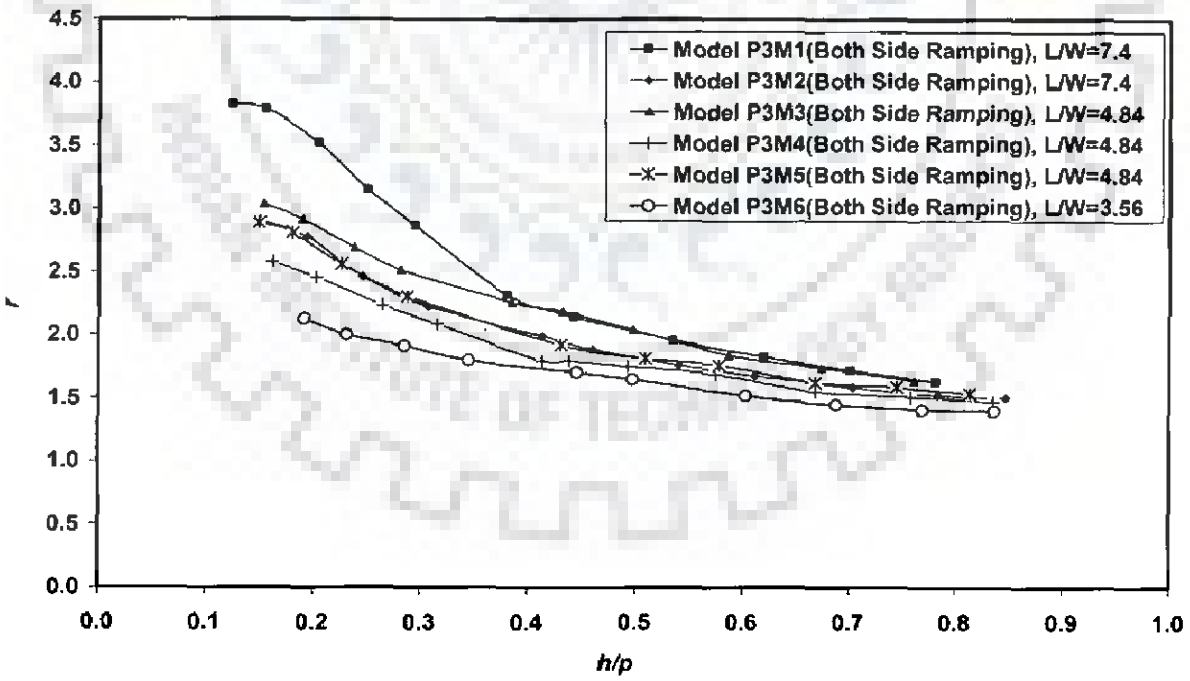

Fig. 4.20 Plot between *r* and *h/p* for all six Models of phase three

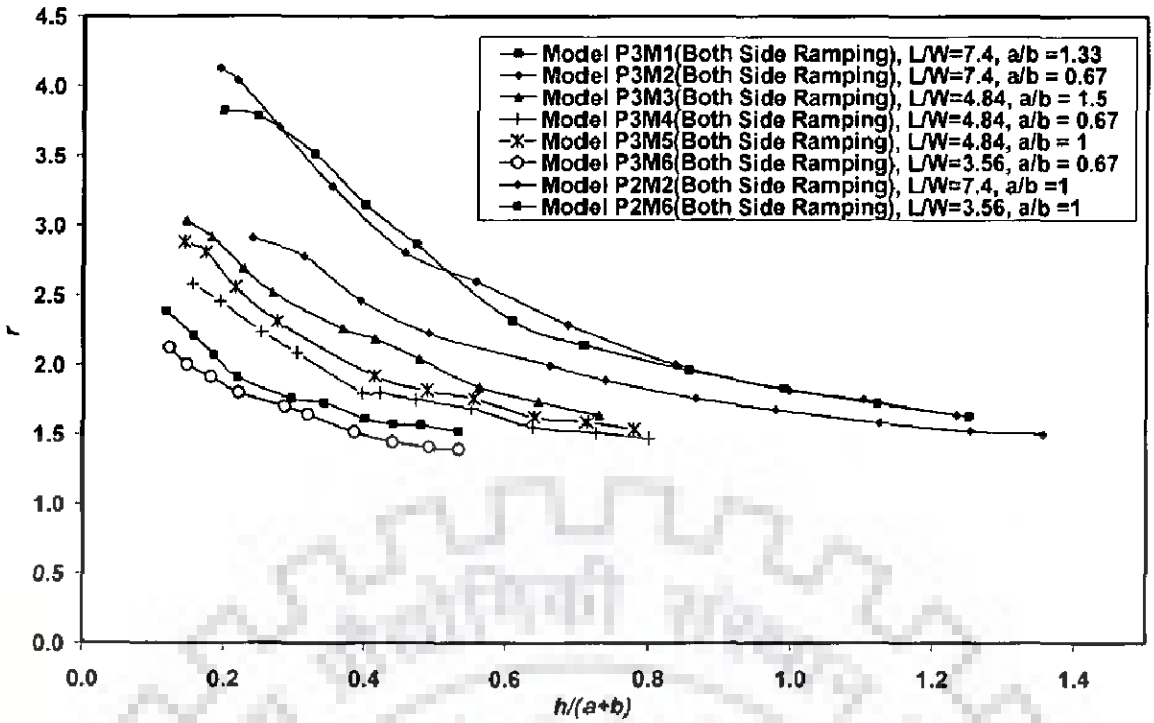

Fig. 4.21 Plot between *r* and *h/(a+b)*

4.7 EVALUATION OF FOURTH PHASE EXPERIMENTS

In the fourth phase of the experiment programme, the models of Piano Key Weir having only downstream side over hanging only are used. Details of the models used in this phase are given in Chapter 3. All the models used are having ratio of inlet to outlet cell widths as unity and mainly, the effect of varying *L/W* is studied.

The graphical representation between discharge and (*h/p*) for all the six models is shown in Figs. (4.22-4.26). In Figs. 4.22 to 4.26, it can be seen that discharge passing through Piano Key Weir (Q_{PK}) is more than discharge passing through rectangular sharp crested weir. Graphical plots between '*r*' and *h/p* for all five models is shown in Fig. 4.27. From Fig. 4.27, model P_4M_4 is found to perform better. It is observed from Fig. 4.27 that effect of length magnification ratio *L/W* reduces as *h/p* becomes greater than 0.6.

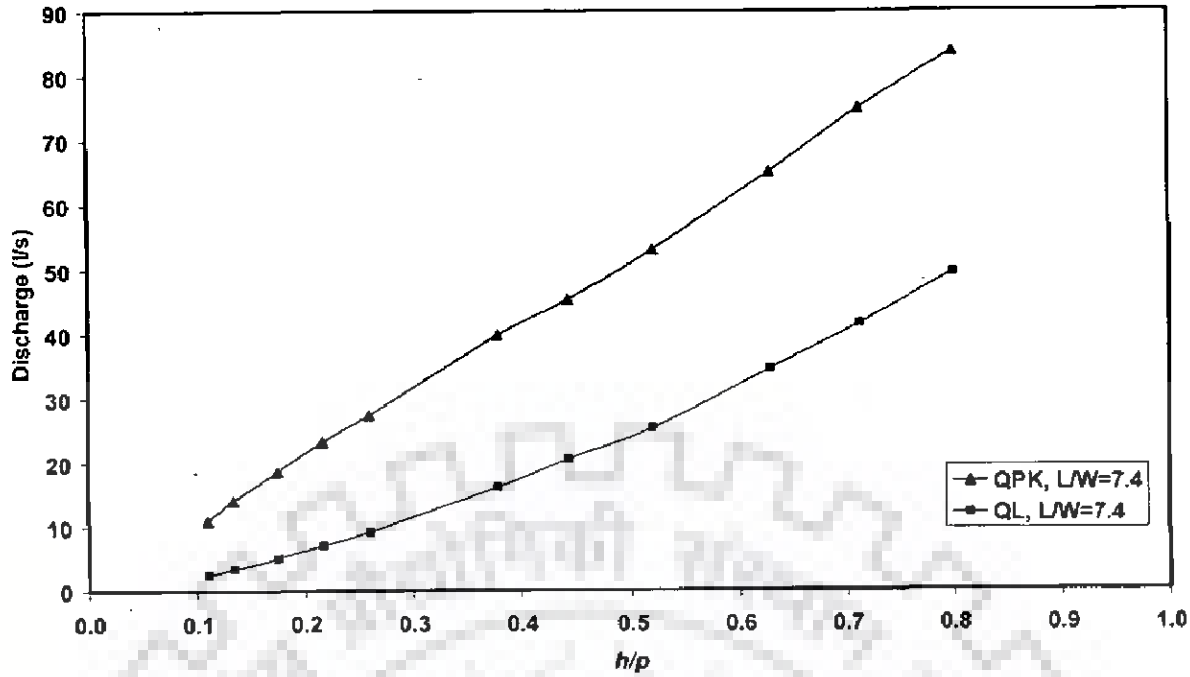

Fig. 4.22 Plot between Q_{PK}, Q_L and h/p for model P_4M_1 with both side ramps

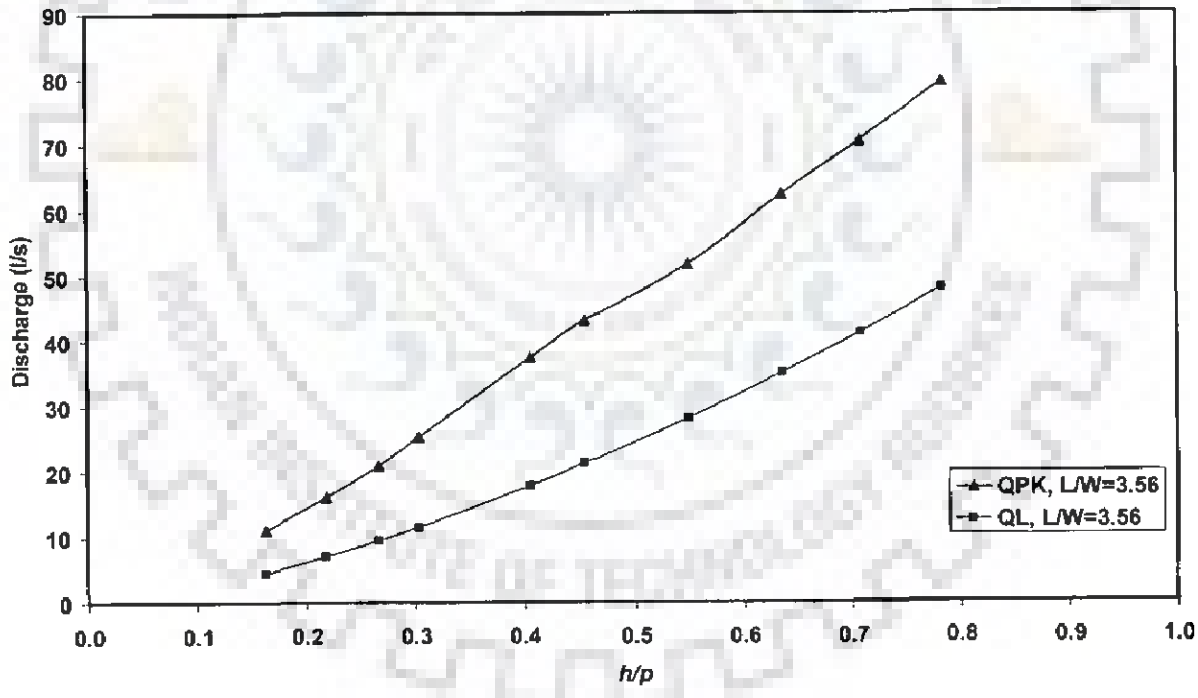

Fig. 4.23 Plot between Q_{PK}, Q_L and h/p for model P_4M_2 with both side ramps

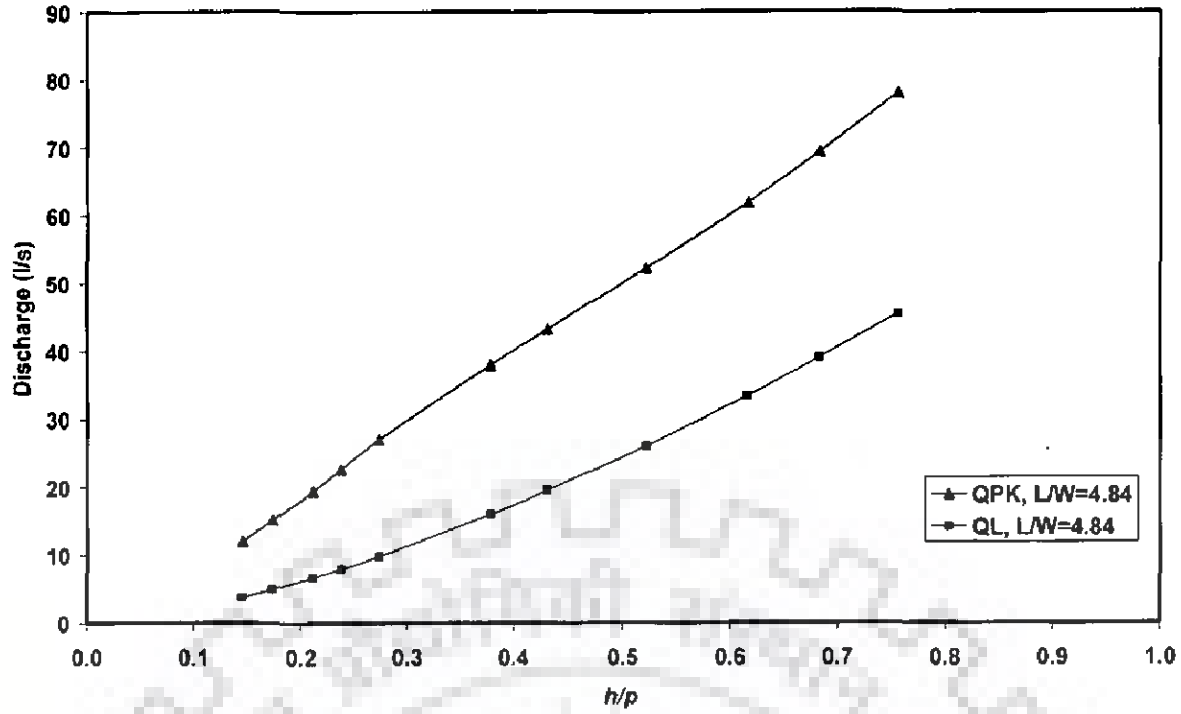

Fig. 4.24 Plot between Q_{PK}, Q_L and h/p for model P_4M_3 with both side ramps

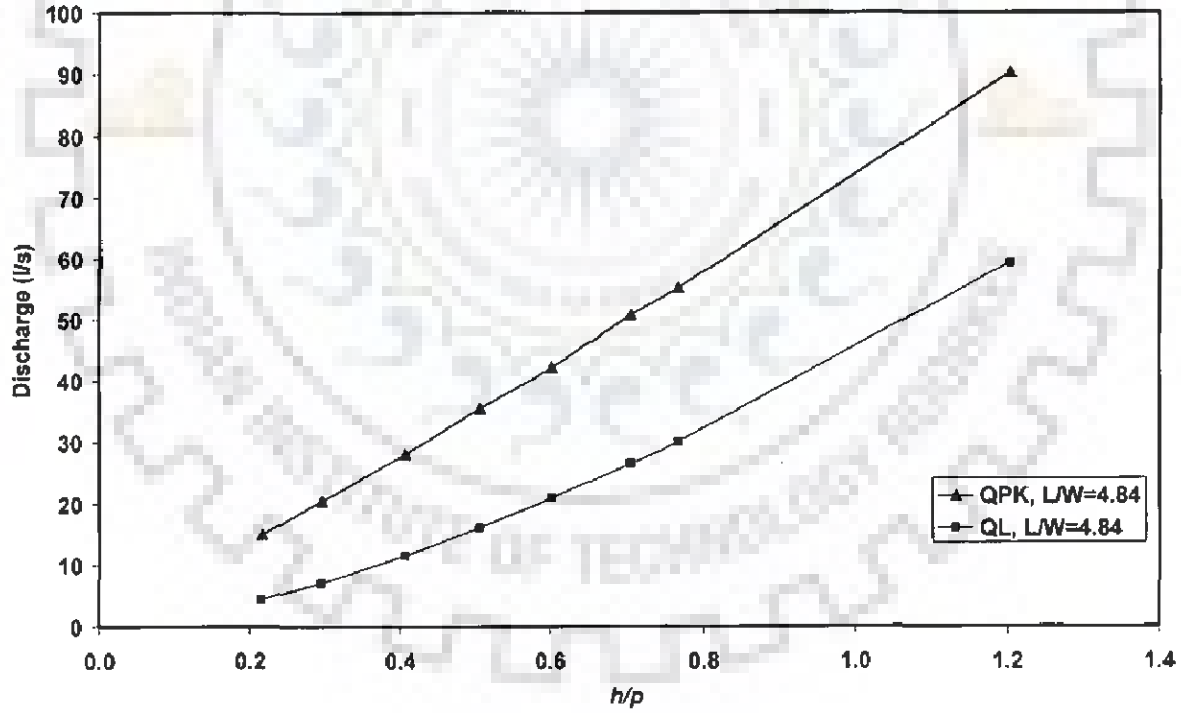

Fig. 4.25 Plot between Q_{PK}, Q_L and h/p for model P_4M_4 with both side ramps

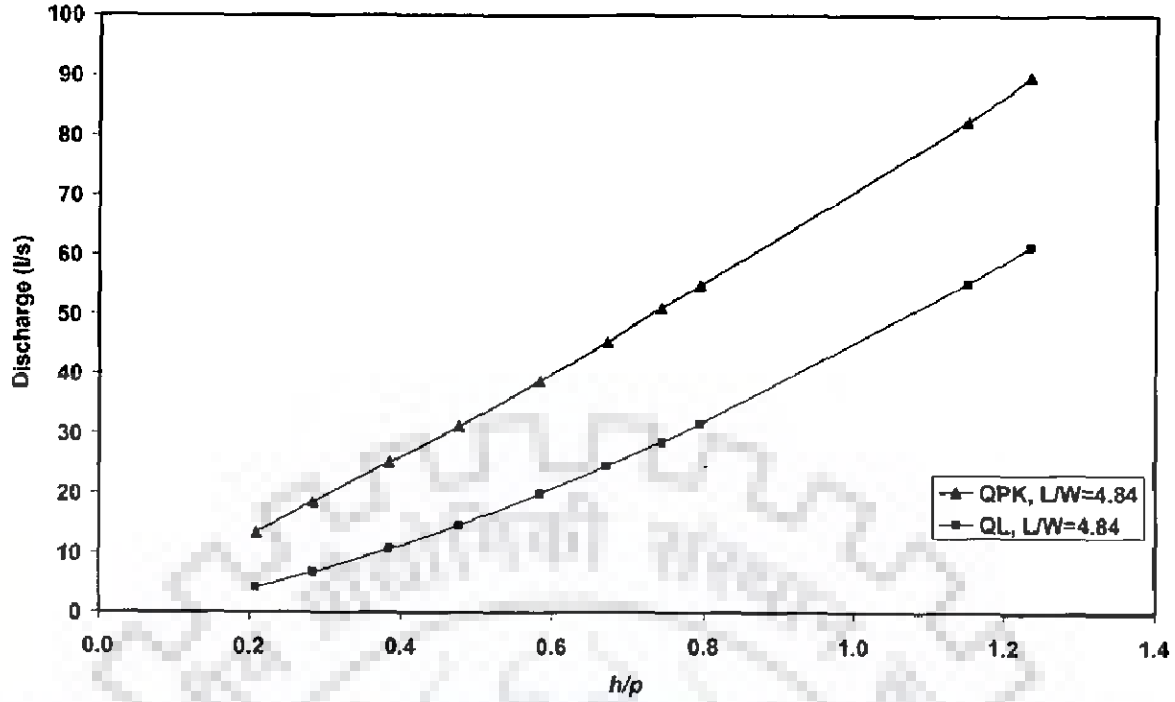

Fig. 4.26 Plot between Q_{PK}, Q_L and h/p for model P_4M_5 with both side ramps

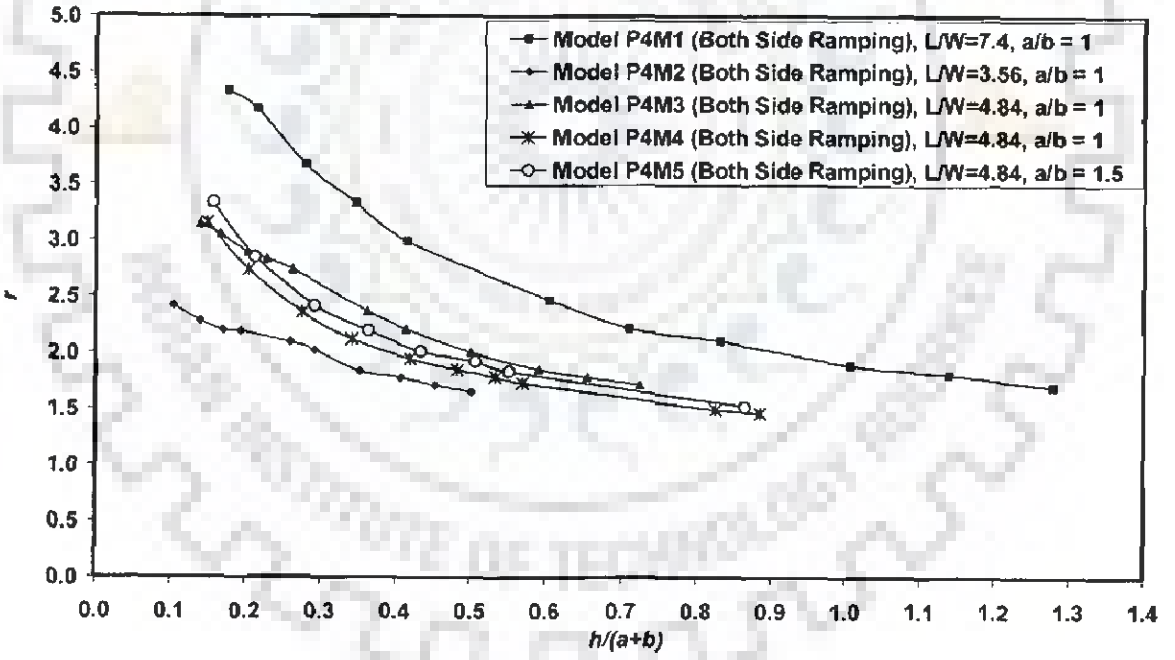

Fig. 4.27 Plot between r and h/p for all five models of phase four

4.8 EVALUATION OF FIFTH PHASE EXPERIMENTS

Here, the focus is modification of inlet and outlet cells by providing filling to ramps so that one ramp now consists of two steps and thus, a planar discontinuity. In total, three models are fabricated. Also, in two models, inlet portion is modified from a flat plate to a triangular prism shaped configuration. Details of these models are given in preceding chapter.

In Figs. 4.28 to 4.32, it could be seen that net absolute value of discharge increment ΔQ is not normally increased for all the modified models.

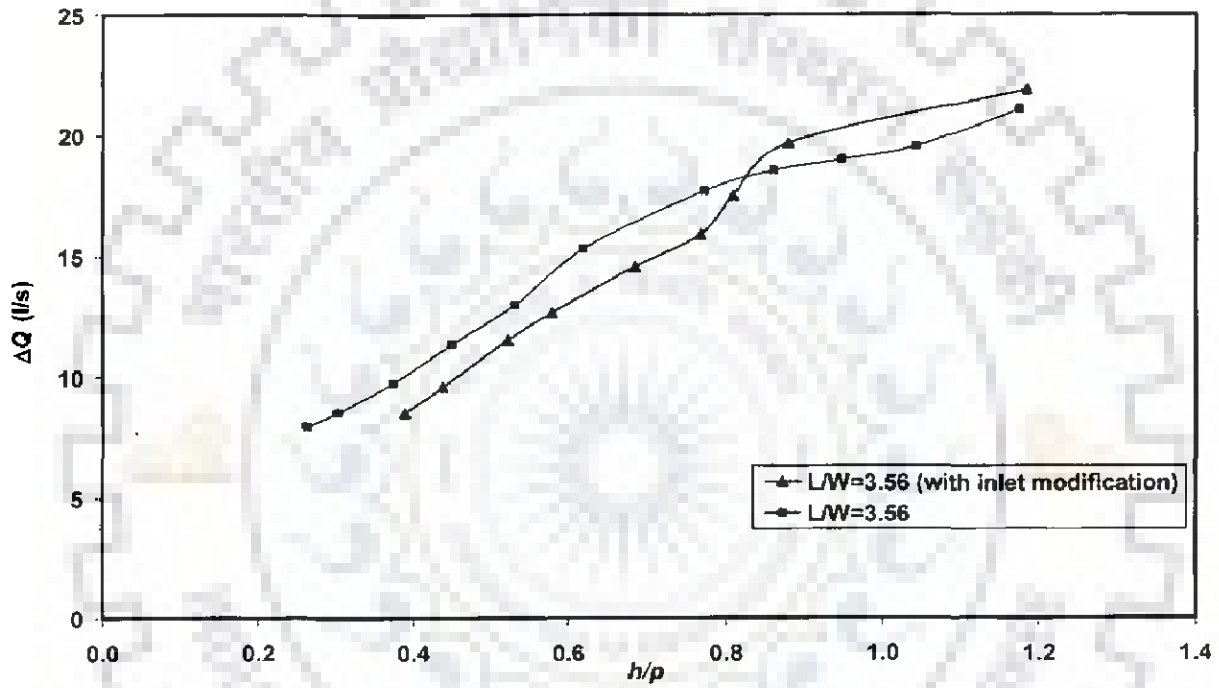

Fig. 4.28 Plot between ΔQ and h/p for model P_2M_4 & model P_2M_4 (with improving the hydraulic shape of inlet)

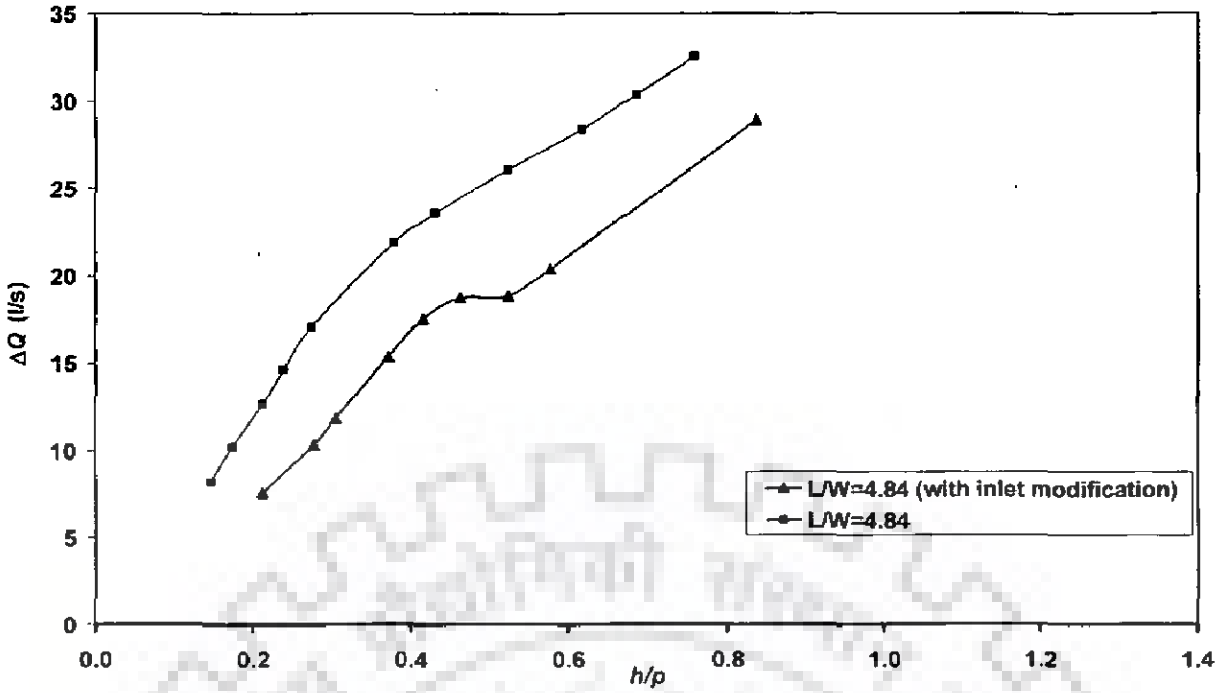

Fig. 4.29 Plot between ΔQ and h/p for model P_4M_3 & model P_4M_3 (with improving the hydraulic shape of inlet)

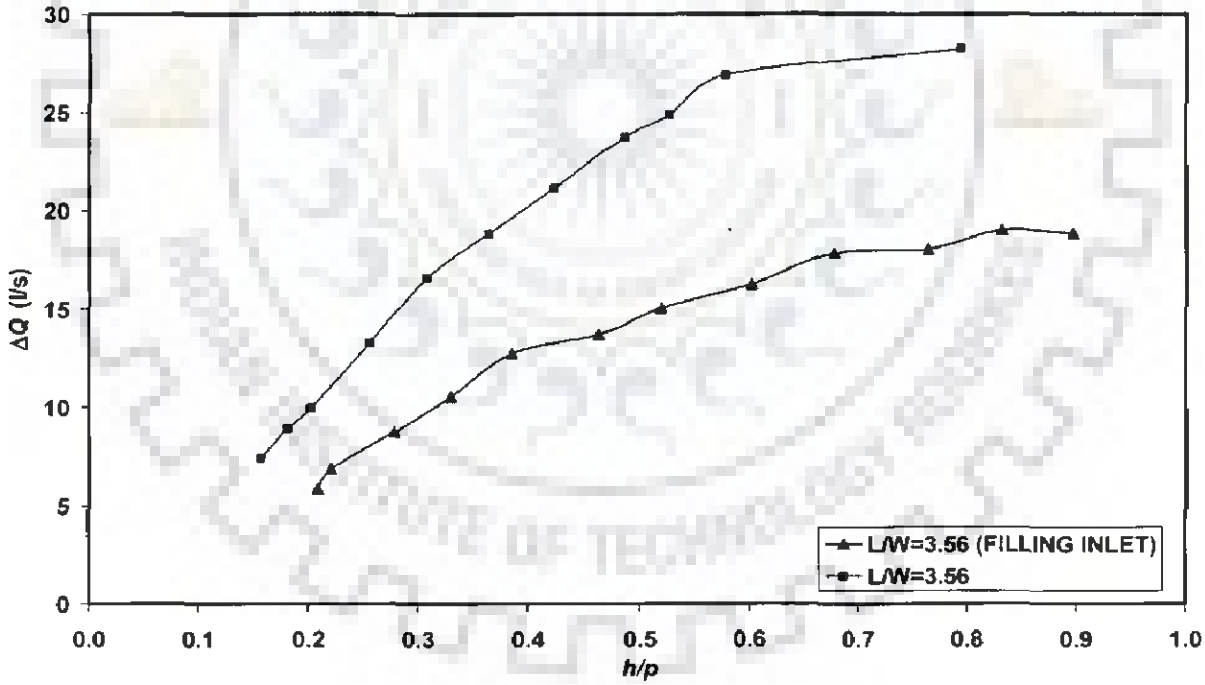

Fig. 4.30 Plot between ΔQ and h/p for model P_2M_6 (filling inlet cell)

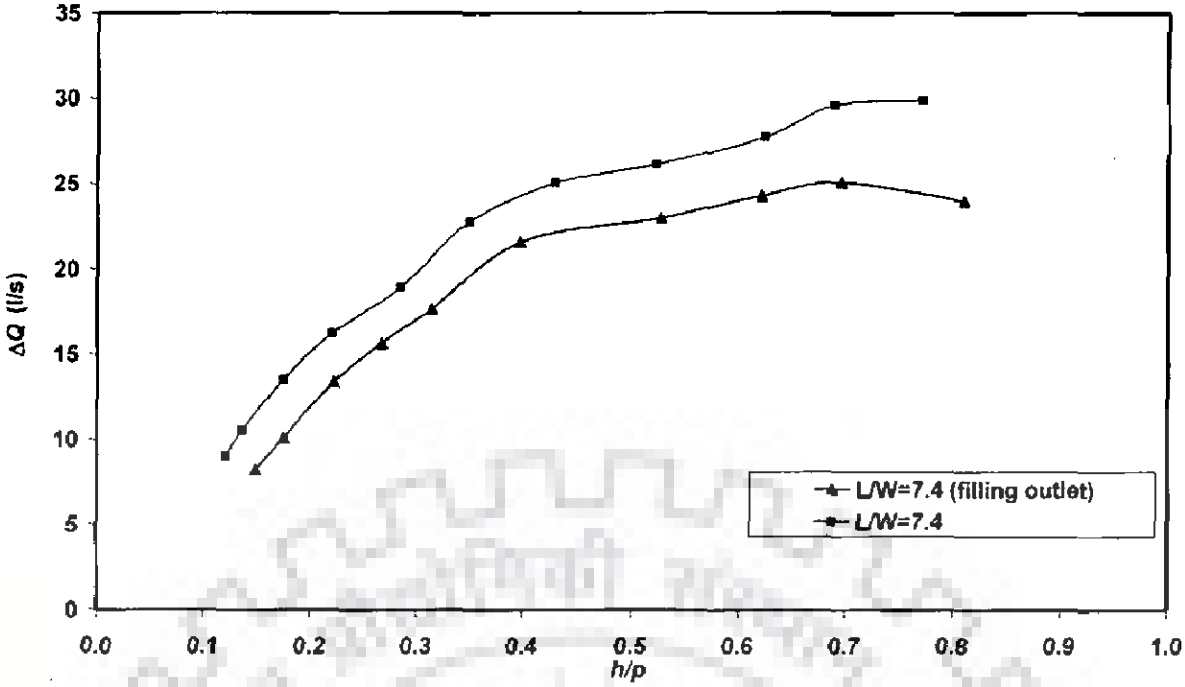

Fig. 4.31 Plot between ΔQ and h/p for model P_2M_2 (filling outlet cell)

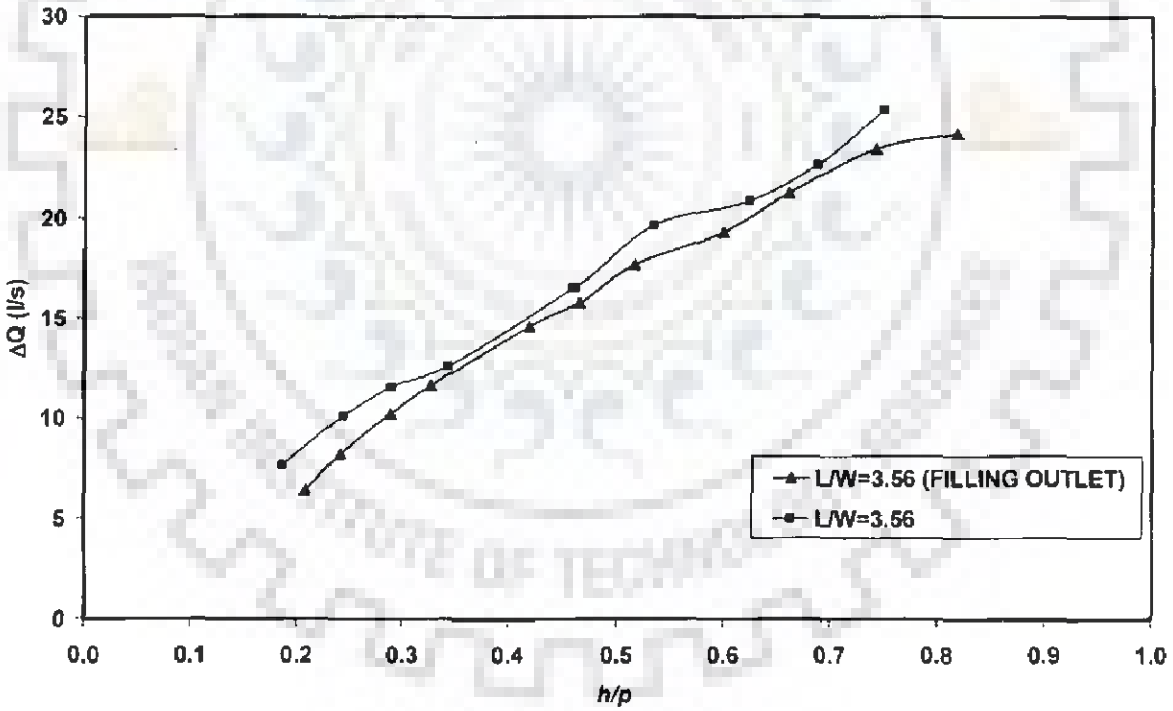

Fig. 4.32 Plot between ΔQ and h/p for model P_2M_5 (filling outlet cell)

4.9 SUMMARY

In this chapter, the experimental data collected in the present study towards evaluation of a most efficient shape of Piano Key Weir are subjected to a preliminary analysis. It is found that during all the phases of experiments, Piano Key Weir discharge is higher than linear weir discharge for a given head. Similarly, the discharge passing capacity of Piano Key Weir at a given head improves with increasing *L/W* ratio and for this reason, the choice of inlet to outlet cell width should be kept as unity, as deviation from this is not helpful in the magnification of discharge. Various modifications to inlet and outlet cells are also not found useful. Piano Key Weir with ramps and having overhanging sides are found to perform better. A further interpretation of performance of both sides overhanging (u/s and d/s) and one side overhanging (d/s) of Piano Key Weir is also presented in Chapter 6.

CHAPTER – 5

PIANO KEY WEIR –A CASE STUDY

5.1 GENERAL

This chapter presents investigation related to application of typical Piano Key Weir for Sawra Kuddu Hydro Electric Project. Sawra Kuddu HEP with an installed capacity of 111 MW is located on Pabbar River in Himachal Pradesh. Laugier (2007) has studied other form of Piano Key Weir for Goulours Dam in France. He conducted the model test in flume with geometrical similar scale based on Froude law. Laugier has reported that Piano Key Weir is used for rehabilitation project in Goulours dam. In Sawra Kuddu HEP, the flow diversion structure consists of four under-sluices bays on the left and three on the right bank, each of 8.00 m width with 1.50 m thick intermediate piers. A 138 m long Piano Key Weir is proposed in between the two sets of under-sluices. The design discharge of the project is 6880 m^3/s. The Piano Key Weir is designed to handle 3900 m^3/s and the balance discharge 2980 m^3/s passes through under-sluices. This chapter focuses on the experimental results and optimization procedure of the evacuation system of Sawra Kuddu HEP with the Piano Key Weir. The physical modeling has been carried out at the laboratory of River engineering at the Water Resources Development and Management department (WRD&M), IITR, Roorkee, India. A comprehensive investigation based on physical model studies on a flume has been undertaken to evolve the best suitable Piano Key Weir elements to assess the behaviour of the Sawra Kuddu HEP. A comparison of observed and computed discharges is presented in Chapter 6, after developing different functional relationships for C_d variation.

5.2 EXPERIMENTAL STUDIES

Combining the experience of preceding experiments, some more physical model studies have been conducted to evolve optimal Piano Key Weir elements of the Sawra Kuddu HEP. A wide flume having perspex walls to visualize the flow was installed at River Engineering Lab of WRD&M IIT-Roorkee. Six Piano Key Weir models built to non-distorted geometrically similar scale of 1:50 molded in transparent acrylic sheet were installed in the flume during experimentation. The models were developed based on Froude law. These models represent a gross waterway of 50.00 m. The dimensions of Piano Key Weir for physical model study in laboratory are indicated in Table 5.1. The plan and sectional view of Piano Key Weir for physical model study are shown in Figs.

5.1 to 5.6. 1.00 m out of 2.76 m width of Piano Key Weir is selected from centre for physical model study in the flume. The total width of Piano Key Weir is 2.76 m. The maximum discharge adopted for model studies was 2500 m^3/s. The discharge scale as per Froude Law was worked out to 1/17678. Using this, the maximum flume discharge was found as 51.23 l/s. The studies were aimed mainly on assessing the better hydraulic efficiency.

The discharge was measured over a V-notch installed at the downstream of the flume. The water levels were measured by pointer gauge having least count of 0.01 cm. All the models were run for 8 to 10 different nappe heights. Pictorial view of all the models is shown in plate no. 5.1 to 5.6.

A comprehensive investigation has been done based on physical model studies on a flume to evolve best suitable Piano Key Weir elements to assess the behaviour of the Sawra Kuddu Barrage system. Comprehensive model constructed at outdoor lab of WRD&M, IIT, Roorkee has reproduced the actual topography of the valley including part of reservoir, designed Piano Key Weir and down stream side of weir. The model extends approximately 400 m upstream of the weir and 150 m down stream of the weir. Here, the Piano Key Weir is installed with full width of 2.76 m in geometric similar model i.e. 138.00 m in Prototype dimension.

The dimensions of Piano Key Weir for prototype are as indicated below in Table 5.2. The plan and sectional view of Piano Key Weir for comprehensive physical model study are shown in Fig. 5.7 and the plan and sectional view of Piano Key Weir for prototype with dimension are shown in Figs. 5.8. The pictorial view of model C_1M_6 in field is shown in Plate No. 5.7.

Table 5.1: Piano Key Weir dimensions for model study

Model No.	Height of Model (p) (cm)	a (cm)	b (cm)	$a+b$ (cm)	L/W	No. of Element
C_1M_1	18.40	14.80	26.28	41.08	3.74	2.5
C_1M_2	18.40	26.30	26.3	52.6	2.96	2
C_1M_3	18.40	19.72	19.72	39.44	3.74	2.5
C_1M_4	18.40	13.14	13.14	26.28	5.10	4
C_1M_5	18.40	16.00	11.60	27.6	4.91	3.5
C_1M_6	18.40	13.80	13.80	27.6	4.91	3.5

Table 5.2: Piano Key Weir dimensions for prototype

Model No.	Height of Model (p) (m)	a (m)	b (m)	$a+b$ (m)	L/W	No. of Element
C_1M_6	9.20	6.90	6.90	13.82	4.91	10

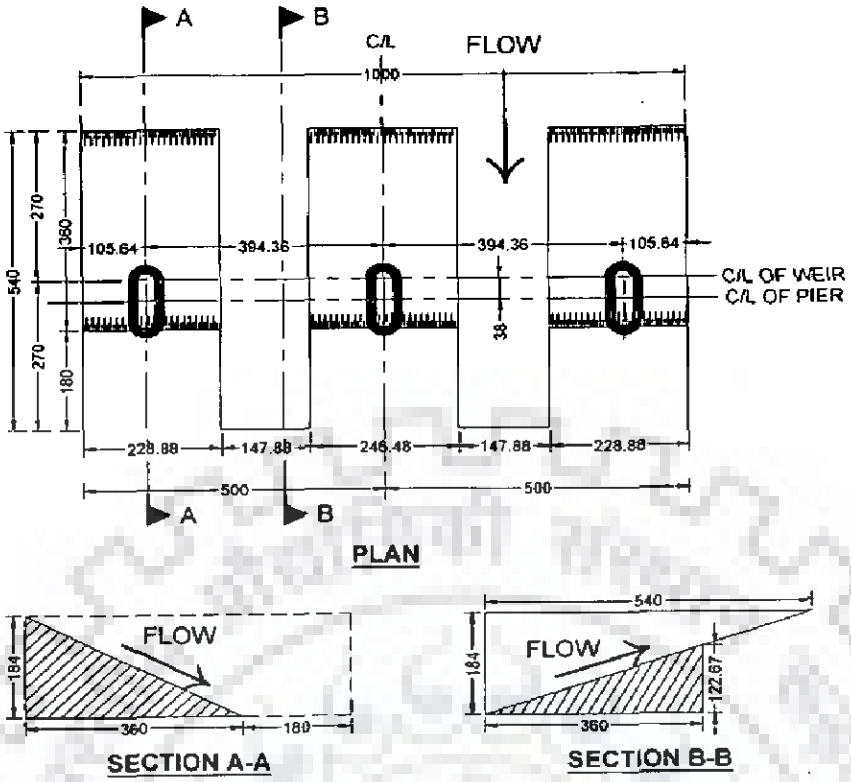

Fig. 5.1 Plan and section of model C_1M_1 for physical model study (dimensions in mm)

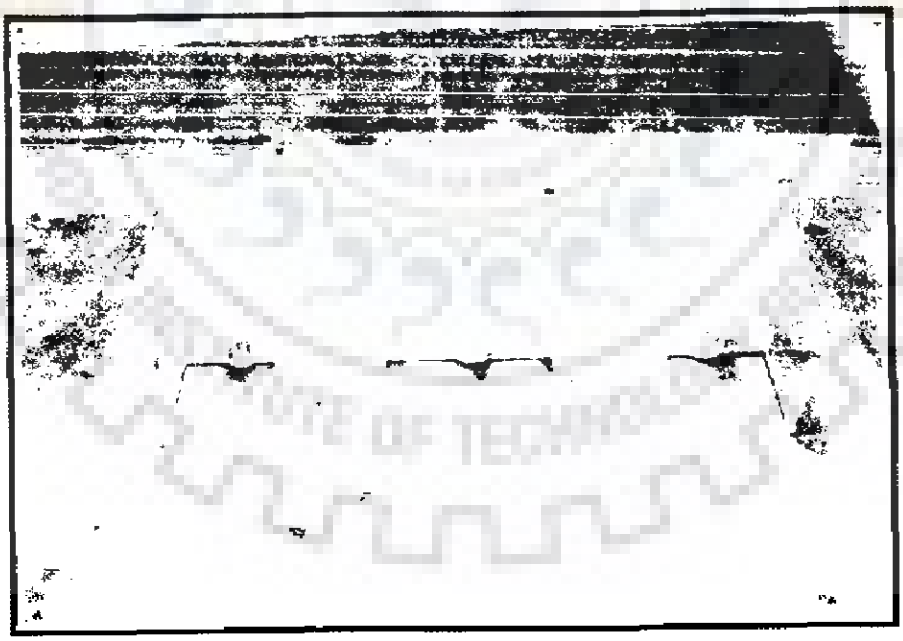

Plate No. 5.1 Model C_1M_1

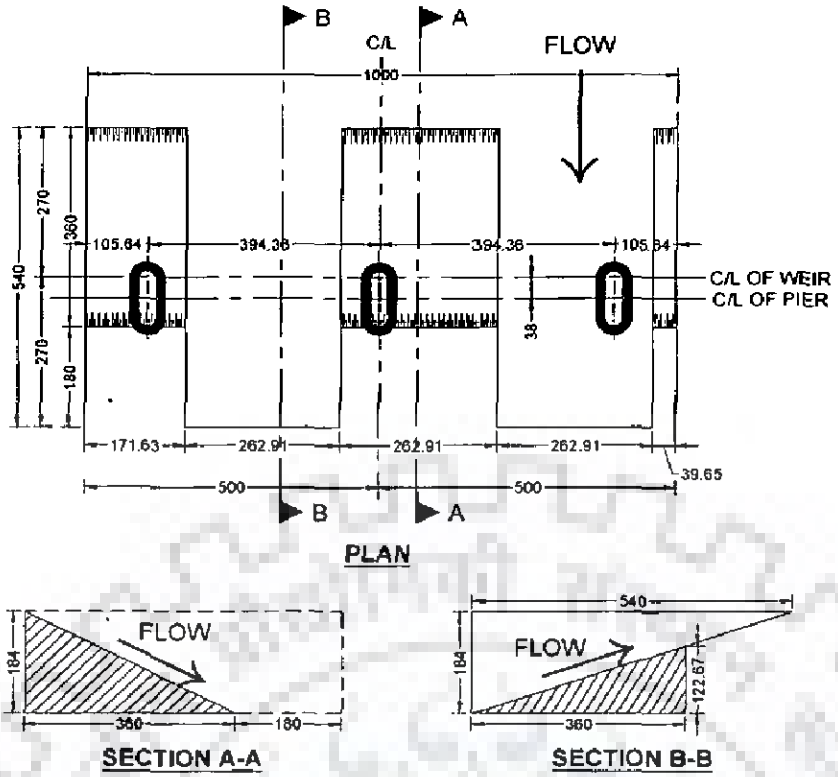

Fig. 5.2 Plan and section of model C_1M_2 for physical model study (dimensions in mm)

Plate No. 5.2 Model C_1M_2

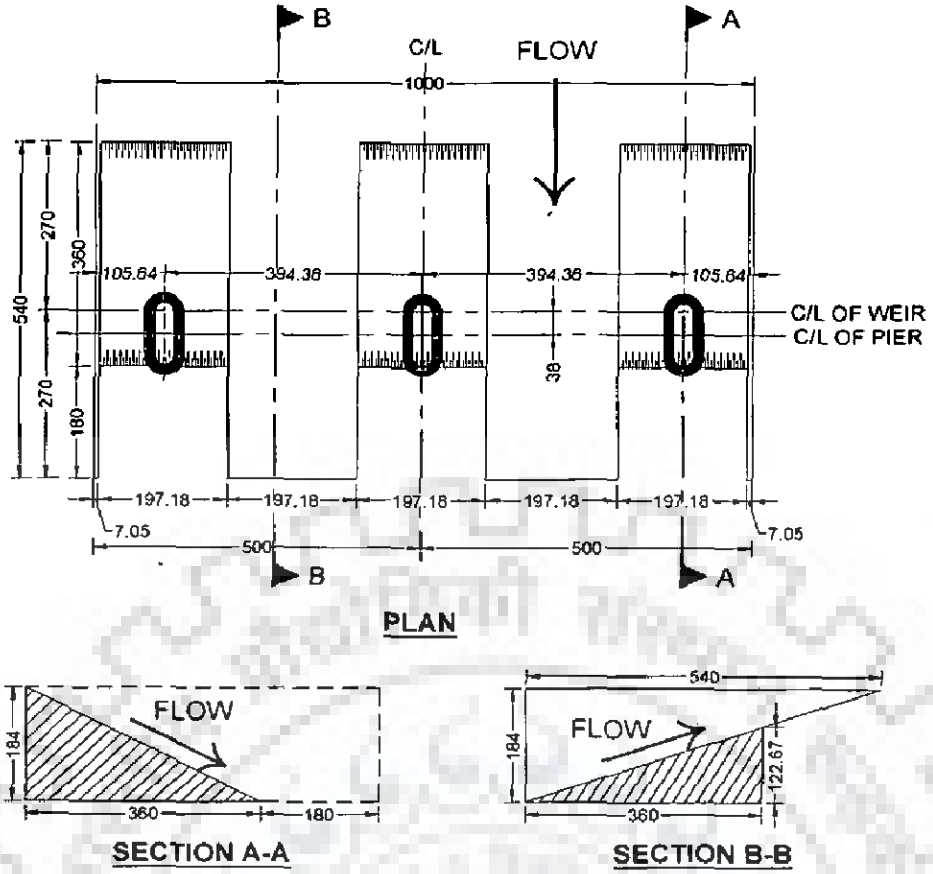

Fig. 5.3 Plan and section of model C_1M_3 for physical model study (dimensions in mm)

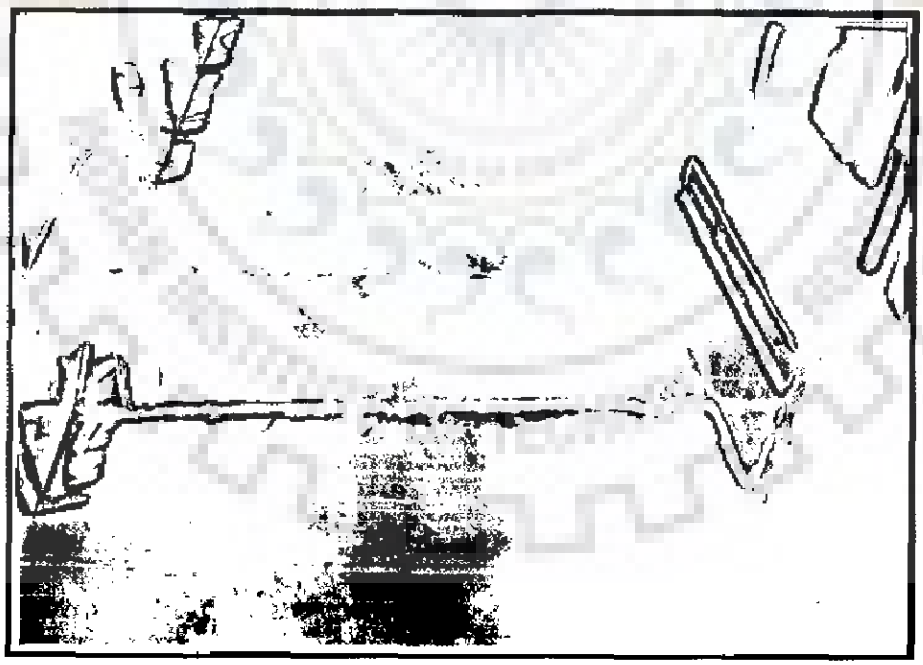

Plate No. 5.3 Model C_1M_3

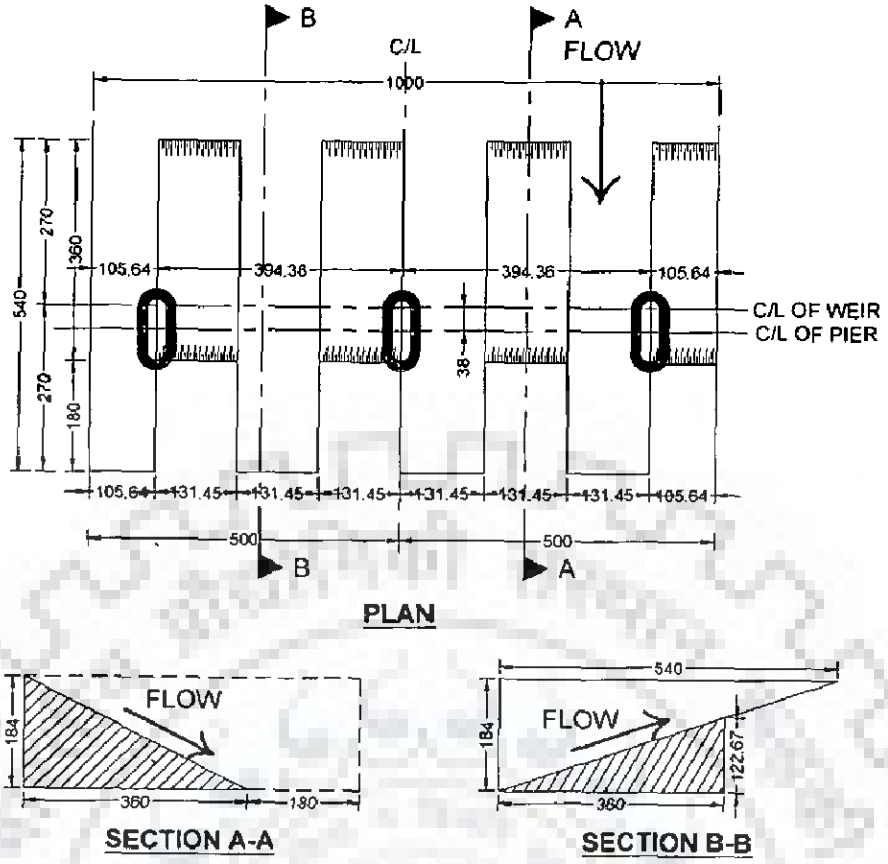

Fig. 5.4 Plan and section of model C_1M_4 for physical model study (dimensions in mm)

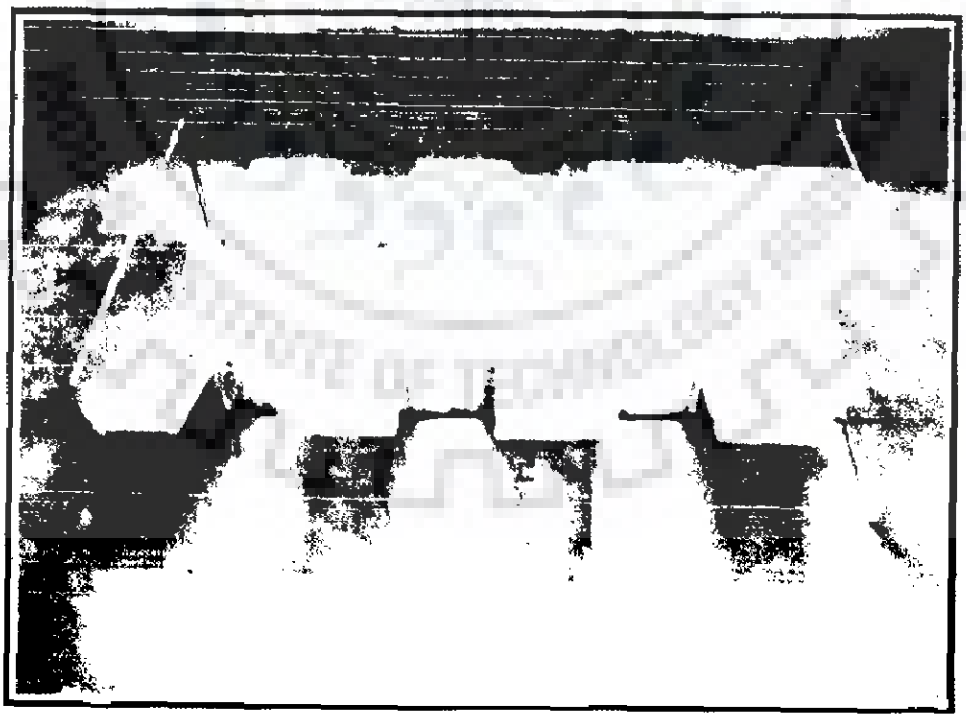

Plate No. 5.4 Model C_1M_4

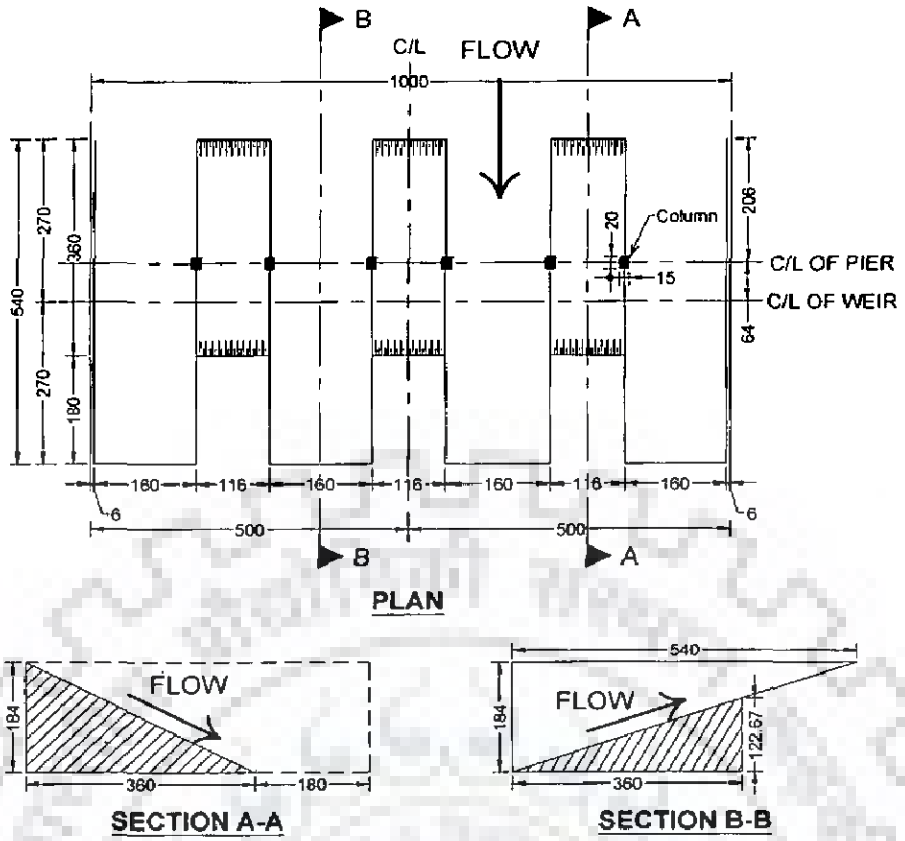

Fig. 5.5 Plan and section of model C_1M_5 for physical model study (dimensions in mm)

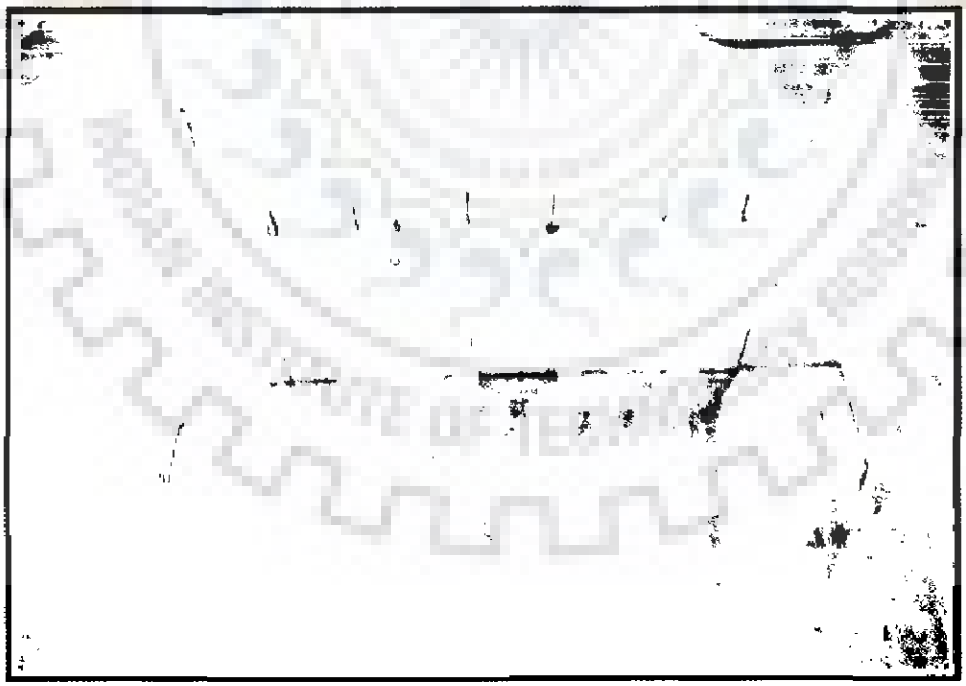

Plate No. 5.5 Model C_1M_5

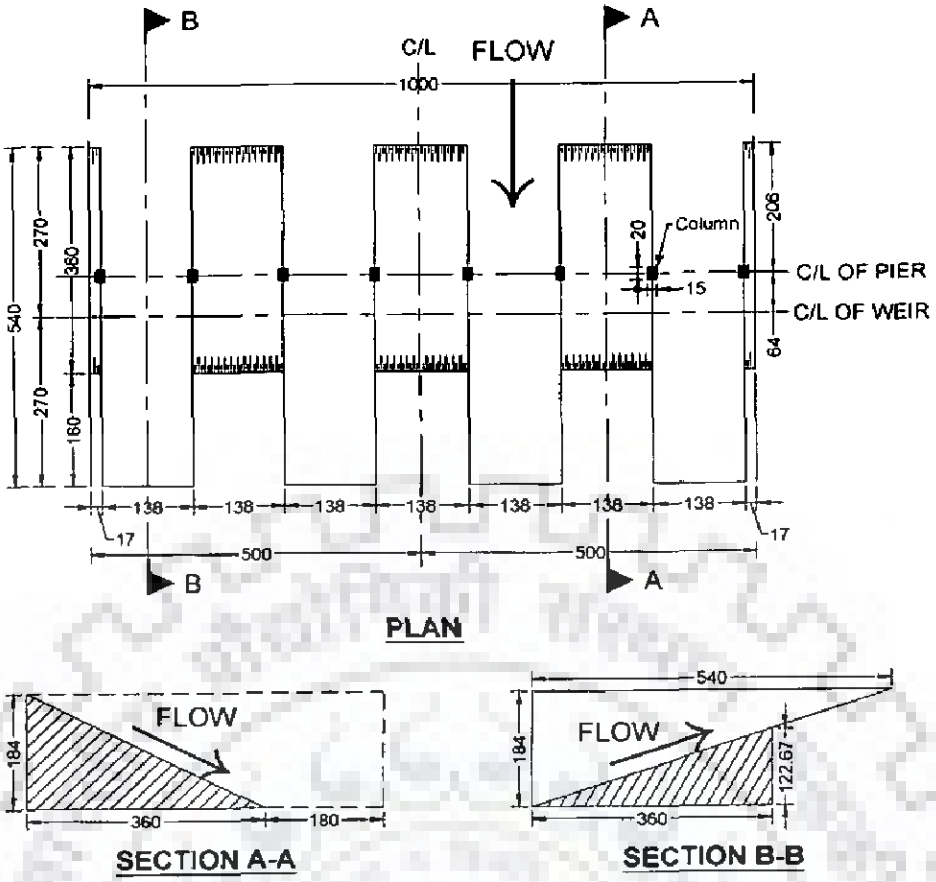

Fig. 5.6 Plan and section of model C_1M_6 for physical model study (dimensions in mm)

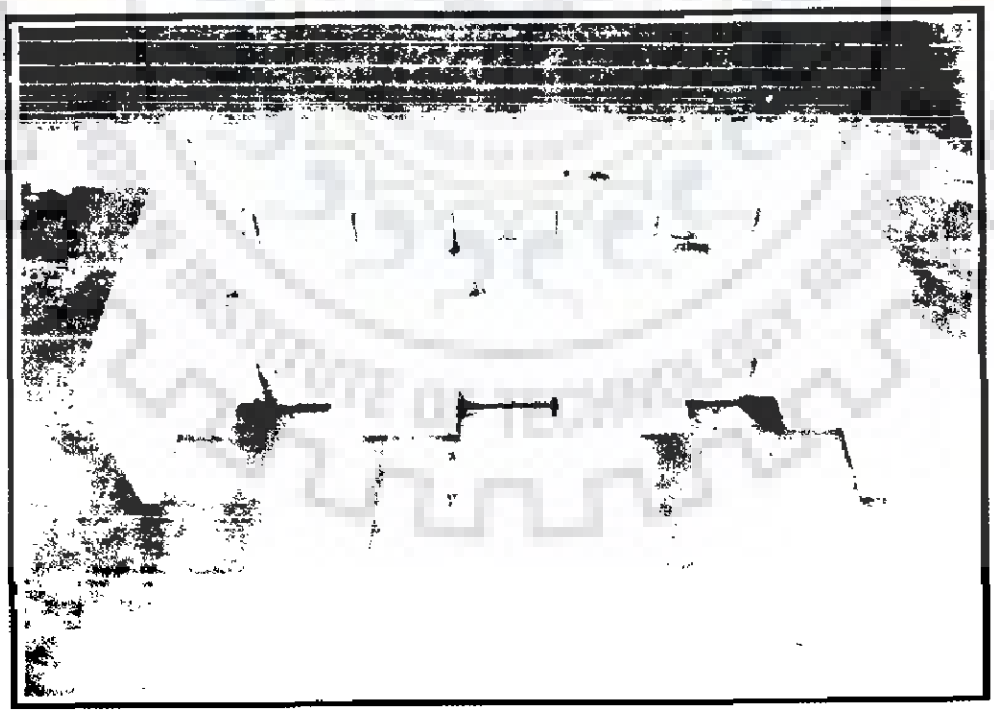

Plate No. 5.6 Model C_1M_6

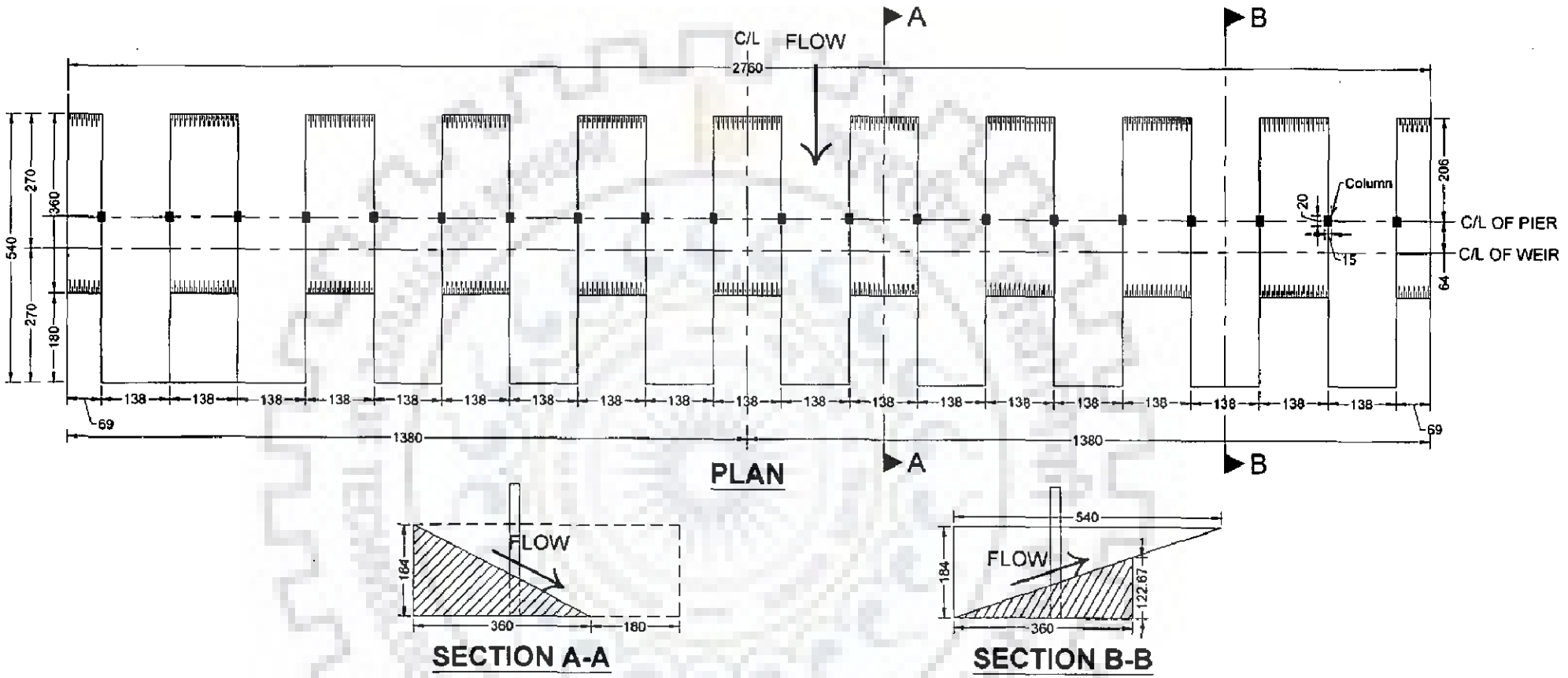

Fig. 5.7 Plan and section of model C_1M_6 for comprehensive model study (dimensions in mm)

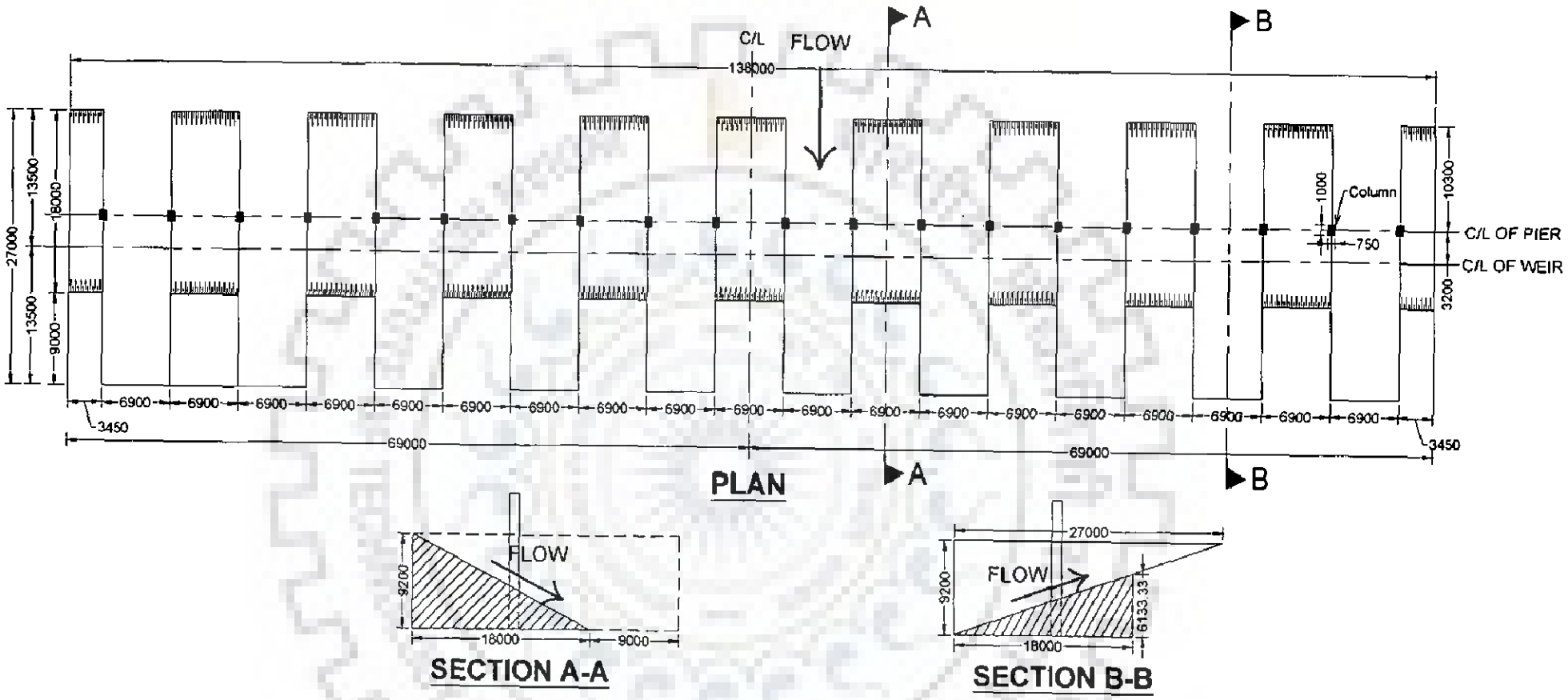

Fig. 5.8 Plan and section of model C_1M_6 for prototype (dimensions in mm)

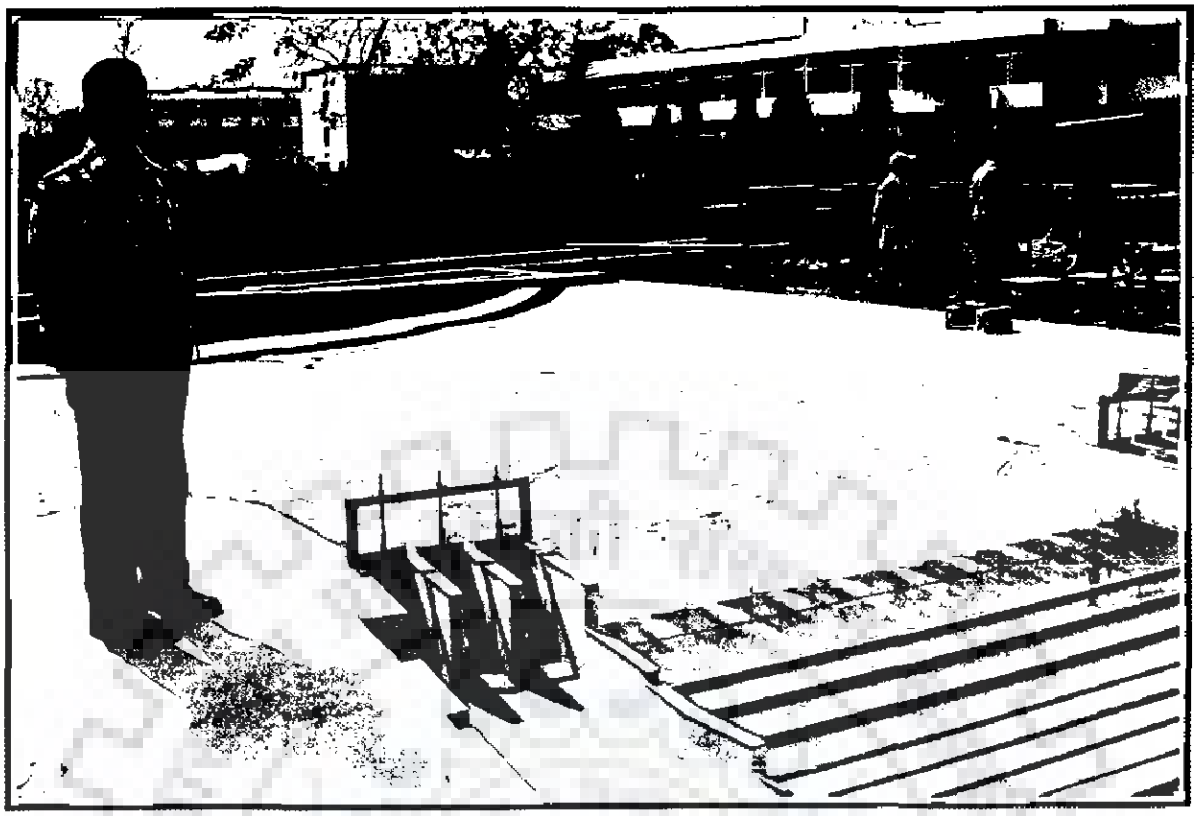

Plate No. 5.7 Pictorial view of Piano Key Weir model C_1M_6 for comprehensive model study

5.3 ANALYSIS OF LAB-BASED MODEL EXPERIMENTS

This is done in two steps. Six different configurations of models are tested for their performance in lab based experiments. The test results in the form of discharge passing capacity as net absolute discharge increment is shown in Fig. 5.9, in which the ordinate 'ΔQ' represents the difference between discharge passing over a Piano Key Weir and sharp crested weir for same *h/p*. The net absolute value of discharge increment for different models is in the range of 5.00 to 30.00 l/s.

The test results for discharge passing capacity is shown in Fig. 5.10 where in the ordinate '*r*' represents the ratio of discharge passing over a Piano Key Weir and sharp crested weir. Fig. 5.10 shows that discharge passing over a Piano Key Weir is 1.54 to 4 times higher than the sharp crested weir. From Figs. 5.9 and 5.10, it is found that lab based model C_1M_6 performs best in terms of *r*. For field scale testing, this model is used for construction.

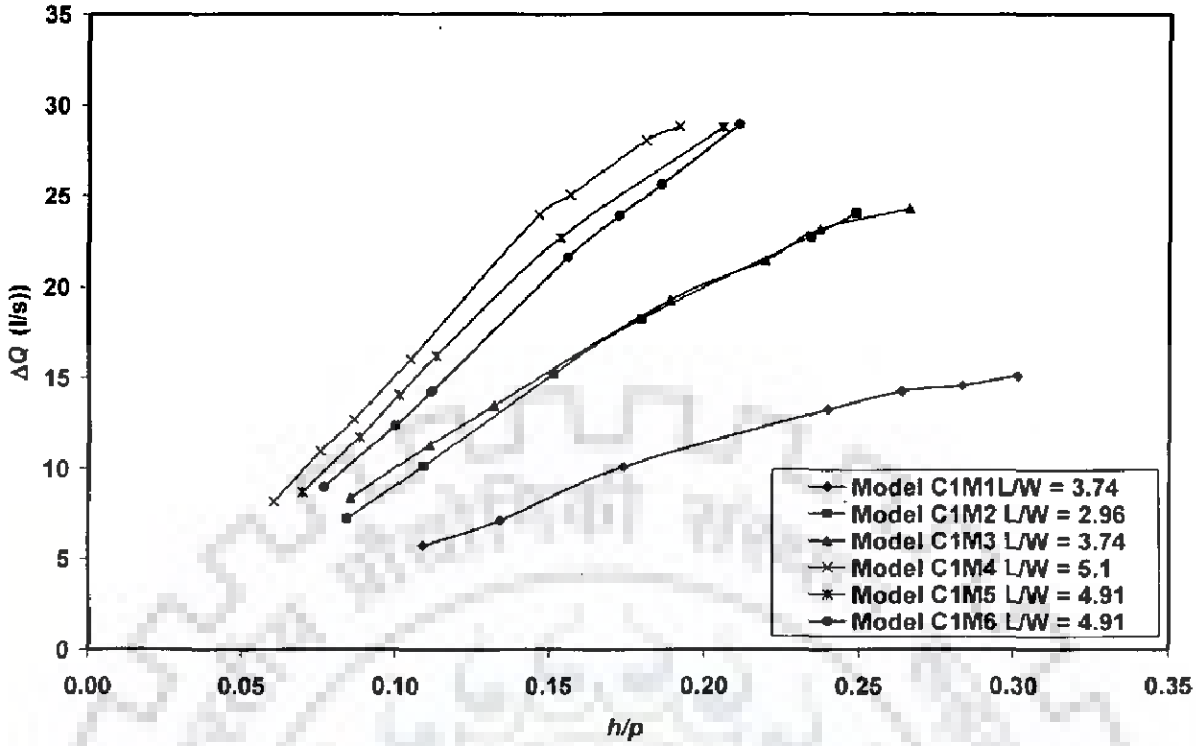

Fig. 5.9 Plot between ΔQ and h/p for all six models

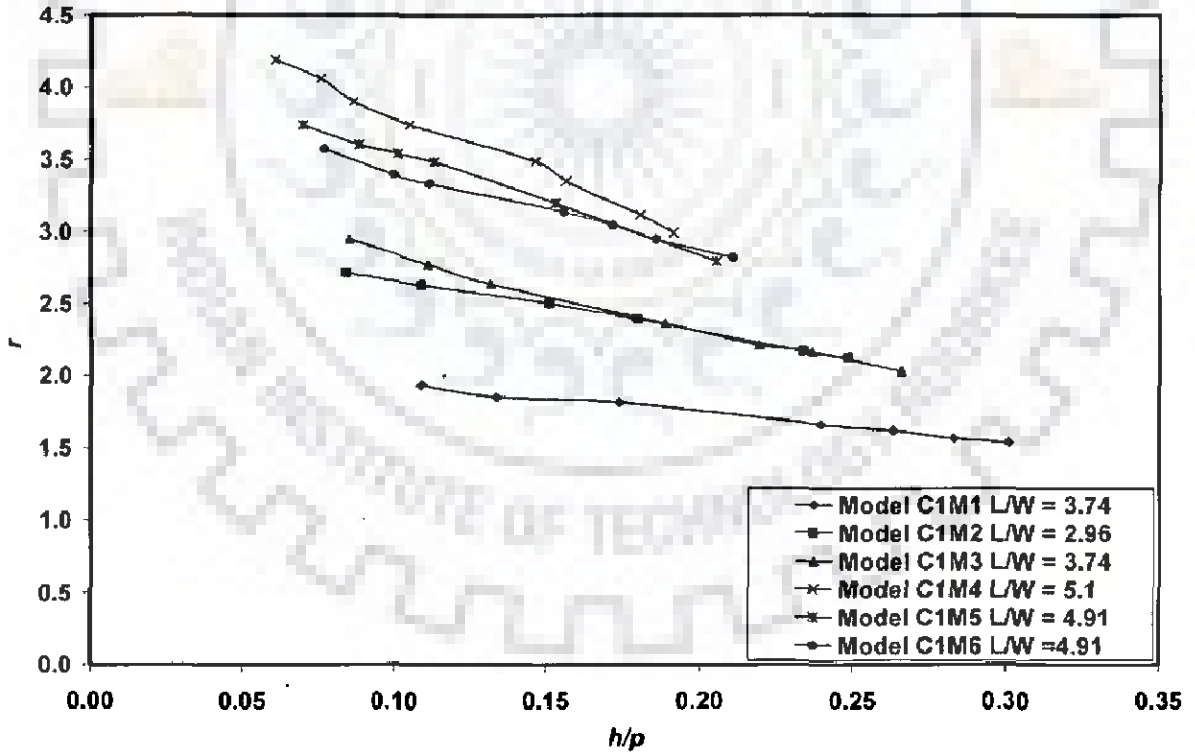

Fig. 5.10 Plot between r and h/p for all six models

5.4 ANALYSIS OF COMPREHENSIVE MODEL EXPERIMENTS RESULTS

From laboratory physical model studies, model C_1M_6 is preferred shape of Piano Key Weir. So this model C_1M_6 of Piano Key Weir is used for comprehensive model experiments. Full length of Piano Key Weir is used in comprehensive model study for better analyses of weir with reservoir area in upstream and downstream of weir.

The test results in the form of discharge passing capacity as net absolute discharge increment is shown in Fig. 5.11, where in the ordinate 'ΔQ' represents the difference between discharge passing over a Piano Key Weir and sharp crested weir for same *h/p*. The net absolute value of discharge increment for model C_1M_6 lies in the range of 450 to 1550 m^3/sec of prototype discharge.

The test results for discharge passing capacity is shown in Fig. 5.12 in which the ordinate '*r*' represents the ratio of discharge passing over a Piano Key Weir and sharp crested weir. Fig. 5.12 shows that discharge passing over a Piano Key Weir is 2.65 to 4.00 times higher than sharp crested weir.

Fig. 5.13 represents the saving of head over the crest of Piano Key Weir against sharp crested weir. This graph shows that saving of head over the crest is 0.80 m (i.e. 58.6 %) in Piano Key Weir against sharp crested weir for lower range of discharge (i.e. 500 m^3/sec) and is 2.00 m (i.e. 47.6 %) in Piano Key Weir against sharp crested weir for higher range of discharge (i.e. 2500 m^3/sec). The running view of the models is shown in Plate no. 5.8 from downstream side of weir and in plate No. 5.9 from upstream side of weir.

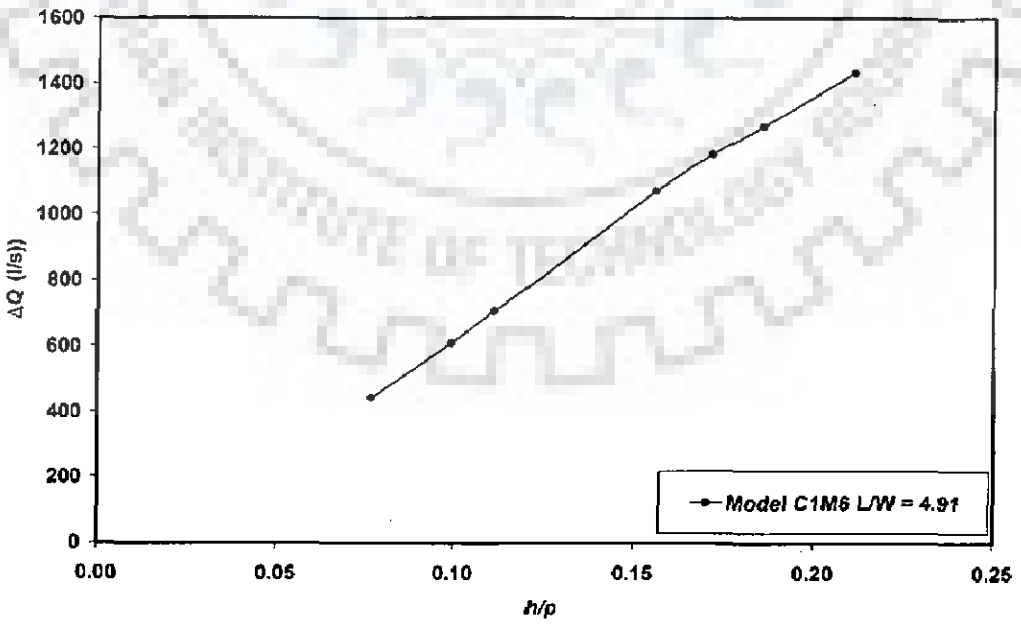

Fig. 5.11 Plot between *r* and *h/p* for model C_1M_6

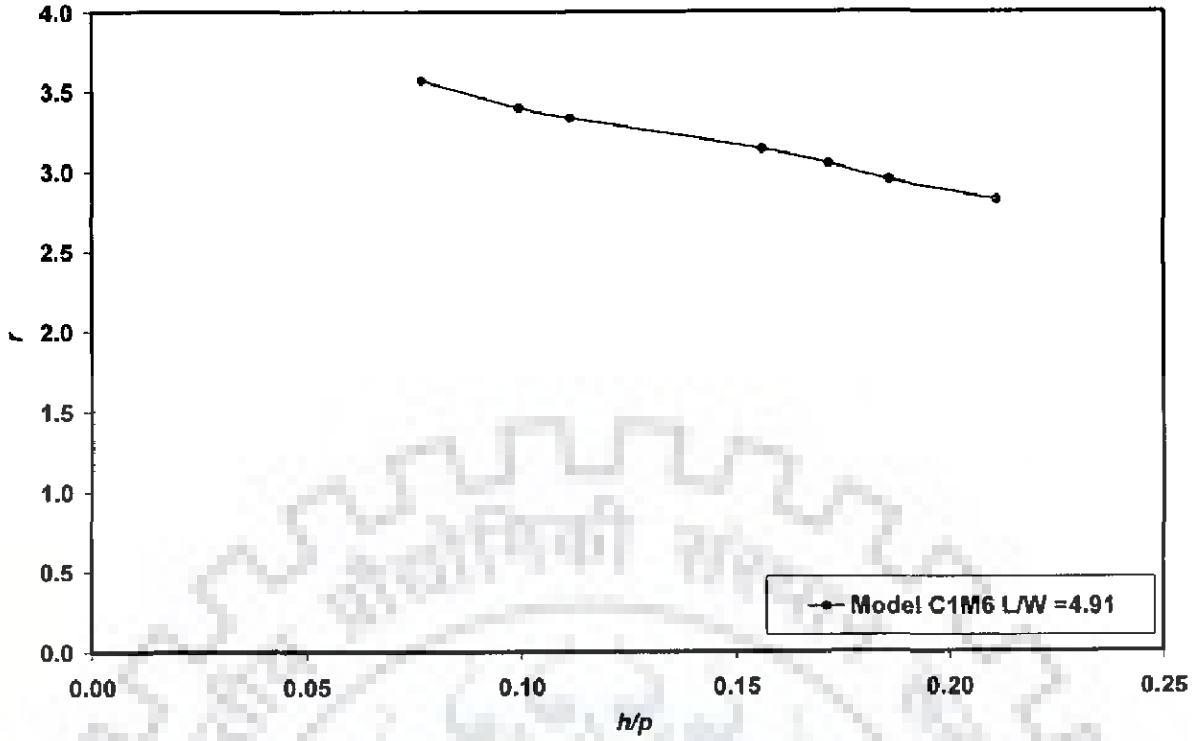

Fig. 5.12 Plot between ΔQ and h/p for model C_1M_6

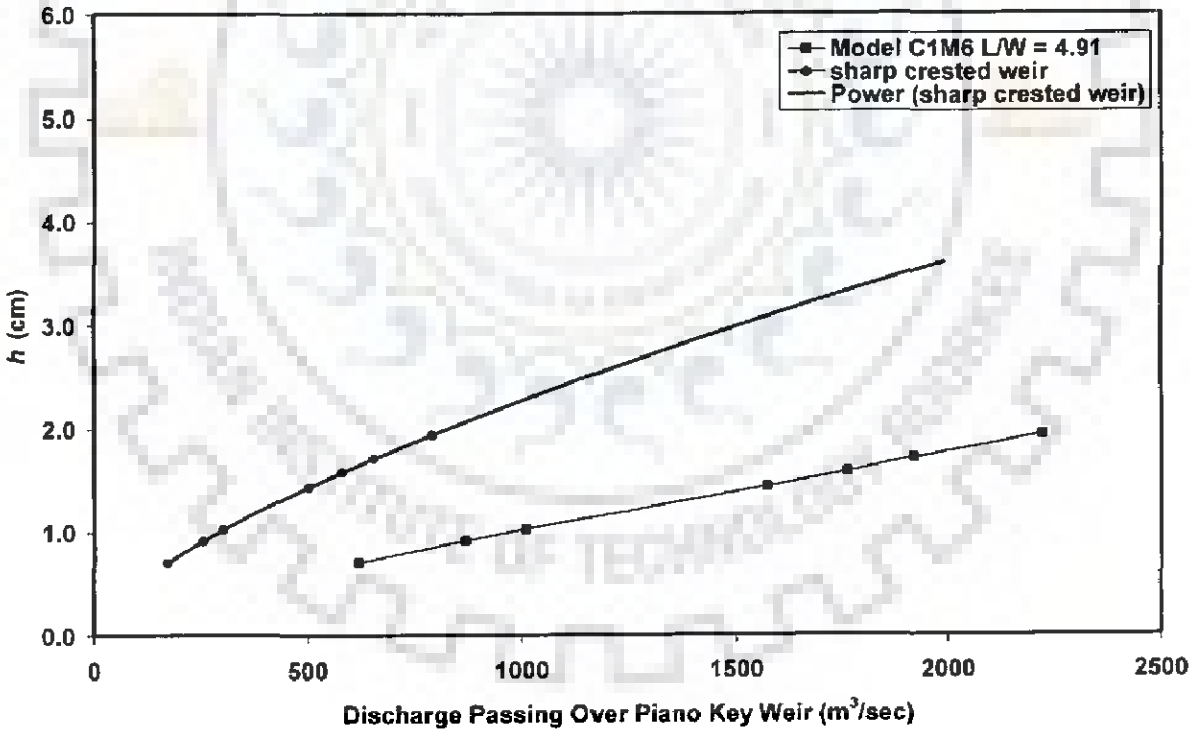

Fig. 5.13 Comparison of Piano Key Weir by to sharp crested weir with head over the crest for model C_1M_6

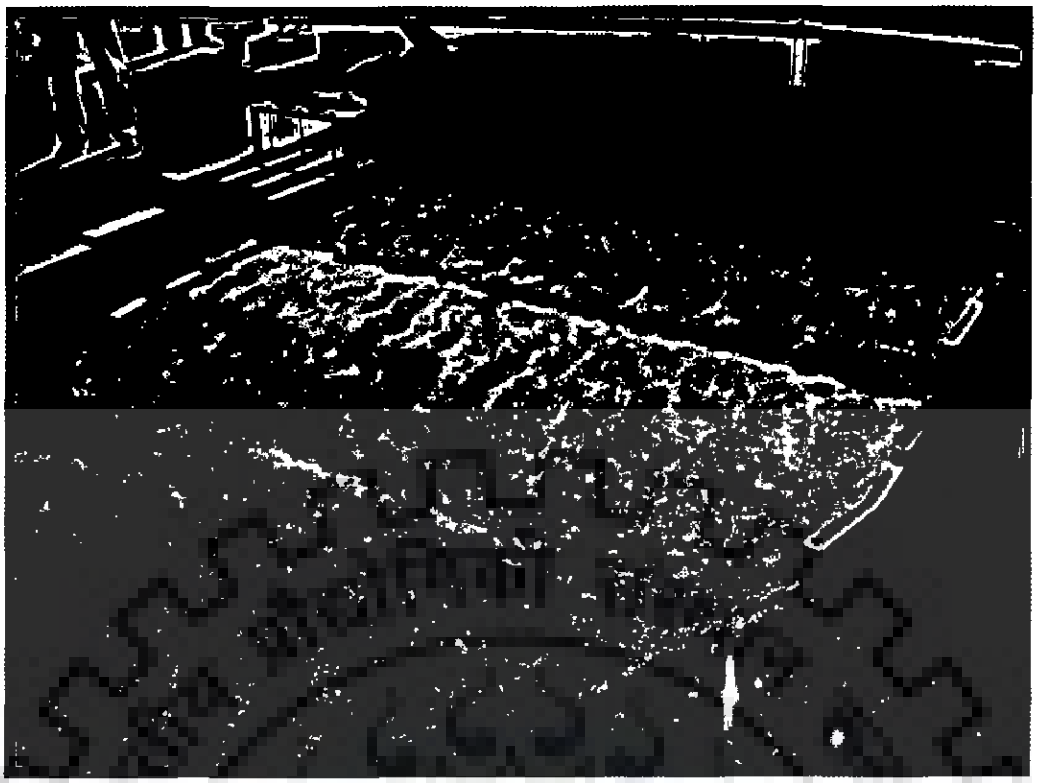

Plate No. 5.8 Running view of Piano Key Weir from d/s with under sluice gate

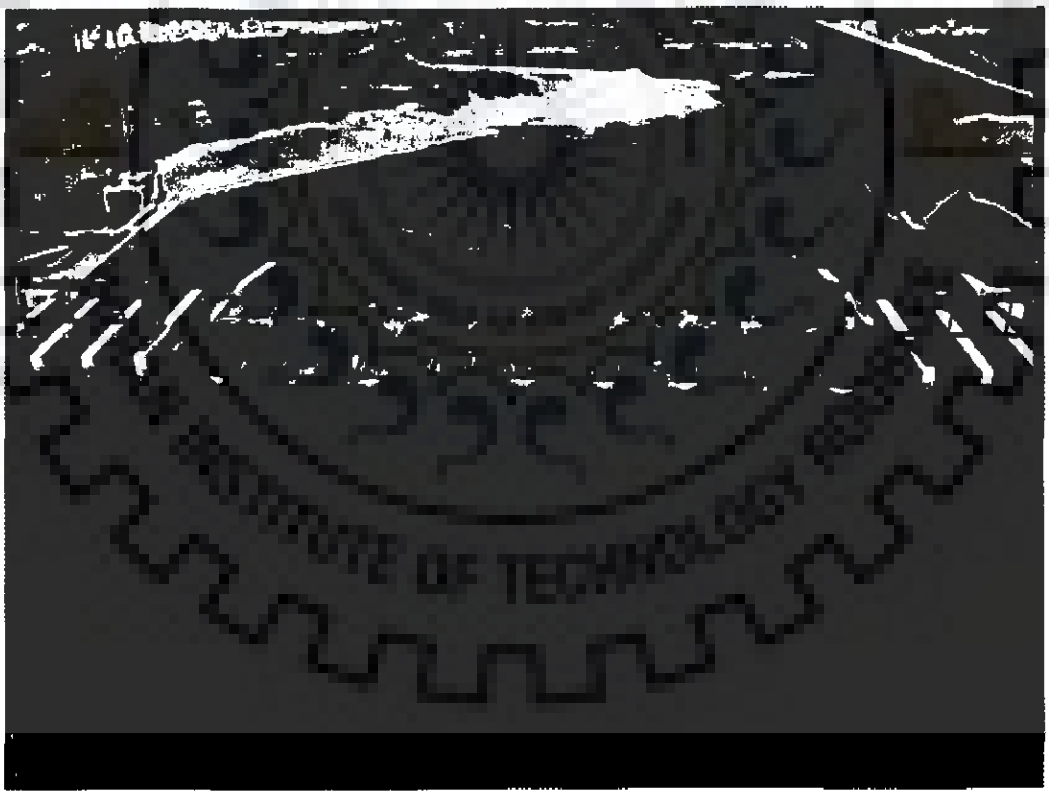

Plate No. 5.9 Running view of Piano Key Weir from u/s with under sluice gate

The maximum water level (MWL) for design flood of 5240 m^3/s was found at El 1423.12 from model study. The rating curve for the discharge passing over Piano Key Weir is depicted in adjoining Fig. 5.14. Reservoir level for 4000 m^3/s passes over Piano Key Weir is 1421.25 m.

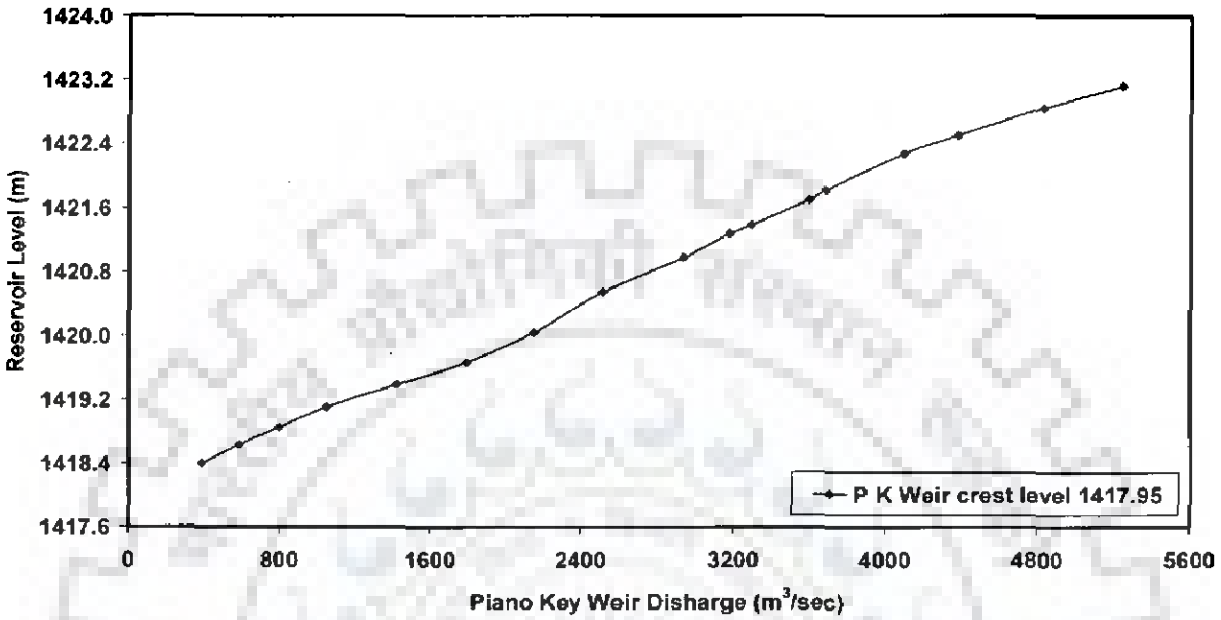

Fig. 5.14 Discharge passing over Piano Key Weir and corresponding reservoir level

5.5 SUMMARY

Design flood of the Sawara Kuddu HEP is 6880 m^3/s and requires high spilling capacity through weir in limited space. Piano Key Weir is designed with geometrically similar scale factor of 1:50. Six different geometries of Piano Key Weirs have been investigated in the lab. Among them, model C_1M_6 was found to be the most efficient with regard to the weir capacity. Study of model C_1M_6 indicated that the Piano Key Weir gives about 2.62 to 4.20 times higher discharge than sharp crested weir for corresponding head. The best evolved shape of Piano Key Weir from laboratory model study has been used for comprehensive model study. Comprehensive model study shows very interesting result that saving of head over the crest in Piano Key Weir lies in the range of 45 to 58 % of sharp crested weir.

CHAPTER 6

ANALYSIS OF DISCHARGE COEFFICIENT

6.1 GENERAL

In case of Labyrinth Weir, Tullis et al. (1995) have developed a large number of relationships for the investigation of discharge coefficient. It is well known that in the design of the Labyrinth Weir, such a relationship enables generalization of various layout of Labyrinth Weir for a given head and discharge data. In the study by Tullis et al. (1995), the discharge coefficient is found related with the ratio H_T/p for a given inclination of the limb of Labyrinth Weir. Furthermore, Tullis et al. (1995) also emphasize the importance of including total head into the analysis. In the earlier investigations on variation of discharge coefficient in case of linear weir, discharge coefficient is related with the Froude number. Thus, existing literature provides a set of objectives for this chapter as follows: (i) to develop a set of relationships for discharge coefficient using set of several parameters, such as Froude number, h/p, L/W, and to identify the best performing relationship; and (ii) to assess the relative merit in using the total head.

6.2 DATA CONSIDERATION

To develop a relationship for discharge coefficient, data in respect of phase two, three, and four are considered. For this data, Piano Key Weir discharge (Q_{PK}) varies from 0-80 l/sec, Froude Number (Fr) varies from 0-0.5, h/p varies from 0-1, and L/W varies from 3.56-7.4. Experiments relate mainly to two types of Piano Key Weir, i.e., one side overhanging and both sides overhanging. It was observed from the preliminary analysis that the performance of Piano Key Weir with both sides overhanging was always superior to the one with only one side overhanging. Thus, experimental data in case of Piano Key Weir with one side overhanging is analysed only for one value of L/W as 4.84. After getting an insight into the functional dependence of C_d variation with various dimensionless parameters for the data of Piano Key Weir with one side overhanging, the data in respect of Piano Key Weir with both sides overhanging are analysed. Here, for both types of Piano Key Weir i.e., one side over hanging and both side over hanging, ramps are provided.

6.3 VARIATION OF DISCHARGE COEFFICIENT

6.3.1 Basics

The main objective of this chapter is to develop a relation between discharge coefficient (C_d), h/p and Froude no. (Fr) for different length magnification ratio L/W and Q_{PK}, i.e.

$$Q_{PK} = f\left(C_d, Fr, h, geometrical\ characteristics\right) \tag{6.1}$$

For different types of spillways, use of the Bazin's formula (Modi et at. 1991), Eq. 6.2, is common for computing discharge Q

$$Q = C_d W \sqrt{2g} h^{\frac{3}{2}} \tag{6.2}$$

The discharge coefficient C_d is independent of the units used to measure W, h, g (acceleration due to gravity) and Q as long as the same units of length is being used throughout (Borghei et al., 1999). Here, W is width of channel, and h is head over crest

For the present case, it was decided to use the Bazin's equation and to develop a relationship for the C_d variation using following functional form, i.e.

$$C_d = f\left(h/p, Fr, L/W\right) \tag{6.3}$$

where C_d using Eq. 6.2 can be written as

$$C_d = \frac{Q_{PK}}{W\sqrt{2g}h^{3/2}} \tag{6.4}$$

where Q_{PK} is discharge passing over Piano Key Weir.

In Eq. (6.3), Fr is Froude no. of the approaching flow and is defined as

$$Fr = \frac{Q_{PK}}{A\sqrt{gH}} \tag{6.5}$$

In the above equation, A is the flow area upstream of weir and H is total depth of water in channel.

To develop empirical relationship using eq. (6.3), a general regression model is considered. The general multiple regression model (Cohen et al., 2003) can be written in as

$$y = \beta_0 + \beta_1 x_1 + \beta_2 x_2 + \beta_3 x_3 + \ldots\ldots\ldots + \beta_i x_i + u \tag{6.6}$$

Where β_0 is the intercept, β_1 is the parameter associated with x_1, and so on. The performance of the regression model is judged in terms of a statistical parameter R^2.

By definition, R^2 is a number between zero and one. R^2 can also be shown to equal the squared correlation coefficient between the actual y_i and the fitted y_i. That is

$$R^2 = \frac{\left(\sum_{i=1}^{n}(y_i - \bar{y})(\hat{y}_i - \bar{\hat{y}})\right)^2}{\left(\sum_{i=1}^{n}(y_i - \bar{y})^2\right)\left(\sum_{i=1}^{n}(\hat{y}_i - \bar{\hat{y}})^2\right)} \tag{6.7}$$

A high value of R^2, suggests that the regression model explains the relationship in a better way.

6.3.2 Cases Considered

To study the variation of discharge coefficient, various options are explored. The relationships are developed separately for Piano-Key Weirs having both sides over-hanging and only one side (d/s side) over hanging. For each of these two geometrically different configurations of Piano Key Weir, many options are explored. These options include (i) variation of discharge coefficient with *Fr* for a given *L/W* (ii) variation of discharge coefficient with *h/p* for a given *L/W* (iii) variation of discharge coefficient with *Fr* and *h/p* for a given *L/W* (iv) variation of discharge coefficient with *Fr*, *h/p* and *L/W*. Of these, the fourth option is the most generalized one.

6.4 VARIATION OF DISCHARGE COEFFICIENT FOR DOWNSTREAM SIDES OVER-HANGING TYPE OF PIANO KEY WEIR

Variation of discharge coefficient is analysed here for value of *L/W* as 4.84 only. The experimental data used for the analysis is given in Table C.13 to C.15 (see Appendix C).

6.4.1 *Variation of Discharge Coefficient with Froude No. for L/W as 4.84*

Fig. 6.1 shows discharge coefficient variation for different values of *Fr*. The following equation best describes the experimental data

$$C_d = 0.4665 Fr^{-0.6011};\ R^2 = 0.87 \tag{6.8}$$

Fig. 6.2 shows that the error between observed and computed discharge coefficient lies in the range of -22 to +17 % for *L/W* as 4.84. Average absolute

percentage error between computed and observed discharge coefficient using Eq. (6.8) is found to be 6.84.

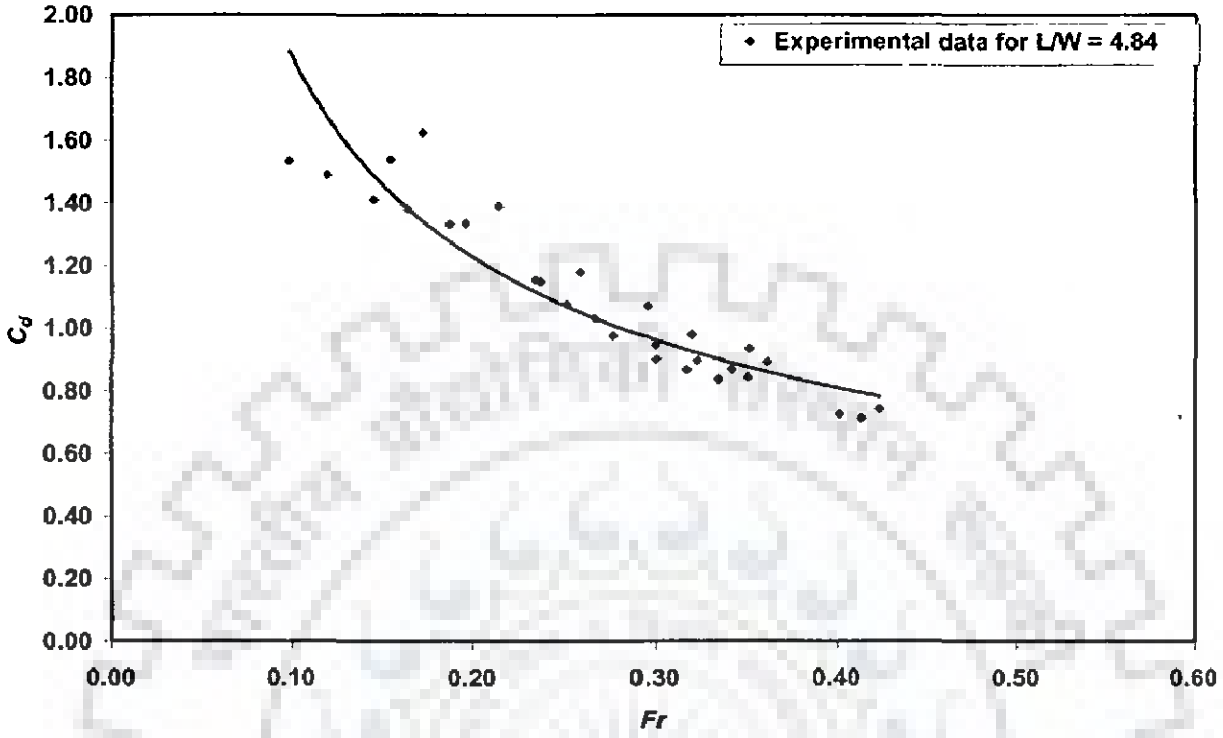

Fig. 6.1 Plot between Fr and C_d for $L/W = 4.84$

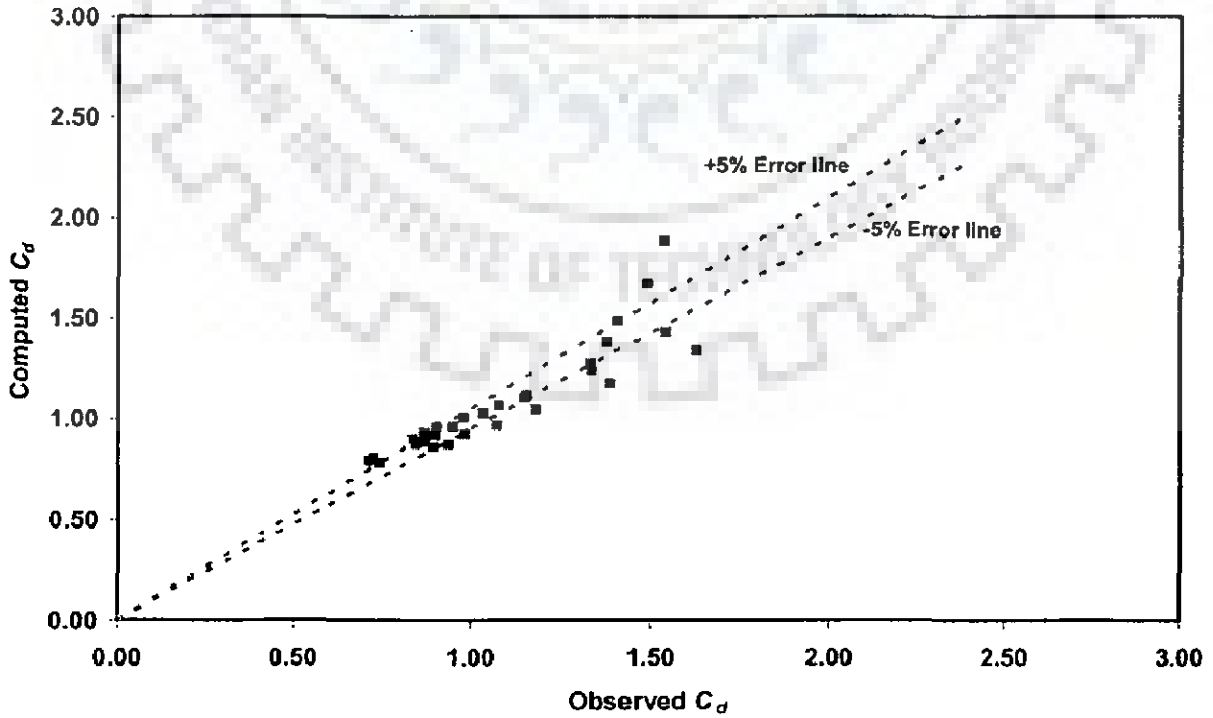

Fig. 6.2 Error analysis between observed and computed C_d for $L/W = 4.84$ using Eq. (6.8)

6.4.2 Variation of Discharge Coefficient with *h/p* for *L/W* as 4.84

Fig. 6.3 shows discharge coefficient variation for different values of *h/p*. If C_d is related with *h/p* only, the following equation best describes the experimental data

$$C_d = 0.778 h/p^{-0.405}; R^2 = 0.96 \quad (6.9)$$

Fig. 6.4 shows that the error between observed and computed discharge coefficient lies in the range of -10 to +10 % for *L/W* as 4.84. Average absolute percentage error between computed and observed discharge coefficient using Eq. (6.9) is found to be 3.46.

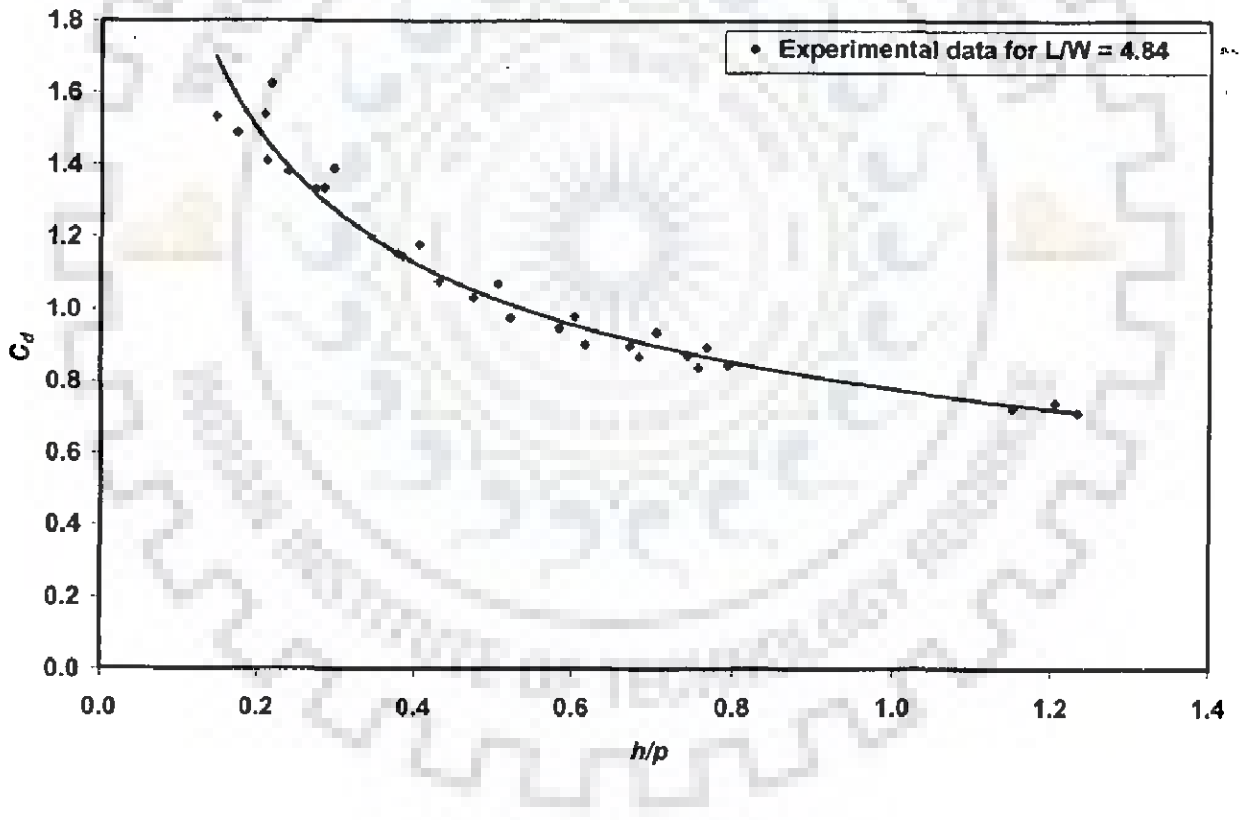

Fig. 6.3 Plot between *h/p* and C_d for *L/W* = 4.84

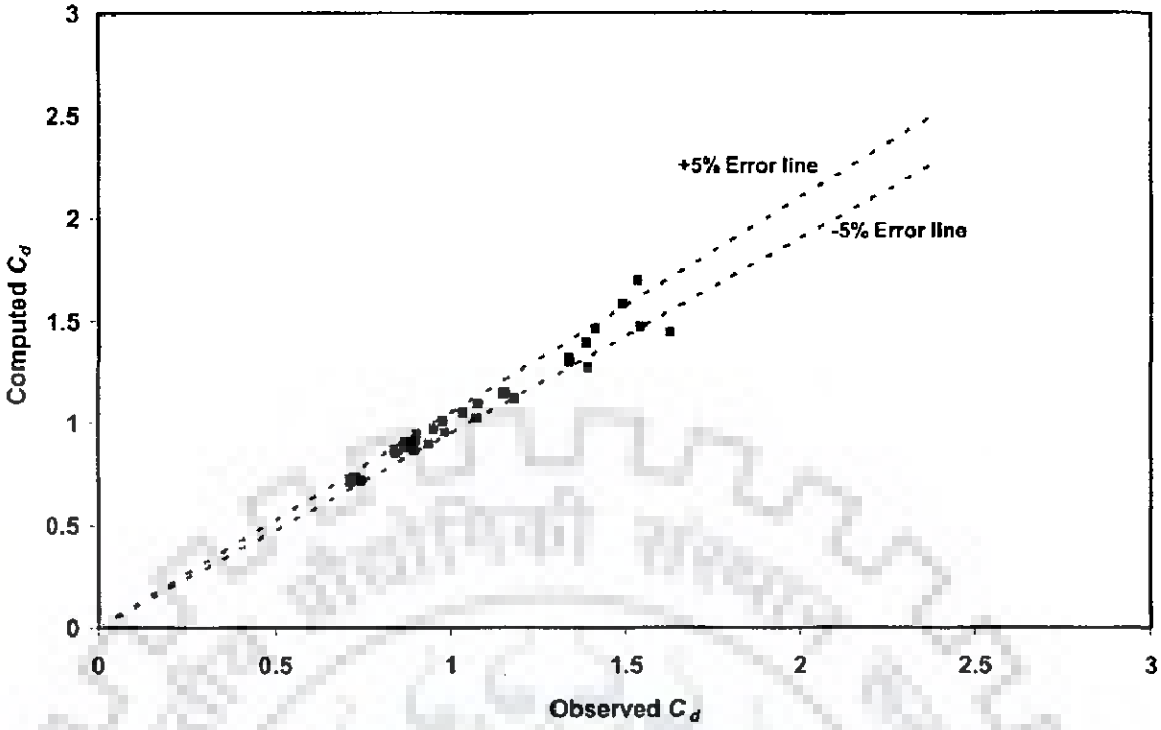

Fig. 6.4 Error analysis between observed and computed C_d for L/W = 4.84 using Eq. (6.9)

6.4.3 Variation of Discharge Coefficient with Froude No. and *h/p* for *L/W* as 4.84

In the previous option, only the upstream (or approach) Froude number (Fr) is taken as the main variable in the development of formula for discharge coefficient analysis. As R^2 was not very high, the option of including an additional variable h/p is explored.

The variation of discharge coefficient with Fr and h/p is shown in Figs. 6.5 and 6.6 respectively. The polynomial regression model for L/W 4.84 yields the following functional form

$$C_d = 1.876 - 0.00954h/p - 2.873Fr\,;\ R^2 = 0.91 \qquad (6.10)$$

Fig. 6.7 shows that the error between observed and computed discharge coefficient lies in the range of -11 to +15 % for L/W as 4.84. Average absolute percentage error between computed and observed discharge coefficient using Eq. (6.10) is found to be 5.85.

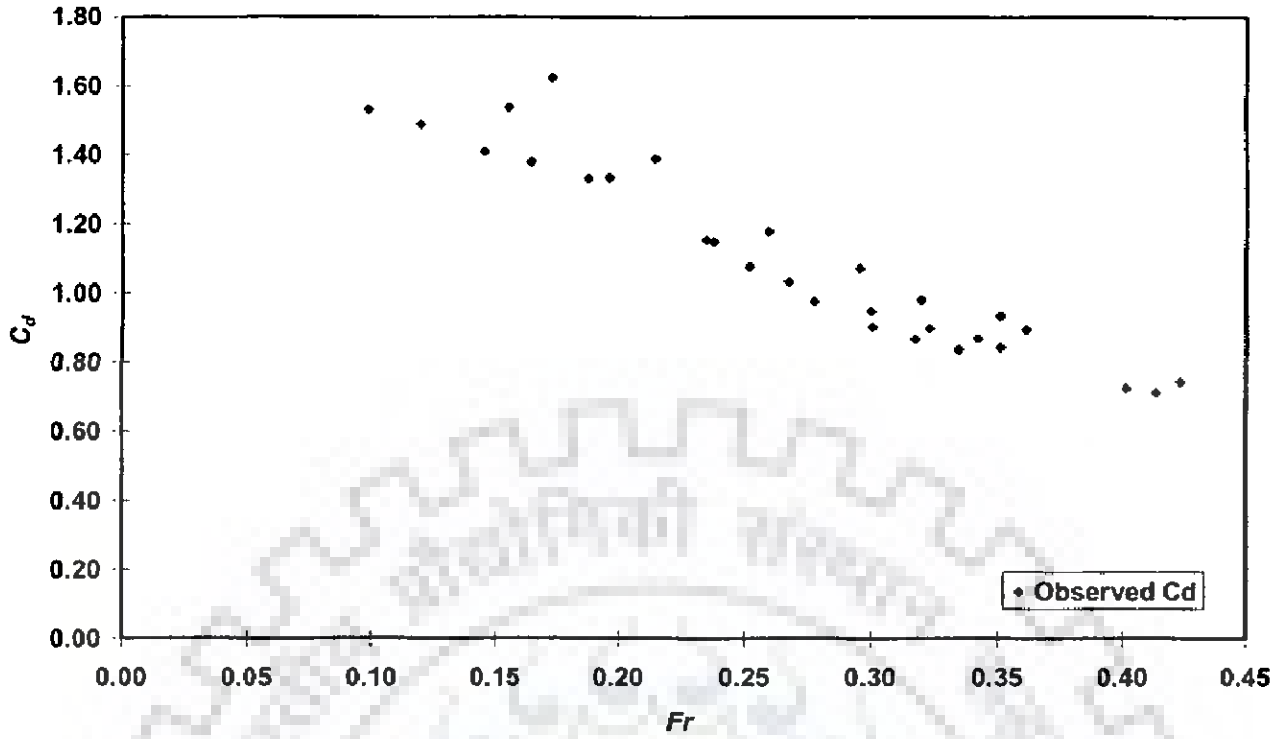

Fig. 6.5 Graphical plot between Fr and C_d for $L/W = 4.84$

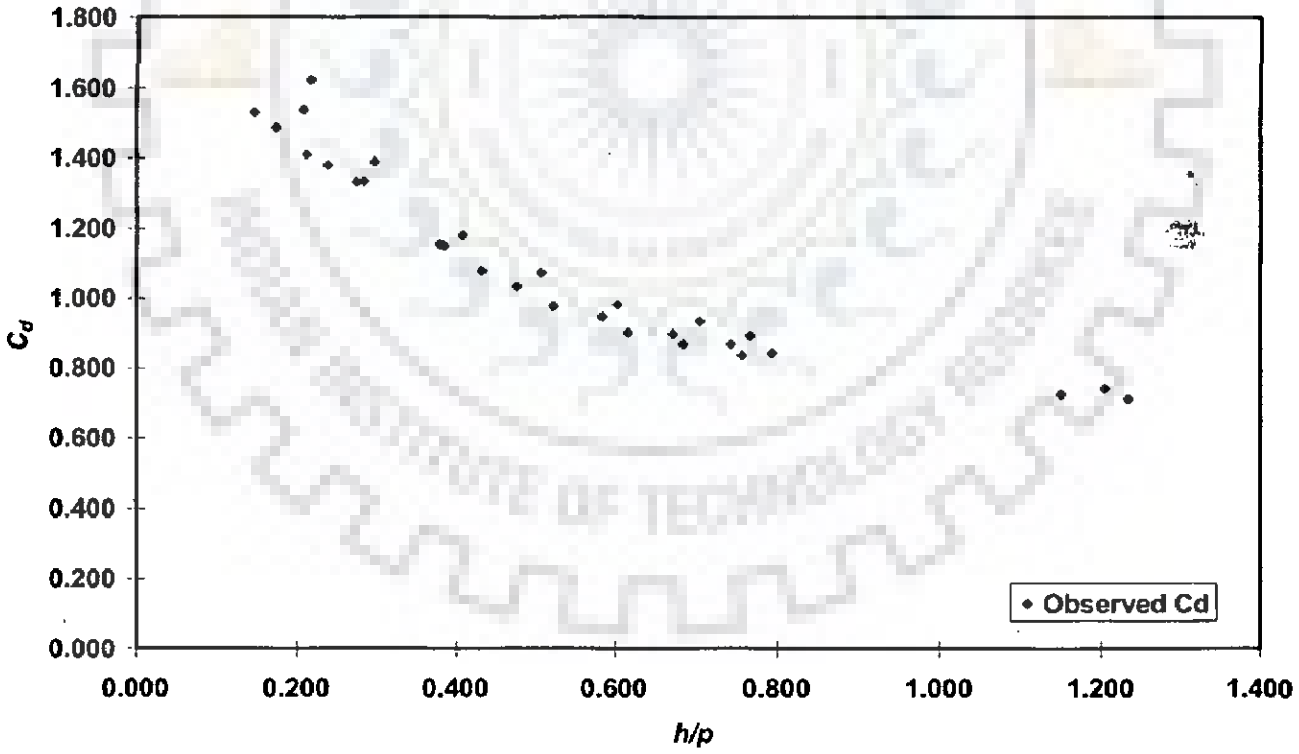

Fig. 6.6 Graphical plot between h/p and C_d for $L/W = 4.84$

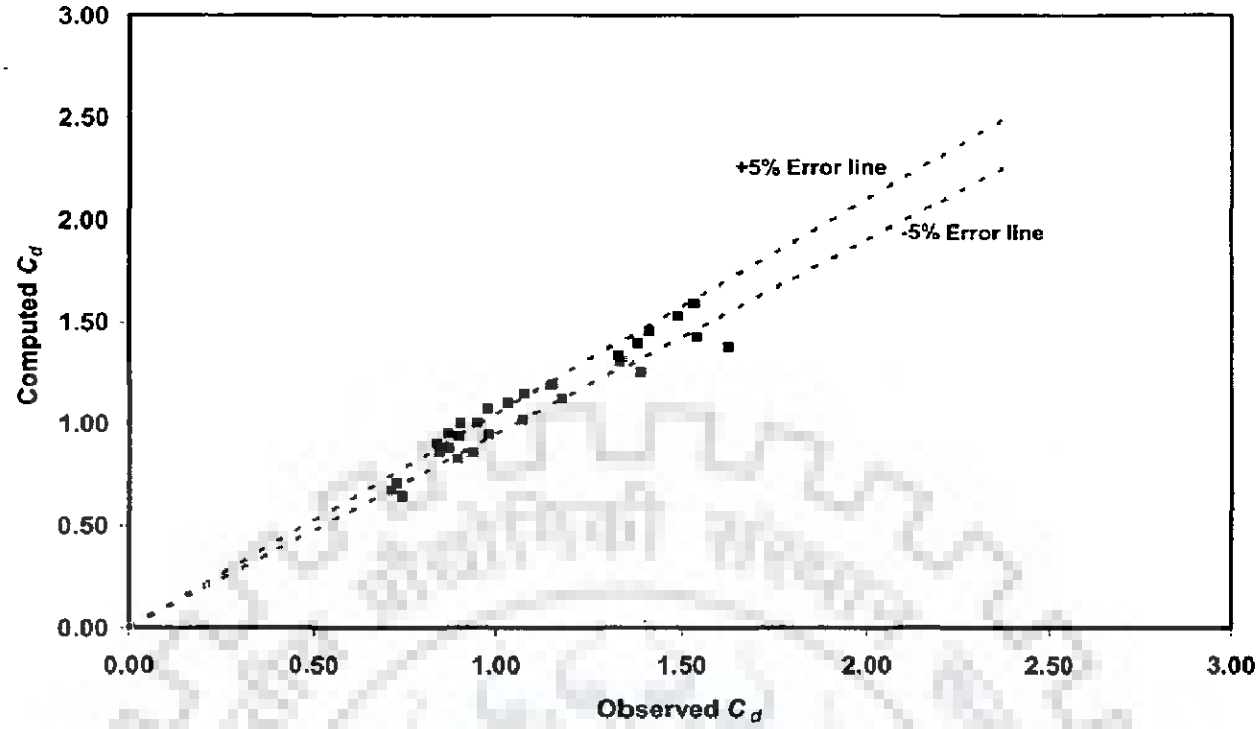

Fig. 6.7 Error analysis between observed and computed C_d for $L/W = 4.84$ using Eq. (6.10)

6.4.4 Variation of Discharge Coefficient with Froude No. and *h/p* in Two Distinct Segments

The analysis done in the previous section indicated the possibility of exploring the refinements in the developed regression relationships between discharge coefficient, *Fr* and *h/p* in different ranges of *h/p*. For this reason, the results of analysis considering two different segments of C_d variation with *h/p* between 0 and 0.4 and greater than 0.4 are presented next.

6.4.4.1 Variation of discharge coefficient with Froude no. and *h/p* upto 0.4 for *L/W* as 4.84

The variation of discharge coefficient with *Fr* and *h/p* upto 0.4 is shown in Figs. 6.8 and 6.9 respectively. The polynomial regression model is developed as follows:

$$C_d = 1.67 - 4.68h/p + 5.23Fr\,;\ R^2 = 0.94 \qquad (6.11)$$

Fig. 6.10 shows that the error between observed and computed discharge coefficient lies in the range of -3 to +3 % for *L/W* as 4.84 and *h/p* upto 0.4. Average absolute percentage error between computed and observed discharge coefficient using Eq. (6.11) is 2.25. Also, R^2 value is found to marginally improve from 0.91 to 0.94.

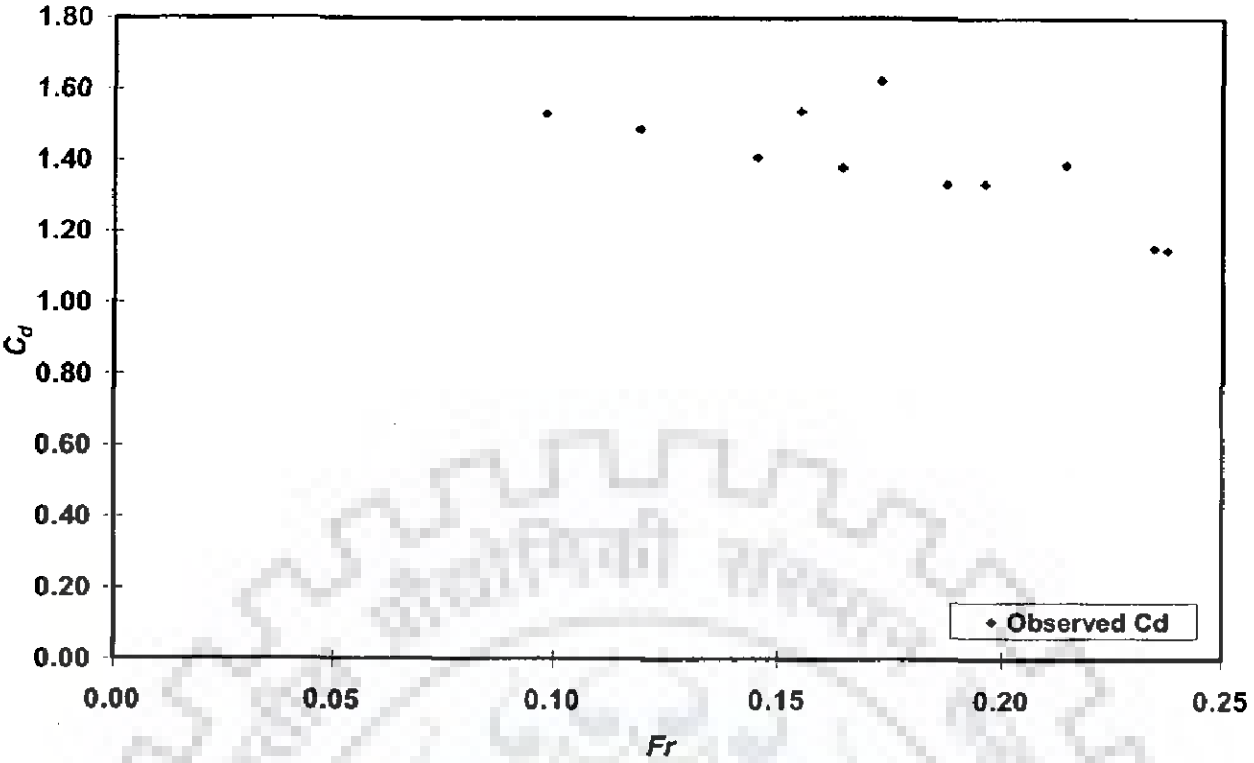

Fig. 6.8 Graphical plot between *Fr* and C_d for *L/W* = 4.84 and *h/p* upto 0.4

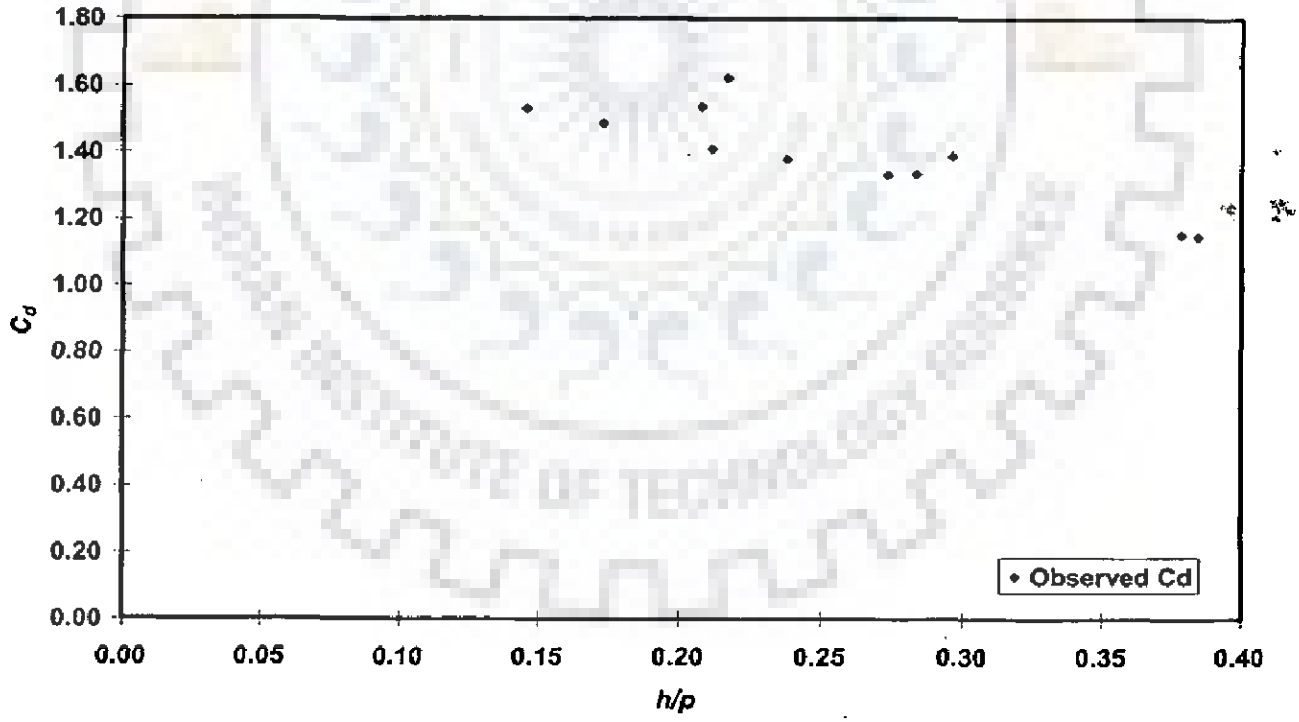

Fig. 6.9 Graphical plot between *h/p* and C_d for *L/W* = 4.84 and *h/p* upto 0.4

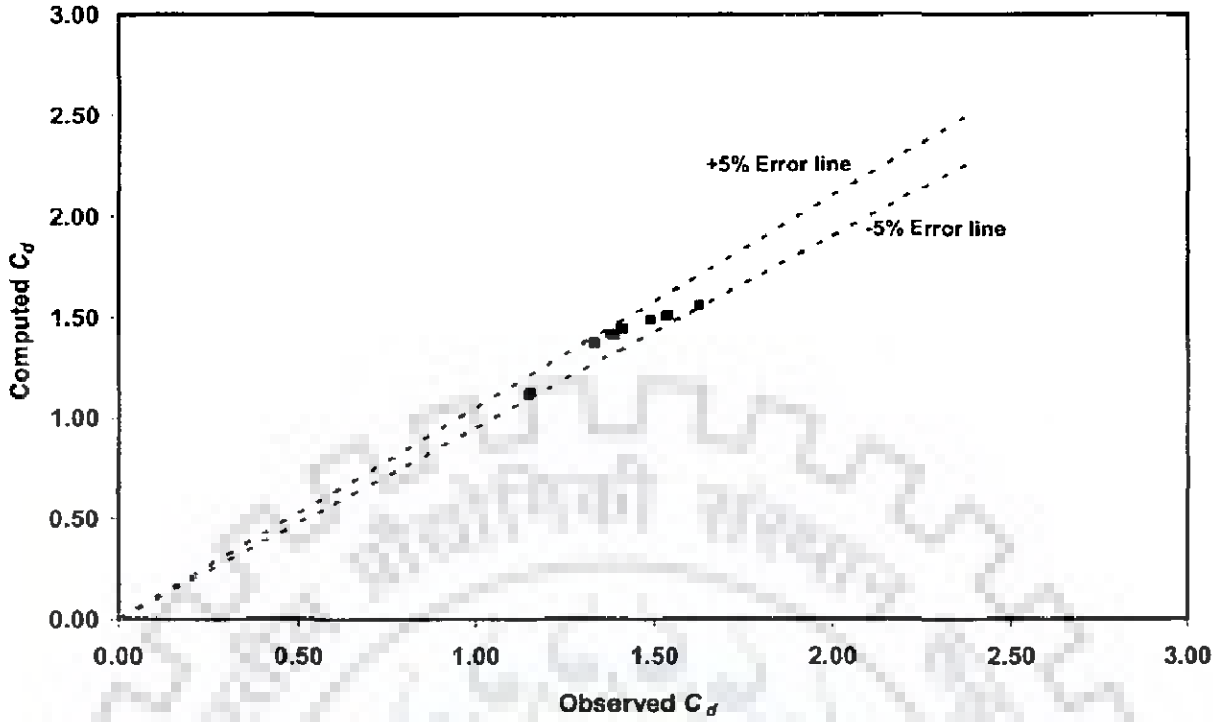

Fig. 6.10 Error analysis between observed and computed C_d for L/W = 4.84 and h/p upto 0.4 using Eq. (6.11)

6.4.4.2 Variation of discharge coefficient with Froude no. and h/p greater than 0.4 for L/W as 4.84

The variation of discharge coefficient with Fr and h/p greater than 0.4 is shown in Figs. 6.11 and 6.12 respectively. The polynomial regression model is developed as follows:

$$C_d = 1.29 - 0.41h/p + 0.26Fr;\ R^2 = 0.85 \qquad (6.12)$$

Fig. 6.13 shows that the error between observed and computed discharge coefficient lies in the range of -7 to +10 % for L/W as 4.84 and h/p greater than 0.4. Average absolute percentage error between computed and observed discharge coefficient using Eq. (6.12) is 4.18. Also, R^2 value is found to marginally reduce from 0.91 to 0.85.

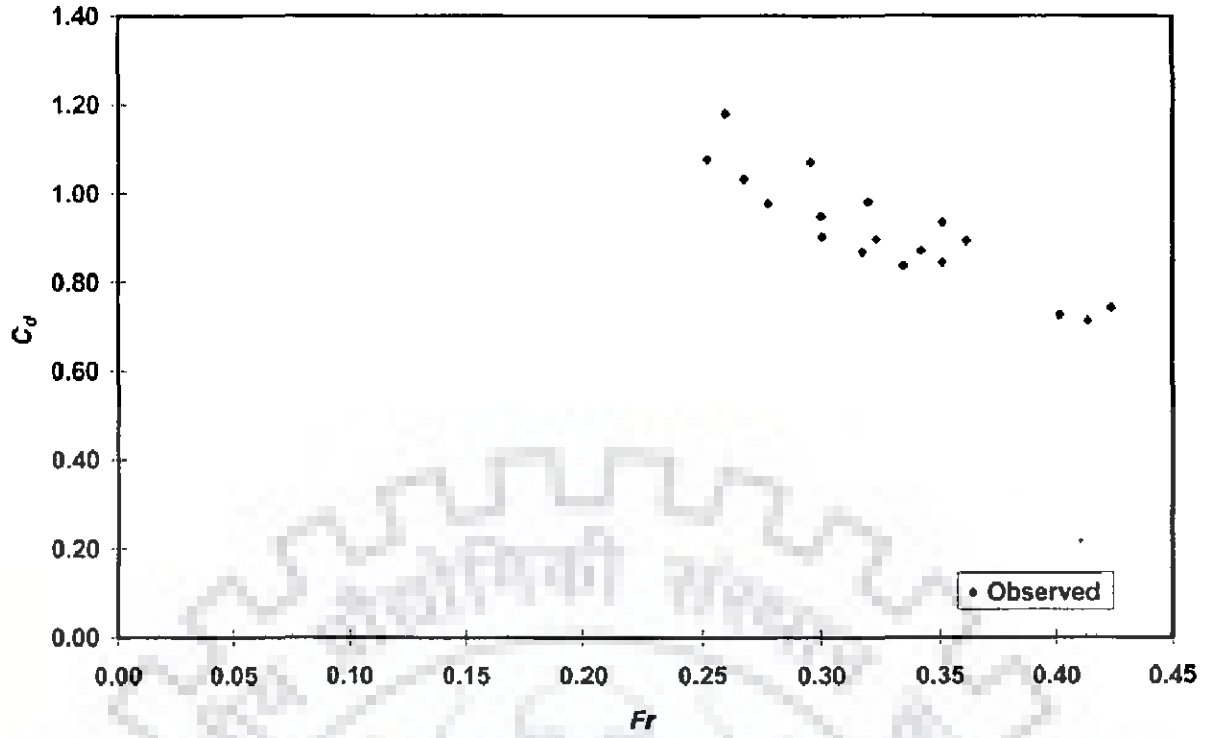

Fig. 6.11 Graphical plot between *Fr* and C_d for *L/W* = 4.84 and *h/p* greater than 0.4

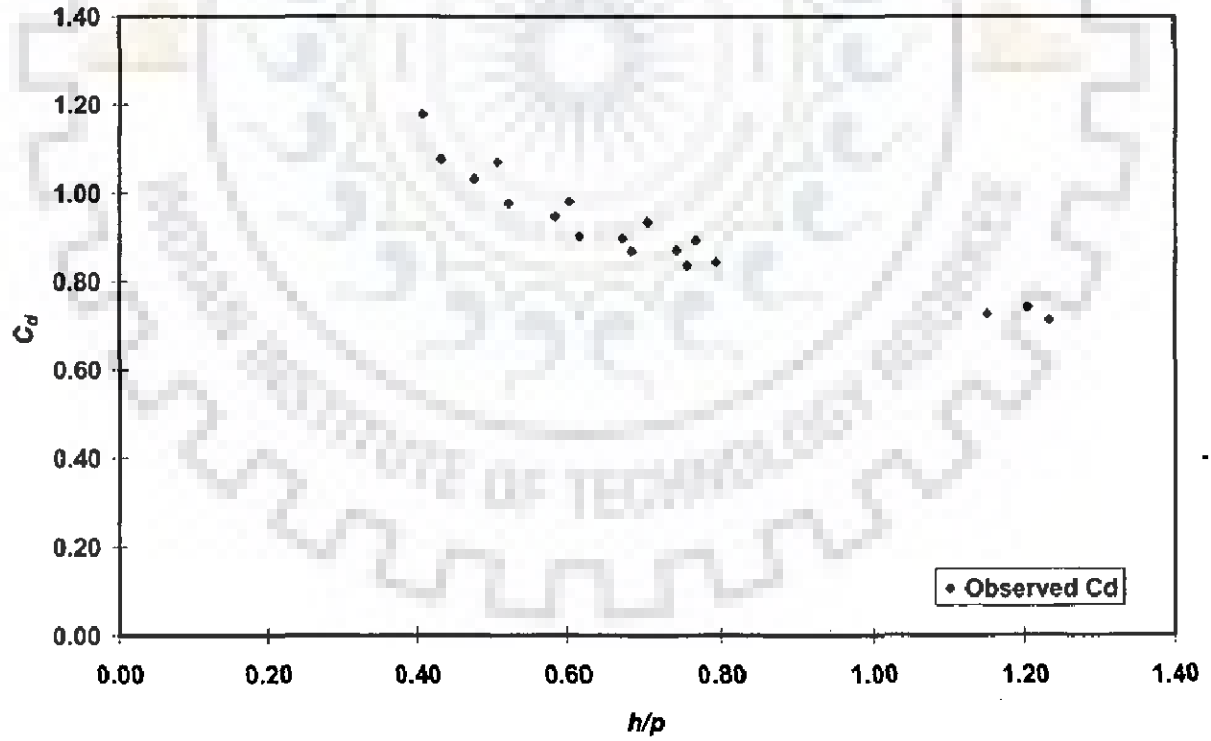

Fig. 6.12 Graphical plot between *h/p* and C_d for *L/W* = 4.84 and *h/p* greater than 0.4

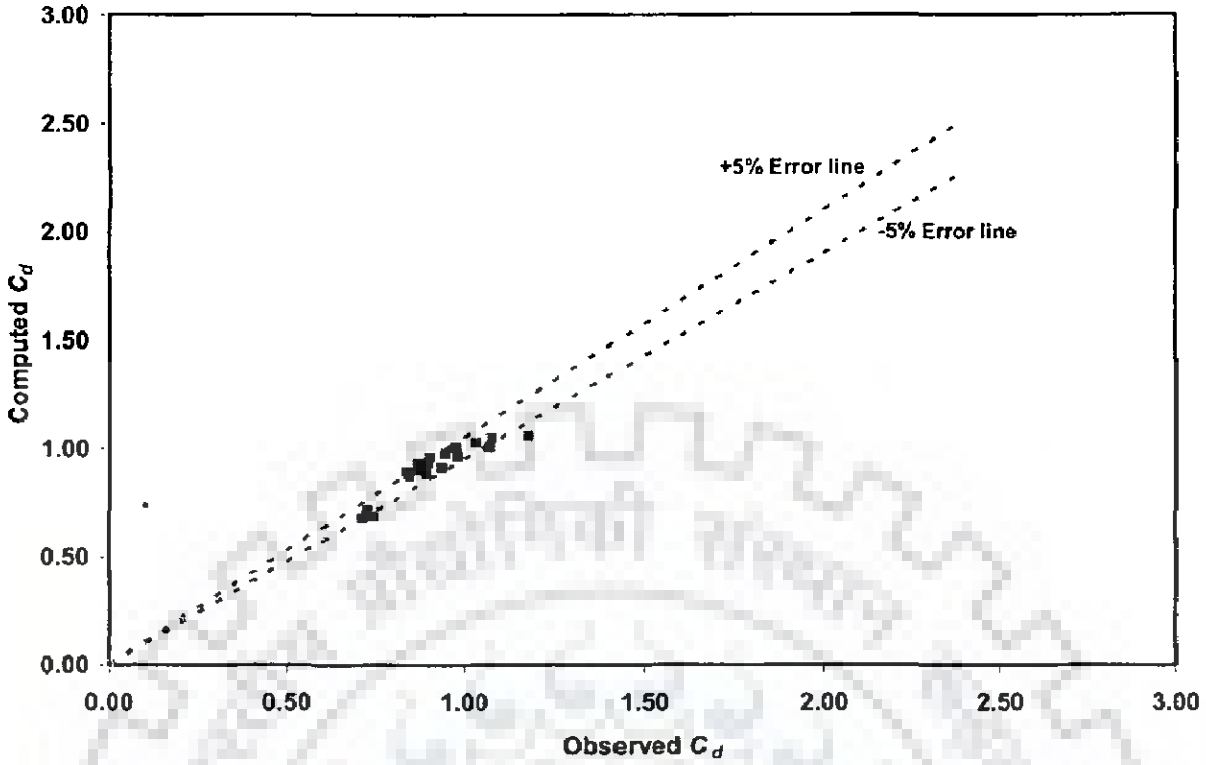

Fig. 6.13 Error analysis between observed and computed C_d for L/W = 4.84 and h/p greater than 0.4 using Eq. (6.12)

6.5 VARIATION OF DISCHARGE COEFFICIENT FOR BOTH SIDES OVER-HANGING TYPE OF PIANO KEY WEIR

Variation of discharge coefficient is analysed here for value of L/W as 3.56, 4.84 and 7.4. The experimental data used for the analysis is given in Table C.1 to C.12 (see Appendix C).

6.5.1 Variation of Discharge Coefficient with Froude No. for L/W as 3.56

Fig. 6.14 shows discharge coefficient variation for different values of Fr. Here, the data used has h/p variation from 0 to 1. If C_d is related with Fr only, the following equation best describes the experimental data

$$C_d = 0.4762 Fr^{-0.3761}; R^2 = 0.7859 \quad (6.13)$$

Fig. 6.15 shows that the error between observed and computed discharge coefficient lies in the range of -14 to +21 % for L/W as 3.56. Average absolute percentage error between computed and observed discharge coefficient using Eq. (6.13) is found to be 5.91.

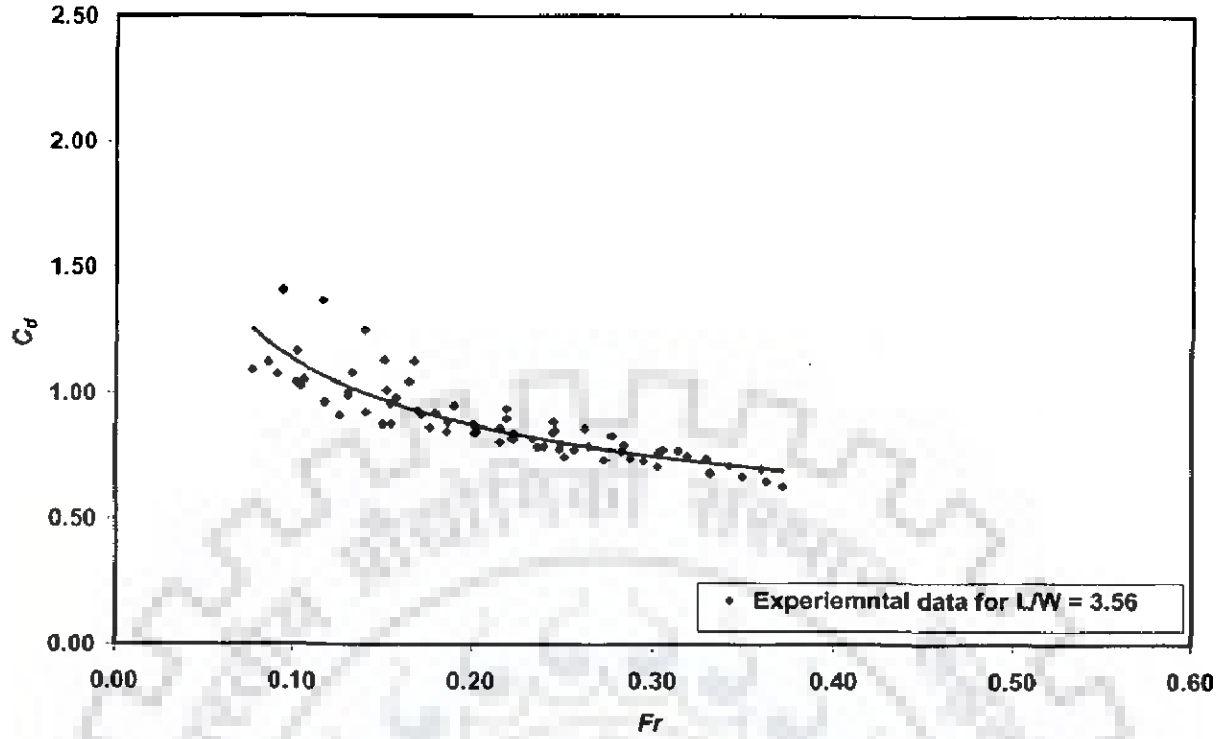

Fig. 6.14 Plot between Fr and C_d for $L/W = 3.56$

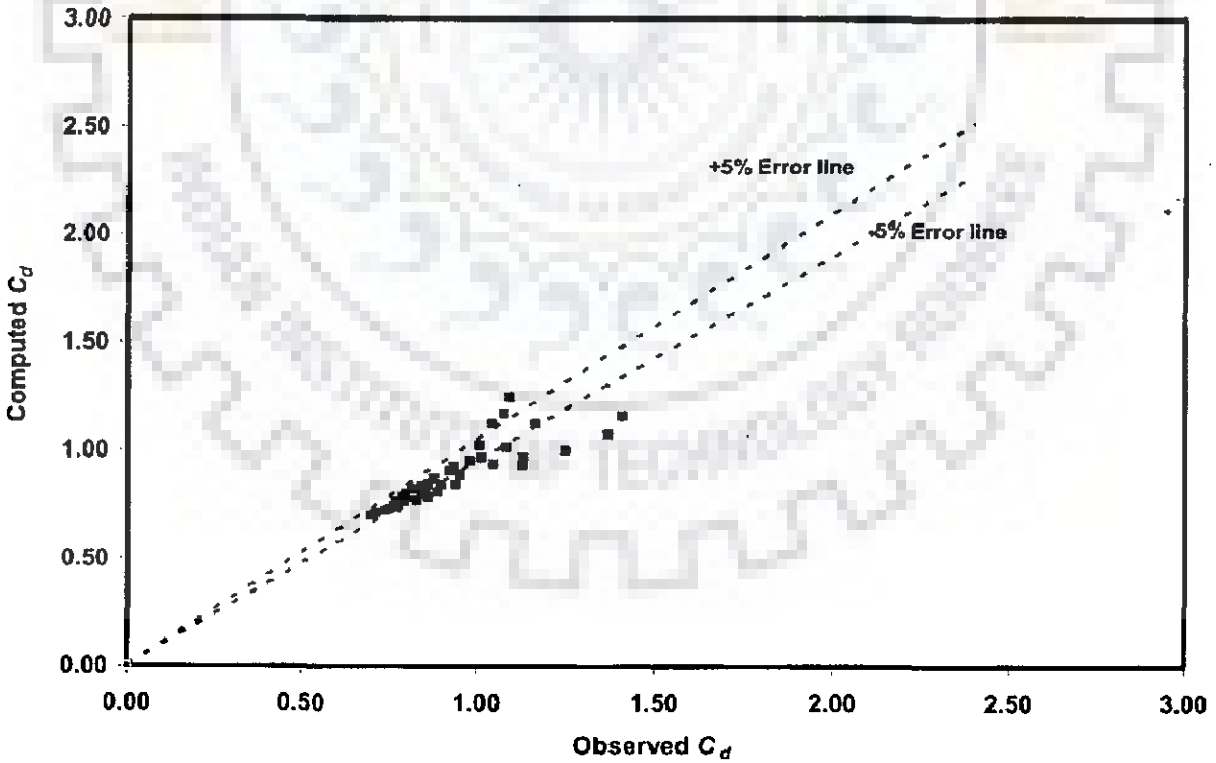

Fig. 6.15 Error analysis between observed and computed C_d for $L/W = 3.56$ using Eq. (6.13)

6.5.2 Variation of Discharge Coefficient with Froude No. for *L/W* as 4.84

Fig. 6.16 shows discharge coefficient variation for different values of Fr. The following equation best describes the experimental data

$$C_d = 0.4691 Fr^{-0.4214}\ ;\ R^2 = 0.5636 \qquad (6.14)$$

Fig. 6.17 shows that the error between observed and computed discharge coefficient lies in the range of -21 to +21 % for *L/W* as 4.84. Average absolute percentage error between computed and observed discharge coefficient using Eq. (6.14) is found to be 11.69.

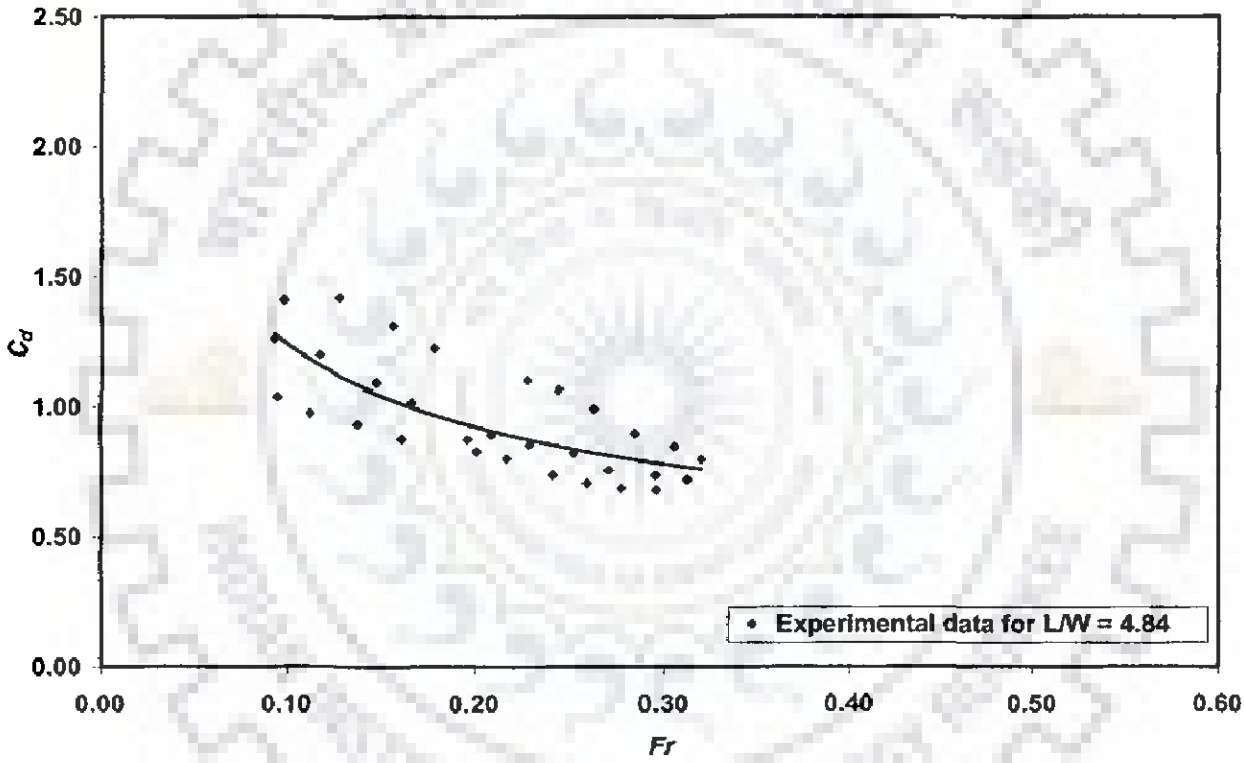

Fig. 6.16 Plot between *Fr* and C_d for *L/W* = 4.84

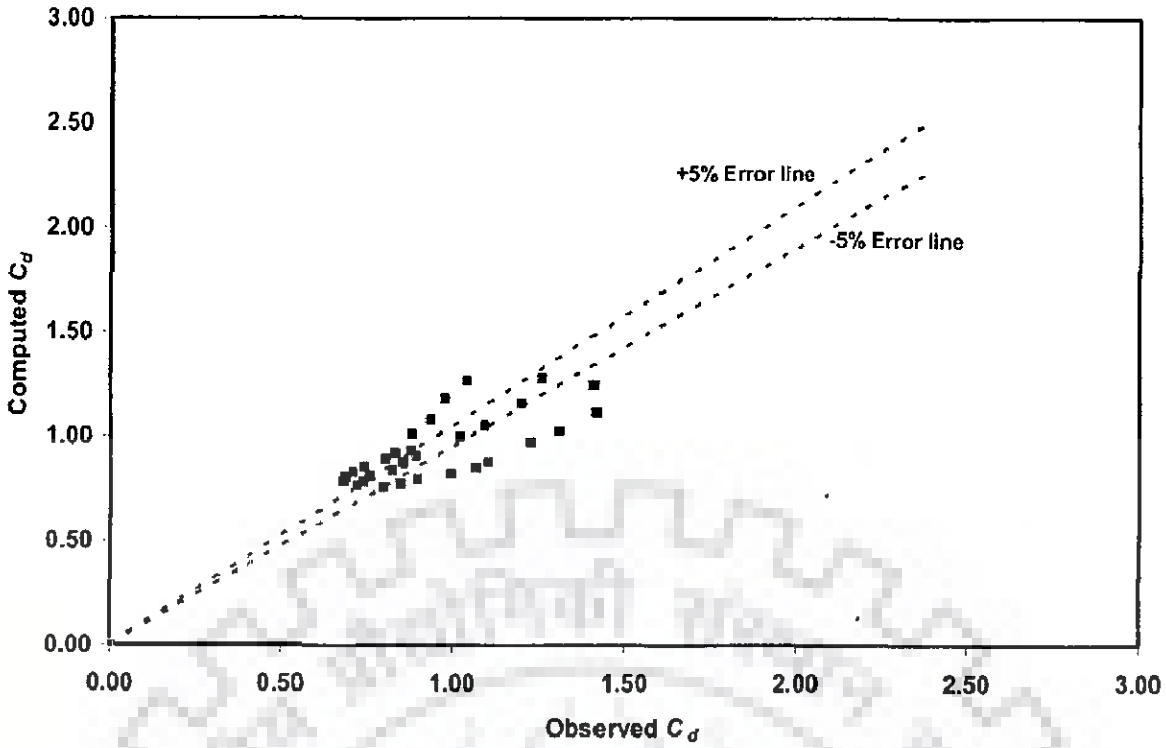

Fig. 6.17 Error analysis between observed and computed C_d for $L/W = 4.84$ using Eq. (6.14)

6.5.3 Variation of Discharge Coefficient with Froude No. for L/W as 7.4

Fig. 6.18 shows discharge coefficient variation for different values of Fr. The following equation best describes the experimental data

$$C_d = 0.371 Fr^{-0.6841}; R^2 = 0.8544 \quad (6.15)$$

Fig. 6.19 shows that the error between observed and computed discharge coefficient lies in the range of -31 to +23 % for L/W as 7.4. Average absolute percentage error between computed and observed discharge coefficient using Eq. (6.15) is found to be 11.13.

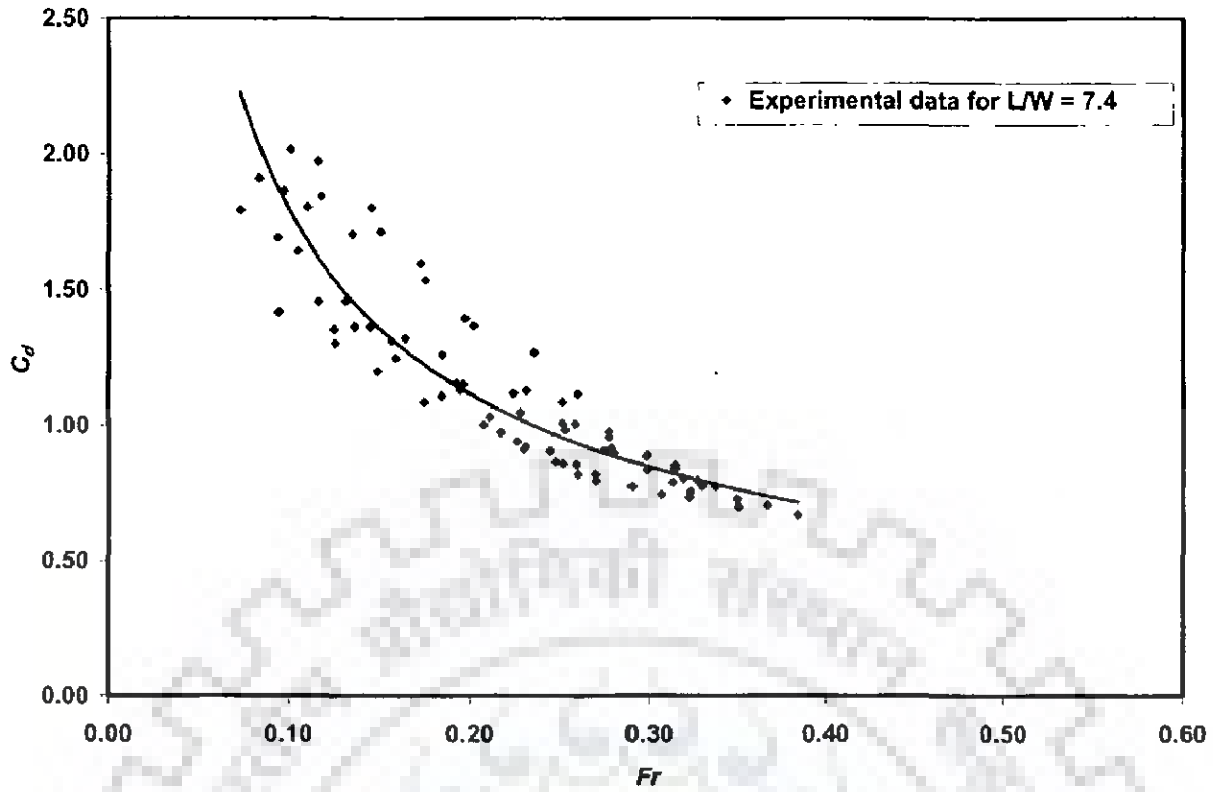

Fig. 6.18 Plot between *Fr* and C_d for *L/W* = 7.4

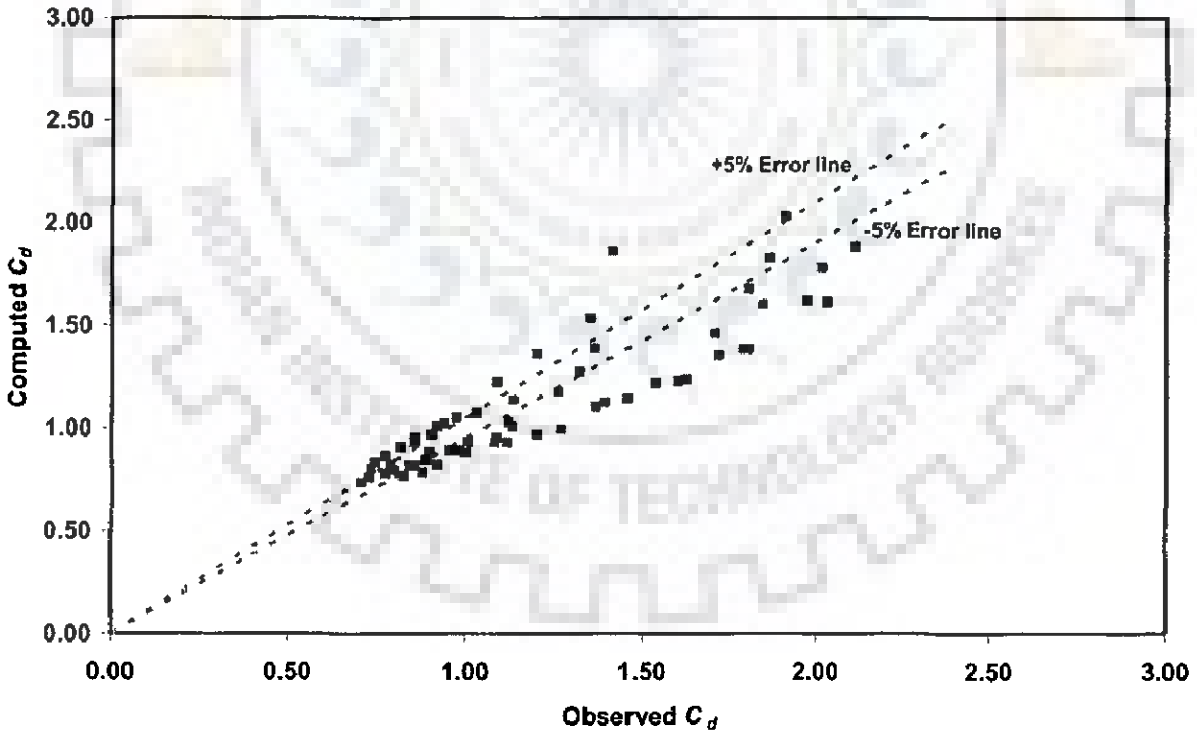

Fig. 6.19 Error analysis between observed and computed C_d for *L/W* = 7.4 using Eq. (6.15)

6.5.4 Variation of Discharge Coefficient with h/p for *L/W* as 3.56

Fig. 6.20 shows discharge coefficient variation for different values of *h/p*. If C_d is related with *h/p* only, the following equation best describes the experimental data

$$C_d = 0.6858 h/p^{-0.305}; R^2 = 0.88 \quad (6.16)$$

Fig. 6.21 shows that the error between observed and computed discharge coefficient lies in the range of -10 to +15 % for *L/W* as 3.56. Average absolute percentage error between computed and observed discharge coefficient using Eq. (6.16) is found to be 4.17.

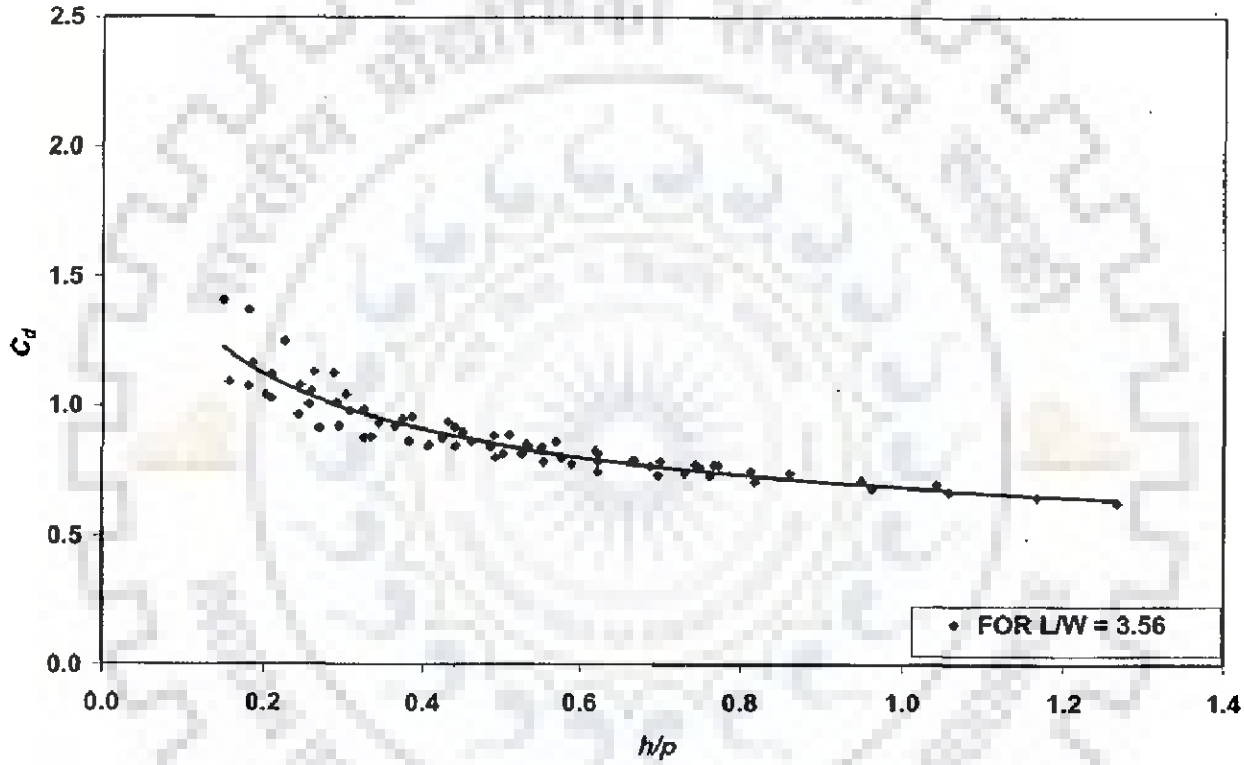

Fig. 6.20 Plot between *h/p* and C_d for *L/W* = 3.56

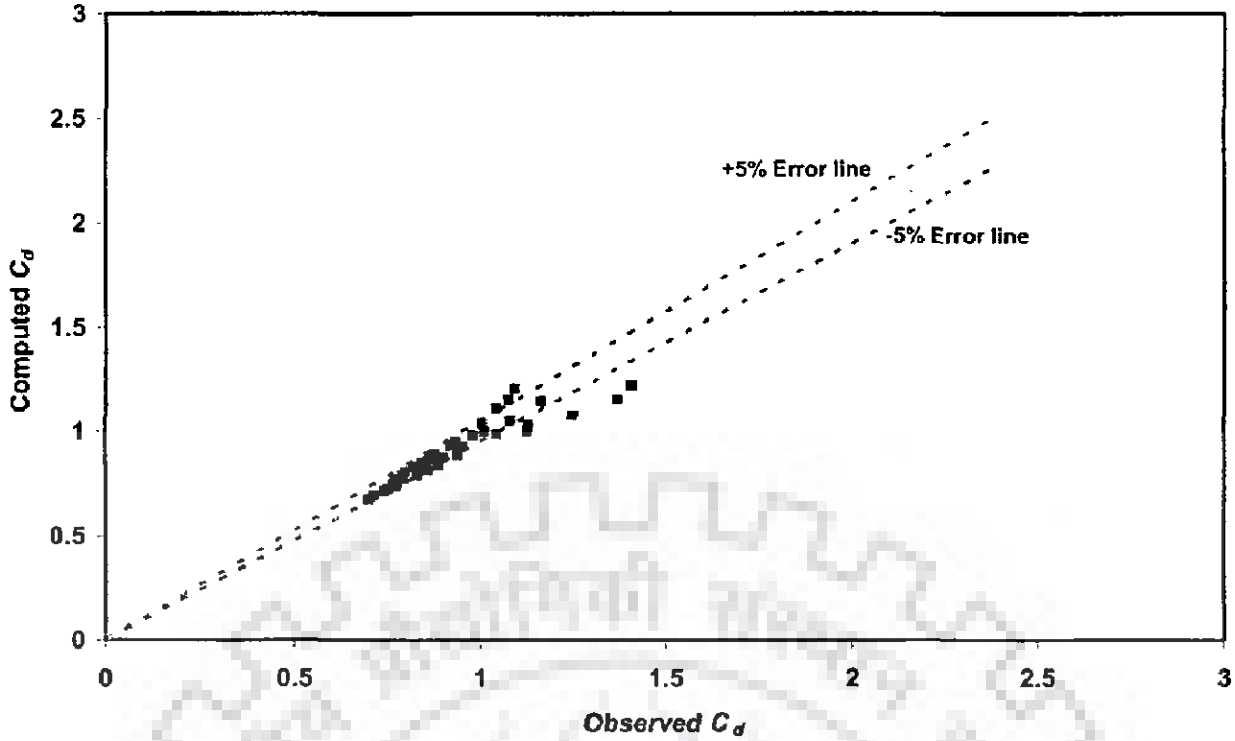

Fig. 6.21 Error analysis between observed and computed C_d for $L/W = 3.56$ using Eq. (6.16)

6.5.5 Variation of Discharge Coefficient with *h/p* for *L/W* as 4.84

Fig. 6.22 shows discharge coefficient variation for different values of *h/p*. If C_d is related with *h/p* only, the following equation best describes the experimental data

$$C_d = 0.667\, h/p^{-0.3703};\ R^2 = 0.80 \qquad (6.17)$$

Fig. 6.23 shows that the error between observed and computed discharge coefficient lies in the range of -18 to +14 % for *L/W* as 4.84. Average absolute percentage error between computed and observed discharge coefficient using Eq. (6.17) is found to be 7.61.

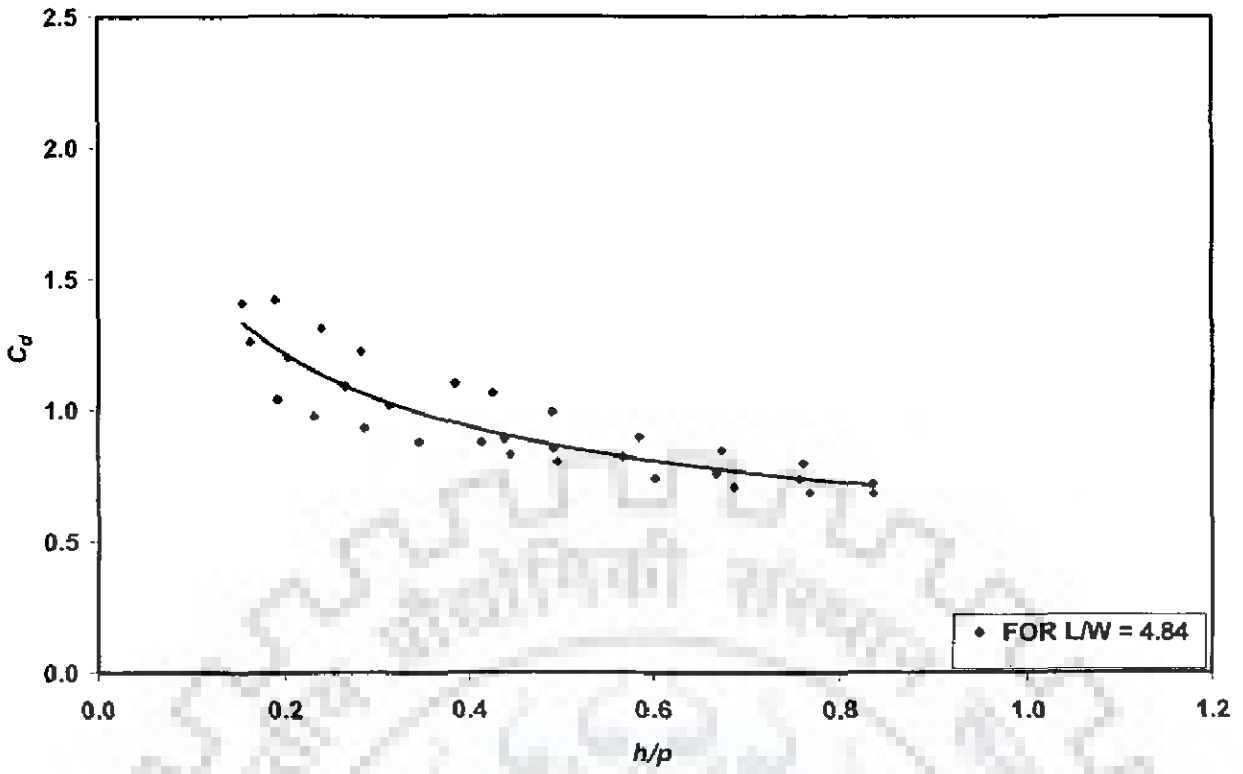

Fig. 6.22 Plot between h/p and C_d for $L/W = 4.84$

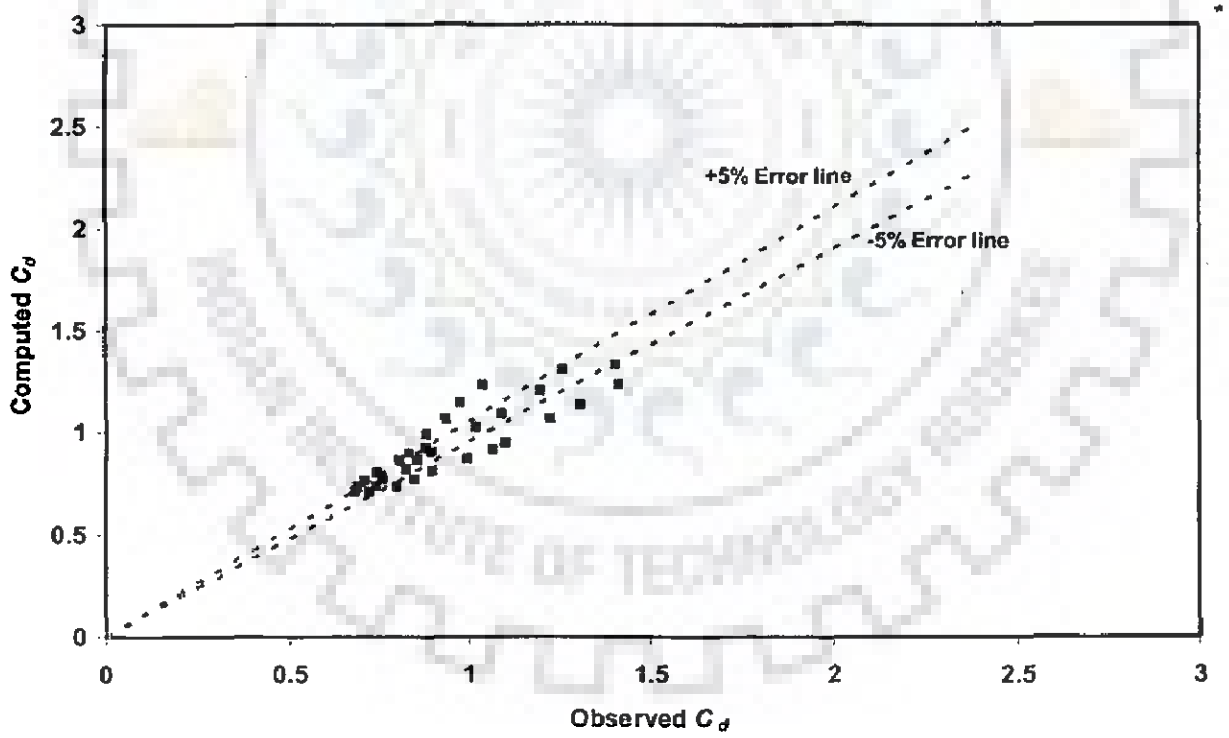

Fig. 6.23 Error analysis between observed and computed C_d for L/W = 4.84 using Eq. (6.17)

6.5.6 Variation of Discharge Coefficient with h/p for *L/W* as 7.4

Fig. 6.24 shows discharge coefficient variation for different values of *h/p*. If C_d is related with *h/p* only, the following equation best describes the experimental data

$$C_d = 0.688\, h/p^{-0.4673};\ R^2 = 0.95 \qquad (6.18)$$

Fig. 6.25 shows that the error between observed and computed discharge coefficient lies in the range of -17 to +13 % for *L/W* as 7.4. Average absolute percentage error between computed and observed discharge coefficient using Eq. (6.18) is found to be 6.67.

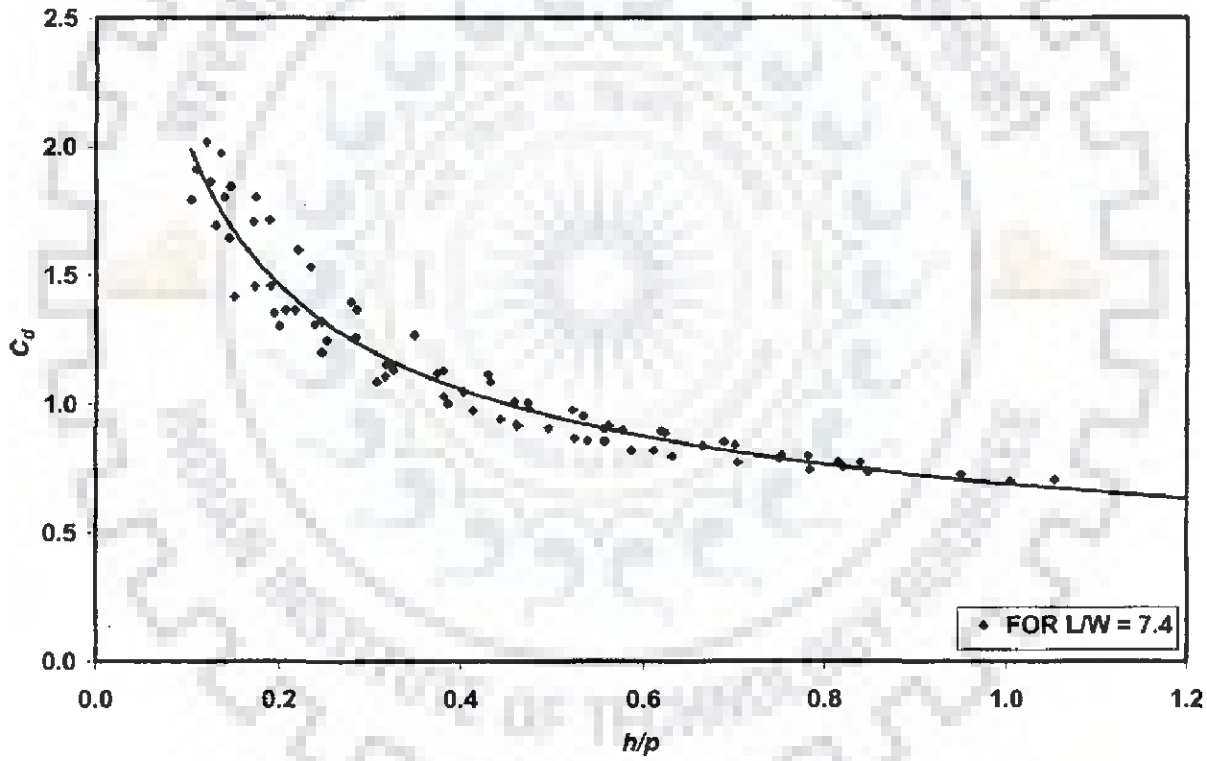

Fig. 6.24 Plot between *h/p* and C_d for *L/W* = 7.4

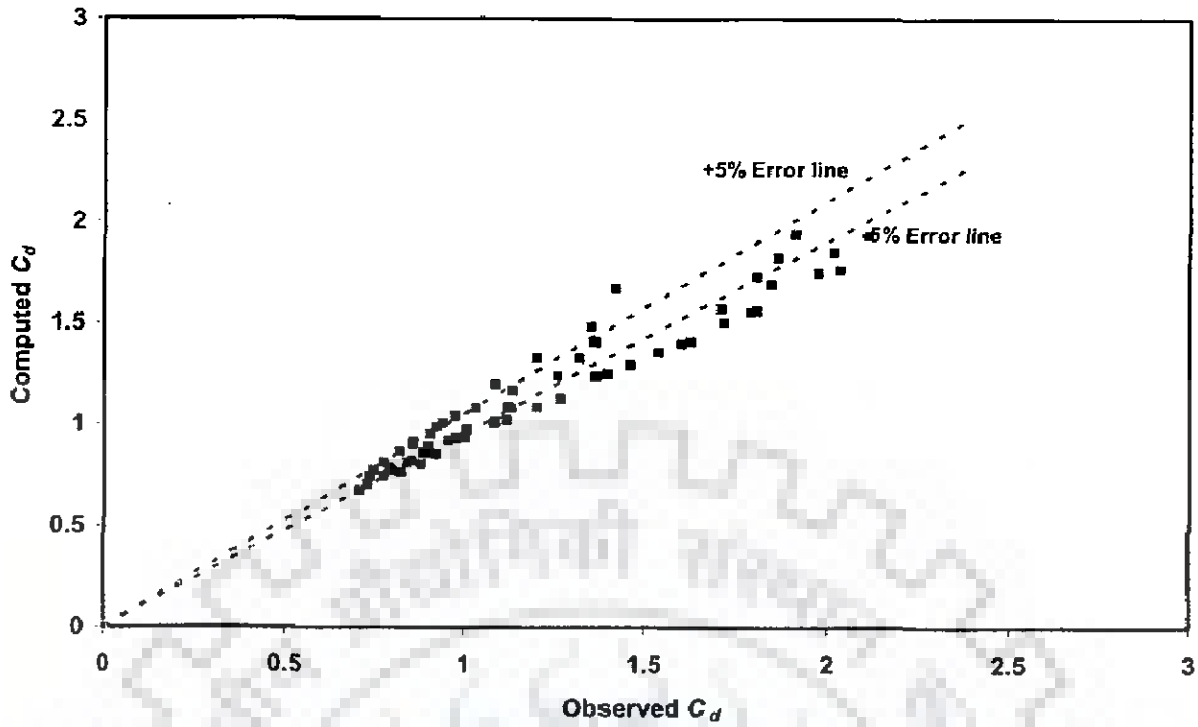

Fig. 6.25 Error analysis between observed and computed C_d for $L/W = 7.4$ using Eq. (6.18)

6.5.7 Variation of Discharge Coefficient with Froude No. and *h/p*

In the previous option, only the upstream (or approach) Froude number (Fr) is taken as the main variable in the development of formula for discharge coefficient analysis. As R^2 was not very high, the option of including an additional variable h/p is explored.

6.5.7.1 Variation of discharge coefficient with Froude No. and *h/p* for *L/W* as 3.56

The variation of discharge coefficient with Fr and h/p is shown in Figs. 6.26 and 6.27 respectively. The polynomial regression model for L/W as 3.56 yields the following functional form

$$C_d = 1.314 - 0.2037h/p - 1.350Fr;\ R^2 = 0.771 \quad (6.19)$$

Fig. 6.28 shows that the error between observed and computed discharge coefficient lies in the range of -9 to +18 % for L/W as 3.56. Average absolute percentage error between computed and observed discharge coefficient using Eq. (6.19) is found to be 6.12.

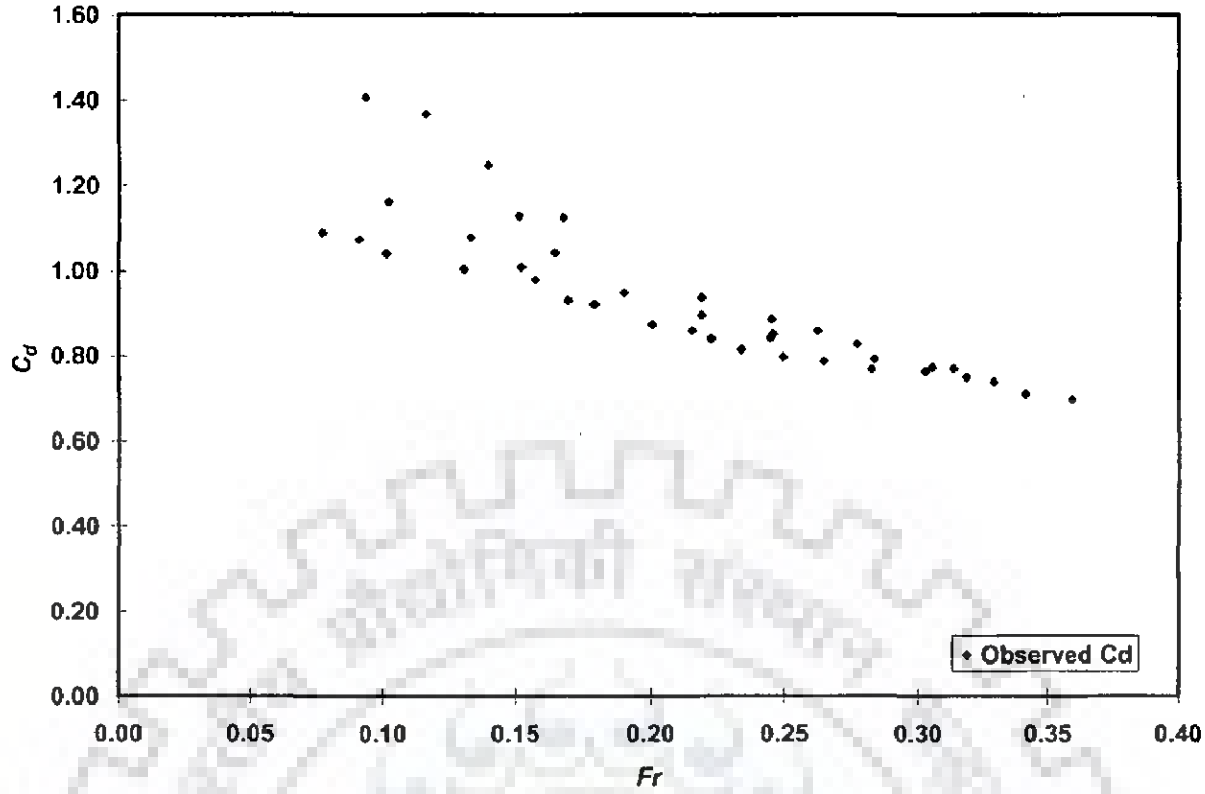

Fig. 6.26 Graphical plot between *Fr* and C_d for *L/W* = 3.56

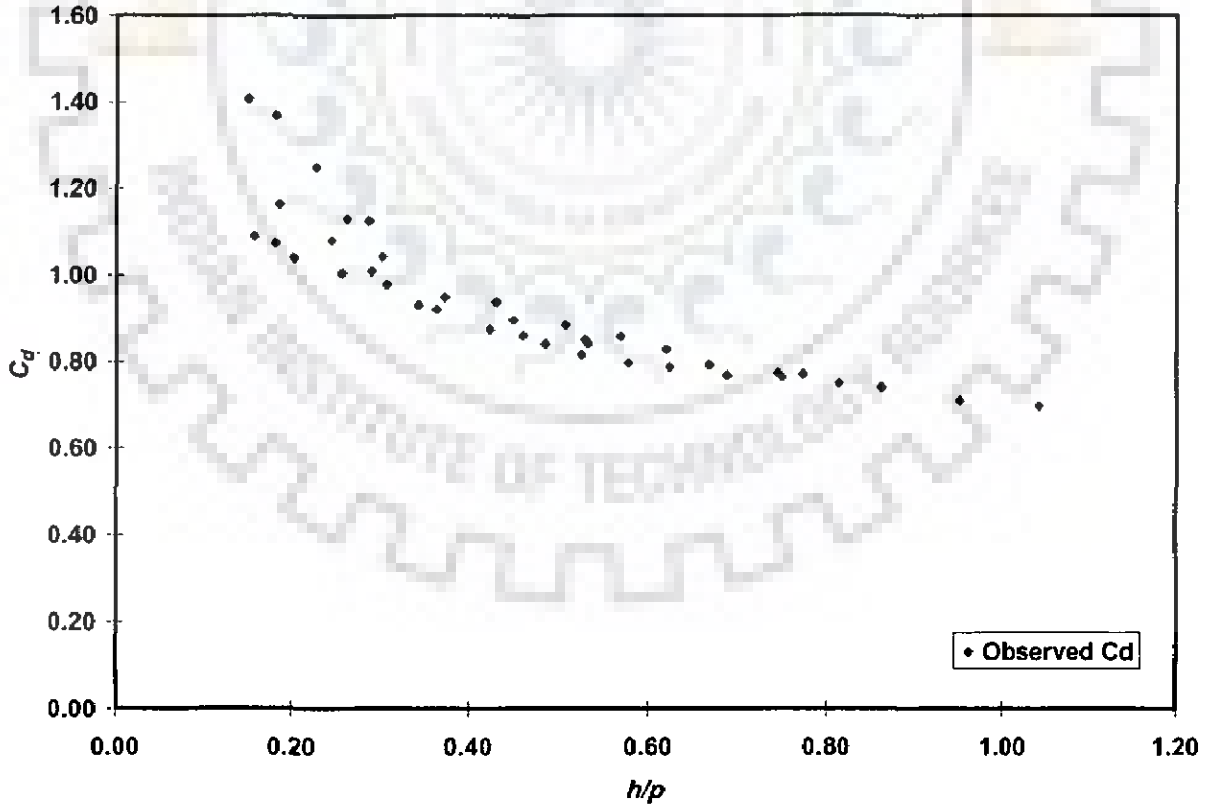

Fig. 6.27 Graphical plot between *h/p* and C_d for *L/W* = 3.56

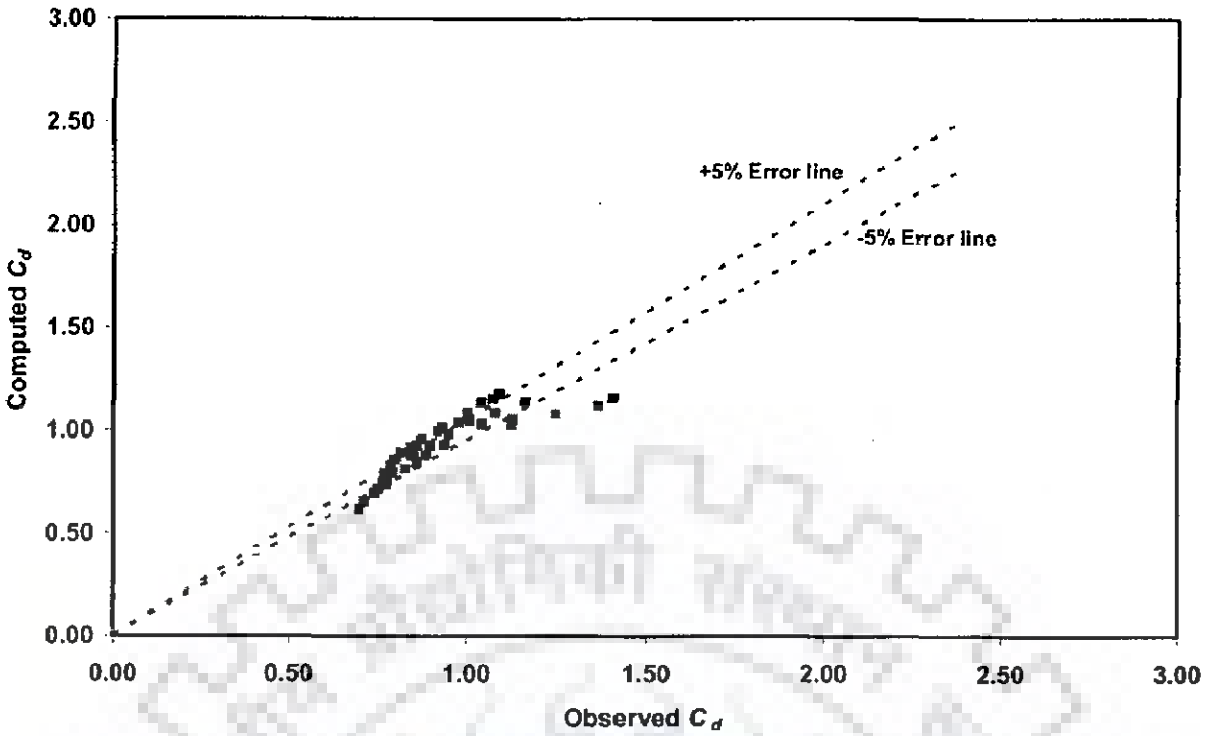

Fig. 6.28 Error analysis between observed and computed C_d for $L/W = 3.56$ using Eq. (6.19)

6.5.7.2 Variation of discharge coefficient with Froude No. and *h/p* for *L/W* as 4.84

The variation of discharge coefficient with *Fr* and *h/p* is shown in Figs. 6.29 and 6.30 respectively. The polynomial regression model for *L/W* as 4.84 yields the following functional form

$$C_d = 1.207 - 1.476h/p + 2.014Fr\,;\ R^2 = 0.771 \qquad (6.20)$$

Fig. 6.31 shows that the error between observed and computed discharge coefficient lies in the range of -16 to +16 % for *L/W* as 4.84. Average absolute percentage error between computed and observed discharge coefficient using Eq. (6.20) is found to be 8.50.

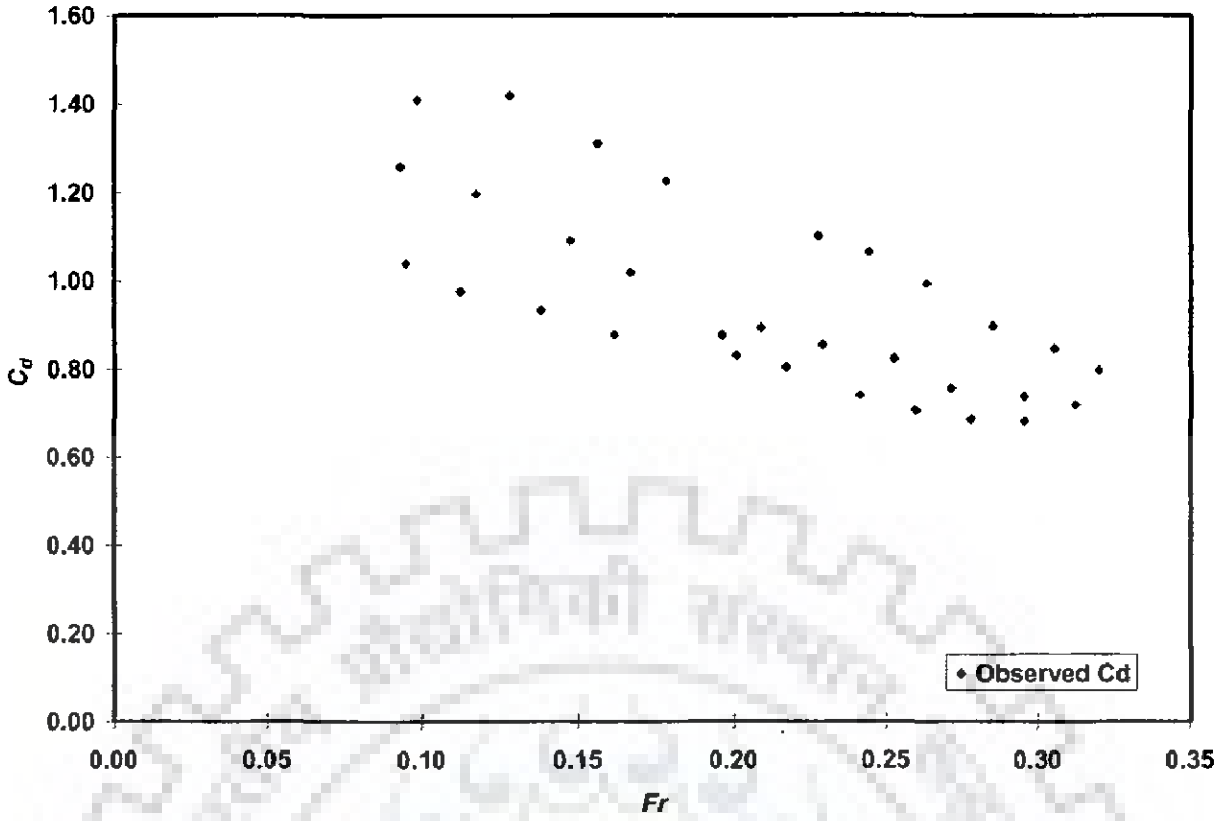

Fig. 6.29 Graphical plot between Fr and C_d for $L/W = 4.84$

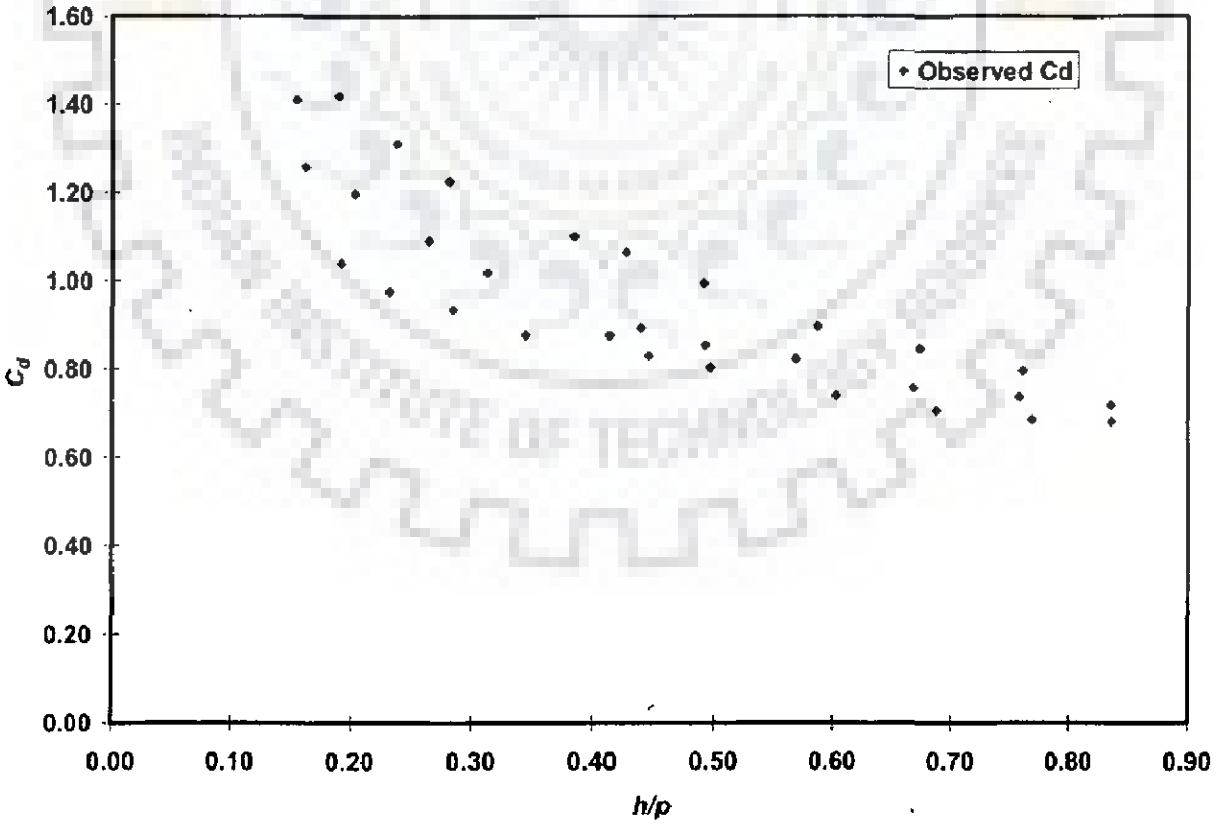

Fig. 6.30 Graphical plot between h/p and C_d for $L/W = 4.84$

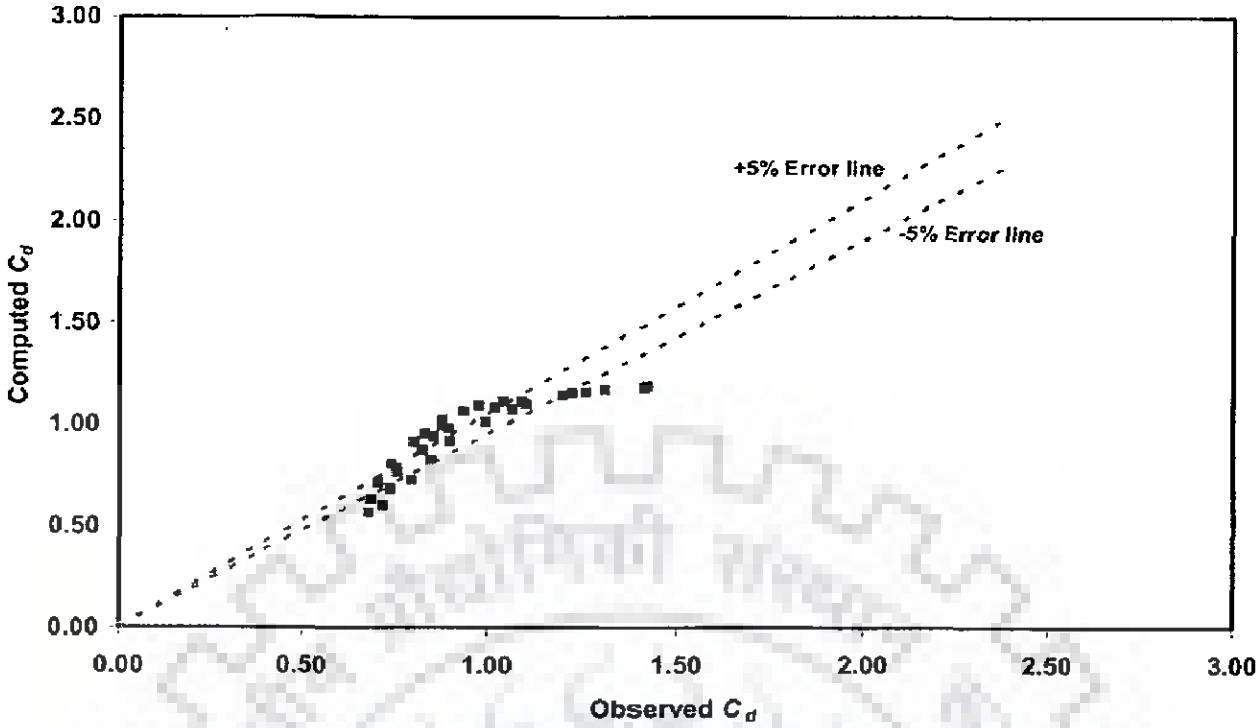

Fig. 6.31 Error analysis between observed and computed C_d for $L/W = 4.84$ using Eq. (6.20)

6.5.7.3 Variation of discharge coefficient with Froude No. and *h/p* for *L/W* as 7.4

The variation of discharge coefficient with Fr and h/p is shown in Figs. 6.32 and 6.33 respectively. The polynomial regression model for L/W as 7.4 yields the following functional form

$$C_d = 2.16 - 0.3619h/p - 3.582Fr\,;\, R^2 = 0.818 \qquad (6.21)$$

Fig. 6.34 shows that the error between observed and computed discharge coefficient lies in the range of -31 to +33 % for L/W as 7.4. Average absolute percentage error between computed and observed discharge coefficient using Eq. (6.21) is found to be 12.02.

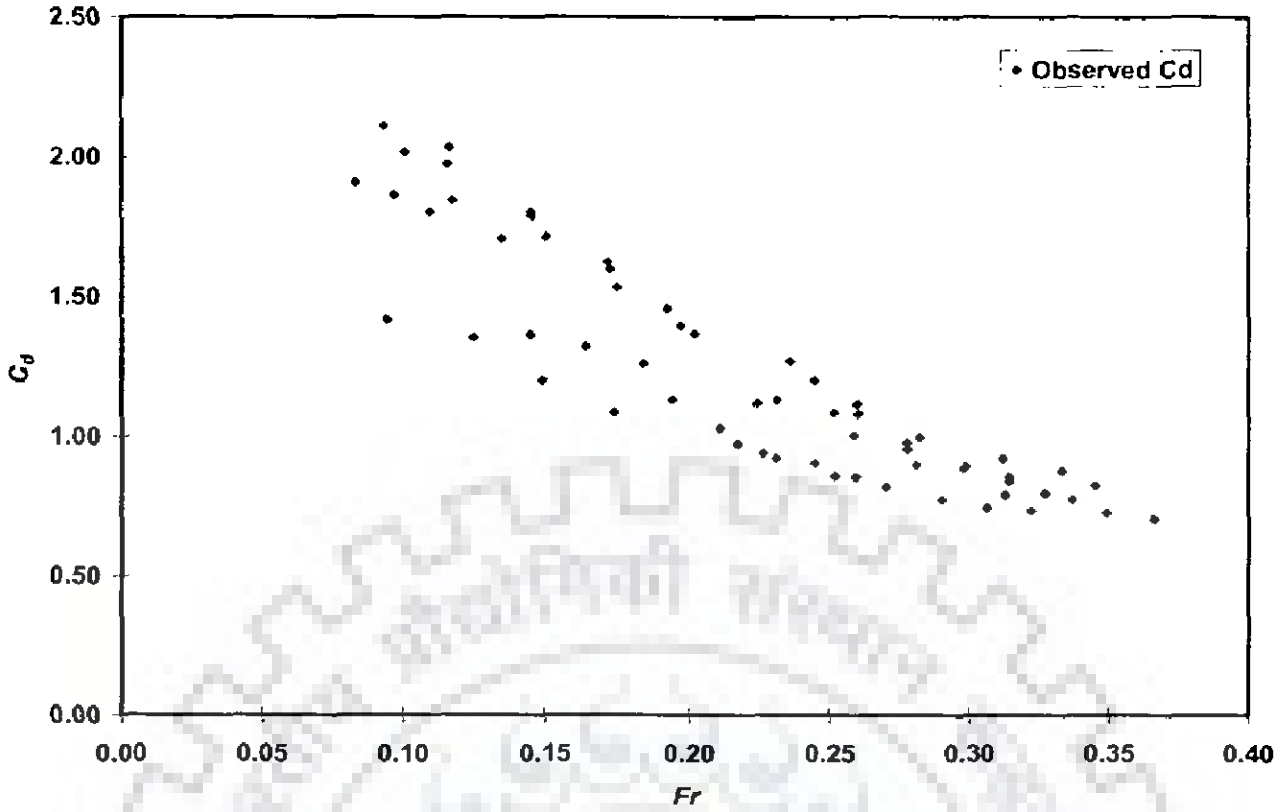

Fig. 6.32 Graphical plot between Fr and C_d for $L/W = 7.4$

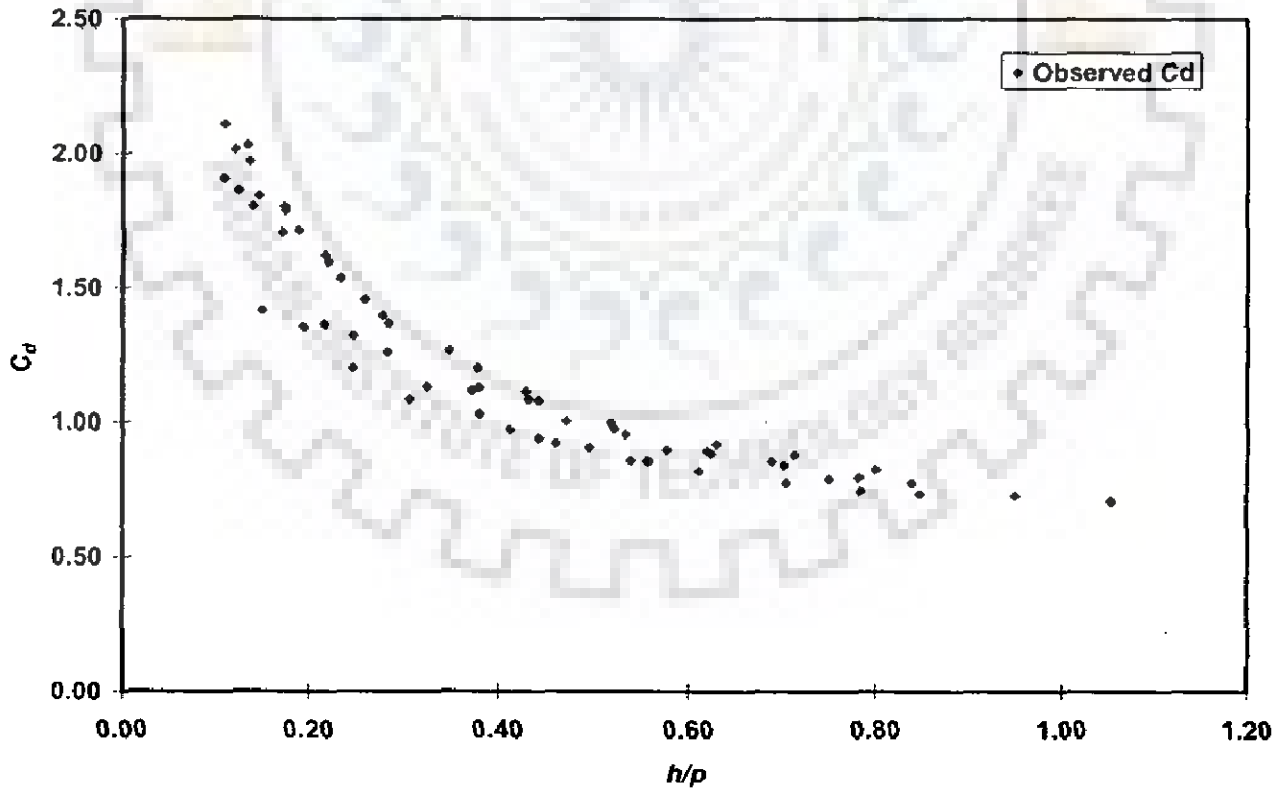

Fig. 6.33 Graphical Plot between h/p and C_d for $L/W = 7.4$

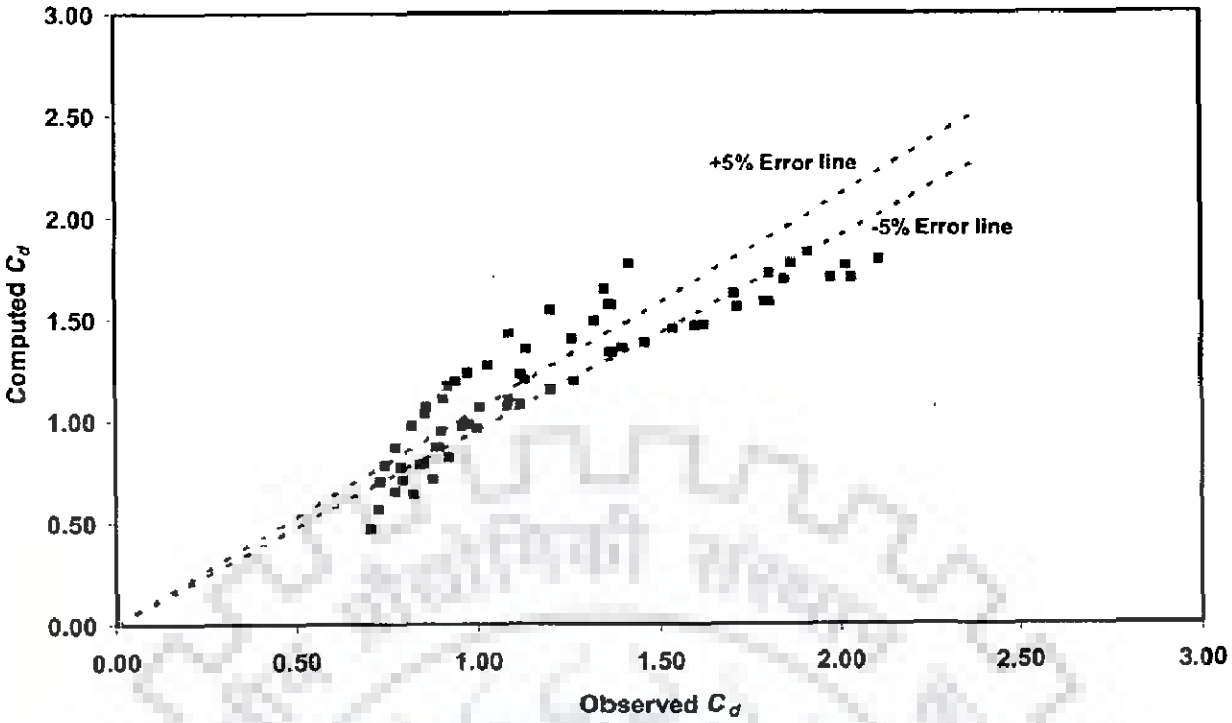

Fig. 6.34 Error analysis between observed and computed C_d for $L/W = 7.4$ using Eq. (6.21)

6.5.8 Variation of Discharge Coefficient with Froude No. and *h/p* in Two Distinct Segments

The analysis done in the previous section indicated the possibility of exploring the refinements in the developed regression relationships between discharge coefficient, *Fr* and *h/p* in different ranges of *h/p*. For this reason, the results of analysis considering two different segments of C_d variation with *h/p* between 0 and 0.4 and greater than 0.4 are presented next.

6.5.8.1 Variation of discharge coefficient with Froude No. and *h/p* upto 0.4 for *L/W* as 3.56

The variation of discharge coefficient with *Fr* and *h/p* upto 0.4 is shown in Figs. 6.35 and 6.36 respectively. The polynomial regression model is developed as follows:

$$C_d = 1.30 - 5.3h/p + 8.42Fr;\ R^2 = 0.92 \qquad (6.22)$$

Fig. 6.37 shows that the error between observed and computed discharge coefficient lies in the range of -4 to +8 % for *L/W* as 3.56 and *h/p* up to 0.4. Average absolute percentage error between computed and observed discharge coefficient using Eq. (6.22) is 3.30. Also, R^2 value is found to improve from 0.771 to 0.92.

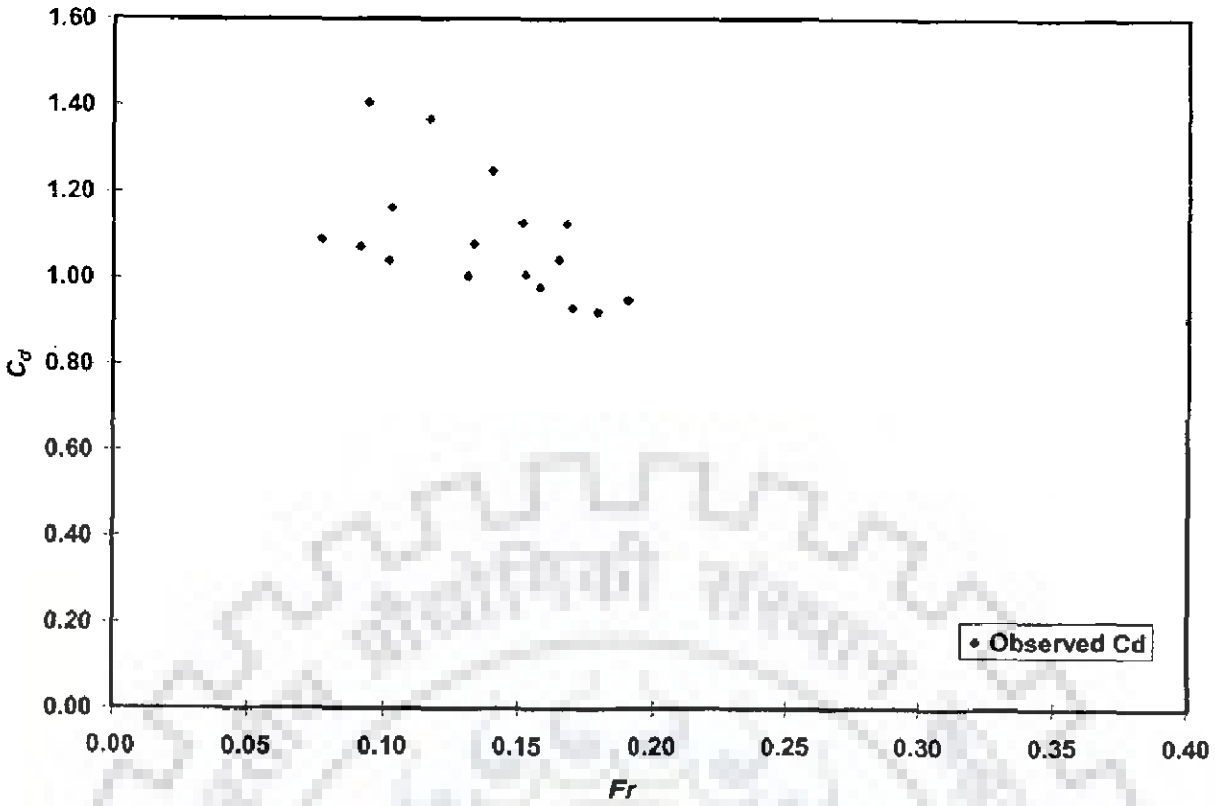

Fig. 6.35 Graphical plot between *Fr* and C_d for *L/W* = 3.56 and *h/p* upto 0.4

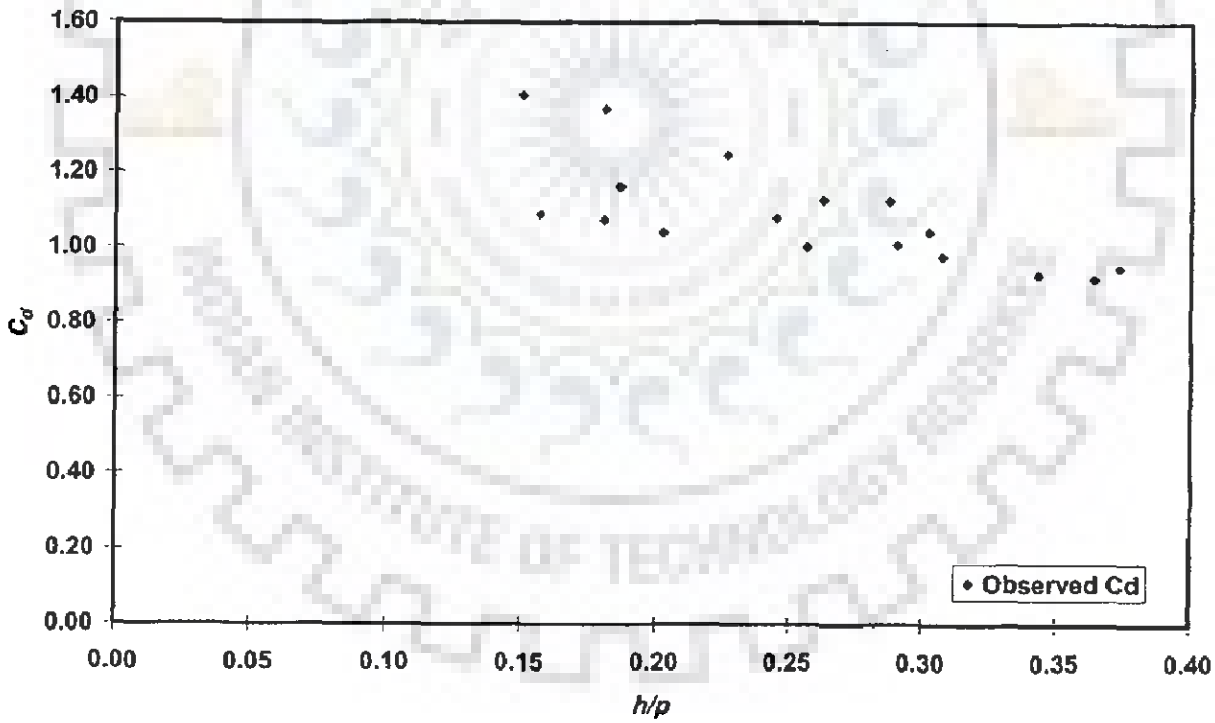

Fig. 6.36 Graphical plot between *h/p* and C_d for *L/W* = 3.56 and *h/p* upto 0.4

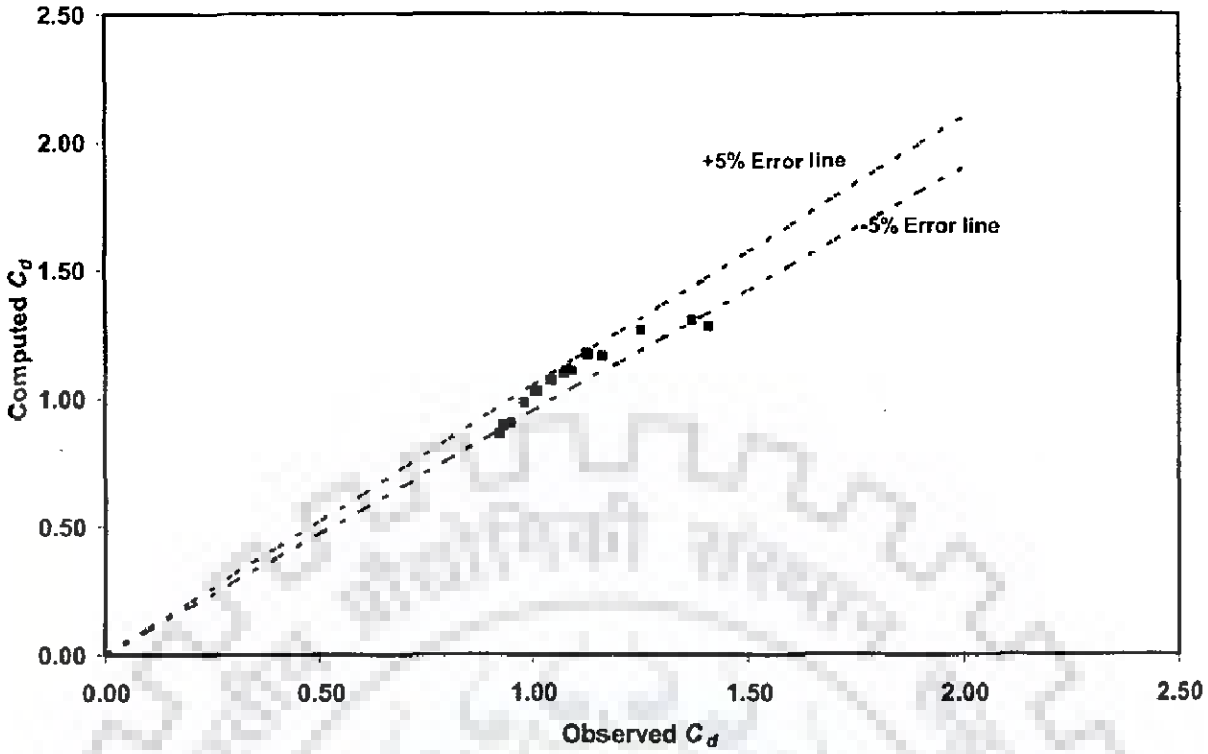

Fig. 6.37 Error analysis between observed and computed C_d for $L/W = 3.56$ and h/p upto 0.4 using Eq. (6.22)

6.5.8.2 Variation of discharge coefficient with Froude No. and *h/p* greater than 0.4 for *L/W* as 3.56

The variation of discharge coefficient with *Fr* and *h/p* greater than 0.4 is shown in Figs. 6.38 and 6.39, respectively. The polynomial regression model is developed as follows:

$$C_d = 0.92 - 0.57h/p + 0.9Fr\,;\ R^2 = 0.90 \qquad (6.23)$$

Fig. 6.40 shows that the error between observed and computed discharge coefficient lies in the range of -4 to +6 % for *L/W* as 3.56 and *h/p* greater than 0.4. Average absolute percentage error between computed and observed discharge coefficient using Eq. (6.23) is 1.93. Also, R^2 value is found to improve from 0.771 to 0.90.

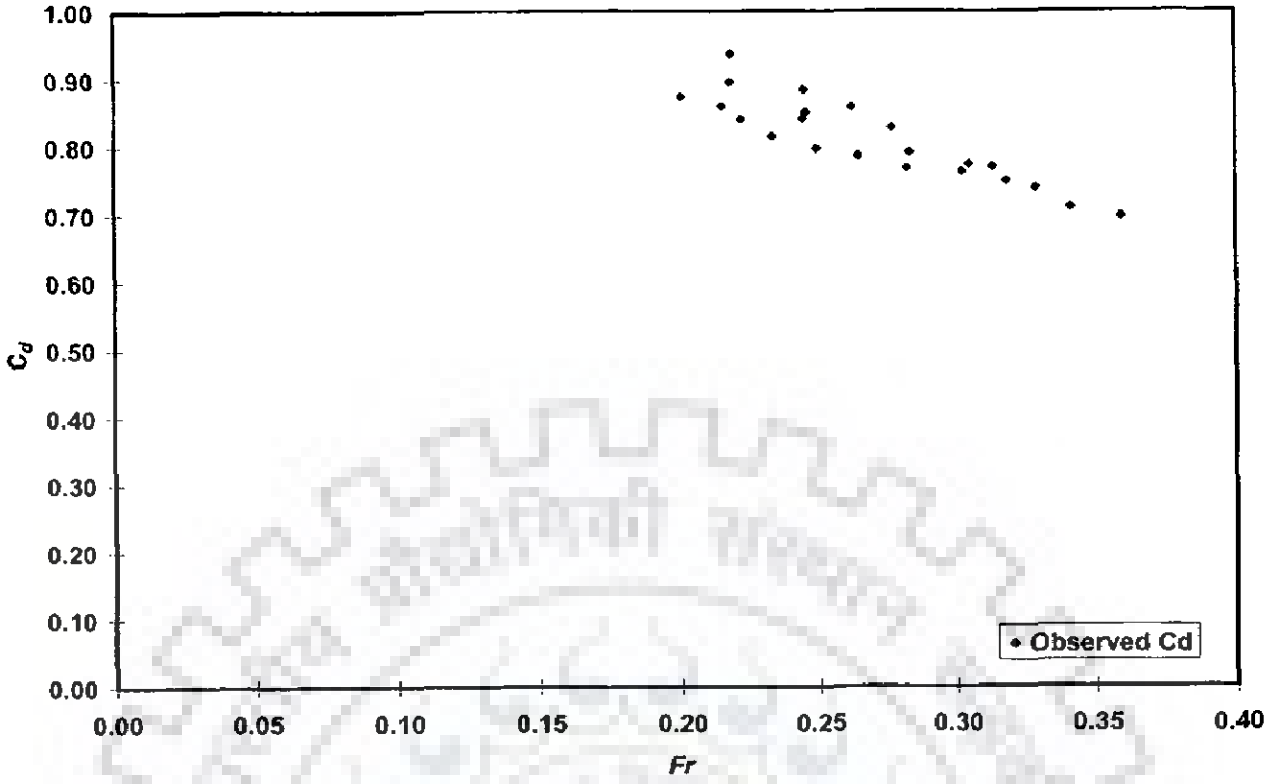

Fig. 6.38 Graphical plot between *Fr* and C_d for *L/W* = 3.56 and *h/p* greater than 0.4

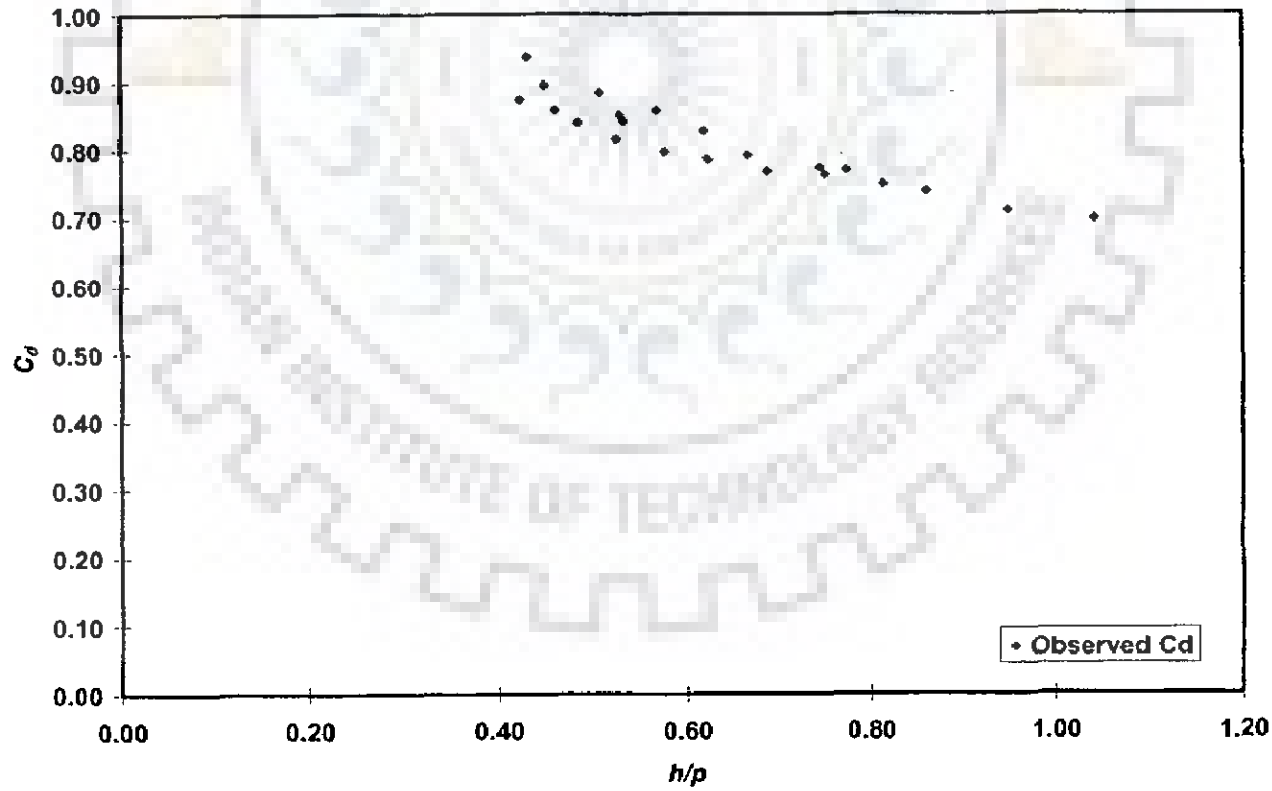

Fig. 6.39 Graphical plot between *h/p* and C_d for *L/W* = 3.56 and *h/p* greater than 0.4

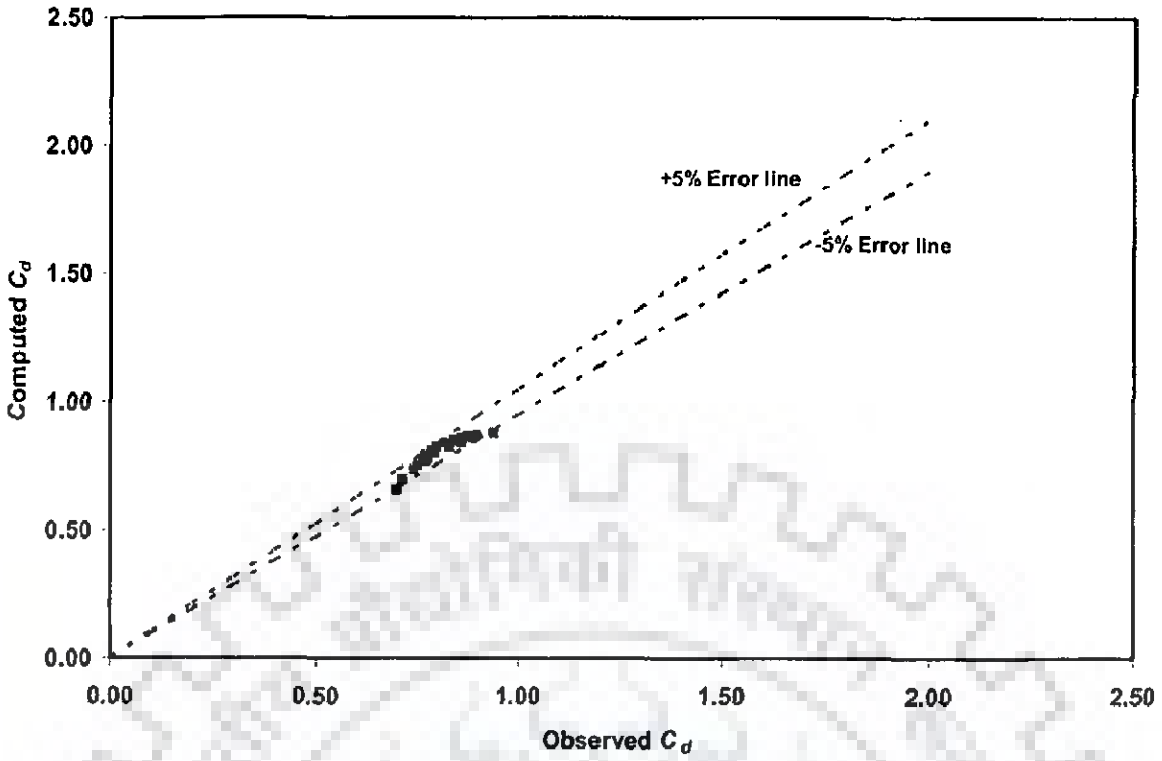

Fig. 6.40 Error analysis between observed and computed C_d for $L/W = 3.56$ and h/p greater than 0.4 using Eq. (6.23)

6.5.8.3 Variation of discharge coefficient with Froude No. and *h/p* upto 0.4 for *L/W* as 4.84

The variation of discharge coefficient with *Fr* and *h/p* upto 0.4 is shown in Figs. 6.41 and 6.42 respectively. The polynomial regression model is developed as follows:

$$C_d = 1.39 - 5.31h/p + 7.66Fr\,;\, R^2 = 0.95 \qquad (6.24)$$

Fig. 6.43 shows that the error between observed and computed discharge coefficient lies in the range of -6 to +9 % for *L/W* as 4.84 and *h/p* upto 0.4. Average absolute percentage error between computed and observed discharge coefficient using Eq. (6.24) is 3.22. Also, R^2 value is found to improve from 0.771 to 0.95.

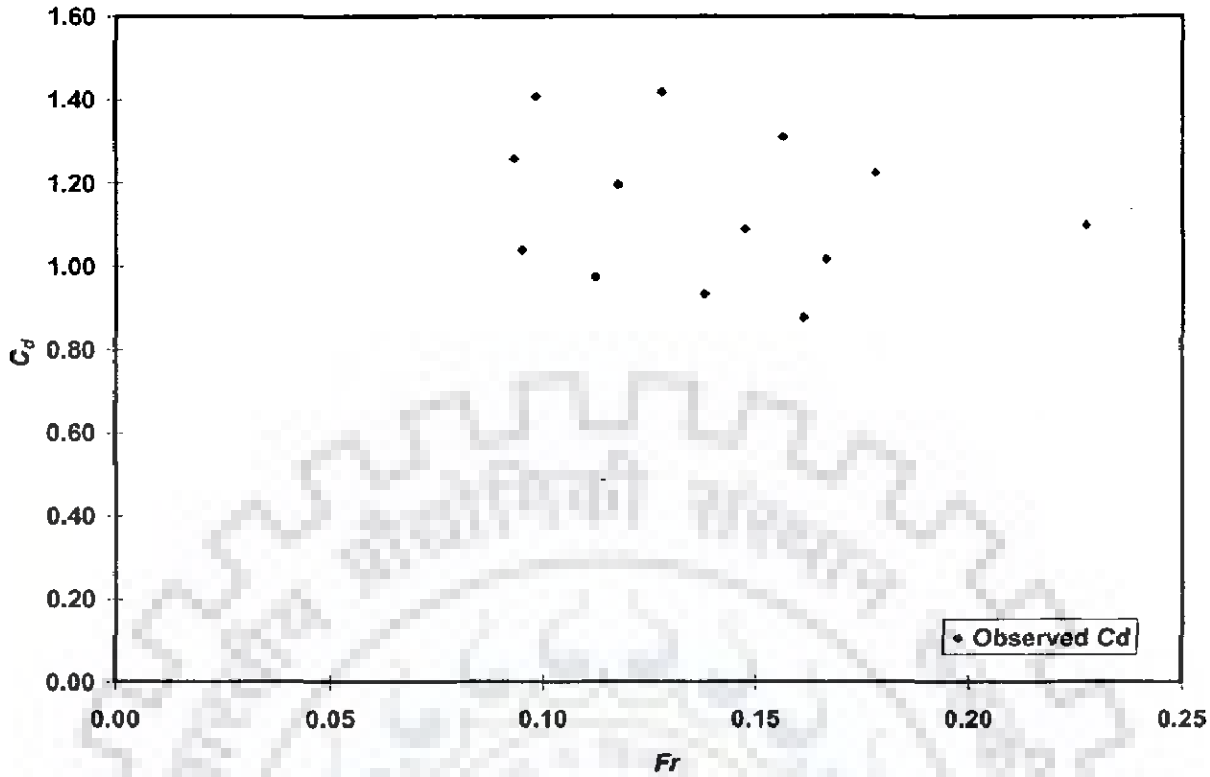

Fig. 6.41 Graphical plot between *Fr* and C_d for *L/W* = 4.84 and *h/p* upto 0.4

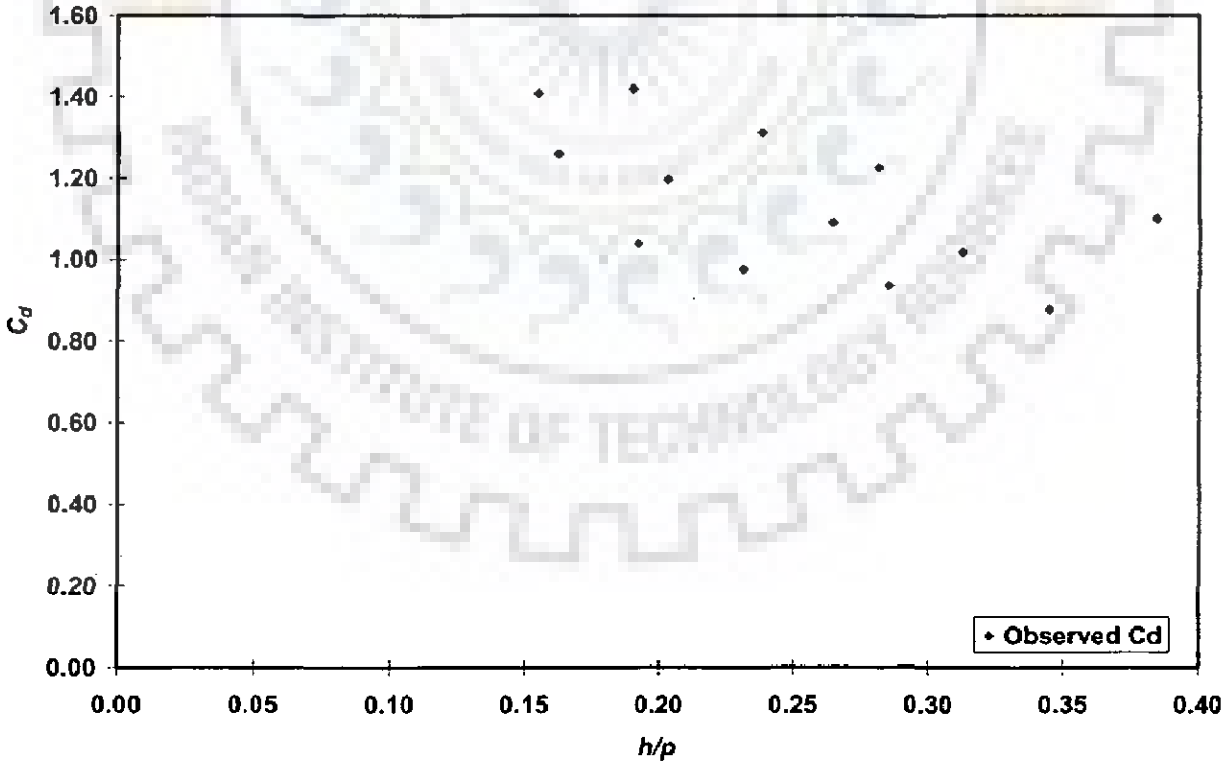

Fig. 6.42 Graphical plot between *h/p* and C_d for *L/W* = 4.84 and *h/p* upto 0.4

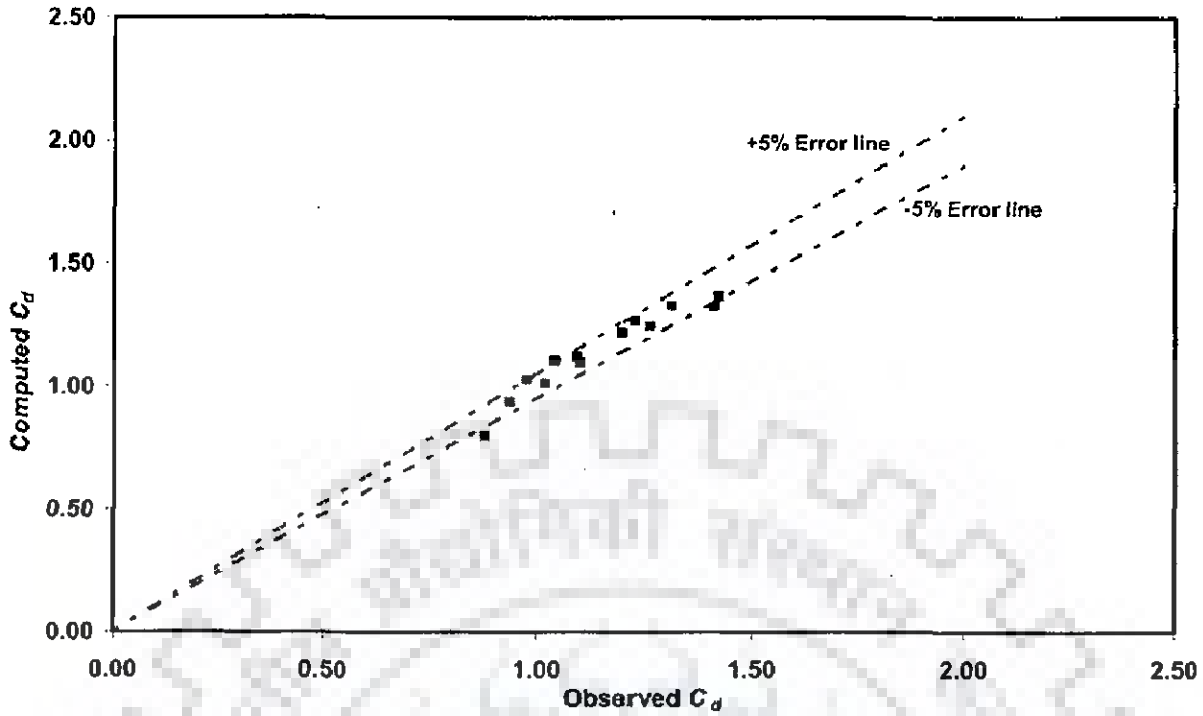

Fig. 6.43 Error analysis between observed and computed C_d for $L/W = 4.84$ and h/p upto 0.4 using Eq. (6.24)

6.5.8.4 Variation of discharge coefficient with Froude No. and h/p greater than 0.4 for L/W as 4.84

The variation of discharge coefficient with Fr and h/p greater than 0.4 is shown in Figs. 6.44 and 6.45 respectively. The polynomial regression model is developed as follows:

$$C_d = 0.77 - 1.27h/p + 3.11Fr\,;\ R^2 = 0.96 \qquad (6.25)$$

Fig. 6.46 shows that the error between observed and computed discharge coefficient lies in the range of -4 to +6 % for L/W as 4.84 and h/p greater than 0.4. Average absolute percentage error between computed and observed discharge coefficient using Eq. (6.25) is 2.63. Also, R^2 value is found to improve from 0.771 to 0.96.

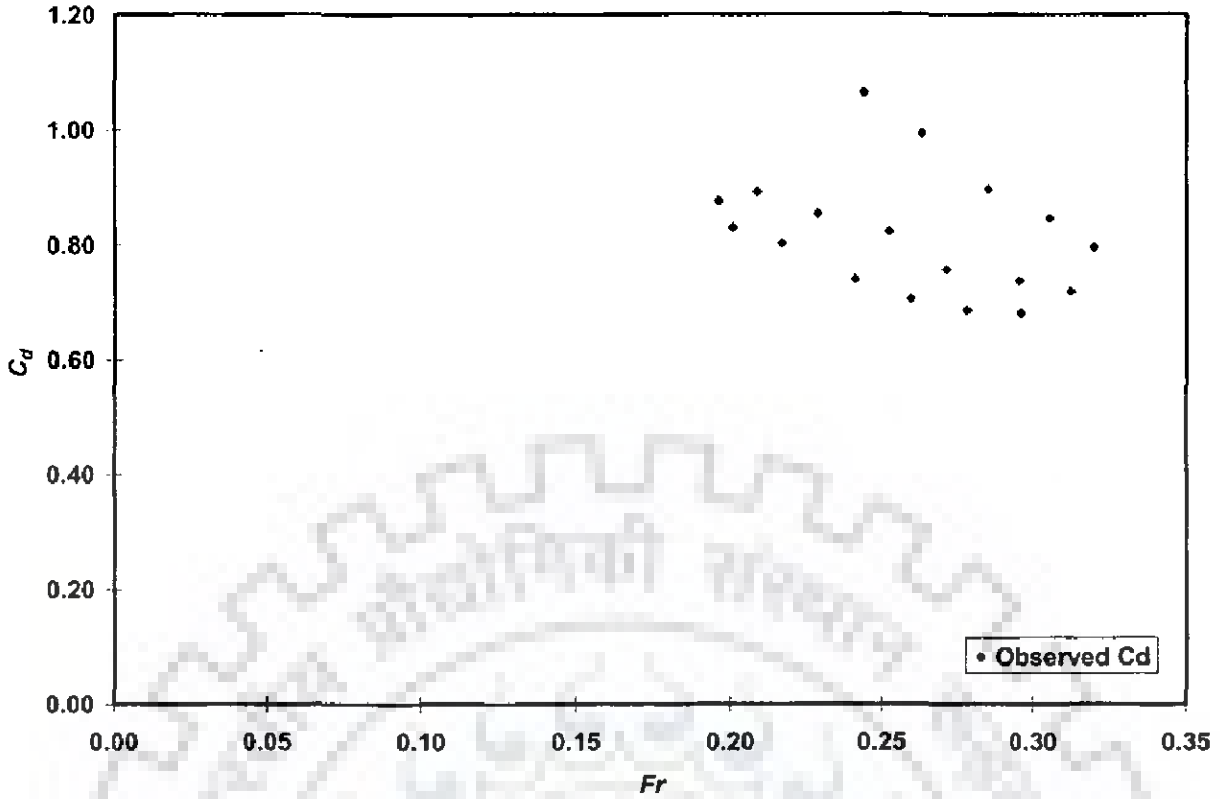

Fig. 6.44 Graphical plot between *Fr* and C_d for *L/W* = 4.84 and *h/p* greater than 0.4

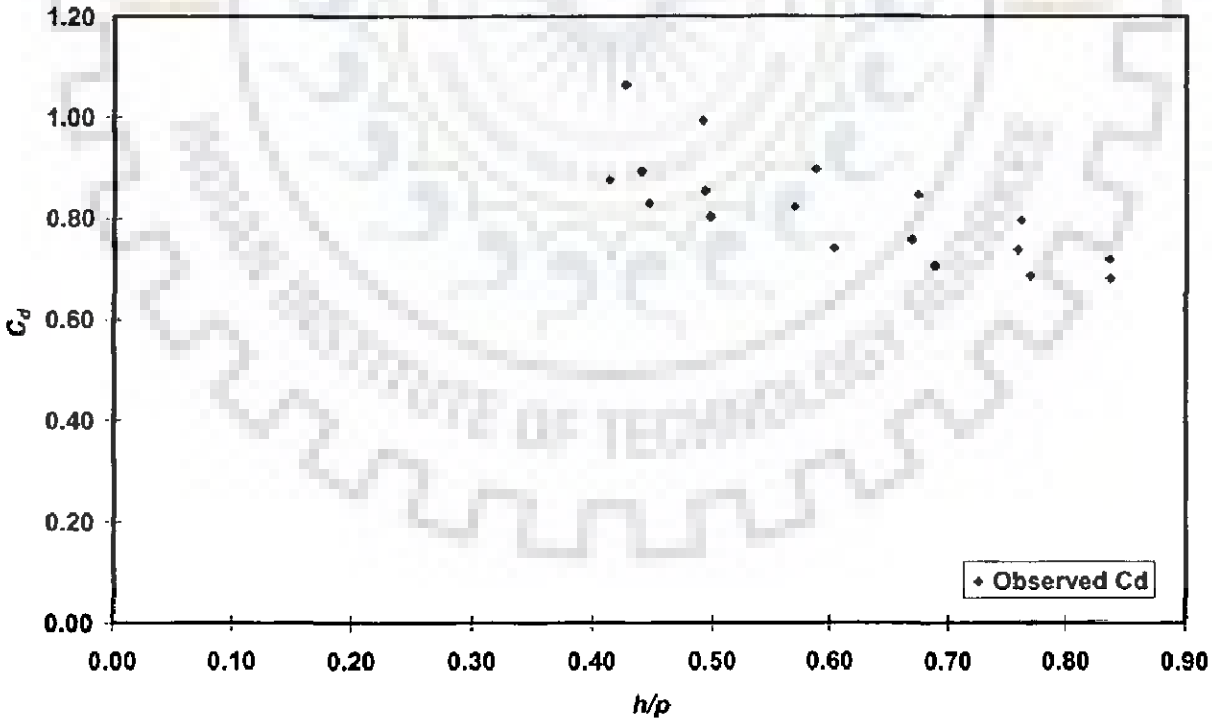

Fig. 6.45 Graphical plot between *h/p* and C_d for *L/W* = 4.84 and *h/p* greater than 0.4

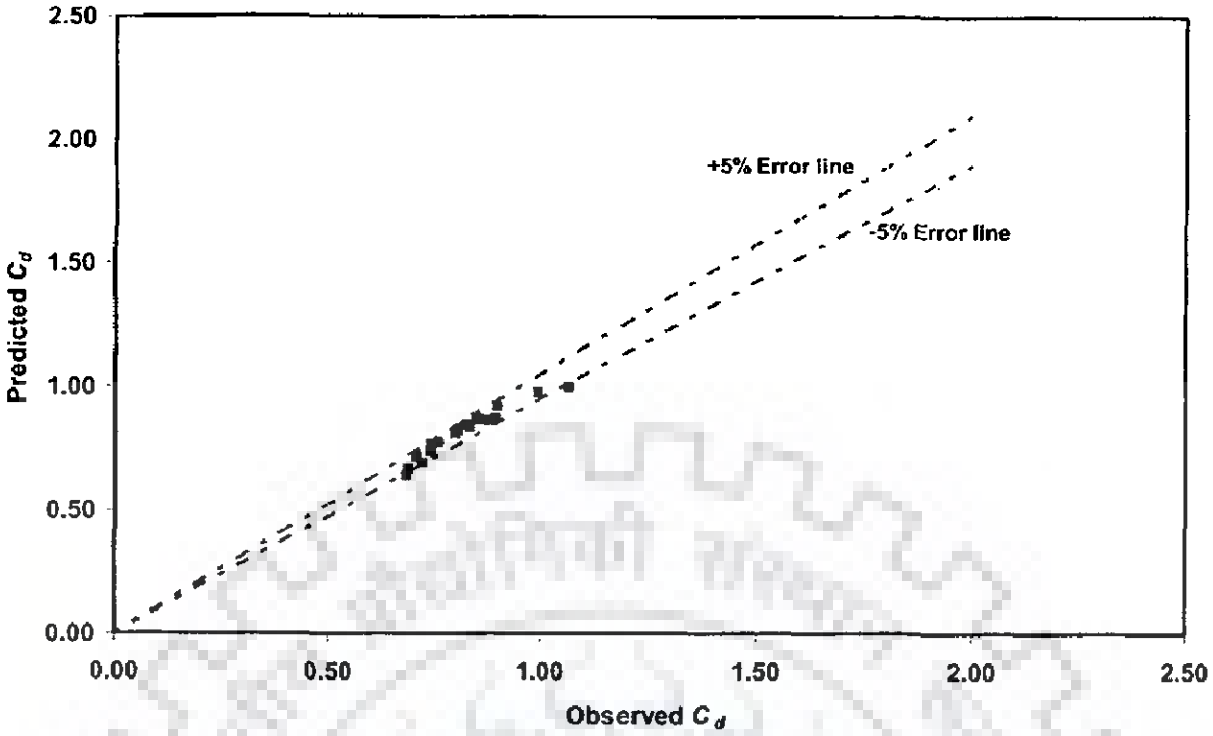

Fig. 6.46 Error analysis between observed and computed C_d for $L/W = 4.84$ and h/p greater than 0.4 using Eq. (6.25)

6.5.8.5 Variation of discharge coefficient with Froude No. and *h/p* upto 0.4 for *L/W* as 7.4

The variation of discharge coefficient with Fr and h/p upto 0.4 is shown in Figs. 6.47 and 6.48 respectively. The polynomial regression model is developed as follows:

$$C_d = 2 - 6.5h/p + 6.36Fr\,;\ R^2 = 0.92 \qquad (6.26)$$

Fig. 6.49 shows that the error between observed and computed discharge coefficient lies in the range of -14 to +15 % for L/W as 7.4 and h/p upto 0.4. Average absolute percentage error between computed and observed discharge coefficient using Eq. (6.26) is 6.28. Also, R^2 value is found to improve from 0.818 to 0.92.

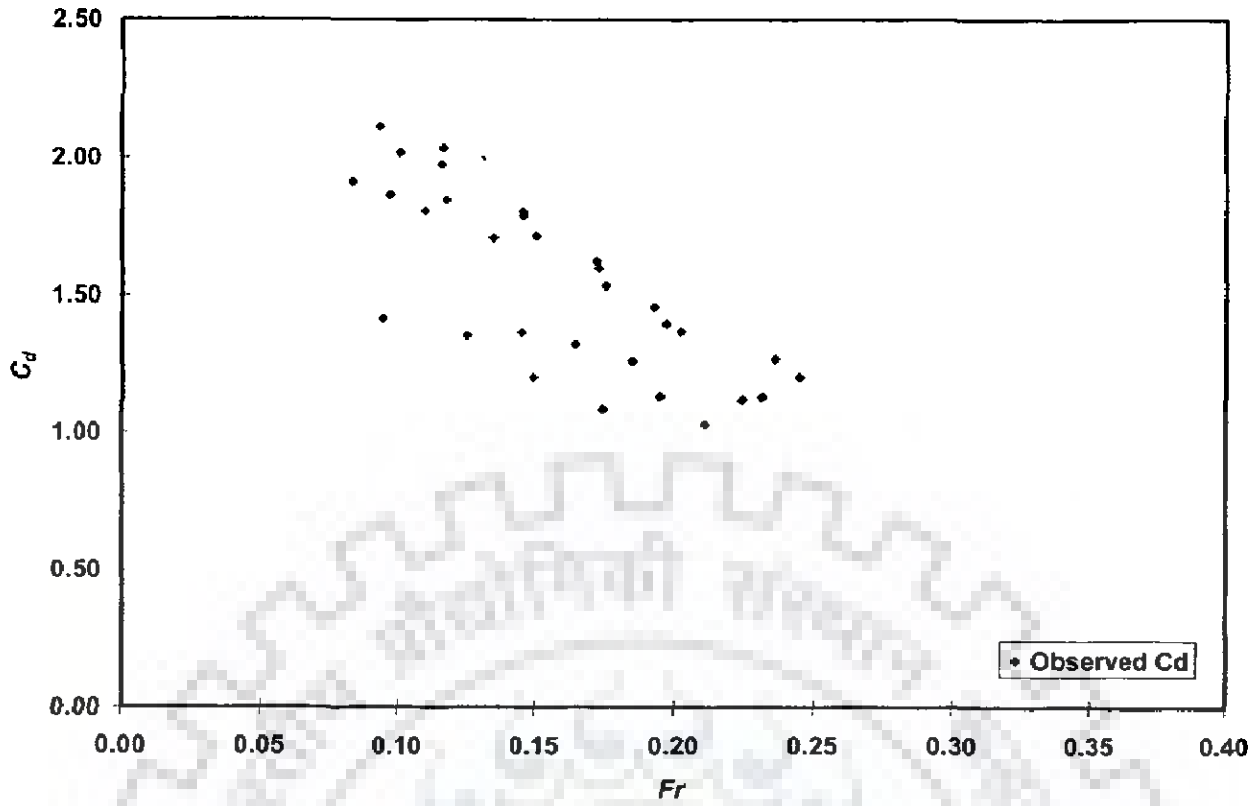

Fig. 6.47 Graphical plot between Fr and C_d for $L/W = 7.4$ and h/p upto 0.4

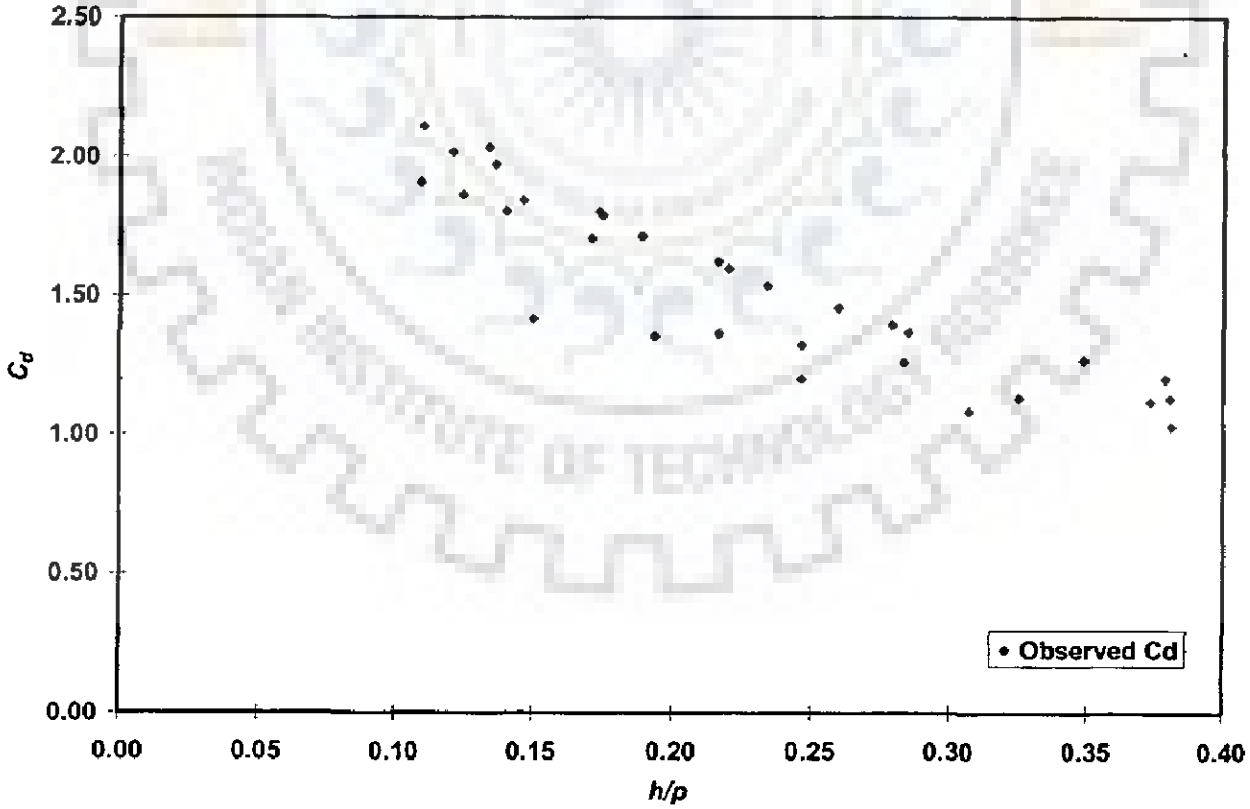

Fig. 6.48 Graphical plot between h/p and C_d for $L/W = 7.4$ and h/p upto 0.4

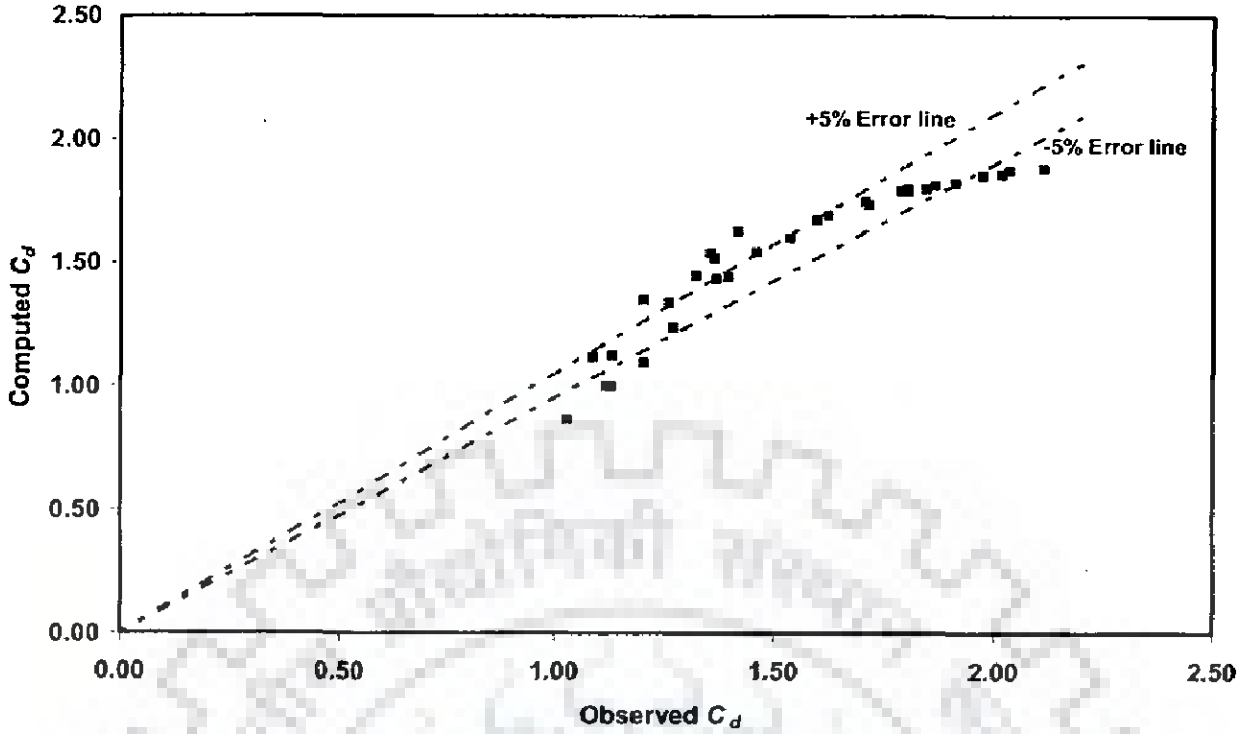

Fig. 6.49 Error analysis between observed and computed C_d for $L/W = 7.4$ and h/p upto 0.4 using Eq. (6.26)

6.5.8.6 Variation of discharge coefficient with Froude No. and h/p greater than 0.4 For L/W as 7.4

The variation of discharge coefficient with Fr and h/p greater than 0.4 is shown in Figs. 6.50 and 6.51 respectively. The polynomial regression model is developed as follows:

$$C_d = 0.87 - 1.09h/p + 2.43Fr\,;\, R^2 = 0.90 \qquad (6.27)$$

Fig. 6.52 shows that the error between observed and computed discharge coefficient lies in the range of -5 to +13 % for L/W as 7.4 and h/p greater than 0.4. Average absolute percentage error between computed and observed discharge coefficient using Eq. (6.27) is 3.24. Also, R^2 value is found to improve from 0.818 to 0.96.

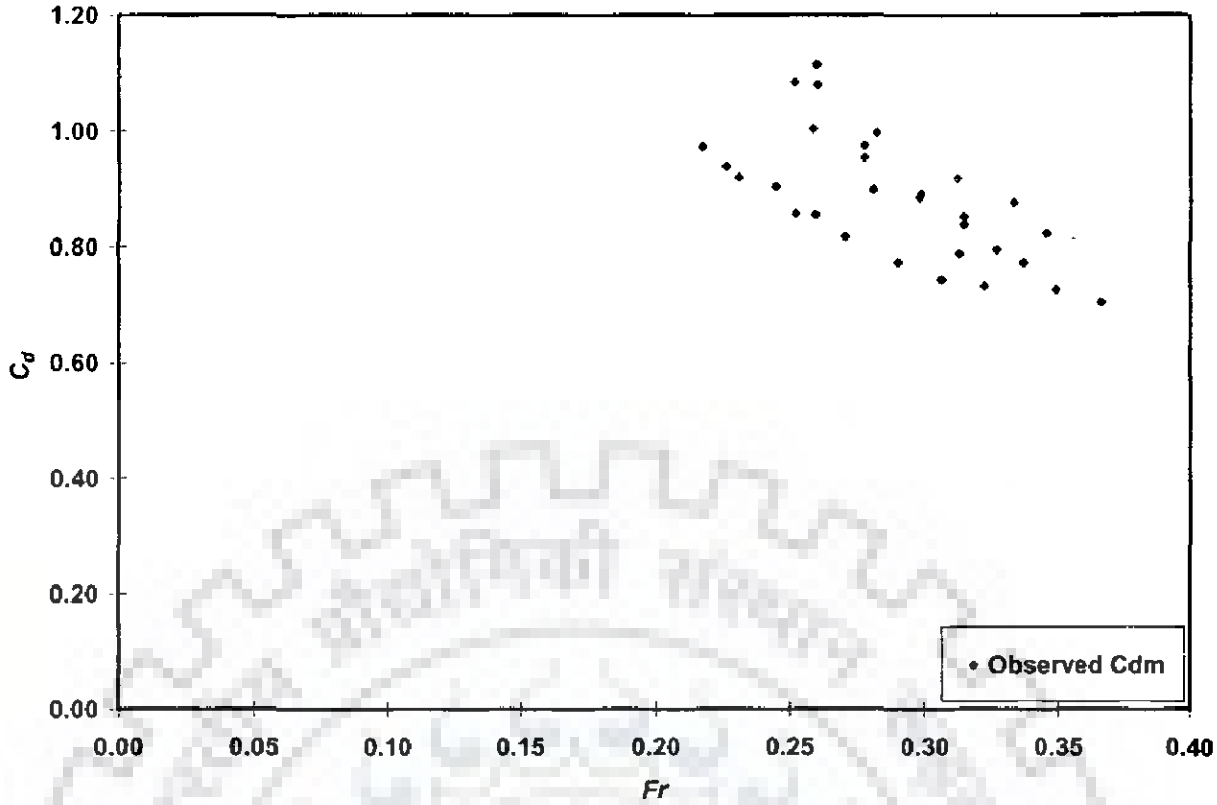

Fig. 6.50 Graphical plot between *Fr* and C_d for *L/W* = 7.4 and *h/p* greater than 0.4

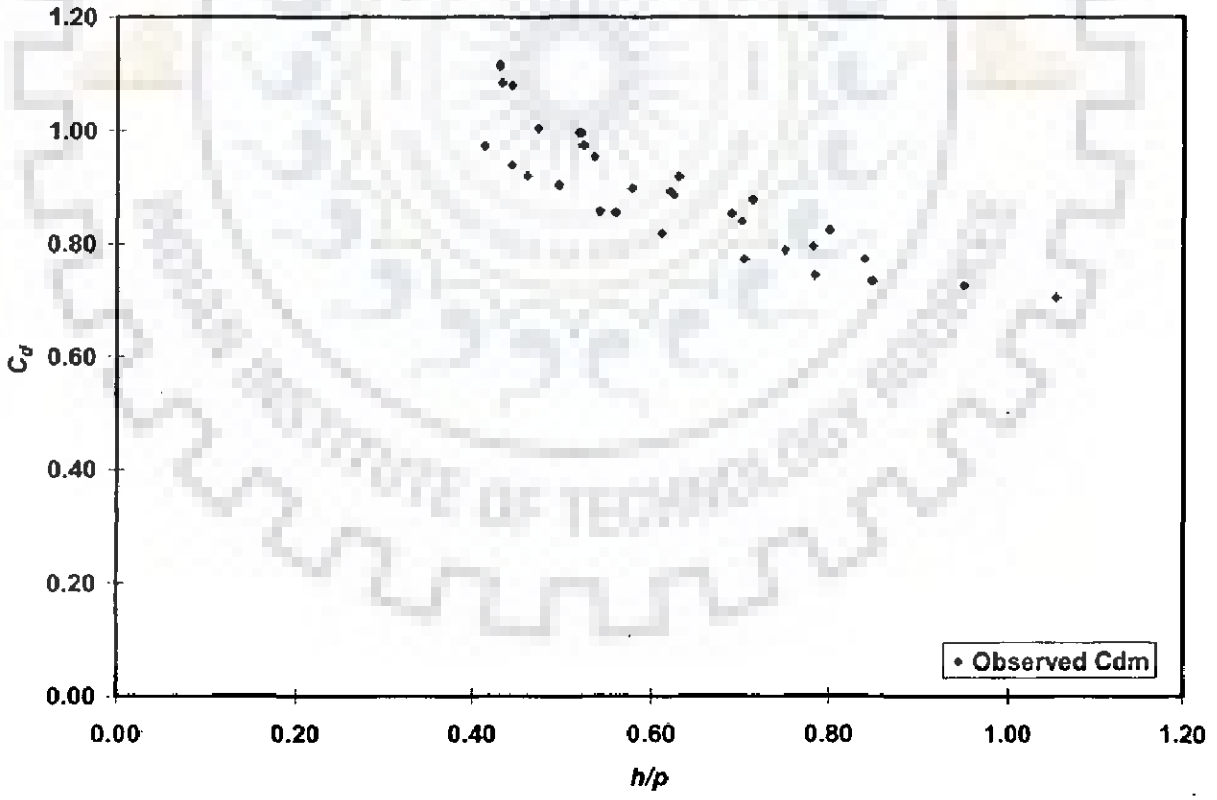

Fig. 6.51 Graphical plot between *h/p* and C_d for *L/W* = 7.4 and *h/p* greater than 0.4

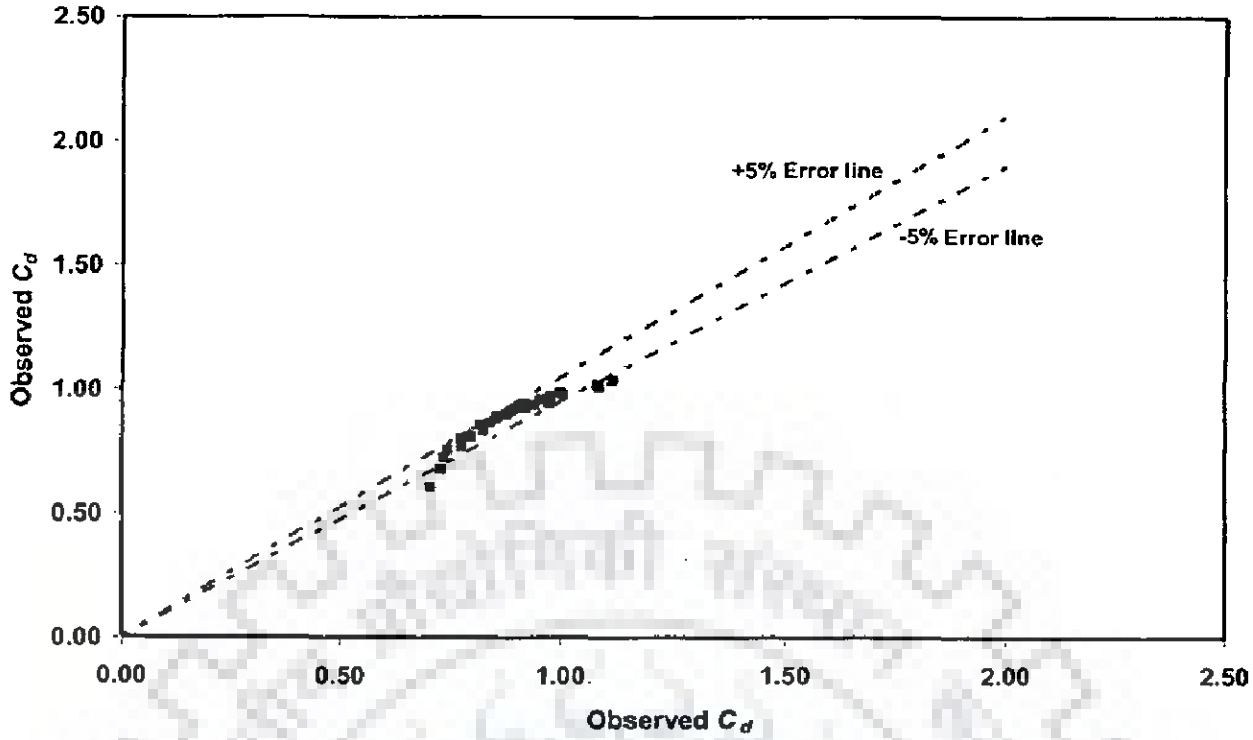

Fig. 6.52 Error analysis between observed and computed C_d for $L/W = 7.4$ and h/p greater than 0.4 using Eq. (6.27)

6.5.9 Variation of Discharge Coefficient with Froude No., *h/p* and *L/W*

So far, the relationships have been developed in terms of Fr and h/p. A generalized linear relationship for the discharge coefficient can be also written as:

$$C_d = a + bL/W + ch/p + dFr \tag{6.28}$$

where a, b, c, and d are constants. To find these constants, the polynomial linear regression method has been adopted. The resultant equation is obtained as

$$C_d = 1.218 + 0.06L/W - 0.791h/p - 0.754Fr\ ;\ R^2 = 0.73 \tag{6.29}$$

Fig. 6.53 shows that the error between observed and computed discharge coefficient lies in the range of -28 to +50 % for all value of L/W. Average absolute percentage error between computed and observed discharge coefficient using Eq. (6.29) is 12.062. It can be seen that R^2 is significantly reduced with a generalized model.

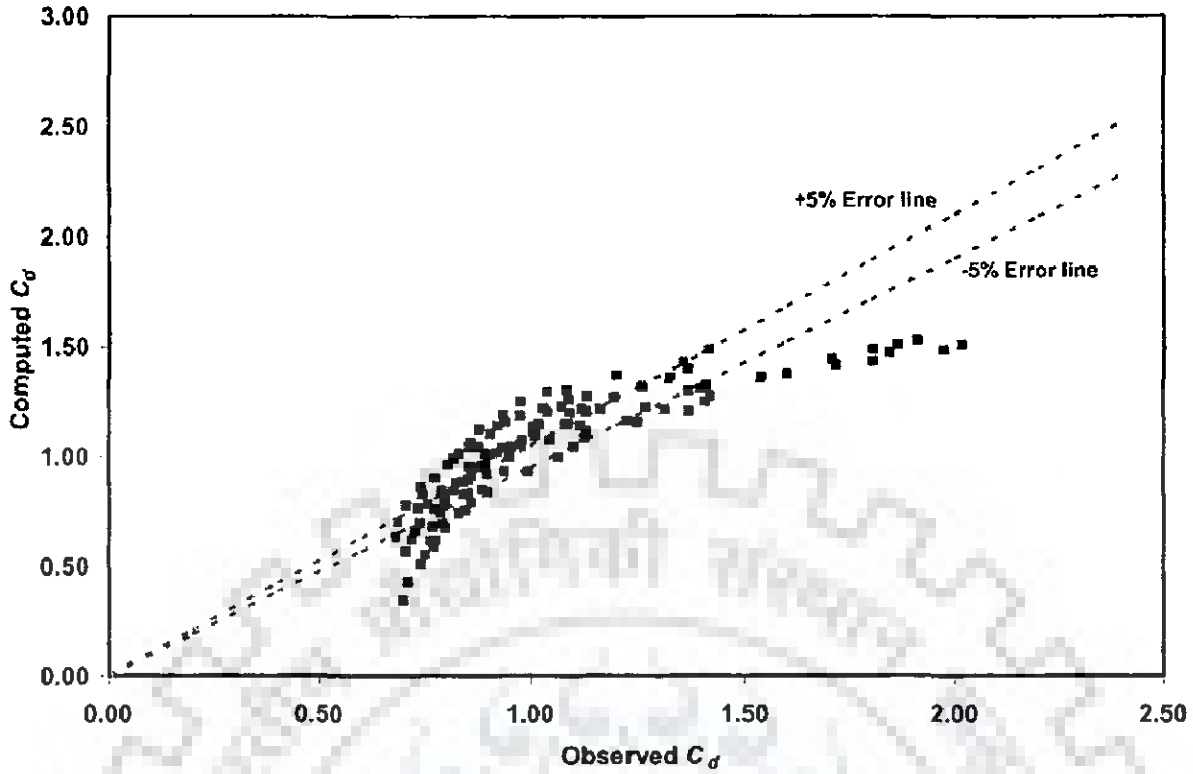

Fig. 6.53 Error analysis between observed and computed C_d for all value of L/W using Eq. (6.29)

6.6 VARIATION OF DISCHARGE COEFFICIENT FOR DOWNSTREAM SIDES OVER-HANGING TYPE OF PIANO KEY WEIR WITH CONSIDERING VELOCITY HEAD OF APPROACH FLOW

Variation of discharge coefficient is analysed here for value of L/W as 4.84. The experimental data used for the analysis is given in Table C.13 to C.15 (see Appendix C).

6.6.1 Variation of Discharge Coefficient with H_T/p for L/W as 4.84

If C_d is related with H_T/p only, the following equation best describes the experimental data

$$C_d = 0.778 h/p^{-0.405}; R^2 = 0.96 \quad (6.30)$$

Fig. 6.54 shows that the error between observed and computed discharge coefficient lies in the range of -10 to +10 % for L/W as 4.84. Average absolute percentage error between computed and observed discharge coefficient using Eq. (6.30) is found to be 3.46.

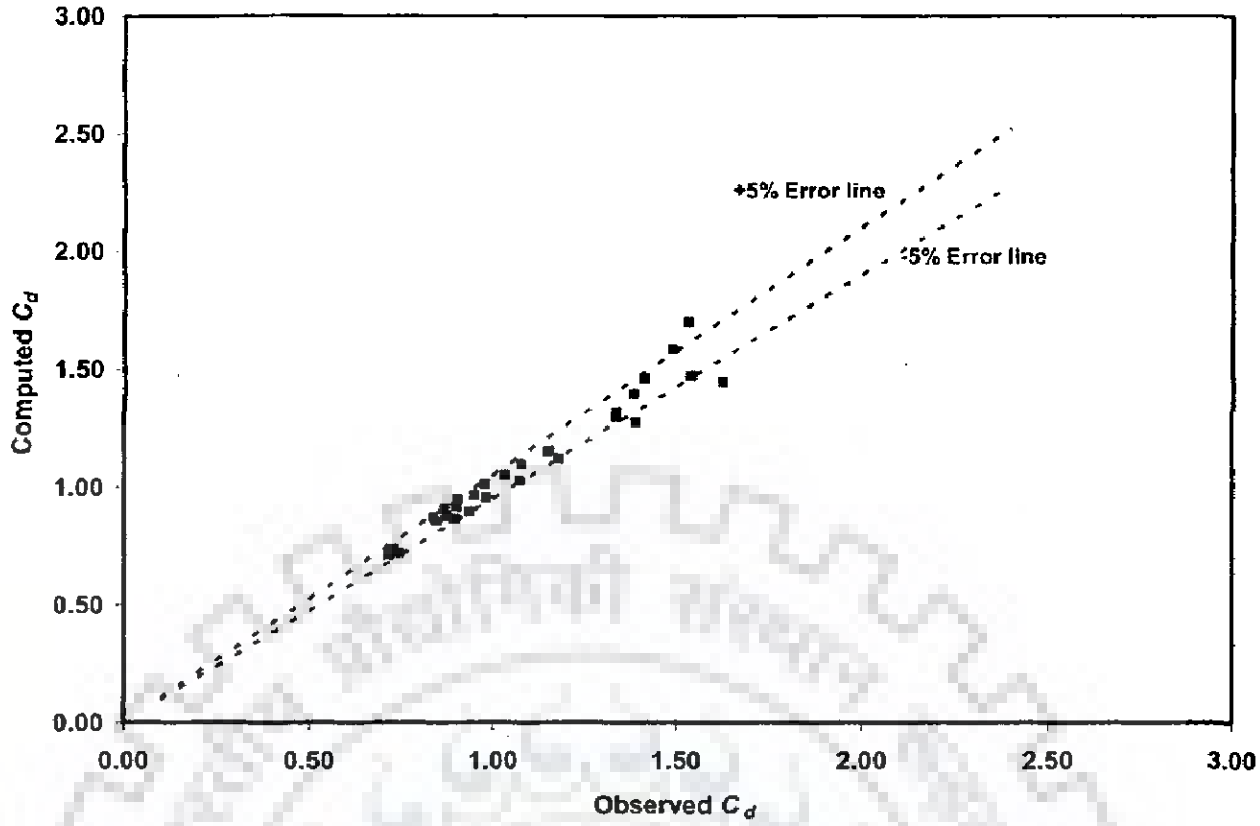

Fig. 6.54 Error analysis between observed and computed C_d for $L/W = 4.84$ using Eq. (6.30)

6.6.2 Variation of Discharge Coefficient with Froude No. and H_T/p for L/W as 4.84

In the previous option, only the upstream (or approach) Froude number (Fr) is taken as the main variable in the development of formula for discharge coefficient analysis. As R^2 was not very high, the option of including an additional variable h/p is explored.

The polynomial regression model for L/W 4.84 yields the following functional form

$$C_d = 1.876 - 0.00914 H_T / p - 2.873 Fr \; ; R^2 = 0.91 \qquad (6.31)$$

Fig. 6.55 shows that the error between observed and computed discharge coefficient lies in the range of -11 to +15 % for L/W as 4.84. Average absolute percentage error between computed and observed discharge coefficient using Eq. (6.31) is found to be 5.85.

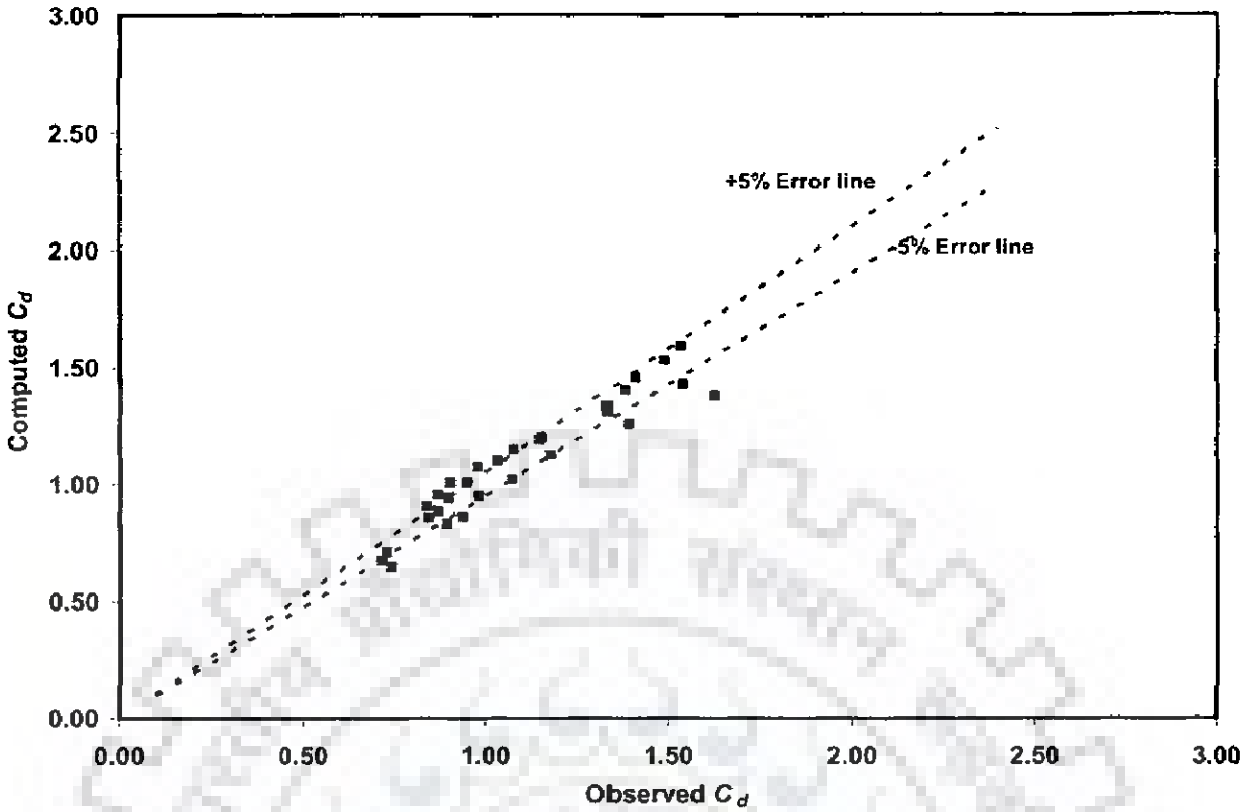

Fig. 6.55 Error analysis between observed and computed C_d for $L/W = 4.84$ using Eq. (6.31)

6.6.3 Variation of Discharge Coefficient with Froude No. and H_T/p in Two Distinct Segments

The analysis done in the previous section indicated the possibility of exploring the refinements in the developed regression relationships between discharge coefficient, Fr and H_T/p in different ranges of H_T/p. For this reason, the results of analysis considering two different segments of C_d variation with H_T/p between 0 and 0.4 and greater than 0.4 are presented next.

6.6.3.1 Variation of discharge coefficient with Froude No. and H_T/p upto 0.4 for L/W as 4.84

The polynomial regression model is developed as follows:

$$C_d = 1.65 - 4.57 H_T / p + 5.21 Fr \; ; R^2 = 0.94 \qquad (6.32)$$

Fig. 6.56 shows that the error between observed and computed discharge coefficient lies in the range of -4 to +4 % for L/W as 4.84 and H_T/p upto 0.4. Average absolute percentage error between computed and observed discharge coefficient using Eq. (6.32) is 2.29. Also, R^2 value is found to marginally improve from 0.91 to 0.94.

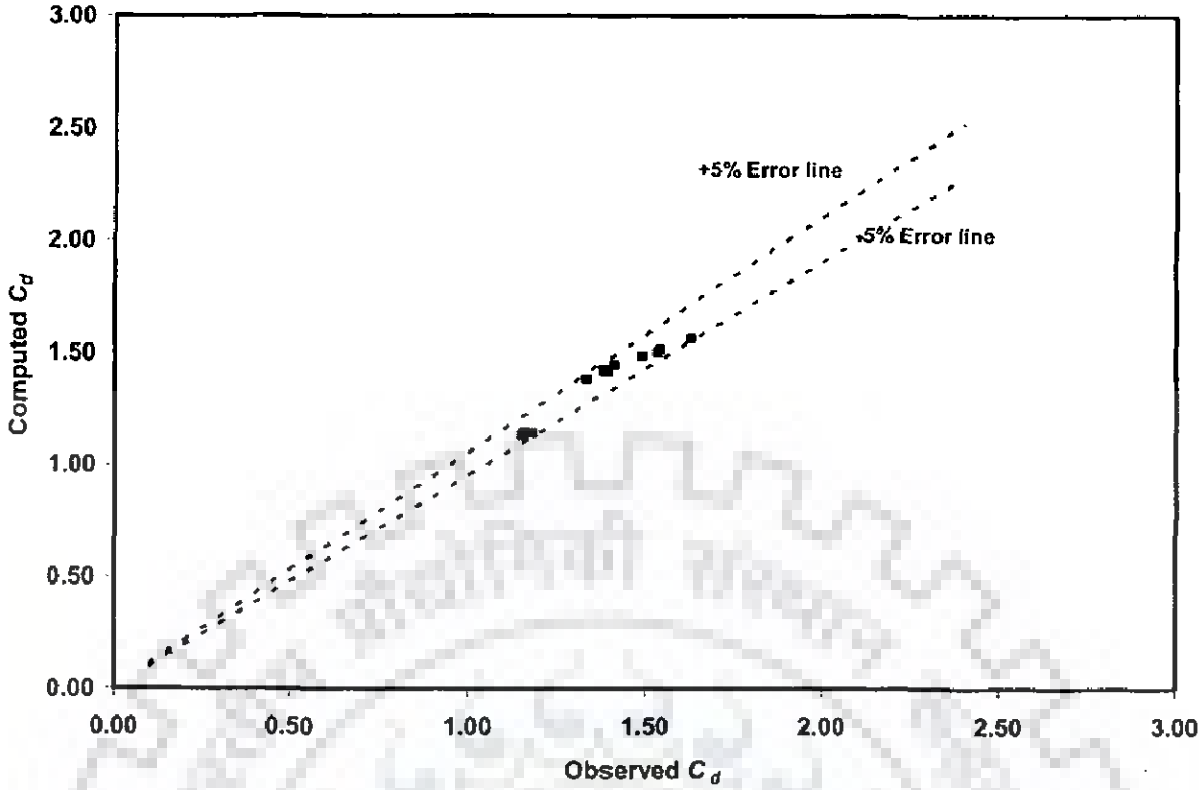

Fig. 6.56 Error analysis between observed and computed C_d for L/W = 4.84 and H_T/p upto 0.4 using Eq. (6.32)

6.6.3.2 Variation of discharge coefficient with Froude No. and H_T/p greater than 0.4 for L/W as 4.84

The polynomial regression model is developed as follows:

$$C_d = 1.18 - 0.44H_T / p + 0.26Fr \; ; R^2 = 0.88 \qquad (6.33)$$

Fig. 6.57 shows that the error between observed and computed discharge coefficient lies in the range of -6 to +7 % for L/W as 4.84 and H_T/p greater than 0.4. Average absolute percentage error between computed and observed discharge coefficient using Eq. (6.33) is 3.47. Also, R^2 value is found to marginally reduce from 0.91 to 0.88.

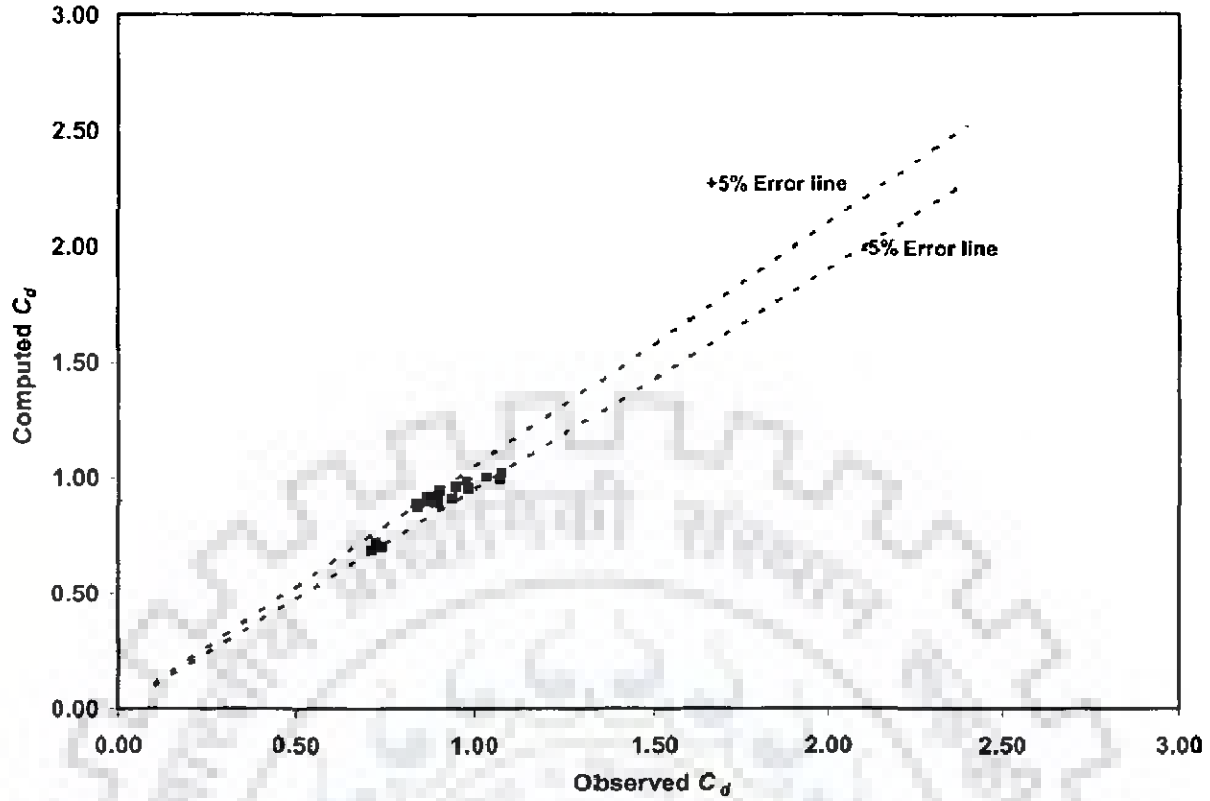

Fig. 6.57 Error analysis between observed and computed C_d for $L/W = 4.84$ and H_T/p greater than 0.4 using Eq. (6.33)

6.7 VARIATION OF DISCHARGE COEFFICIENT FOR BOTH SIDES OVER-HANGING TYPE OF PIANO KEY WEIR WITH CONSIDERING VELOCITY HEAD OF APPROACH FLOW

It is shown that discharge coefficient is a function of different parameters such as Fr, H_T/p, L/W. However, with the help of the experimental results, the effect of variables was tested, either one by one or altogether. Variation of discharge coefficient is analysed here for different value of L/W. The experimental data used for the analysis is given in Table C.1 to C.12 (see Appendix C).

6.7.1 Variation of Discharge Coefficient with H_T/p for L/W as 3.56

If C_d is related with H_T/p only, the following equation best describes the experimental data

$$C_d = 0.6965\, h/p^{-0.3121};\ R^2 = 0.90 \qquad (6.34)$$

Fig. 6.58 shows that the error between observed and computed discharge coefficient lies in the range of -13 to +13 % for L/W as 3.56. Average absolute percentage error between computed and observed discharge coefficient using Eq. (6.34) is found to be 3.90.

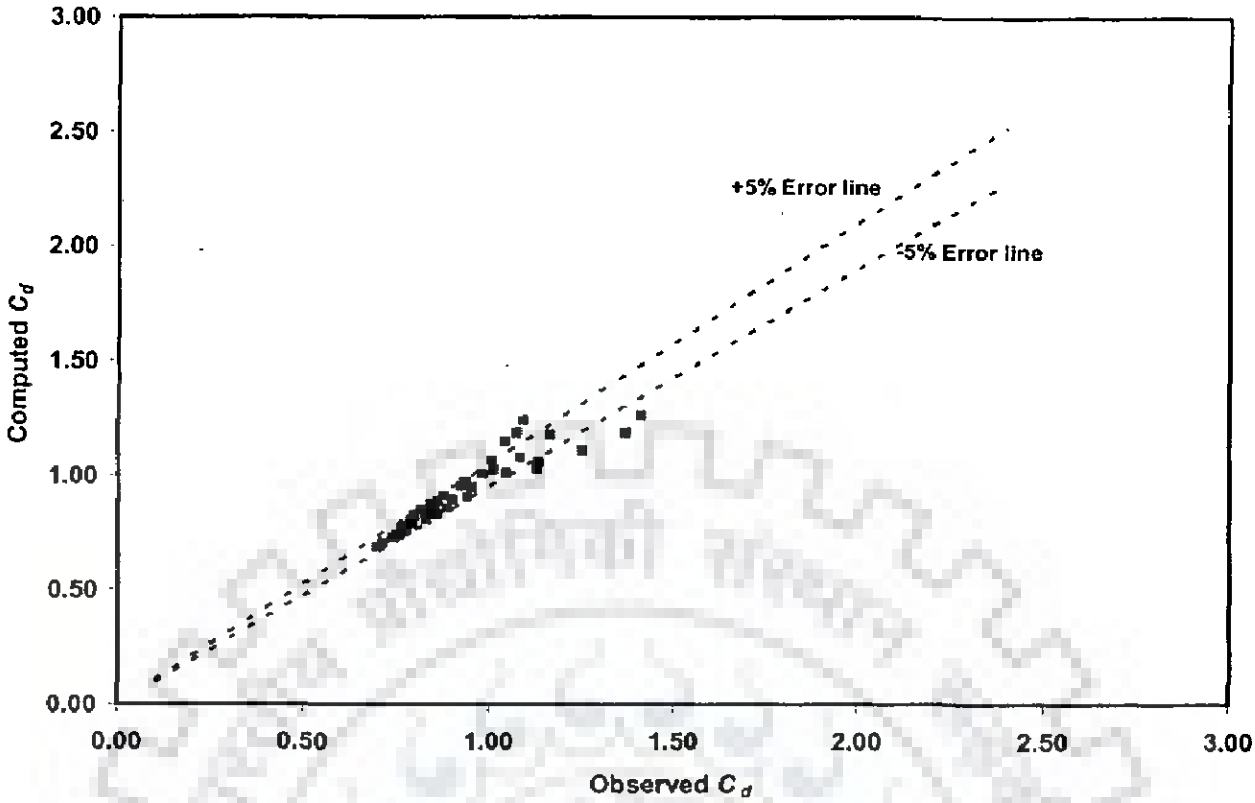

Fig. 6.58 Error analysis between observed and computed C_d for $L/W = 3.56$ using Eq. (6.34)

6.7.2 Variation of Discharge Coefficient with H_T/p for L/W as 4.84

If C_d is related with H_T/p only, the following equation best describes the experimental data

$$C_d = 0.667\, h/p^{-0.3701};\ R^2 = 0.80 \qquad (6.35)$$

Fig. 6.59 shows that the error between observed and computed discharge coefficient lies in the range of -18 to +14 % for L/W as 4.84. Average absolute percentage error between computed and observed discharge coefficient using Eq. (6.35) is found to be 7.61.

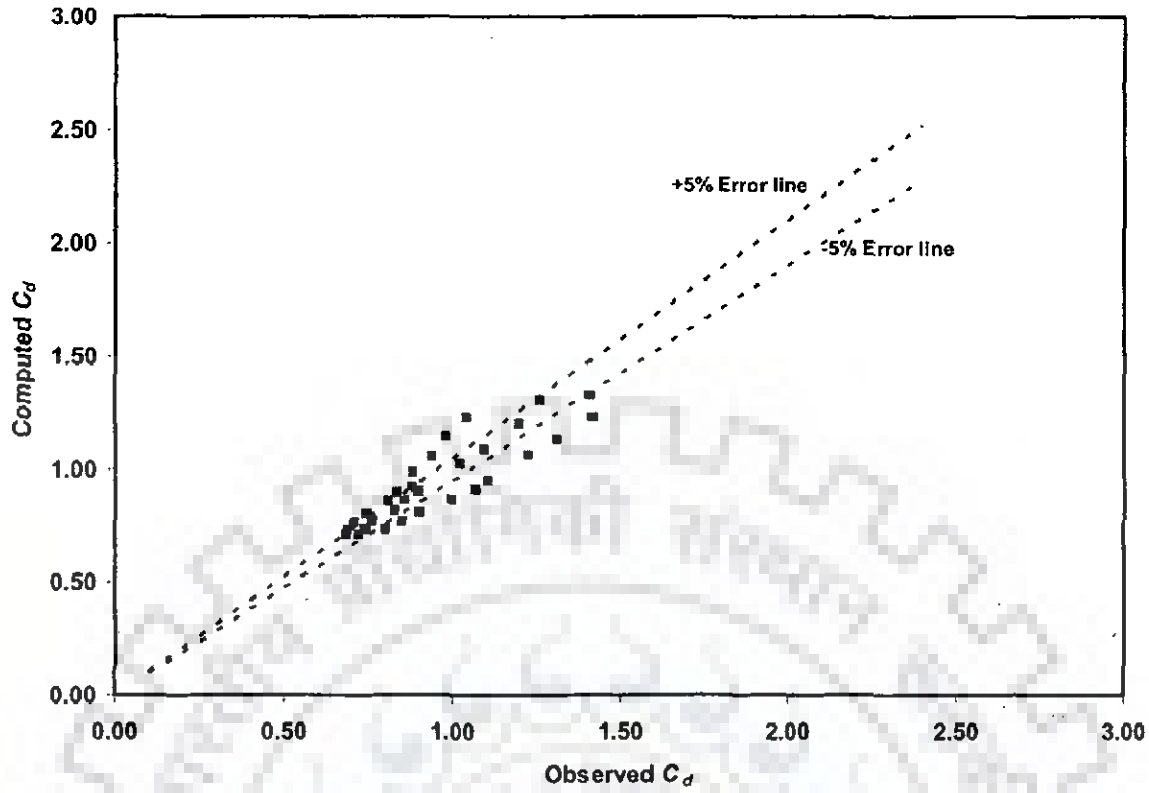

Fig. 6.59 Error analysis between observed and computed C_d for L/W = 4.84 using Eq. (6.35)

6.7.3 Variation of Discharge Coefficient with H_T/p for L/W as 7.4

If C_d is related with H_T/p only, the following equation best describes the experimental data

$$C_d = 0.684 h/p^{-0.4899}\ ;\ R^2 = 0.95 \qquad (6.36)$$

Fig. 6.60 shows that the error between observed and computed discharge coefficient lies in the range of -22 to +10 % for L/W as 7.4. Average absolute percentage error between computed and observed discharge coefficient using Eq. (6.36) is found to be 5.85.

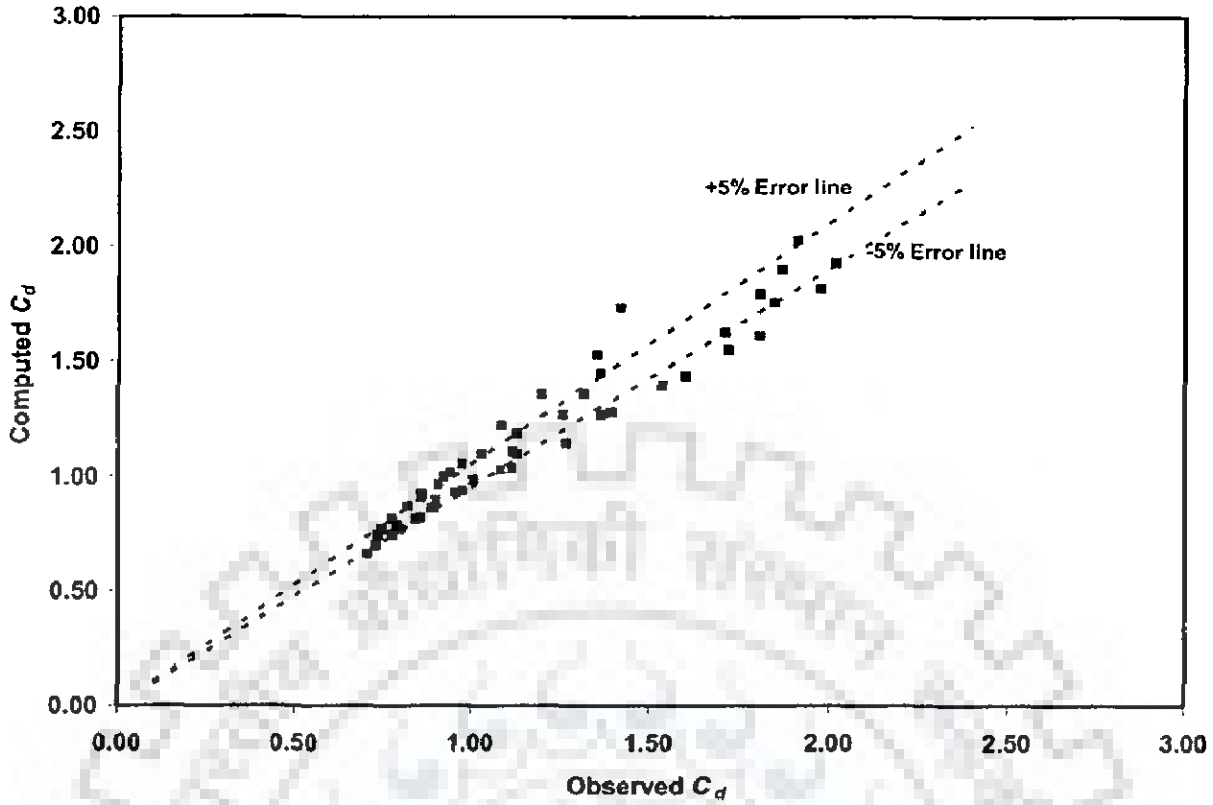

Fig. 6.60 Error analysis between observed and computed C_d for L/W = 7.4 using Eq. (6.36)

6.7.4 Variation of Discharge Coefficient with Froude No. and H_T/p

In the previous option, only the upstream (or approach) Froude number (Fr) is taken as the main variable in the development of formula for discharge coefficient analysis. As R^2 was not very high, the option of including an additional variable h/p is also explored.

6.7.4.1 Variation of discharge coefficient with Froude No. and H_T/p for L/W as 3.56

The polynomial regression model for L/W 3.56 yields the following functional form

$$C_d = 1.314 - 0.201 H_T / p - 1.354 Fr \; ; R^2 = 0.77 \qquad (6.37)$$

Fig. 6.61 shows that the error between observed and computed discharge coefficient lies in the range of -9 to +18 % for L/W as 3.56. Average absolute percentage error between computed and observed discharge coefficient using Eq. (6.37) is found to be 6.12.

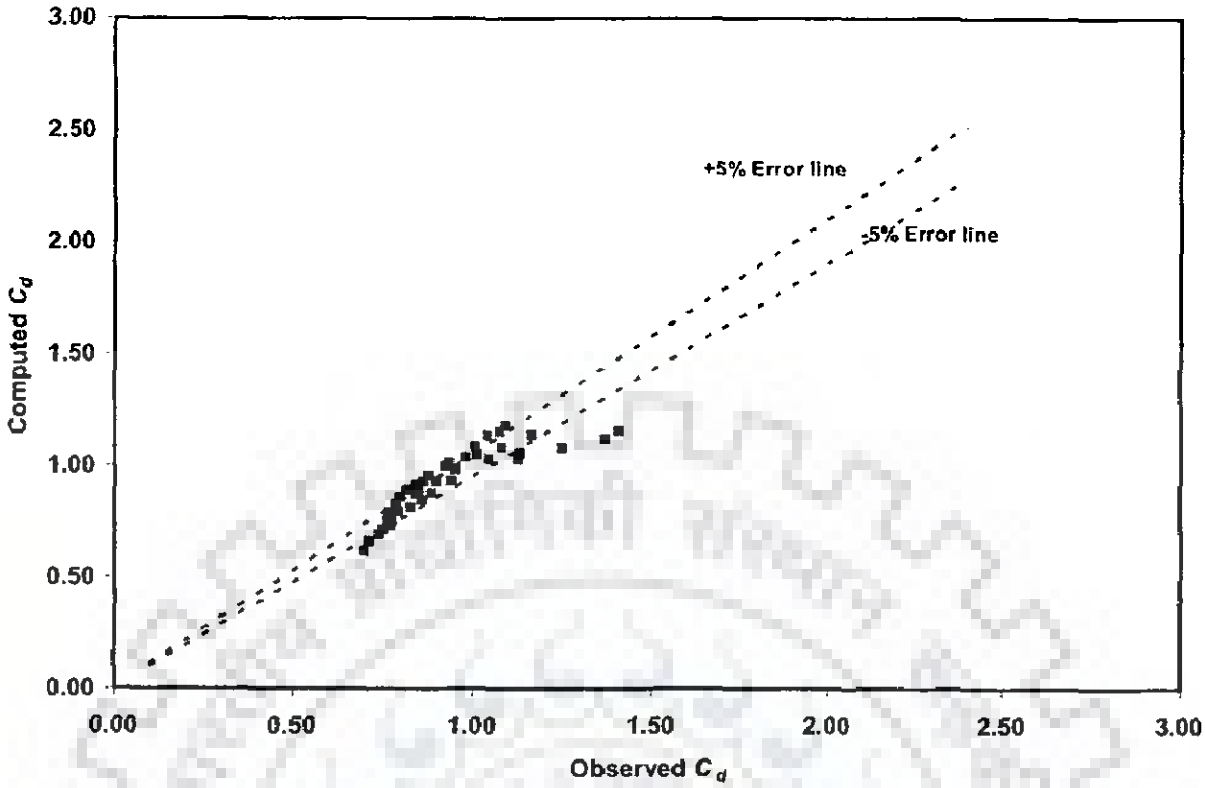

Fig. 6.61 Error analysis between observed and computed C_d for $L/W = 3.56$ using Eq. (6.37)

6.7.4.2 Variation of discharge coefficient with Froude No. and H_T/p for L/W as 4.84

The polynomial regression model for L/W 4.84 yields the following functional form

$$C_d = 1.207 - 1.476H_T / p + +2.014Fr\,;\, R^2 = 0.77 \qquad (6.38)$$

Fig. 6.62 shows that the error between observed and computed discharge coefficient lies in the range of -16 to +16 % for L/W as 4.84. Average absolute percentage error between computed and observed discharge coefficient using Eq. (6.38) is found to be 8.50.

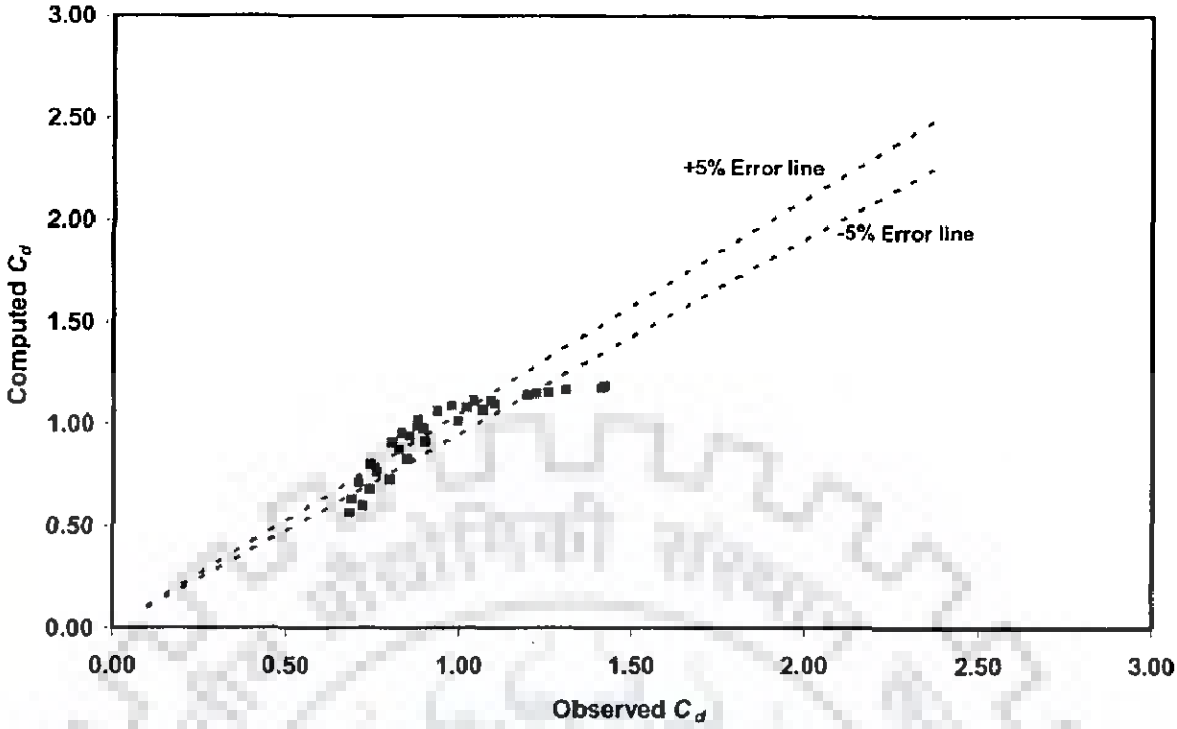

Fig. 6.62 Error analysis between observed and computed C_d for L/W = 4.84 using Eq. (6.38)

6.7.4.3 Variation of discharge coefficient with Froude No. and H_T/p for L/W as 7.4

The polynomial regression model for L/W 7.4 yields the following functional form

$$C_d = 2.11 - 0.255H_T / p - 3.739Fr \; ; R^2 = 0.818 \qquad (6.39)$$

Fig. 6.63 shows that the error between observed and computed discharge coefficient lies in the range of -27 to +31 % for L/W as 7.4. Average absolute percentage error between computed and observed discharge coefficient using Eq. (6.39) is found to be 12.04.

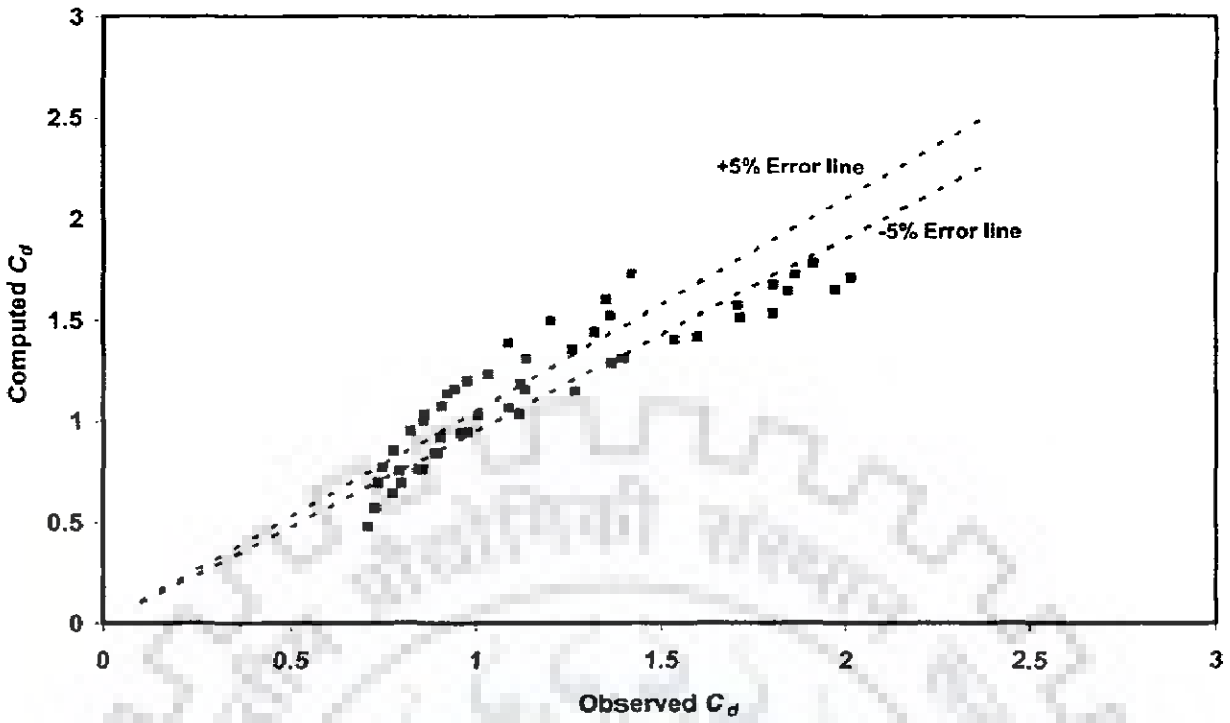

Fig. 6.63 Error analysis between observed and computed C_d for $L/W = 7.4$ using Eq. (6.39)

6.7.5 Variation of Discharge Coefficient with Froude No. and H_T/p in Two Distinct Segments

The analysis done in the previous section indicated the possibility of exploring the refinements in the developed regression relationships between discharge coefficient, Fr and H_T/p in different ranges of H_T/p. For this reason, the results of analysis considering two different segments of C_d variation with H_T/p between 0 and 0.4 and greater than 0.4 are presented next.

6.7.5.1 Variation of discharge coefficient with Froude No. and H_T/p upto 0.4 for L/W as 3.56

The polynomial regression model is developed as follows:

$$C_d = 1.30 - 5.35H_T / p + 8.43Fr\,;\ R^2 = 0.92 \qquad (6.40)$$

Fig. 6.64 shows that the error between observed and computed discharge coefficient lies in the range of -4 to +8 % for L/W as 3.56 and H_T/p upto 0.4. Average absolute percentage error between computed and observed discharge coefficient using Eq. (6.40) is 3.30. Also, R^2 value is found to improve from 0.77 to 0.92.

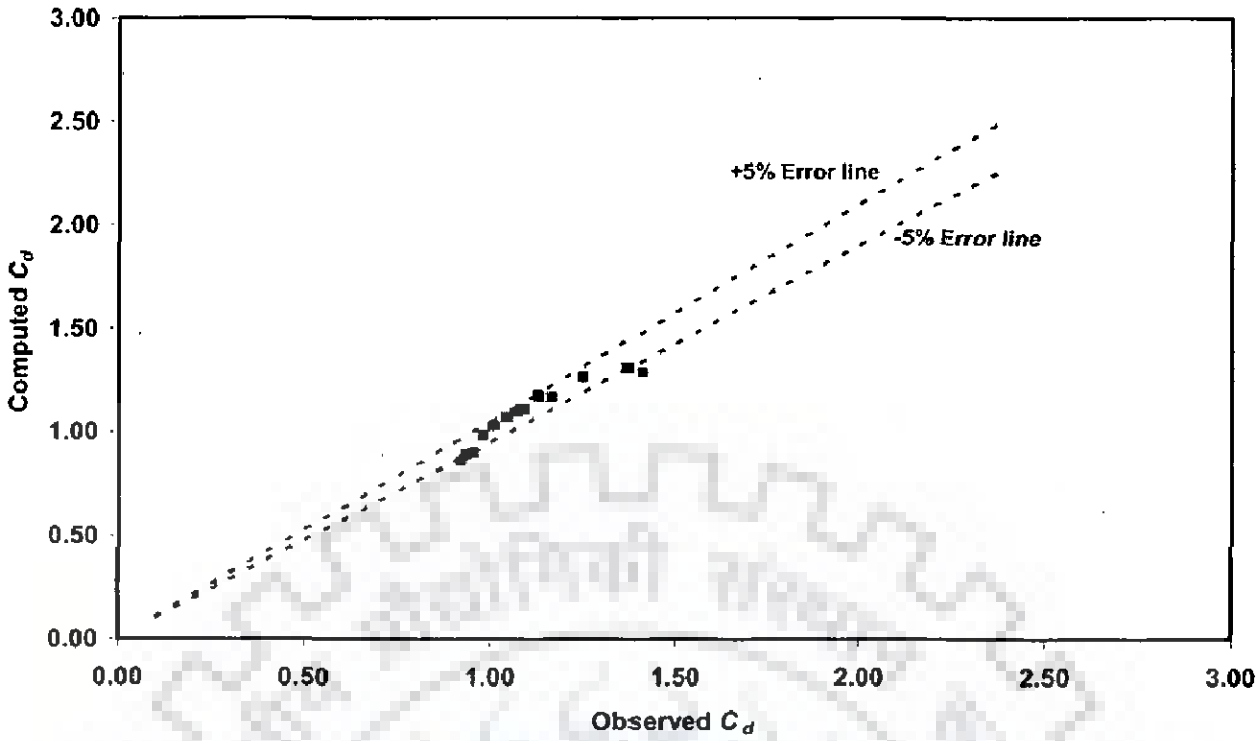

Fig. 6.64 Error analysis between observed and computed C_d for L/W = 3.56 and H_T/p upto 0.4 using Eq. (6.40)

6.7.5.2 Variation of discharge coefficient with Froude No. and H_T/p greater than 0.4 for L/W as 3.56

The polynomial regression model is developed as follows:

$$C_d = 0.92 - 0.568 H_T / p + 0.90 Fr \; ; R^2 = 0.90 \qquad (6.41)$$

Fig. 6.65 shows that the error between observed and computed discharge coefficient lies in the range of -4 to +6 % for L/W as 3.56 and H_T/p greater than 0.4. Average absolute percentage error between computed and observed discharge coefficient using Eq. (6.41) is 1.93. Also, R^2 value is found to improve from 0.77 to 0.90.

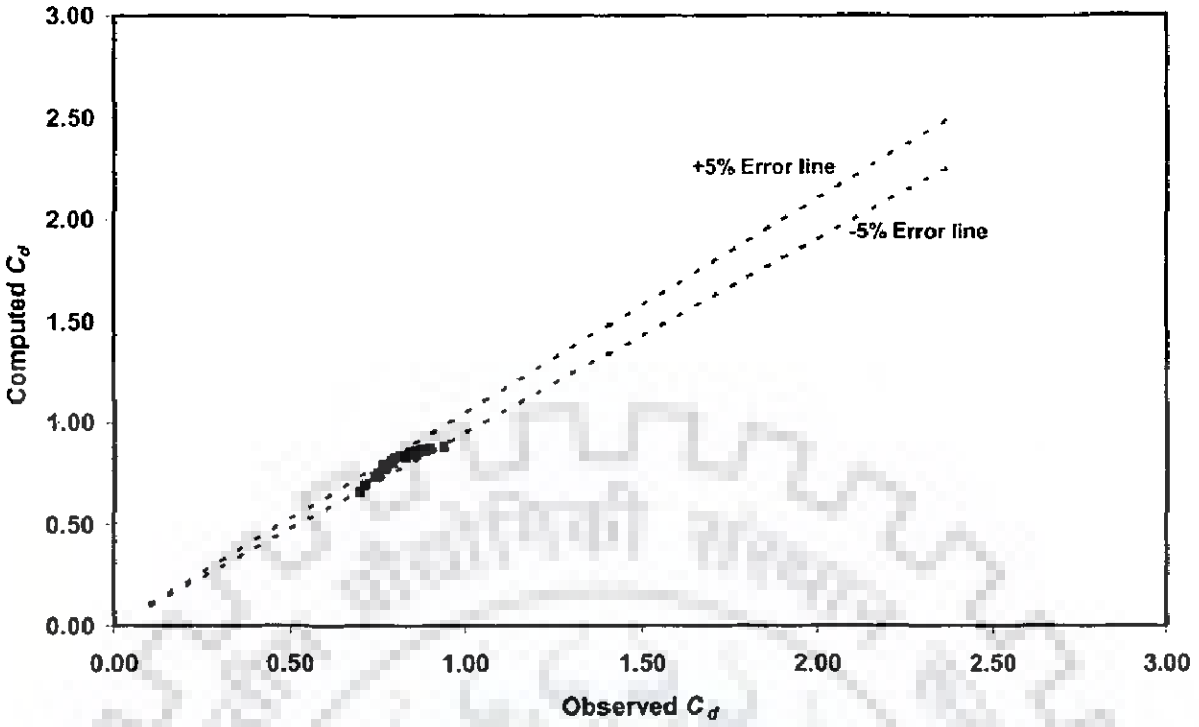

Fig. 6.65 Error analysis between observed and computed C_d for $L/W = 3.56$ and H_T/p greater than 0.4 using Eq. (6.41)

6.7.5.3 Variation of discharge coefficient with Froude No. and H_T/p upto 0.4 for L/W as 4.84

The polynomial regression model is developed as follows:

$$C_d = 1.39 - 5.31 H_T / p + 7.66 Fr \; ; R^2 = 0.95 \qquad (6.42)$$

Fig. 6.66 shows that the error between observed and computed discharge coefficient lies in the range of -6 to +9 % for L/W as 4.84 and H_T/p upto 0.4. Average absolute percentage error between computed and observed discharge coefficient using Eq. (6.42) is 3.22. Also, R^2 value is found to improve from 0.77 to 0.95.

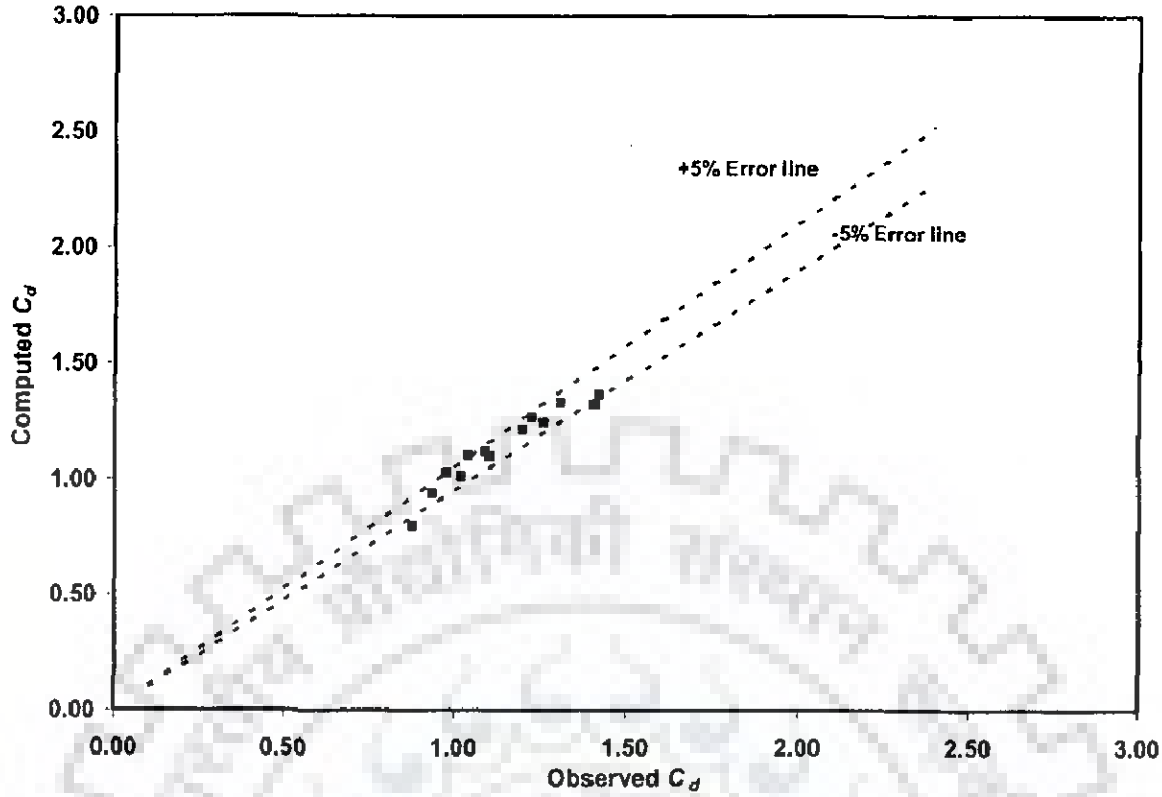

Fig. 6.66 Error analysis between observed and computed C_d for L/W = 4.84 and H_T/p upto 0.4 using Eq. (6.42)

6.7.5.4 Variation of discharge coefficient with Froude No. and H_T/p greater than 0.4 for L/W as 4.84

The polynomial regression model is developed as follows:

$$C_d = 0.77 - 1.268 H_T / p + 3.121 Fr \; ; R^2 = 0.96 \qquad (6.43)$$

Fig. 6.67 shows that the error between observed and computed discharge coefficient lies in the range of -3 to +6 % for L/W as 4.84 and H_T/p greater than 0.4. Average absolute percentage error between computed and observed discharge coefficient using Eq. (6.43) is 2.63. Also, R^2 value is found to improve from 0.77 to 0.96.

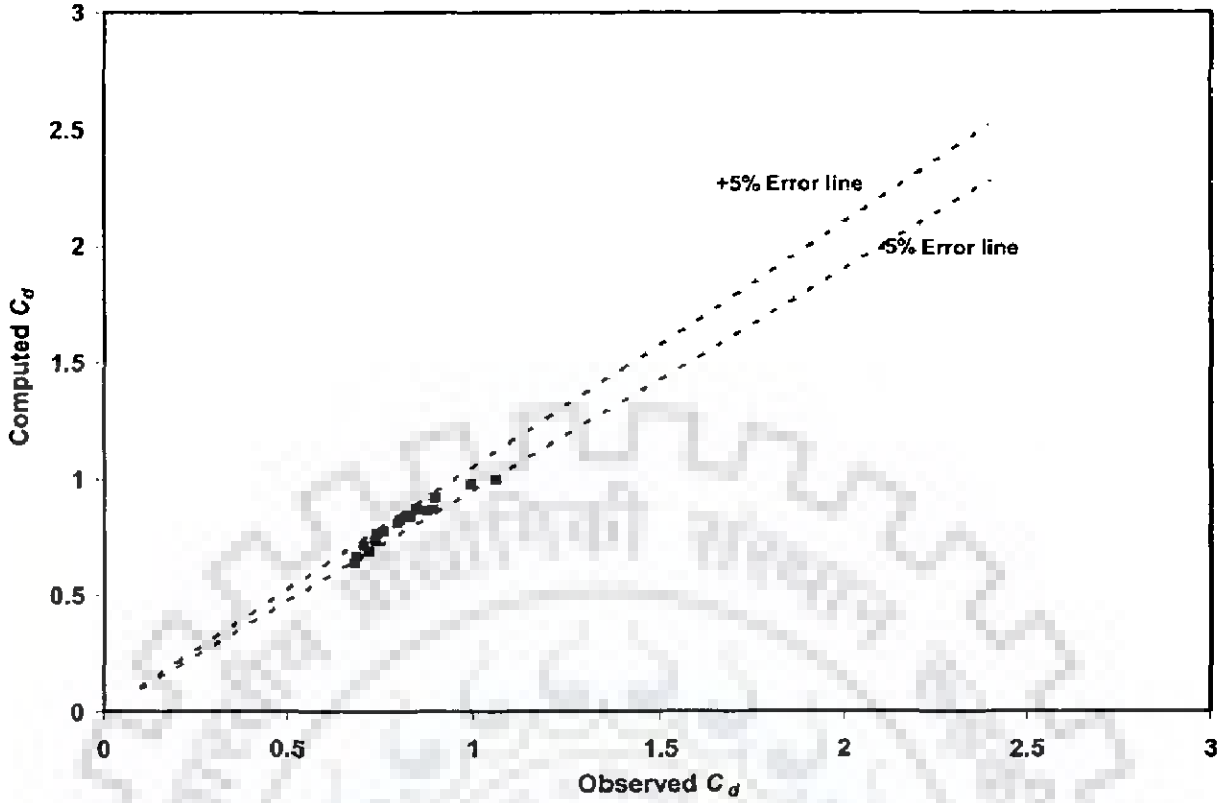

Fig. 6.67 Error analysis between observed and computed C_d for $L/W = 4.84$ and H_T/p greater than 0.4 using Eq. (6.43)

6.7.5.5 Variation of discharge coefficient with Froude No. and H_T/p upto 0.4 for L/W as 7.4

The polynomial regression model is developed as follows:

$$C_d = 1.93 - 6.53H_T / p + 6.74Fr\,;\ R^2 = 0.90 \qquad (6.44)$$

Fig. 6.68 shows that the error between observed and computed discharge coefficient lies in the range of -12 to +15 % for L/W as 7.4 and H_T/p upto 0.4. Average absolute percentage error between computed and observed discharge coefficient using Eq. (6.44) is 6.13. Also, R^2 value is found to improve from 0.81 to 0.90.

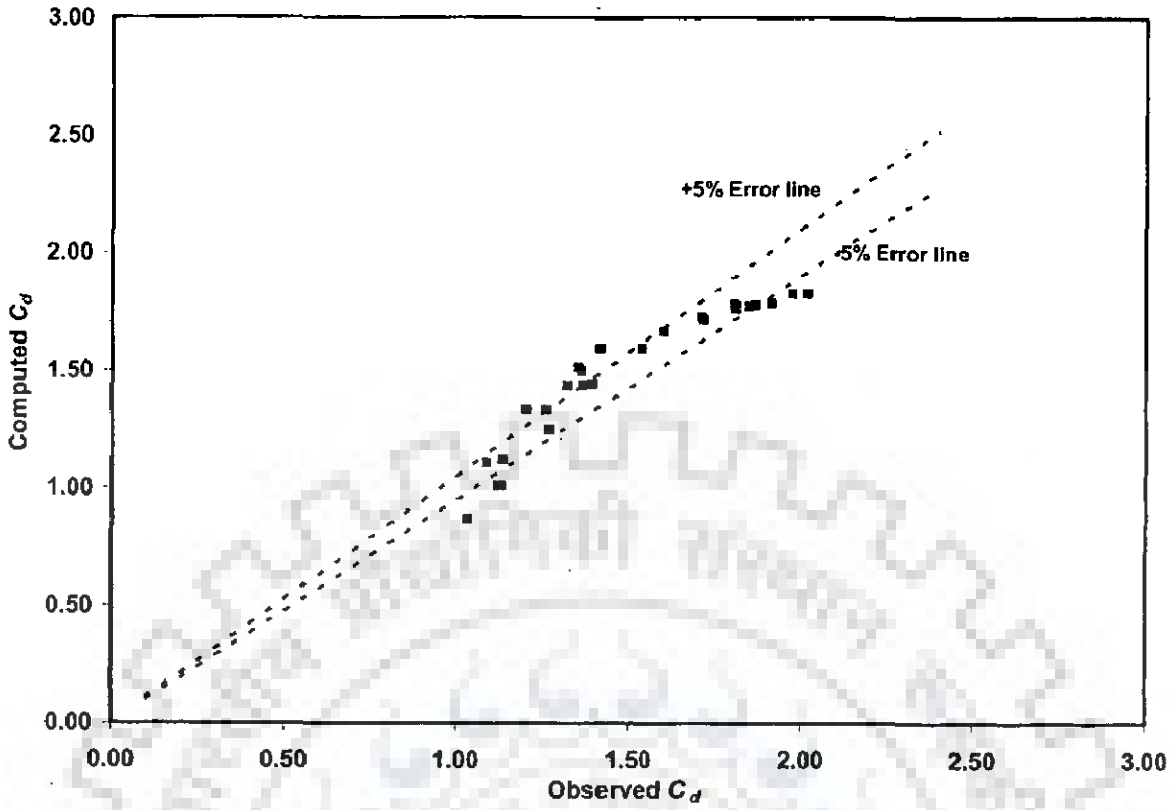

Fig. 6.68 Error analysis between observed and computed C_d for L/W = 7.4 and H_T/p upto 0.4 using Eq. (6.44)

6.7.5.6 Variation of Discharge Coefficient with Froude No. and H_T/p greater than 0.4 for L/W as 7.4

The polynomial regression model is developed as follows:

$$C_d = 0.837 - 1.1H_T / p + 2.56Fr\,;\, R^2 = 0.89 \qquad (6.45)$$

Fig. 6.69 shows that the error between observed and computed discharge coefficient lies in the range of -5 to +12 % for L/W as 7.4 and H_T/p greater than 0.4. Average absolute percentage error between computed and observed discharge coefficient using Eq. (6.45) is 3.37. Also, R^2 value is found to improve from 0.81 to 0.89.

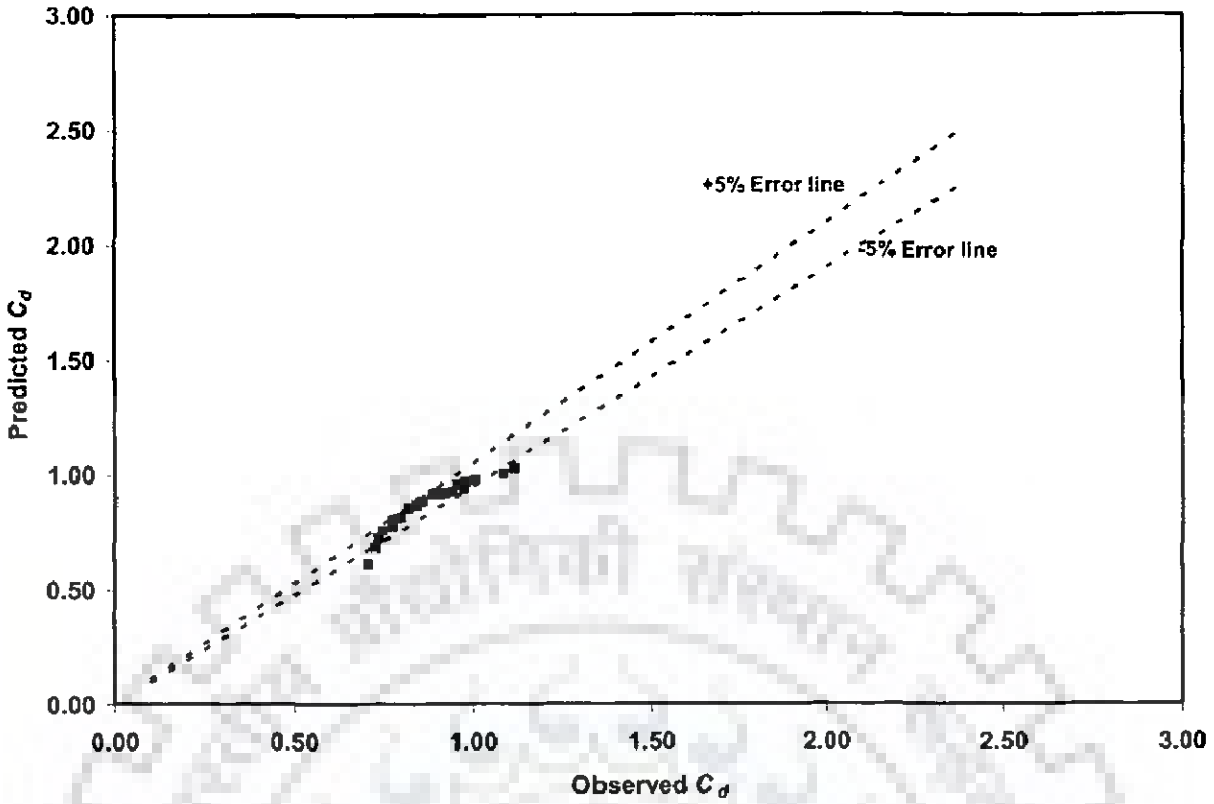

Fig. 6.69 Error analysis between observed and computed C_d for $L/W = 7.4$ and H_T/p greater than 0.4 using Eq. (6.45)

6.7.6 Variation of Discharge Coefficient with Froude No., H_T/p and L/W

The polynomial linear regression method is obtained as

$$C_d = 1.21 + 0.062L/W - 0.788H_T/p - 0.758Fr\,;\, R^2 = 0.73 \qquad (6.46)$$

Fig. 6.70 shows that the error between observed and computed discharge coefficient lies in the range of -28 to +50 % for all value of L/W. Average absolute percentage error between computed and observed discharge coefficient using Eq. (6.46) is 12.06. It can be seen that R^2 is significantly reduced with a generalized model.

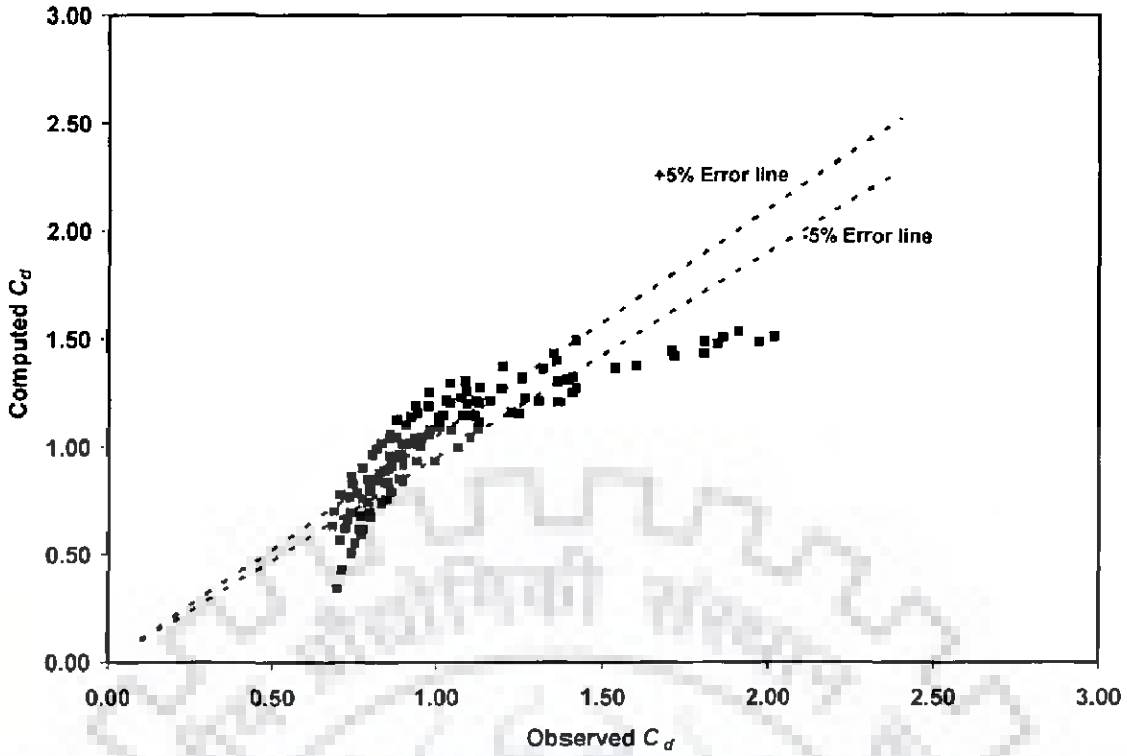

Fig. 6.70 Error analysis between observed and computed C_d for all value of L/W using Eq. (6.46)

6.8 RESULT AND DISCUSSION

In preceding section several options are attempted to develop relationship for C_d variations for two different configurations of Piano Key Weir, i.e. one side and both side overhanging. Table 6.1 summarized the functional relationship for the experimental conditions corresponding to L/W as 4.84. It can be seen from the table, normally one side overhanging relationships are having higher values of R^2 indicating the appropriateness of different functional relationships. However, the perusal of function relationships for both side overhanging indicates relatively poor performance of C_d variation only as function of Fr. Also, the C_d variation with h/p as only variational parameter doesn't appear to work so well ($R^2 = 0.80$) when compared with counterpart for one side overhanging ($R^2 = 0.96$). Table 6.1 clearly indicates that for a given L/W as 4.84 the most suitable relationship is that which involves h/p and Fr both as variational parameters.

To further validate this, data collected at field scale model (see chapter 5) is used Fig. 6.71 shows the agreement diagram between observed and computed discharge using (i) $C_d = f(Fr)$, (ii) $C_d = f(h/p)$ & (iii) $C_d = f(h/p, Fr)$ and it can be seen that use of $C_d = f(h/p, Fr)$ very well works with the field scale model results.

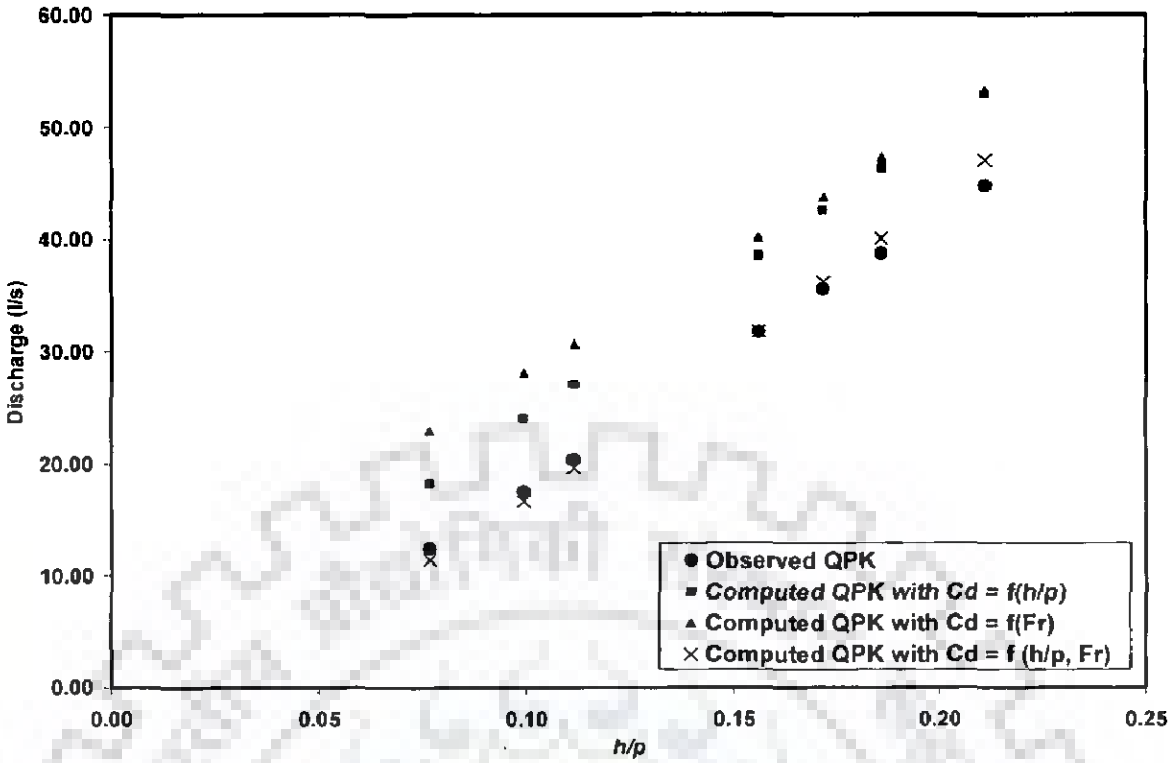

Fig. 6.71 Performance of C_d relationships using field scale data of Piano Key Weir

As discussed in the beginning the use of total head can make significant difference to the developed relationship. Table 6.2 is developed which only contains measure of error in terms of average absolute percentage error and R^2. A case pertaining to C_d variation with Fr contained head. Same is not included in table 6.2. The last line of the table 6.2 indicates only a marginal improvement in the developed relationship for C_d variation with H_T/P greater than 0.4 and Fr.

Table 6.3 to 6.5 summaries the measure of error statics with different functional relationships in case of Piano Key Weir with both side overhanging. For lower value of L/W say as 3.56 and 4.84, the functional relationship of C_d variation in term of Fr and h/p again appears to be most suitable choice. However for larger value of L/W as 7.4, it is interesting to observe that relationship strongly dominated by h/p. It is probably because of this reason that the development of generalized relationship for C_d variation with Fr, h/p, and L/W does not work very well as indicated by lower value of R^2 as 0.73 (see the last row in the table 6.3 to 6.5).

Table 6.1: Average absolute percentage error between observed and computed C_d for one side and both sides overhanging type of Piano Key Weir for L/W as 4.84

$C_d = f()$	For one side overhanging		Both sides overhanging	
	Equation	R^2	Equation	R^2
Fr	$C_d = 0.4665 Fr^{-0.6011}$	.0.87	$C_d = 0.4691 Fr^{-0.4214}$	0.56
h/p	$C_d = 0.778 h/p^{-0.405}$	0.96	$C_d = 0.667 h/p^{-0.3703}$	0.80
Fr, h/p	$C_d = 1.876 - 0.00954 h/p - 2.873 Fr$	0.91	$C_d = 1.207 - 1.476 h/p + 2.014 Fr$	0.77
Fr, h/p upto 0.4	$C_d = 1.67 - 4.68 h/p + 5.23 Fr$	0.94	$C_d = 1.39 - 5.31 h/p + 7.66 Fr$	0.95
Fr, h/p greater than 0.4	$C_d = 1.29 - 0.41 h/p + 0.26 Fr$	0.85	$C_d = 0.77 - 1.27 h/p + 3.11 Fr$	0.96

Table 6.2: Comparison of average absolute percentage error between observed and computed C_d for L/W as 4.84 with h/p and H_T/p for single side overhanging

$C_d = f()$	Average absolute % error	R^2	$C_d = f()$	Average absolute % error	R^2
Fr	6.84	0.87	-	-	-
h/p	3.46	0.96	H_T/p	3.46	0.96
Fr, h/p	5.85	0.91	Fr, H_T/p	5.85	0.91
Fr, h/p upto 0.4	2.25	0.94	Fr, H_T/p upto 0.4	2.87	0.94
Fr, h/p greater than 0.4	4.18	0.85	Fr, H_T/p greater than 0.4	3.47	0.88

Table 6.3: Comparison of Average absolute percentage difference between observed and computed C_d for L/W as 3.56 with h/p and H_T/p for both side overhanging

$C_d = f()$	Average absolute % error	R^2	$C_d = f()$	Average absolute % error	R^2
Fr	5.91	0.78	-	-	-
h/p	4.17	0.88	H_T/p	3.90	0.90
Fr, h/p	6.12	0.77	*Fr*, H_T/p	6.12	0.77
Fr, h/p upto 0.4	3.30	0.92	*Fr*, H_T/p upto 0.4	3.30	0.92
Fr, h/p greater than 0.4	1.93	0.90	*Fr*, H_T/p greater than 0.4	1.93	0.90
Fr, h/p, L/W	12.06	0.73	*Fr*, H_T/p, *L/W*	12.06	0.73

Table 6.4: Comparison of Average absolute percentage error between observed and computed C_d for L/W as 4.84 with h/p and H_T/p for both side overhanging

$C_d = f()$	Average absolute % error	R^2	$C_d = f()$	Average absolute % error	R^2
Fr	11.69	0.56	-	-	-
h/p	7.61	0.80	H_T/p	7.61	0.80
Fr, h/p	8.50	0.77	*Fr*, H_T/p	8.50	0.77
Fr, h/p upto 0.4	3.22	0.95	*Fr*, H_T/p upto 0.4	3.22	0.95
Fr, h/p greater than 0.4	2.63	0.96	*Fr*, H_T/p greater than 0.4	2.63	0.96
Fr, h/p, L/W	12.06	0.73	*Fr*, H_T/p, *L/W*	12.06	0.73

Table 6.5: Comparison of Average absolute percentage error between observed and computed C_d for L/W as 7.4 with h/p and H_T/p for both side overhanging

$C_d = f(\ )$	Average absolute % error	R^2	$C_d = f(\ )$	Average absolute % error	R^2
Fr	11.13	0.85	-	-	-
h/p	6.67	0.95	H_T/p	5.85	0.95
Fr, h/p	12.02	0.81	Fr, H_T/p	12.04	0.81
Fr, h/p upto 0.4	6.28	0.92	Fr, H_T/p upto 0.4	6.13	0.90
Fr, h/p greater than 0.4	3.24	0.90	Fr, H_T/p greater than 0.4	3.37	0.89
Fr, h/p, L/W	12.06	0.73	Fr, H_T/p, L/W	12.06	0.73

6.9 SUMMARY

In this chapter, analysis of C_d variation as a function of Fr, h/p, H_T/p, L/W is presented for two configurations of Piano Key Weir having one side and both side overhanging. The relationship is found sensitive to the range of variables considered for the analysis. For relatively lesser value of L/W, the C_d variation can be described in terms of h/p (or H_T/p) and Fr for a given L/W. Analysis for larger values of L/W indicated that C_d relationship was very much influenced by h/p. For the data considered in this study, it was observed that h/p or H_T/p can be used interchangeably in the development of C_d relationship.

7.1 CONCLUSIONS

Based on this study, the following conclusions can be inferred:

1. Initial phase of experiments (phase -I to IV) which were planned with different configurations of Piano Key Weir, i.e. with or without ramp and one or two side overhanging (u/s & d/s) indicate that Piano Key Weir with presence of ramp and two sides overhanging provides a higher discharge under same head when compared with other Piano Key Weir configurations with lesser number of ramps and/or over-hangings.
2. In phase-V experiments, filling were introduced in the ramps but these were not found to increase the discharge. Thus, ramps with no planar discontinuity were found to be best performing. In phase-V experiments, also modification were introduced into inlet limb of Piano Key Weir but it was again observed (experiment set P_5M_1 & P_5M_2) that such a inlet modification was of no practical significance as it did not lead to any increase in the discharge.
3. The ratio (r) of Piano Key Weir to linear weir discharge for a given head was always more than one and when compared with Labyrinth weir (based on computational only) was always higher than the Labyrinth weir. This finding is in conformity with the literature.
4. The ratio (r) was found to increase with magnification ratio L/W. However, at larger value of L/W, the ratio (r) was observed to tend to approach a limiting value in the proximity of four.
5. For a very large value of L/W, it was observed that variation of ratio of inlet and outlet cell width did influence the ratio r and the performance was best when two cells were of same width. Any deviation from this ratio was found to have a negative effect on r at larger L/W ratios.
6. Among the several options attempted to develop relationship for C_d variations for two different configurations of Piano Key Weir, i.e. one side and both side overhanging, it was found that for one side overhanging Piano Key Weir, C_d variations as a function of (i) Fr (ii) h/p and (iii) Fr and h/p lead to development of several relationships with a relatively higher values of R^2 indicating the appropriateness of different functional relationships. However, the perusal of function relationships for both side overhanging indicates relatively poor performance of C_d variation only as function of Fr. Also, the

C_d variation with h/p as only variational parameter doesn't appear to work so well when compared with counterpart for one side overhanging.

7. The use of total head is also explored in the analysis of C_d variations. However, no significant improvements are observed into development of C_d relationships. This may be because of the reason that velocity heads are very small in the experiments performed.
8. From a summary of results given in chapter 6, for lower values of L/W say as 3.56 and 4.84, the functional relationship of C_d variation in term of Fr and h/p appears to be most suitable choice. However, for larger value of L/W as 7.4, it is interesting to observe that relationship is strongly dominated by h/p. It is probably because of this reason that the development of generalized relationship for C_d variation with Fr, h/p, and L/W does not work very well as indicated by lower values of R^2.
9. Evaluation of the data collected at field scale model (see chapter 5) using (i) $C_d = f(Fr)$, (ii) $C_d = f(h/p)$ & (iii) $C_d = f(h/p, Fr)$ indicates that the use of $C_d = f(h/p, Fr)$ very well works with the field scale model results.

7.2 FUTURE SCOPE OF WORK

- Detailed flow characteristics over a typical Piano Key Weir model may be studied to provide an insight into the internal flow distribution characteristics through the different flow paths constituting the overall magnified crest length and the flow characteristics in the upstream of the Piano Key Weir.
- The model study is required for higher discharges.
- Detailed study on crest shape of Piano Key Weir is also required.

REFERENCES

1. Afshar, A., (1988) "The Development of Labyrinth Weir Design", Water Power and Dam Construction, 40(5), 36-39.

2. Baud O., Hager W.H., Minor H.-E. (2002) "Non-intrusive Discharge Measurements During Floods" Proc. Int. Conf. Flood Estimation March, 6-8, Berne, Switzerland.

3. Blanc, P., and Lemperiere, F., (2001) "Labyrinth Spillways Have a Promising Future", International Journal of Hydropower & Dams, Issue 4.

4. Borghei S.M., Jalili M.R. and Ghodsian M. (1999) "Discharge Coefficient for Sharp Crested Weir in Subcritical Flow", American Society of Civil Engineering, Journal of Hydraulic Engineering, 125(10), 1051-1056.

5. Chi Hien, T., Thanh Son, H. and Ho Ta Khanh, M. (2006) "Results of Some Piano Keys Weir Hydraulic Model Tests in Vietnam", CIGB/ICOLD, Barcelona, Spain.

6. Chow V.T. (1959), "Open Channel Hydraulics", Mc Graw-Hill, Inc., New York.

7. Cohen J, Cohen P, Aiken L, & West S. (2003) "Applied Multiple Regression/Correlation Analysis for the Behavioral Sciences", 3rd ed. Hillsdale NJ: Lawrence Erlbaum.

8. Darvas, L. A. (1971) "Performance and Design of Labyrinth Weirs", American Society of Civil Engineering, Journal of Hydraulic Engineering, 97(80), 1246-1251.

9. Emiroglu, M. E. and A. Baylar (2005) "Influence of Included Angle and Sill Slope of Air Entrainment of Triangular Planform Labyrinth Weirs", American Society of Civil Engineering, Journal of Hydrualic Engineering, 131(3): 184-189.

10. Falvey H.T. (2003) "Hydraulic Design of Labyrinth Weir", ACSE Press, USA.

11. Hay, N., and Taylor, G., (1970) "Performance and Design of Labyrinth Weirs", *American Society of Civil Engineering, Journal of Hydraulic Engineering, 96(11),* 2237-2357.

12. Kindsvater, C. E., and Carter R. W. (1959), "discharge characteristics of rectangular thin plate weirs", American Society of Civil Engineering, Journal of Hydraulic Engineering, 124, 772-822.

13. Laugier, F. (2007) "Design and Construction of the First Piano Key Weir (PKW) Spillway at the Goulours Dam", Hydropower & Dams. Issue 5,

14. Leite Ribeiro M., Bieri M., Boillat J.-L., Schleiss A., Laugier F., (2009) "Improving Hydraulic Capacity of existing spillway, Pani key weir design", Q.90-R.1, International Commission on the Large Barrage, Brasilia, Mai.

15. Leite Ribeiro M., Boillat J.-L., Kantoush S., Albalat C., Laugier F., Lochu A. (2007) "Rehabilitation of St-Marc dam: Model studies for the spillways", Hydro 2007 "New approaches for a new era", Granada, Spain,15-17 October 2007.

16. Lempérière F. and Jun G. (2005) "Low Cost Increase of Dams Storage and Flood Mitigation: The Piano Keys Weir", Q. 53 R. 2.06 International Commission on Irrigation and Drainage Nineteenth Congress Beijing.

17. Lempérière, F. and Ouamane, A. (2003) "The Piano Keys weir: a new cost-effective solution for spillways", Hydropower & Dams Issue 5, 144-149.

18. Lux, F., (1989) "Design and Application of Labyrinth weir", Design of Hydraulic Structures 89, Balkema/Rotterdam/Brookfield.

19. Lux, F., and Hinchliff, D.L., (1985) "Design and construction of labyrinth spillways", 15th Congress ICOLD, Vol. IV, Q59-R15, Lausanne, Switzerland, 249-274.

20. Magalhaes, A. P., and M. Lorena (1989) "Hydraulic Design of Labyrinth Weir", Report No. 736, National Laboratory of Civil Engineering, Lisbon, Portugal.

21. Meglhaes, A. P., (1985) "Labyrinth weir spillway", Transactions of the 15th Congress ICOLD, Vol. VI, Q59-R24, Lausanne, Switzerland, 395-407.

22. Modi P.N. and seth S.M. (1991) "Hydraulics and Fluid Mechanics", Edition 10, Standard Book House, New Delhi.

23. Ouamane, A. and Lempérière F. (2006) "Design of a new economic shape of weir", Proceedings of the International Symposium on Dams in the Societies of the 21st Century, 463-470. Barcelona, Spain,

24. Pinheiro, A.N., and Silva, I., (1999) "Discharge coefficient of side weirs, Experimental study and comparative analysis of different formulas", XXVIII IAHR Proceedings, Garz, Austria.

25. Taylor G. (1968), "The Performance of Labyrinth Weir", Ph.D. Thesis, University of Nottingham, Nottingham, U.K.

26. Tullis, J. P., Nosratollah, A., and Waldron, D., (1995). "Design of labyrinth spillways", American Society of Civil Engineering, Journal of Hydraulic Engineering, 121(3), 247-255.

27. Weber, L.J., Shumate, E.D. and Mawer, (2001) "Experimental on Flow at a 90° Open-Channel Junction", Journal of Hydraulic Engineering, ASCE, Vol. 127, No. 5.

28. Wormleaton, P. R. and C. C. Tsang (2000) "Aeration performance of rectangular plan-form labyrinth weirs", Journal of Hydrualic Environmental Engineering 126(5): 456-465.

APPENDIX-A

DATA RELATED TO FIVE PHASE EXPERIEMNTS

This appendix contains the experimental data collected in five phase experiments. The data presented here have been used in Chapter 4.

P = height of weir (cm)
L = Perimeter of Piano Key weir crest (cm)
W = Width of channel (cm)
Q_{PK} = Piano Key Weir discharge (l/s)
Q_L = Linear Weir discharge (l/s)
r = Q_{PK}/Q_L
ΔQ = Q_{PK}-Q_L

Table A.1: Data for discharge coefficient variation analysis for Model P_1M_1

h	h/p	Q_{PK}	Q_L	r	ΔQ
14.56	1.21	82.24	60.00	1.37	22.24
12.06	1.01	64.68	45.23	1.43	19.45
9.84	0.82	51.61	33.34	1.55	18.27
6.70	0.56	34.84	18.73	1.86	16.11
5.69	0.47	29.51	14.66	2.01	14.85
3.87	0.32	19.42	8.22	2.36	11.20
2.40	0.20	10.73	4.02	2.67	6.71

Table A.2: Data for discharge coefficient variation analysis for Model P_1M_2

h	h/p	Q_{PK}	Q_L	r	ΔQ
13.04	0.82	80.75	50.86	1.59	29.89
12.04	0.75	74.19	45.12	1.64	29.07
10.65	0.67	64.26	37.54	1.71	26.72
8.97	0.56	54.56	29.01	1.88	25.54
7.35	0.46	44.46	21.52	2.07	22.94
6.45	0.40	37.98	17.69	2.15	20.29
5.07	0.32	29.17	12.33	2.37	16.84
3.82	0.24	21.68	8.06	2.69	13.62
3.30	0.21	18.12	6.47	2.80	11.64
2.76	0.17	14.80	4.95	2.99	9.84

Table A.3: Data for discharge coefficient variation analysis for Model P_1M_3

h	h/p	Q_{PK}	Q_L	r	ΔQ
12.63	0.63	78.98	48.48	1.63	30.50
11.74	0.59	72.96	43.44	1.68	29.51
10.53	0.53	65.50	36.90	1.77	28.60
9.26	0.46	57.03	30.43	1.87	26.59
7.70	0.39	47.41	23.08	2.05	24.33
6.32	0.32	38.99	17.16	2.27	21.83
5.03	0.25	31.18	12.18	2.56	19.00
3.80	0.19	23.94	8.00	2.99	15.94
2.90	0.15	17.99	5.33	3.37	12.66
2.60	0.13	15.72	4.53	3.47	11.19
2.07	0.10	11.83	3.22	3.68	8.61

Table A.4: Data for discharge coefficient variation analysis for Model P_1M_4

h	h/p	Q_{PK}	Q_L	r	ΔQ
15.19	1.27	82.41	63.94	1.29	18.47
14.00	1.17	75.19	56.57	1.33	18.62
12.70	1.06	67.07	48.88	1.37	18.19
11.55	0.96	59.28	42.39	1.40	16.89
9.82	0.82	48.23	33.23	1.45	15.00
8.77	0.73	42.58	28.05	1.52	14.54
7.08	0.59	32.43	20.35	1.59	12.09
6.03	0.50	26.75	15.99	1.67	10.76
5.30	0.44	22.84	13.18	1.73	9.66
4.58	0.38	18.69	10.59	1.77	8.10
3.90	0.33	14.93	8.32	1.80	6.61
3.23	0.27	11.71	6.27	1.87	5.44

Table A.5: Data for discharge coefficient variation analysis for Model P_1M_5

h	h/p	Q_{PK}	Q_L	r	ΔQ
13.31	1.11	77.14	52.44	1.47	24.70
12.20	0.76	69.06	46.02	1.50	23.04
11.17	0.70	60.66	40.32	1.50	20.35
9.97	0.62	52.09	34.00	1.53	18.09
8.87	0.55	45.92	28.53	1.61	17.39
7.89	0.49	39.42	23.94	1.65	15.48
6.50	0.41	31.05	17.90	1.74	13.16
5.34	0.33	23.97	13.33	1.80	10.64
4.70	0.29	20.79	11.00	1.89	9.79
3.89	0.24	16.36	8.29	1.97	8.08
3.34	0.21	13.86	6.59	2.10	7.27

Table A.6: Data for discharge coefficient variation analysis for Model P_1M_6

h	h/p	Q_{PK}	Q_L	r	ΔQ
13.16	0.82	80.16	51.56	1.55	28.60
12.30	0.77	73.83	46.59	1.58	27.24
11.22	0.70	65.52	40.59	1.61	24.93
9.97	0.62	57.03	34.00	1.68	23.03
8.82	0.55	48.77	28.29	1.72	20.48
7.84	0.49	42.92	23.71	1.81	19.22
7.04	0.44	37.83	20.17	1.87	17.65
6.17	0.39	32.43	16.55	1.96	15.88
5.20	0.33	25.89	12.81	2.02	13.08
4.15	0.26	19.74	9.13	2.16	10.61
3.35	0.21	15.21	6.62	2.30	8.58

Table A.7: Data for discharge coefficient variation analysis for Model P_2M_1

h	h/p	Q_{PK}	Q_L	r	ΔQ
14.16	1.18	80.08	57.55	1.39	22.53
12.65	1.05	70.20	48.59	1.44	21.61
11.40	0.95	61.92	41.57	1.49	20.35
10.07	0.84	54.74	34.51	1.59	20.23
9.00	0.75	47.16	28.46	1.66	18.70
6.92	0.58	36.22	19.66	1.84	16.56
5.68	0.47	30.12	14.62	2.06	15.50
4.48	0.37	23.50	10.24	2.29	13.26
3.40	0.28	17.50	6.77	2.58	10.73
2.60	0.22	12.67	4.53	2.80	8.14

Table A.8: Data for discharge coefficient variation analysis for Model P_2M_2

h	h/p	Q_{PK}	Q_L	r	ΔQ
12.34	0.77	76.73	46.81	1.64	29.92
11.02	0.69	69.12	39.50	1.75	29.62
9.98	0.62	61.83	34.05	1.82	27.78
8.37	0.52	52.32	26.15	2.00	26.17
6.88	0.43	44.58	19.49	2.29	25.09
5.58	0.35	37.03	14.23	2.60	22.80
4.56	0.29	29.50	10.52	2.80	18.98
3.52	0.22	23.38	7.13	3.28	16.25
2.78	0.17	18.52	5.00	3.70	13.52
2.18	0.14	14.07	3.48	4.04	10.59
1.93	0.12	11.98	2.90	4.13	9.08

Table A.9: Data for discharge coefficient variation analysis for Model P_2M_3

h	h/p	Q_{PK}	Q_L	r	ΔQ
11.17	0.56	70.72	40.32	1.75	30.40
9.94	0.50	62.77	33.84	1.85	28.93
8.87	0.44	54.98	28.53	1.93	26.45
7.62	0.38	47.97	22.72	2.11	25.25
6.50	0.33	41.56	17.90	2.32	23.66
4.93	0.25	32.05	11.82	2.71	20.23
3.42	0.17	23.92	6.83	3.50	17.09
2.80	0.14	18.73	5.06	3.70	13.67
2.18	0.11	13.62	3.48	3.91	10.14

Table A.10: Data for discharge coefficient variation analysis for Model P_2M_4

h	h/p	Q_{PK}	Q_L	r	ΔQ
14.10	1.18	78.25	57.18	1.37	21.07
12.51	1.04	68.31	48.79	1.40	19.52
11.40	0.95	60.56	41.57	1.46	18.99
10.34	0.86	54.43	35.90	1.52	18.53
9.28	0.77	48.23	30.53	1.58	17.70
7.44	0.62	37.23	21.92	1.70	15.31
6.37	0.53	30.32	17.36	1.75	12.96
5.40	0.45	24.90	13.55	1.84	11.35
4.48	0.37	19.93	10.24	1.95	9.69
3.63	0.30	15.98	7.47	2.14	8.51
3.15	0.26	13.98	6.04	2.31	7.94

Table A.11: Data for discharge coefficient variation analysis for Model P_2M_5

h	h/p	Q_{PK}	Q_L	r	ΔQ
13.35	1.11	80.49	52.68	1.53	27.81
12.00	0.75	70.27	44.89	1.57	25.38
11.01	0.69	62.15	39.45	1.58	22.70
9.98	0.62	54.92	34.05	1.61	20.87
8.55	0.53	46.64	27.00	1.73	19.64
7.38	0.46	38.18	21.65	1.76	16.53
5.49	0.34	26.52	13.89	1.91	12.63
4.65	0.29	22.41	10.82	2.07	11.59
3.92	0.25	18.55	8.38	2.21	10.17
2.98	0.19	13.25	5.55	2.39	7.70

Table A.12: Data for discharge coefficient variation analysis for Model P_2M_6

h	h/p	Q_{PK}	Q_L	r	ΔQ
12.70	0.79	77.10	48.88	1.58	28.22
11.55	0.58	69.30	42.39	1.63	26.91
10.54	0.53	61.83	36.95	1.67	24.88
9.73	0.49	56.53	32.78	1.72	23.75
8.48	0.42	47.81	26.67	1.79	21.14
7.28	0.36	40.05	21.21	1.89	18.84
6.15	0.31	33.05	16.47	2.01	16.58
5.13	0.26	25.83	12.55	2.06	13.28
4.05	0.20	18.78	8.80	2.13	9.98
3.62	0.18	16.37	7.44	2.20	8.93
3.14	0.16	13.43	6.00	2.24	7.43

Table A.13: Data for discharge coefficient variation analysis for Model P_3M_1

h	h/p	Q_{PK}	Q_L	r	ΔQ
12.51	0.78	77.98	47.78	1.63	30.20
11.22	0.70	69.90	40.58	1.72	29.32
9.91	0.62	61.68	33.69	1.83	27.99
8.56	0.54	52.95	27.04	1.96	25.91
7.10	0.44	43.76	20.43	2.14	23.33
6.09	0.38	37.62	16.23	2.32	21.39
4.72	0.30	29.11	10.17	2.86	18.94
4.00	0.25	24.60	7.81	3.15	16.79
3.28	0.21	19.94	5.67	3.52	14.27
2.48	0.16	14.63	3.86	3.79	10.77
1.99	0.12	11.59	3.03	3.83	8.56

Table A.14: Data for discharge coefficient variation analysis for Model P_3M_2

h	h/p	Q_{PK}	Q_L	r	ΔQ
13.56	0.85	81.12	53.92	1.50	27.20
12.54	0.78	73.19	47.96	1.53	25.23
11.26	0.70	64.70	40.80	1.59	23.90
9.78	0.61	55.42	33.03	1.68	22.39
8.65	0.54	48.32	27.47	1.76	20.85
7.38	0.46	40.88	21.65	1.89	19.23
6.63	0.41	36.64	18.35	2.00	18.29
4.91	0.31	26.16	11.75	2.23	14.41
3.94	0.25	20.80	8.45	2.46	12.35
3.12	0.20	16.37	5.89	2.78	10.48
2.40	0.15	11.67	4.01	2.91	7.66

Table A.15: Data for discharge coefficient variation analysis for Model P_3M_3

h	h/p	Q_{PK}	Q_L	r	ΔQ
12.18	0.76	74.98	45.90	1.63	29.08
10.78	0.67	66.30	38.22	1.73	28.08
9.39	0.59	57.14	31.07	1.84	26.07
7.97	0.50	48.40	23.75	2.04	24.65
6.92	0.43	42.00	19.23	2.18	22.77
6.15	0.38	37.17	16.47	2.26	20.70
4.50	0.28	25.90	10.30	2.51	15.60
3.81	0.24	21.60	8.03	2.69	13.57
3.04	0.19	16.66	5.72	2.91	10.94
2.45	0.15	12.19	4.02	3.03	8.17

Table A.16: Data for discharge coefficient variation analysis for Model P_3M_4

h	h/p	Q_{PK}	Q_L	r	ΔQ
13.37	0.84	77.83	52.80	1.47	25.03
12.13	0.76	69.01	45.63	1.51	23.38
10.69	0.67	58.57	37.74	1.55	20.83
9.20	0.58	50.03	29.65	1.69	20.38
7.88	0.49	41.84	23.89	1.75	17.95
7.03	0.44	36.14	20.13	1.80	16.01
6.62	0.41	33.05	18.39	1.80	14.66
5.06	0.32	25.21	12.07	2.09	13.14
4.23	0.26	21.02	9.39	2.24	11.63
3.25	0.20	15.54	6.33	2.45	9.21
2.60	0.16	11.69	4.53	2.58	7.16

Table A.17: Data for discharge coefficient variation analysis for Model P_3M_5

h	h/p	Q_{PK}	Q_L	r	ΔQ
13.02	0.81	78.02	50.73	1.54	27.29
11.92	0.75	70.56	44.44	1.59	26.12
10.69	0.67	61.30	37.74	1.62	23.56
9.25	0.58	52.18	29.64	1.76	22.54
8.15	0.51	45.60	25.12	1.82	20.48
6.90	0.43	37.62	19.57	1.92	18.05
4.60	0.29	24.60	10.65	2.31	13.95
3.62	0.23	19.04	7.44	2.56	11.60
2.90	0.18	14.97	5.33	2.81	9.64
2.40	0.15	11.59	4.02	2.88	7.57

Table A.18: Data for discharge coefficient variation analysis for Model P_3M_6

h	h/p	Q_{PK}	Q_L	r	ΔQ
13.38	0.84	73.78	52.85	1.40	20.93
12.30	0.77	65.53	46.59	1.41	18.94
11.00	0.69	57.03	39.40	1.45	17.63
9.64	0.60	49.05	32.32	1.52	16.73
7.95	0.50	39.84	24.21	1.65	15.63
7.13	0.45	34.99	20.56	1.70	14.43
5.52	0.35	25.21	14.00	1.80	11.21
4.56	0.29	20.14	10.52	1.91	9.62
3.70	0.23	15.38	7.68	2.00	7.70
3.07	0.19	12.38	5.82	2.13	6.56

Table A.19: Data for discharge coefficient variation analysis for Model P_4M_1

h	h/p	Q_{PK}	Q_L	r	ΔQ
12.80	0.80	83.56	49.45	1.69	34.11
11.40	0.71	74.83	41.57	1.80	33.26
10.07	0.63	65.03	34.51	1.88	30.52
8.32	0.52	53.00	25.26	2.10	27.74
7.10	0.44	45.28	20.43	2.22	24.85
6.06	0.38	39.70	16.11	2.46	23.59
4.15	0.26	27.29	9.13	2.99	18.16
3.46	0.22	23.15	6.95	3.33	16.20
2.80	0.18	18.57	5.06	3.67	13.51
2.14	0.13	14.10	3.38	4.17	10.72
1.76	0.11	10.92	2.52	4.33	8.40

Table A.20: Data for discharge coefficient variation analysis for Model P_4M_2

h	h/p	Q_{PK}	Q_L	r	ΔQ
12.55	0.78	79.27	48.01	1.65	31.26
11.34	0.71	70.46	41.24	1.71	29.22
10.18	0.64	62.36	35.07	1.78	27.29
8.80	0.55	51.70	28.19	1.83	23.51
7.30	0.46	43.11	21.30	2.02	21.81
6.50	0.41	37.43	17.89	2.09	19.54
4.86	0.30	25.30	11.57	2.19	13.73
4.27	0.27	20.94	9.53	2.20	11.41
3.50	0.22	16.13	7.07	2.28	9.06
2.62	0.16	11.11	4.59	2.42	6.52

Table A.21: Data for discharge coefficient variation analysis for Model P_4M_3

h	h/p	Q_{PK}	Q_L	r	ΔQ
12.10	0.76	78.01	45.45	1.72	32.56
10.93	0.68	69.41	39.02	1.78	30.39
9.86	0.62	61.83	33.43	1.85	28.40
8.35	0.52	52.18	26.05	2.00	26.13
6.90	0.43	43.20	19.57	2.21	23.63
6.05	0.38	38.02	16.07	2.37	21.95
4.37	0.27	26.97	9.86	2.74	17.11
3.80	0.24	22.65	8.00	2.83	14.65
3.38	0.21	19.40	6.71	2.89	12.69
2.77	0.17	15.20	4.98	3.05	10.22
2.33	0.15	12.07	3.84	3.14	8.23

Table A.22: Data for discharge coefficient variation analysis for Model P_4M_4

h	h/p	Q_{PK}	Q_L	r	ΔQ
14.45	1.20	90.22	59.32	1.52	30.90
9.20	0.77	55.22	30.14	1.83	25.08
8.45	0.70	50.84	26.53	1.92	24.31
7.23	0.60	42.21	21.00	2.01	21.21
6.08	0.51	35.56	16.19	2.20	19.37
4.88	0.41	28.16	11.64	2.42	16.52
3.55	0.30	20.58	7.22	2.85	13.36
2.60	0.22	15.09	4.53	3.33	10.56

Table A.23: Data for discharge coefficient variation analysis for Model P_4M_5

h	h/p	Q_{PK}	Q_L	r	ΔQ
14.80	1.23	89.88	61.49	1.46	28.39
13.80	1.15	82.39	55.37	1.49	27.02
9.52	0.79	54.87	31.72	1.73	23.15
8.91	0.74	51.22	28.72	1.78	22.50
8.05	0.67	45.39	24.67	1.84	20.72
7.00	0.58	38.87	20.00	1.94	18.86
5.71	0.48	31.20	14.74	2.12	16.46
4.61	0.38	25.17	10.69	2.35	14.48
3.40	0.28	18.54	6.77	2.74	11.77

Table A.24: Data for discharge coefficient variation analysis for Model P_5M_1

h	h/p	Q_{PK}	Q_L	r	ΔQ
14.22	1.19	79.81	57.91	1.38	21.90
10.55	0.88	56.68	37.01	1.53	19.67
9.72	0.81	50.23	32.73	1.53	17.50
9.22	0.77	46.14	30.24	1.53	15.90
8.22	0.69	40.00	25.45	1.57	14.55
6.95	0.58	32.45	19.79	1.64	12.66
6.26	0.52	28.44	16.92	1.68	11.53
5.26	0.44	22.60	13.03	1.73	9.57
4.67	0.39	19.40	10.90	1.78	8.50

Table A.25: Data for discharge coefficient variation analysis for Model P_5M_2

h	h/p	Q_{PK}	Q_L	r	ΔQ
13.36	0.84	81.63	52.74	1.55	28.89
9.23	0.58	50.69	30.28	1.67	20.41
8.38	0.52	45.07	26.20	1.72	18.87
7.40	0.46	40.53	21.74	1.86	18.79
6.64	0.42	36.06	18.48	1.95	17.58
5.93	0.37	30.99	15.60	1.99	15.39
4.88	0.31	23.50	11.64	2.02	11.86
4.43	0.28	20.41	10.07	2.03	10.34
3.38	0.21	14.30	6.71	2.13	7.59

Table A.26: Data for discharge coefficient variation analysis for Model P_5M_3

h	h/p	Q_{PK}	Q_L	r	ΔQ
14.35	0.90	78.63	59.80	1.31	18.83
13.31	0.83	71.43	52.44	1.36	18.99
12.22	0.76	64.15	46.13	1.39	18.02
10.84	0.68	56.37	38.54	1.46	17.83
9.63	0.60	48.60	32.37	1.50	16.23
8.31	0.52	40.89	25.87	1.58	15.02
7.44	0.47	35.61	21.91	1.63	13.70
6.17	0.39	29.28	16.55	1.77	12.73
5.28	0.33	23.64	13.10	1.80	10.54
4.45	0.28	18.88	10.13	1.86	8.75
3.53	0.22	14.03	7.16	1.96	6.87

Table A.27: Data for discharge coefficient variation analysis for Model P_5M_4

h	h/p	Q_{PK}	Q_L	r	ΔQ
12.96	0.81	74.38	50.38	1.48	24.00
11.13	0.70	65.19	40.10	1.63	25.09
9.94	0.62	58.16	33.84	1.72	24.32
8.43	0.53	49.42	26.43	1.87	22.99
6.35	0.40	38.89	17.28	2.25	21.61
5.03	0.31	29.85	12.18	2.45	17.67
4.27	0.27	25.21	9.53	2.65	15.68
3.55	0.22	20.60	7.22	2.85	13.38
2.80	0.18	15.17	5.06	3.00	10.11
2.38	0.15	12.19	3.96	3.08	8.23

Table A.28: Data for discharge coefficient variation analysis for Model P_5M_5

h	h/p	Q_{PK}	Q_L	r	ΔQ
13.10	0.82	75.43	51.20	1.47	24.23
11.89	0.74	67.75	44.27	1.53	23.48
10.58	0.66	58.42	37.16	1.57	21.26
9.59	0.60	51.37	32.07	1.60	19.30
8.28	0.52	43.42	25.73	1.69	17.69
7.45	0.47	37.74	21.96	1.72	15.78
6.72	0.42	33.42	18.81	1.78	14.61
5.24	0.33	24.60	12.95	1.90	11.65
4.63	0.29	21.00	10.76	1.95	10.24
3.87	0.24	16.49	8.22	2.01	8.27
3.33	0.21	13.00	6.56	1.98	6.44

APPENDIX-B

DATA RELATED TO CASE STUDY

This appendix contains the experimental data collected in case study experiments. The data presented here have been used in Chapter 5.

P = height of weir (cm)
L = Perimeter of Piano Key weir crest (cm)
W = Width of channel (cm)
Q_{PK} = Piano Key Weir discharge (l/s)
Q_L = Linear Weir discharge (l/s)
r = Q_{PK}/Q_L
ΔQ = $Q_{PK}-Q_L$

Table B.1: Data for discharge coefficient variation analysis for Model C_1M_1

h	h/p	Q_L	Q_{PK}	r	ΔQ
5.540	0.301	28.166	43.251	1.536	15.086
5.210	0.283	25.687	40.222	1.566	14.535
4.850	0.264	23.071	37.323	1.618	14.252
4.410	0.240	20.004	33.217	1.661	13.213
3.200	0.174	12.365	22.423	1.814	10.059
2.460	0.134	8.334	15.432	1.852	7.098
2.000	0.109	6.109	11.836	1.937	5.727

Table B.2: Data for discharge coefficient variation analysis for Model C_1M_2

h	h/p	Q_L	Q_{PK}	r	ΔQ
4.610	0.249	21.380	45.451	2.126	24.071
4.340	0.234	19.529	42.285	2.165	22.756
3.330	0.180	13.126	31.362	2.389	18.236
2.800	0.151	10.120	25.300	2.500	15.180
2.020	0.109	6.201	16.304	2.629	10.103
1.560	0.084	4.209	11.414	2.712	7.205

Table B.3: Data for discharge coefficient variation analysis for Model C_1M_3

h	h/p	Q_L	Q_{PK}	r	ΔQ
4.930	0.266	23.644	47.952	2.028	24.307
4.390	0.237	19.868	43.031	2.166	23.163
4.070	0.220	17.736	39.172	2.209	21.436
3.500	0.189	14.143	33.406	2.362	19.263
2.440	0.132	8.233	21.685	2.634	13.453
2.060	0.111	6.386	17.693	2.770	11.306
1.580	0.085	4.290	12.645	2.948	8.355

Table B.4: Data for discharge coefficient variation analysis for Model C_1M_4

h	h/p	Q_L	Q_{PK}	r	ΔQ
3.550	0.191	14.448	43.251	2.994	28.804
3.350	0.181	13.244	41.289	3.118	28.045
2.900	0.156	10.667	35.725	3.349	25.058
2.710	0.146	9.636	33.596	3.486	23.960
1.940	0.105	5.837	21.832	3.741	15.995
1.600	0.086	4.372	17.053	3.901	12.682
1.400	0.076	3.578	14.519	4.058	10.941
1.120	0.060	2.560	10.731	4.191	8.170

Table B.5: Data for discharge coefficient variation analysis for Model C_1M_5

h	h/p	Q_L	Q_{PK}	r	ΔQ
3.810	0.206	16.064	44.816	2.790	28.752
2.840	0.153	10.338	33.029	3.195	22.691
2.090	0.113	6.526	22.723	3.482	16.196
1.870	0.101	5.524	19.559	3.541	14.036
1.630	0.088	4.495	16.181	3.600	11.686
1.290	0.070	3.165	11.836	3.740	8.671

Table B.6: Data for discharge coefficient variation analysis for Model C_1M_6

h	h/p	Q_L	Q_{PK}	r	ΔQ
3.880	0.211	15.897	44.816	2.819	28.919
3.420	0.186	13.155	38.756	2.946	25.601
3.160	0.172	11.684	35.568	3.044	23.884
2.870	0.156	10.113	31.728	3.137	21.615
2.050	0.111	6.105	20.338	3.331	14.232
1.830	0.099	5.149	17.486	3.396	12.337
1.410	0.077	3.483	12.434	3.570	8.952

APPENDIX-C

DATA RELATED TO STUDY OF C_d VARATION

This appendix contains the data related to study of variation of discharge coefficient analysis. The data presented here have been used in Chapter 6.

P = height of weir (cm)
L = Perimeter of Piano Key weir crest (cm)
W = Width of channel (cm)
H_T = Total head of water (cm)
Fr = Froude number
C_d = Discharge coefficient

Table C.1: Data for discharge coefficient variation analysis for Model P_2M_1

p	h/p	L/W	H_T/p	Fr	C_d
12	1.054	7.40	1.056	0.366	0.704
12	0.950	7.40	0.951	0.349	0.726
12	0.839	7.40	0.840	0.337	0.773
12	0.750	7.40	0.751	0.313	0.788
12	0.577	7.40	0.577	0.281	0.898
12	0.473	7.40	0.474	0.259	1.004
12	0.373	7.40	0.374	0.224	1.119
12	0.283	7.40	0.284	0.185	1.260
12	0.217	7.40	0.217	0.145	1.364

Table C.2: Data for discharge coefficient variation analysis for Model P_2M_2

p	h/p	L/W	H_T/p	Fr	C_d
16	0.689	7.40	0.690	0.314	0.853
16	0.624	7.40	0.624	0.298	0.885
16	0.523	7.40	0.524	0.278	0.975
16	0.430	7.40	0.430	0.260	1.115
16	0.349	7.40	0.349	0.236	1.268
16	0.285	7.40	0.285	0.202	1.367
16	0.220	7.40	0.220	0.173	1.598
16	0.174	7.40	0.174	0.145	1.803
16	0.136	7.40	0.136	0.116	1.973
16	0.121	7.40	0.121	0.101	2.017

Table C.3: Data for discharge coefficient variation analysis for Model P_2M_3

p	h/p	L/W	H_T/p	Fr	C_d
20	0.559	7.40	0.559	0.259	0.855
20	0.497	7.40	0.497	0.245	0.904
20	0.444	7.40	0.444	0.226	0.939
20	0.381	7.40	0.381	0.211	1.029
20	0.325	7.40	0.325	0.195	1.132
20	0.247	7.40	0.247	0.164	1.321
20	0.171	7.40	0.171	0.135	1.707
20	0.140	7.40	0.140	0.110	1.804
20	0.109	7.40	0.109	0.083	1.910

Table C.4: Data for discharge coefficient variation analysis for Model P_2M_4

p	h/p	L/W	H_T/p	Fr	C_d
12	1.043	3.56	1.044	0.359	0.697
12	0.950	3.56	0.951	0.342	0.710
12	0.862	3.56	0.863	0.329	0.739
12	0.773	3.56	0.774	0.314	0.770
12	0.620	3.56	0.621	0.277	0.828
12	0.531	3.56	0.531	0.246	0.851
12	0.450	3.56	0.450	0.219	0.896
12	0.373	3.56	0.374	0.190	0.949
12	0.303	3.56	0.303	0.165	1.043
12	0.263	3.56	0.263	0.151	1.129

Table C.5: Data for discharge coefficient variation analysis for Model P_2M_5

p	h/p	L/W	H_T/p	Fr	C_d
16	0.750	3.56	0.751	0.303	0.763
16	0.688	3.56	0.689	0.283	0.768
16	0.624	3.56	0.624	0.265	0.786
16	0.534	3.56	0.535	0.245	0.842
16	0.461	3.56	0.462	0.216	0.859
16	0.343	3.56	0.343	0.170	0.930
16	0.291	3.56	0.291	0.152	1.009
16	0.245	3.56	0.245	0.133	1.079
16	0.186	3.56	0.186	0.102	1.162

Table C.6: Data for discharge coefficient variation analysis for Model P_2M_6

p	h/p	L/W	H_T/p	Fr	C_d
20	0.578	3.56	0.578	0.250	0.797
20	0.527	3.56	0.527	0.234	0.816
20	0.487	3.56	0.487	0.223	0.841
20	0.424	3.56	0.424	0.201	0.874
20	0.364	3.56	0.364	0.179	0.920
20	0.308	3.56	0.308	0.158	0.978
20	0.257	3.56	0.257	0.131	1.003
20	0.203	3.56	0.203	0.102	1.040
20	0.181	3.56	0.181	0.091	1.073
20	0.157	3.56	0.157	0.077	1.089

Table C.7: Data for discharge coefficient variation analysis for Model P_3M_1

p	h/p	L/W	H_T/p	Fr	C_d
16	0.782	7.40	0.783	0.327	0.795
16	0.701	7.40	0.702	0.314	0.839
16	0.619	7.40	0.620	0.299	0.892
16	0.535	7.40	0.536	0.278	0.954
16	0.433	7.40	0.433	0.252	1.085
16	0.381	7.40	0.381	0.231	1.130
16	0.279	7.40	0.279	0.197	1.395
16	0.234	7.40	0.234	0.176	1.535
16	0.189	7.40	0.189	0.150	1.715
16	0.146	7.40	0.146	0.118	1.845
16	0.124	7.40	0.124	0.097	1.863

Table C.8: Data for discharge coefficient variation analysis for Model P_3M_2

p	h/p	L/W	H_T/p	Fr	C_d
16	0.848	7.40	0.848	0.322	0.733
16	0.784	7.40	0.785	0.307	0.744
16	0.704	7.40	0.704	0.290	0.773
16	0.611	7.40	0.612	0.270	0.818
16	0.541	7.40	0.541	0.252	0.857
16	0.461	7.40	0.462	0.231	0.920
16	0.413	7.40	0.413	0.217	0.973
16	0.307	7.40	0.307	0.175	1.085
16	0.246	7.40	0.246	0.149	1.200
16	0.194	7.40	0.194	0.125	1.354
16	0.150	7.40	0.150	0.094	1.417

Table C.9: Data for discharge coefficient variation analysis for Model P_3M_3

p	h/p	L/W	H_T/p	Fr	C_d
16	0.761	4.84	0.762	0.320	0.796
16	0.674	4.84	0.675	0.305	0.845
16	0.587	4.84	0.588	0.285	0.896
16	0.491	4.84	0.491	0.263	0.993
16	0.426	4.84	0.427	0.244	1.064
16	0.384	4.84	0.385	0.228	1.100
16	0.281	4.84	0.281	0.178	1.225
16	0.238	4.84	0.238	0.156	1.311
16	0.190	4.84	0.190	0.128	1.419
16	0.155	4.84	0.155	0.098	1.409

Table C.10: Data for discharge coefficient variation analysis for Model P_3M_4

p	h/p	L/W	H_T/p	Fr	C_d
16	0.836	4.84	0.837	0.312	0.719
16	0.758	4.84	0.759	0.295	0.737
16	0.668	4.84	0.669	0.271	0.756
16	0.569	4.84	0.569	0.253	0.823
16	0.493	4.84	0.493	0.229	0.854
16	0.439	4.84	0.440	0.209	0.892
16	0.414	4.84	0.414	0.196	0.876
16	0.313	4.84	0.313	0.167	1.018
16	0.264	4.84	0.265	0.148	1.090
16	0.203	4.84	0.203	0.117	1.197
16	0.163	4.84	0.163	0.093	1.258

Table C.11: Data for discharge coefficient variation analysis for Model P_3M_5

p	h/p	L/W	H_T/p	Fr	C_d
16	0.814	3.56	0.815	0.319	0.750
16	0.745	3.56	0.746	0.305	0.774
16	0.668	3.56	0.669	0.284	0.792
16	0.569	3.56	0.569	0.263	0.858
16	0.509	3.56	0.510	0.245	0.885
16	0.431	3.56	0.432	0.219	0.937
16	0.288	3.56	0.288	0.168	1.125
16	0.226	3.56	0.226	0.140	1.248
16	0.181	3.56	0.181	0.116	1.368
16	0.150	3.56	0.150	0.094	1.407

Table C.12: Data for discharge coefficient variation analysis for Model P_3M_6

p	h/p	L/W	H_T/p	Fr	C_d
16	0.836	4.84	0.837	0.296	0.680
16	0.769	4.84	0.769	0.278	0.686
16	0.688	4.84	0.688	0.260	0.706
16	0.603	4.84	0.603	0.241	0.740
16	0.497	4.84	0.497	0.217	0.802
16	0.446	4.84	0.446	0.201	0.829
16	0.345	4.84	0.345	0.161	0.877
16	0.285	4.84	0.285	0.138	0.933
16	0.231	4.84	0.231	0.112	0.975
16	0.192	4.84	0.192	0.095	1.039

Table C.13: Data for discharge coefficient variation analysis for Model P_4M_3

p	h/p	L/W	H_T/p	Fr	C_d
16	0.756	4.84	0.757	0.334	0.837
16	0.683	4.84	0.684	0.317	0.867
16	0.616	4.84	0.617	0.300	0.901
16	0.522	4.84	0.522	0.277	0.976
16	0.431	4.84	0.432	0.252	1.076
16	0.378	4.84	0.379	0.234	1.153
16	0.273	4.84	0.273	0.187	1.332
16	0.238	4.84	0.238	0.164	1.380
16	0.211	4.84	0.211	0.145	1.409
16	0.173	4.84	0.173	0.119	1.488
16	0.146	4.84	0.146	0.098	1.532

Table C.14: Data for discharge coefficient variation analysis for Model P_4M_4

p	h/p	L/W	H_T/p	Fr	C_d
12	1.204	4.84	1.206	0.424	0.741
12	0.767	4.84	0.768	0.361	0.893
12	0.704	4.84	0.705	0.351	0.934
12	0.603	4.84	0.603	0.320	0.980
12	0.507	4.84	0.507	0.295	1.071
12	0.407	4.84	0.407	0.259	1.179
12	0.296	4.84	0.296	0.214	1.389
12	0.217	4.84	0.217	0.173	1.624

Table C.15: Data for discharge coefficient variation analysis for Model P_4M_5

p	h/p	L/W	H_T/p	Fr	C_d
12	1.233	4.84	1.235	0.414	0.712
12	1.150	4.84	1.152	0.401	0.725
12	0.793	4.84	0.794	0.351	0.843
12	0.743	4.84	0.744	0.342	0.869
12	0.671	4.84	0.672	0.323	0.897
12	0.583	4.84	0.584	0.300	0.947
12	0.476	4.84	0.476	0.267	1.032
12	0.384	4.84	0.385	0.237	1.148
12	0.283	4.84	0.284	0.196	1.335
12	0.208	4.84	0.208	0.155	1.538